KATHOLIEKE UNIVERSITEIT LEUVEN
FACULTEIT INGENIEURSWETENSCHAPPEN
DEPARTEMENT BURGERLIJKE BOUWKUNDE
LABORATORIUM VOOR HYDRAULICA
Kasteelpark Arenberg 40, B-3001 Heverlee, Belgium

Climate change impacts on hydrological extremes and water resources in Lake Victoria catchments, upper Nile basin

Promotoren:

Prof. P. Willems
Prof. G. Ngirane-Katashaya (Makerere University Kampala, Uganda)
Prof. J. Berlamont

Dissertation presented in partial fulfillment of the requirements for the degree of Doctor of Engineering

by

Paul OGIRAMOI NYEKO

November 2011

KATHOLIEKE UNIVERSITEIT LEUVEN
FACULTEIT INGENIEURSWETENSCHAPPEN
DEPARTEMENT BURGERLIJKE BOUWKUNDE
LABORATORIUM VOOR HYDRAULICA
Kasteelpark Arenberg 40, B-3001 Heverlee, Belgium

Climate change impacts on hydrological extremes and water resources in Lake Victoria catchments, upper Nile basin

Jury members:

Prof. P. Willems, Promoter
Prof. G. Ngirane-Katashaya, Promoter
(Makerere University Kampala, Uganda)
Prof. J. Berlamont, Promoter
Prof. D. Raes
Prof. J. van Dyck
Prof. N. van Lipzig
Prof. F. M. Mutua, (University of Nairobi, Kenya)
Prof. W. Bauwens (Vrije Univeristeit Brussels, Belgium)

Proefschrift voorgedragen tot
het behalen van het doctoraat
in de ingenieurswetenschapen

door

Paul OGIRAMOI NYEKO

November 2011

© 2011 Katholieke Universiteit Leuven – Faculteite Ingenieurswetenschappen,
Arenberg Doctoraatsschool, Kasteelpark Arenberg 40, B-3001 Heverlee, Belgium.

All rights reserved. No part of the publication may be reproduced in any form by print, photoprint, microfilm, electronic or any other means without written permission from the publisher, Department of Civil Engineering, Katholieke Universiteit Leuven Kasteelpark Arenberg 40, 3001 Heverlee, Belgium.

Legal deposit D/2011/7515/140
ISBN 978-94-6018-439-0

DEDICATION

This research is dedicated to my brother Dan E. Okello Tudi to remember him for the faithful role he played in laying the foundation of my education.

ACKNOWLEDGEMENTS

A journey without an end is not one. A finished journey comes with lots of mixed feelings. One such feeling is characterized by a reflection on how troublesome it was, which in Kiswahili is popularly known as *safari tabu*. However, at the end of it all, the feeling of the achievement attained is overwhelming, which brings joys and gratitude. Indeed, I feel extremely happy for the successful completion of this academic journey. The time and opportunity to remember the genesis and in-between events of this academic research is here. I was a seed, and successfully grew well to harvest time because I was watered, weeded and pruned. It is one harvest but many laborers played different roles. The one who tirelessly watered me was Prof. Patrick Willems. I am wholeheartedly grateful for his academic guidance, gentility and diligence he demonstrated during the course of the research. He sowed the seed and pruned it well with all his unquestionable talents. Thanks to him many more. I did not also stagger in the absence of Prof. Patrick Willems because he was not alone. Many thanks to Prof. Gaddi Ngirane-Katashaya for the supports he rendered. He filled the gaps while I was not in Belgium. Thanks for being very instrumental during the decisive stages of the research. I would like also to acknowledge the roles of Prof. Jean Berlamont, especially in filling the administrative gap. Thanks to the hydraulic research team and its administration at the Civil Engineering Department, KULeuven.

This research was powered by the funding from the Flemish Interuniversity Council – University Development Cooperation (VLIR-OUS) under the ICP-PhD programme, administered at KULeuven, Belgium and Makerere University Kampala, Uganda. In the absence of the powerhouse (VLIR-OUS), it would not have been possible to implement this research. I am honored and very grateful for its role it played and I want to say long live VLIR-OUS. I am particularly grateful to Inge Vanderveren and Chistel Vancauwenbergh who were involved in the day-to-day official administrative works at the international office, KULeuven. Thanks to all the officials at the VLIR-OUS secretariat in Brussels; particularly to Stefan Wellen for being instrumental during the decisive moments of my contract with VLIR-OUS. I am further grateful to Prof. Gaddi Ngirane-Katasaya, together with Dr. Umaru Bagampadde for administering the programme well at the Department of Civil Engineering, Makerere University Kampala, Uganda.

I am also indebted to the Ministry of Water and Environment, Uganda, for the institutional supports rendered and the data provided for this research. I am particularly thankful to the Director, Eng. Sottie Bomukama, commissioner, Eng. Aaron Kabirizi and his two assistants, Eng. Aus-Ali Tushabe and Eng. Joseph Oriono Eyatu, for being supportive. This research was linked to the

FRIEND/Nile research activities, which increased its visibility and facilitated its dissemination. Thanks to all the FRIEND/Nile team members for all the intellectual interactions and I pledge my commitment for further collaborations.

I am also thankful to all the examination and advisory committee members for being critical of the research. Your remarks were meant to put more weights on the harvest. My assurance to you is that the good knowledge that I have reaped shall be put to good use for the benefits of others as well.

To my colleagues and friends; you have been helpful in one way or another during the period of this research. You have supported me directly or indirectly. I heartily thank you for the supports you rendered kindly, morally, technically or resourcefully. I am particularly thankful to my colleague Victor for the many useful ideas that we shared during the course of this research.

To my family who has stood behind me since I was born. You have made me what I am today. Thanks to my late father. I wish he was alive to witness the harvest of the fruit that he sowed. Thanks to my mother for shaping my life to unforgettable time. Thanks to my brother, Dan, and his wife, Florence, for the roles played in laying all the necessary foundations for my education.

For a successful man, there is always a glittering woman behind. Thanks to my dear wife, Janet, for all the supports, for being a woman of my heart and for shouldering both the weights of a man and woman in our home while I was away in Leuven. Thanks for looking after the children (Ogira, Lengcwiny, Itaba and Piri) well in my absence. I love you very much.

While in Leuven, I was seeking spiritual nourishment together with others in the University Parish International Community (UPIC). Thanks to all the parishioners and to all the fellow choir members for the spiritual environment that we shared together. God, may you bless UPIC community.

To all the people I have not mentioned; many thanks for being part of my life and for supporting me in this research unknowingly or knowingly. Your voluntary and involuntary actions have pushed my academic achievements and career to the next level. May God bless you all.

God has made me into being and I want to crown my gratitude to him. I want to thank you, oh God, for all what you have done in my life. Thanks you God for this academic achievement; many things have happened in my life because of your wishes. I put my future into thy hands.

N. P. Ogiramoi

ENGLISH SUMMARY

Climate is indubitably a key driver of change determining different characteristics and distributions of natural and managed systems. Change in climate is hypothesized to be a result of mainly increase in greenhouse gases concentrations in the atmosphere and has been widely documented in literatures as involving increase in global temperature. Human activities, primarily burning of fossil fuels and clearing of forests are also widely documented to have greatly intensified the natural greenhouse effect resulting into an enhancement of global warming. Due to global warming, several of the constituents of the components of the climate system, including hydrological cycle, will be severely perturbed.

Scientists around the globe are using climate models such as Global Climate Models (GCMs) to facilitate the understanding of the changes in the climate system with optimistic attempts to project future climate based on, for example, socioeconomic scenarios. Corroborated studies have conspicuously shown that change in climate is a real threat to a global society and its environment. The threat is mainly extremes of climate such as severe droughts and prolonged or intense wet spells resulting into floods, among others, which have very strong negative impacts on both natural and managed systems.

Change in climate may potentially alter the frequency, quantity, location and duration of hydrological regimes. Changed hydrological extremes will have significant implications on the planning and design of hydraulic structures and general characteristics of water resources such as quantities and qualities. The changes could aggravate periodic and cyclic shortfalls of water supply in addition to other factors such as landuse malpractices.

Increasing accumulation and availability of climate related information such as scientific publications and more especially the data for future possible climate states obtained through application of GCMs and past climate are rapidly driving the climate change impacts studies to the next level. The demand for hydrological implications of climate change is one big area of concern because of the significant role hydrology plays in the sustainability of human and ecological lives. The main objective of this study was thus to investigate the possible impacts of climate change on the hydrological extremes and water resources in the upper Nile basin, Lake Victoria catchments, with a yawning focus on the hydrological consequences for the River Katonga and River Ruizi catchment responses.

Investigation of trends in the historical hydrometeorological records formed the first objective of this study. Trend analysis results do not only provide information on the general direction of observed change but also unravel significant changes that have occurred over and above the expected natural climate variability and may link them to past consequences. Since the effects of climate change are unleashed more through the occurrence of extremes, the presence of a significant linear trend in a long term climate record of extremes may provide evidence of a significant shift from the natural trend to that which is enhanced by, for example, anthropogenic forcing. Analysis of long term records of extremes for rainfall, temperature and streamflows from selected stations within the study area were considered in this study. The findings indicated that these extremes are generally experiencing a positive trend. Albeit positive trend was generally demonstrated in the extremes for the selected variables, the presence of significant linear trend was only manifested in the extremes of the data for the stations located in the northern and eastern parts of the Lake Victoria basin. This may suggest that the monotony in the linear trend is probably an indicator of the sensitivity of the region's extremes to climate change due to possible external enhancement of the natural climate agitation. The latter has implications for flood risks if the trend is maintained. Furthermore, the higher significant anomalies for the 1990s as compared to that of the 1960s may suggest a more intense enhancement of the change in the natural variability in the recent climate. Correlation between change in the extremes of rainfall and that of the minimum temperature was demonstrated to be stronger compared to other variables. This may suggest that in the absence of extreme rainfall data, minimum temperature may be a good indicator of the rainfall extremes.

The credibility of the GCMs in representing the current and past climate needs to be assessed before the GCM data are employed to aid assessment of hydrological impacts of climate change. Thus, the second objective of this study was to test the reliability of the GCMs based on their simulation runs for the 20th century (present day climate). The present day simulations were evaluated against the observed hydrometeorological records using mainly statistical metrics. The findings showed that several GCMs are quite implausible with respect to simulation of the climate of the Lake Victoria basin and more tasks still lie ahead for the climate modelers. However, the evaluation results for some of the GCMs provided motivation for their employment in the impact assessment for the region.

Change in hydrological regimes due to projected change in climate necessitates comparing the future hydrological time series with that of the current or observed climate. GCMs directly provide future hydrological time series such as rainfall and temperature based on Special Report on Emission Scenarios (SRES) of the Intergovernmental Panel on Climate Change (IPCC). Nevertheless, the scales in the GCM experimental runs still need to be similar

with the one needed for the study of local hydrology if a meaningful comparison is being sought. Convention approach to match the scales in GCMs with that of the hydrology at catchment level is through what is termed downscaling. The third objective of the study was to formulate a methodology for the improvement of the perturbation approach for downscaling rainfall. The innovated technique ensures the extraction of climate change signals at larger scale and transferring them to local scale is carried out while accounting for the climate change signals of the wet spells in the time series. The results demonstrated the plausibility of the technique.

The downscaled hydrometeorological variables enabled the investigation of climate change impacts on rainfall in the study area. The fourth objective was to analyze change in rainfall extremes because of their apparent manifestation in the face of climate change. Extremes from selected stations across the study area were considered and comparison was done based mainly on extreme value analysis. The findings showed that the magnitude of rainfall extremes are projected to be altered significantly with the extremes for the eastern part of the Lake Victoria basin increasing higher than those for the western part. The rainfall extremes for the south and the southwestern parts of the basin are projected to decrease. Analysis of the possible change in rainfall Intensity-duration-frequency (IDF) relationships was also carried out using extreme value technique. The results showed that change in the IDF would have significant implications for hydraulic design practices and other related engineering applications.

The other objective was to carry out a rigorous analysis of the possible hydrological responses of the River Katonga and Ruizi catchments, given possible future climate states, based on rainfall-runoff model simulations. The rainfall-runoff model was driven by the downscaled variables from a suit of selected GCM runs under three different SRES scenarios code-named A1, A1B and B1 of the IPCC and for two different future periods, 2050s and 2090s. Since the focus of the study was centered on high flows, considerable efforts were devoted to ensure that the development of the rainfall-runoff model take into account good fits with the high flow peaks during calibration and validation stages. Impacts of climate change on the streamflows from the two catchments were executed by comparing the future streamflows with that of the present day (control) streamflows. The results showed that the hydrological response of the respective catchment is likely to underscore the integrity of the water balance of the catchments. The water balance of each of the two catchments is projected to experience a significant deficit and may severely affect the hydrologic demands from the two catchments in addition to other constraints. Furthermore, the flood frequency is projected to be affected and this has implications on the engineering practices and other water resources planning involving flood frequency estimations.

In conclusive remarks, assessment of the possible impacts of climate change on the hydrological extremes and water resources of the upper Nile basin was carried out based on a suit of GCM runs, which were also used for AR4 IPCC. This should set the stage for the subsequent relevant research tasks that seek to address hydrological impacts of climate change for the region. Water managers in the catchments are advised to take a step that may lead to the revision of the current relevant hydraulic design guidelines in order to take into account the future hydrologic risks imposed by change in climate. In addition, a collaborative effort is needed across relevant research disciplines and the responsible water agencies in the region for a more holistic and integrated research syntheses that can, unanimously, translate into a regional strategy and policy for adaptation to climate change. It should be noted also that a number of uncertainty sources are known and constitute one of the most setbacks in climate change impacts assessment, which cannot be shirked.

NERDERLANDSE SAMENVATTING

Klimaat heeft een sterke invloed op vele natuurlijke en kunstmatige systemen. Zoals uitgebreid gedocumenteerd in de literatuur wordt verwacht dat veranderingen in het klimaat voor een belangrijk deel worden veroorzaakt door de toename in de uitstoot aan broeikasgassen in de atmosfeer. Deze toename veroorzaakt onder meer een globale mondiale temperatuurstijging. Ook andere menselijke activiteiten zoals ontbossing zouden een significante invloed hebben op het klimaat. Deze klimaatveranderingen beïnvloeden op hun beurt de hydrologische cyclus, waaronder rivierafvoeren (overstromingen, laagwater) en waterbeschikbaarheid.

Om de klimaatverandering te bestuderen, maken wetenschappers wereldwijd gebruik van klimaatmodellen, zowel mondiale als regionale klimaatmodellen. In deze modellen worden scenario's gesimuleerd van mogelijke toekomstige socio-economische evoluties. Recente studies hebben aangetoond dat de vooropgestelde klimaatscenario's een sterke wereldwijde bedreiging vormen voor de maatschappij en het milieu. Vooral de verhoogde kans op het voorkomen van extreme klimaatcondities zoals droogte en periodes met intense neerslag kunnen een catastrofale invloed hebben.

De invloed van de klimaatverandering op de hydrologie varieert van veranderingen in de frequentie, de kwantiteit, de tijdsduur, tot de locatie van hydrologische gebeurtenissen (zoals overstromingen en watertekorten). Zulke veranderingen kunnen een belangrijke invloed hebben op de kwantiteit en de kwaliteit van beschikbare watervoorraden, dus op de planning en het ontwerp van waterbeheerstrategieën en gerelateerde hydraulische structuren. De veranderingen kunnen de watervoorziening in het gedrang brengen, kunnen meer overstromingen veroorzaken, maar kunnen ook indirecte problemen induceren zoals een niet-duurzaam landgebruik.

De toename en verhoogde beschikbaarheid aan klimaatgerelateerde informatie zoals wetenschappelijke publicaties, langdurige historische meetreeksen van temperatuur, neerslag en rivierdebieten, en simulatieresultaten met klimaatmodellen, zorgden de laatste jaren voor een sterke stijging in het aantal impactstudies m.b.t. klimaatverandering. Ze zorgen er ook voor dat het niveau van deze studies naar een hoger niveau wordt getild. Vooral het aantal hydrologische impactstudies kent een sterke stijging, omwille van het grote belang van water voor mens en milieu. De voorliggende doctoraatsstudie moet in deze context gezien worden. De hoofddoelstelling van de studie bestond erin om de mogelijke invloed te bestuderen van de klimaatverandering op de hydrologie van het meest opwaartse deelbekken van de Nijl in Africa: dat van de stroomgebieden die afwateren naar het Victoriameer opwaarts van de Witte Nijl. Terwijl de klimaatverandering voor

het ganse deelbekken van het Victoriameer werd bestudeerd, werd de hydrologische impactanalyse beperkt tot de stroomgebieden van de rivieren Katonga en Ruizi in Uganda.

In een eerste stap van het onderzoek werden de trends in de beschikbare historische hydrometeorologische tijdreeksen onderzocht. Dit onderzoek gaf informatie over de recente historische veranderingen en of deze veranderingen statistisch significant zijn in vergelijking met de natuurlijke variabiliteit. Op basis van langdurige meetreeksen van neerslag, temperatuur en rivierdebieten beschikbaar in de bestudeerde stroomgebieden werden de extreme waarden geëxtraheerd en nagegaan of er significante trends zijn die mogelijks kunnen toegeschreven worden aan de antropogene klimaatopwarming. Resultaten gaven aan dat de temperatuur- en neerslagextremen multidecadale oscillaties vertonen door het gegroepeerd in de tijd voorkomen van deze extremen (over tijdschalen van 1 tot 2 decaden). Naast deze oscillaties, vertonen vooral de stations in het noorden en het oosten van het Victoriabekken een recente stijgende trend. De afwijkingen in het voorkomen van neerslag- en debietextremen blijken sterker voor de jaren 1990 dan de jaren 1960. Het is duidelijk dat wanneer deze trend zich verder zet, dit grote socio-economische gevolgen kan hebben voor de regio. Of deze trend zich effectief zal verder zetten werd in het vervolg van het onderzoek geschat op basis van simulatieresultaten met klimaatmodellen.

In een tweede stap van het onderzoek werd de performantie van de klimaatmodellen in het beschrijven van hydrometeorologische extremen bestudeerd. De simulatieresultaten voor de twintigste eeuw werden hiervoor vergeleken met historische waarnemingen. Op basis van modelperformantiestatistieken werd aangetoond dat meerdere mondiale klimaatmodellen erg onnauwkeurig zijn in het simuleren van het lokale klimaat in de omgeving van het Victoriameer. Het verder verbeteren van deze modellen is dus noodzakelijk, onder meer via dynamische neerschaling van de modelresultaten in tijd en ruimte door gebruik te maken van fijnmazigere regionale klimaatmodellen. Omdat op basis van extern klimaatonderzoek verwacht wordt dat de regionale veranderingen in klimaat vooral bepaald worden door de grootschalige antropogene invloeden en klimaatprocessen, kan verondersteld worden dat de simulatieresultaten voor de klimaatveranderingen nauwkeuriger zijn dan deze voor het regionale klimaat zelf. Op basis van deze argumentatie en omwille van de behoorlijke nauwkeurigheid van bepaalde modellen voor het recente en huidige klimaat, werd geopteerd om de bestaande mondiale klimaatmodellen te gebruiken als basis voor de hydrologische impactanalyse van de klimaatverandering.

De resultaten van de klimaatmodellen konden echter niet rechtstreeks gebruikt worden voor de hydrologische impactanalyse. Enerzijds is er de afwijking van de klimaatmodellen met de historische waarnemingen wat een correctie van

deze afwijking noodzaakt. Anderzijds is er het verschil in ruimtelijke schaal tussen de klimaatmodelresultaten en de schaal waarop de hydrologische impactanalyse gebeurt. Dit laatste probleem werd opgelost door het gebruik van een statistische neerschalingstechniek. In een derde stap van het onderzoek werd daarom een analyse gemaakt van de bestaande statistische neerschalingstechnieken, werd een beloftevolle methode geselecteerd, en getest en verfijnd voor gebruik in de semi-ariede en semi-humiede gebieden van het opwaartse Nijlbekken. De grofschalige klimaatmodelresultaten voor en na simulatie van de emissiescenario's van de Intergouvernementele Werkgroep rond Klimaatverandering (IPCC) van de Verenigde Naties werden statistisch vergeleken, en getransformeerd naar veranderingen in de lokale neerslag- en temperatuurreeksen. Dit gebeurde op basis van een kwantielperturbatiemethode, die in voorafgaandelijk onderzoek aan de Afdeling Hydraulica van de K.U.Leuven werd ontwikkeld en uitgebreid getest voor Belgische condities. Voor toepassing in het Nijlbekken werd de methode verder verfijnd door rekening te houden met de nauwkeurige veranderingen in de lengte van droge perioden in de neerslagreeksen.

In een vierde stap van het onderzoek warden de veranderingen in neerslagextremen, na statistische neerschaling, uitgebreid bestudeerd en gemodelleerd op basis van een statistische extreme-waarden-analyse. Ook de regionale verschillen in de opwaartse stroomgebieden van het Victoriameer in Kenya, Tanzania en Uganda werden geanalyseerd. De toename in neerslagextremen bleek sterker in het oosten van die regio dan in het westen. In het zuiden en het zuidwesten stellen de resultaten een toekomstige daling in de neerslagextremen voorop voor de komende decennia. De analyse werd uitgevoerd voor toekomstprojecties tot de jaren 2050 en tot de jaren 2090. De resultaten werden samengevat in veranderingen aan de intensiteit/duur/frequentie-verbanden (IDF-verbanden) van extreme neerslag. De onzekerheid op de veranderingen werd geschat door de resultaten van alle beschikbare klimaatmodelsimulaties met elkaar te vergelijken. Deze omvatten een ruime set aan verschillende klimaatmodellen en drie verschillende IPCC-emissiescenario's.

In een volgende, vijfde stap van het onderzoek werden de veranderingen in hydrometeorologische variabelen getransformeerd naar overeenkomstige veranderingen in hydrologische variabelen. Dit gebeurde op basis van neerslagafstromingsmodellen voor de Katonga- en Ruizi-stroomgebieden. Omwille van de focus van het voorliggend onderzoek op extremen, werd bij de opbouw en kalibratie van de neerslagafstromingsmodellen bijzondere aandacht gegeven aan de nauwkeurigheid van de modellen in het beschrijven van piekafvoeren en laagwaterdebieten. Na vergelijking van de neerslagafstromingsresultaten voor en na perturbatie van de modelinvoer op basis van de klimaatscenario's, werd voor beide stroomgebieden enerzijds een daling van de waterbeschikbaarheid gevonden, en anderzijds een stijging van

de piekafvoeren. De daling in de waterbeschikbaarheid in de droge perioden kan – in combinatie met de sterke bevolkingsgroei en toename in welvaart – in de toekomst de hydrologische noden in sterke mate verhogen. Een toename in piekafvoeren tijdens de natte perioden zorgt voor een toename in de overstromingsfrequenties, dus voor bijkomende noden m.b.t. overstromingsbeheersing.

De hydrologische impactresultaten van de klimaatverandering, zoals bekomen in dit doctoraatsonderzoek, kunnen rechtstreeks gebruikt worden door de lokale waterbeheerders en beleidsmakers, o.a. bij het ontwerp van aangepaste waterbeheersstrategieën en hydraulische infrastructuur. Bij de bouw van nieuwe infrastructuur of de opmaak van nieuwe waterbeheersplannen, kan via de ontwikkelde klimaatscenario's en de methode voor hydrologische impactanalyse, rekening worden gehouden met de mogelijke toekomstige evoluties, samen met hun onzekerheid. De grote onzekerheid in de toekomstige klimaatevoluties, die voor een deel veroorzaakt is door de onzekere kennis over het toekomstig gedrag van mensen (onzekerheid in de emissiescenario's), maar ook door de onzekerheid in de klimaatmodellen en fysische processen, noodzaakt een risico-analyse aanpak. Zulke aanpak dient geïntegreerd in het huidig waterbeheer- en de bijhorende planning. Ook heeft het onderzoek, dat gebruik maakte van multidisciplinaire kennis vanuit de klimatologie, de hydrologie en de statistiek en dat tegemoet diende te komen aan het grote verschil tussen wat klimatologen klassiek aanleveren en wat hydrologen en waterbouwkundige ingenieurs nodig hebben, duidelijk gemaakt dat er nood is aan meer interdisciplinaire samenwerking. Ook hebben de resultaten, via de hydrologische impactanalyse en de bijhorende gevaren, zeker voor de ontwikkelingslanden in de regio van het Victoriameer, duidelijk gemaakt dat er nood is aan een duurzame regionale strategie voor klimaatadaptatie. Dit vraagt een holistische en geïntegreerde aanpak, waarbij met verschillende deelaspecten en invloeden rekening wordt gehouden. Dit onderzoek heeft daar voor een deel aan bijgedragen door meer inzicht op te bouwen rond klimaatverandering en –variabiliteit, door – op basis van de huidige kennis en inzicht – klimaatscenario's en een methode voor hydrologische impactanalyse te ontwikkelen, en door de methode en impactresultaten te demonstreren voor twee stroomgebieden in de regio.

ACRONYMS AND ABBREVIATIONS

20C3M	20th Century Climate Simulation
AggL	Aggregation level
AM	Annual Maxima
AMF	Annual Maximum Flood
AR4 IPCC	Fourth Assessment Report of the Intergovernmental Panel on Climate Change
CCS	Climate Change Signal
CDO	Climate Data Operators
CLS	POS Climate Change Signal
CLSa	POSa Climate Change Signal
CS	Control Series
ENSO	El Niño/La Niña-Southern Oscillation
EVD	Extreme Value Distribution
FAO	Food and Agricultural Organization
FRIEND/Nile	Flow Regimes from International and Experimental Networks Data for River Nile basin
GCM	Global Climate Model
GEV	Generalized Extreme Value
GHG	Green House Gases
GLO	Generalized Logistics Distribution
GPD	Generalized Pareto Distribution
IDF	Intensity Duration Frequency
IDW	Inverse Distance Weighting
iid	independently, identically distributed
IWRM	Integrated Water Resources Management
k.d.e	Kernel density estimates
L-CK	L-Coefficient of Kurtosis
L-CS	L-Coefficient of Skewness
L-CV	L-Coefficient of Variation
LN	Lognormal Distribution
MK	Mann-Kendall
MMD	Multi-Model Data
MWE	Ministry of Water and Environment, Uganda
NAO	North Atlantic Oscillation
OS	Observed Series
P3	Pearson type 3 Distribution
PCMDI	Programme for Climate Model Data and Inter-comparison
PDS	Partial Duration Series
POS	Perturbed Observed Series
POSa	Adjusted Perturbed Observed Series

POT	Peak-Over-Threshold
PWM	Probability Weighted Moment
RCM	Regional Climate Model
SMF	Seasonal Mean Flow
SRES	Special Report on Emissions Scenarios
SS	Scenario Series
UNESCO	United Nations Education, Scientific and Cultural Organization
WMO	World Meteorological Organization

CONTENTS

CHAPTER 1

GENERAL INTRODUCTION

1.1 Introduction

Climate is indubitably a key driver of change determining different characteristics and distributions of natural and managed systems. Change in global climate is hypothesized to be a result of increase in greenhouse gas concentrations in the atmosphere and has been widely documented in literatures as involving increase in global temperature. Human activities, primarily burning of fossil fuels and clearing of forests, are also widely documented in literatures to have greatly intensified the natural greenhouse effect with rate of warming over the last 50 years almost doubled that over the last 100 years (0.13°C versus 0.07°C) (Trenberth, et al., 2007). Due to global warming, the global climate will change and as such several of the constituents of the components of the climate system (e.g. hydrological cycle) will be severely perturbed. Change in global climate is conveyed directly to regional and local climate.

Scientists around the globe are using climate models to understand changes in the climate system with optimistic attempts to project future climate (Meehl et al., 2007). Corroborated global studies have conspicuously shown that change in climate is a real threat to a global society and its environment. The threat is mainly extremes of climate such as severe droughts and prolonged wet spells, among others, which have very strong negative impacts on both natural and managed systems. The risks associated with climate change are enormous and critical (Parry, 2001) and need not to be ignored.

Climate change may potentially affect the frequency, quantity, location and duration of hydrometeorological extremes. Changed hydrological extremes will have significant implications on the design of civil structures and general water resources planning and management. The changes could exacerbate periodic and cyclic shortfalls of water, particularly in arid and semi-arid areas of the world (Yanjun et al., 2008; Christensen et al., 2007; Hamlet & Lettenmaier, 1999; Jeong, 2005; Kundzewicz et al., 2007). Strong corroborated conclusions have been made on developing countries regarding their vulnerability to climate change because of the fact that many are located in arid and semi-arid regions and most derive their water resources from single-point systems such as boreholes or isolated reservoirs (e.g. Boko et al., 2007; Christensen et al., 2007). Even in the absence of climate change, present population trends and patterns of water use wave gesticulate that more

developing countries, especially in Africa, will exceed limits of their 'economically usable and land-based water resources before 2025 (Kundzewicz et al., 2008). These warnings call for a twist in thinking about and response to the looming climate change and its impacts especially from local perspective.

The Fourth Assessment Report of Working Group II of the Intergovernmental Panel on Climate Change (AR4 IPCC) critically assessed thousands of recent publications on different aspects of climate change impacts, adaptation and vulnerabilities. The multi-disciplinary and multi-national authorship of the report ensured that a wide variety of available information, opinions and hypotheses was assessed. It also enabled the prioritization of the findings with respect to their importance, likelihood and confidence. One of the priority areas requiring further research, as recommended by IPCC in its AR4, is the assessments of climate change impacts on water resources (Carter et al., 2007).

The study of climate change impacts on water resources is very important in informing decision-making process in the overall planning and management of water resources. Application of the recommended standard IPCC impact approach[1] has been used significantly to study impacts of climate change on hydrology and water resources (e.g. Andersson et al., 2006; Notter et al., 2007; Paturel et al., 2007; Hreiche et al., 2007; Yanjun et al., 2008). However, the climate-sensitive resources of many regions and sectors, for example the River Nile basin, have not yet been subject to adequate impact assessments. The demand for such assessments has grown significantly and presents a very worrying case for the upper River Nile basin, Lake Victoria basin. Nevertheless, there are growing responses from researchers but with few attempts being made (e.g. Setegn et al., 2011; Awange et al., 2008, Githui et al., 2009; Owor et al., 2009; Koutsouris et al., Nyeko-Ogiramoi et al., 2010; Taye et al., 2011). Further actions however are needed to address the disparity in the spatial coverage of the study of the impacts of climate change on hydrological extremes at local scale.

1.2 Research motivation and problem statement

Figure 1.1 shows examples of water-related vulnerability "hot spots" where climate change impacts on freshwater resources in the decades to come are a threat to the pursuit of sustainable development of the affected regions. The map represents the ensemble mean change in annual runoff averaged across a number of different climate models (Nohara et al., 2006) and generally provides a global overview on the problems, which will be associated with the impacts of climate change on water resources.

[1] The approach: 1. Define problem, 2. Select method, 3. Test method/sensitivity, 4. Select scenarios, 5. Assess bio-physical impacts, 6. Assess autonomous adjustments, 7. Evaluate adaptation strategies.

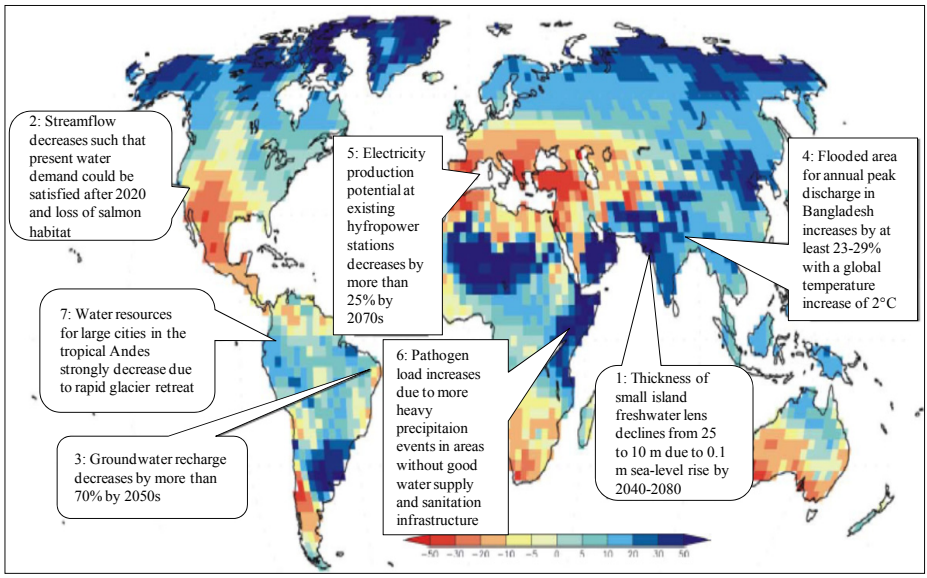

Figure 1.1 Illustrative map of future climate change impacts on freshwater, which are a threat to the sustainable development of the affected regions (modified after Kundzewicz et al., 2007). Background map: ensemble mean change of annual runoff (in percent) between present (1981–2000) and 2081–2100 for the SRES A1B emissions scenario (based on Nohara et al., 2006). References in boxes – 1: Bobba et al. (2000); 2: Barnett et al. (2004); 3: Döll and Flörke (2005); 4: Mirza et al. (2003); 5: Lehner et al. (2005); 6: Kistemann et al. (2002); 7: Vergara et al. (2007).

Runoff is projected to increase in some regions and to decrease in others, exaggerating water resources problems in some catchments and alleviating them in others. By mid-century, annual average river runoff and water availability are projected to decrease by 10–30% over some dry regions at mid-latitudes and in the dry tropics, while increasing by 10–40% at high latitudes and in some wet tropical areas (Milly et al., 2005) and more pronounced changes are likely by the end of this century. Many of the presently water stressed semiarid and arid areas are likely to suffer from decreasing water resource availability due to climate change as both river streamflows and groundwater recharge decline (c.f. Northeast Brazil; Fig. 1 – Box 3; Döll and Flörke, 2005).

Changes in flood and drought frequency and intensity are projected (Arnell, 2004; Barnett et al., 2005). The proportion of total rainfall from heavy precipitation events is very likely to increase over most areas (IPCC, 2007) and tropical and high latitude areas are particularly likely to experience increases in both the frequency and intensity of heavy precipitation events. The flood frequency and magnitude is projected to increase in the regions experiencing increase in precipitation intensity, while drought frequency is projected to increase in many regions, in particular those where reduction of precipitation is projected.

Globally, by the 2090s, drought-affected areas are likely to increase in extent, while the proportion of the land surface in extreme drought at any one time is predicted to increase ten-fold from the present. The overall drying trend is projected with a decrease in global average value of the Palmer Drought Severity Index of 0.3 and 0.56 per decade, respectively, for the first and the second half of this century (Burke et al., 2006). Some drainage basins are projected to experience increase in frequency of both floods and droughts. The beneficial impacts of projected increases in annual runoff in such areas as eastern and southeastern Asia (Figure 1.1), will be tempered by adverse impacts of increased variability and seasonal runoff shifts on water supply and flood risk in particular in heavily populated low-lying river deltas (Figure 1.1 – Box 4; Mirza et al., 2003).

Furthermore, additional precipitation during the wet season in those regions may not alleviate dry season problems if the excess water cannot be stored. Areas in which runoff is projected to decline are likely to face a reduction in the value of the services provided by water resources, for example as habitat for freshwater fauna and flora (Figure 1.1 - Box 5; Barnett et al., 2004), or as energy source (Figure 1.1 – Box 2; Lehner et al., 2005).

Climate change poses a major conceptual challenge to water managers in addition to the challenges caused by population and land-use change. It is now evidently inappropriate to assume that past hydrological conditions will continue into the future due to climate change uncertainty and the dearth of knowledge on future climate. It will also be intricate to detect a clear climate change effect within the next couple of decades, even with an underlying trend. Water managers in some countries are already considering how to incorporate the potential effects of climate change into policies and specific designs explicitly but the challenge being faced is the insufficient research information into the subject matter at local scale, especially for developing countries such as those in the River Nile basin. This demonstrates the need for climate change impacts information at local scale a priority.

For purposes of engineering applications, impacts studies are required on hydrological extremes such as extremes of precipitation and high streamflows (which are mainly floods) and for the Nile basin such studies are very limited (e.g. Taye et al., 2011). Incorporation of the findings from the limited available information on climate change impact assessment on water resources in the Nile basin into policy practice is inevitably hindered by transboundary issues and different, but parallel local policies. The problem is complicated by the fact that water is effectively managed at catchment scale and adaptation is local and application of findings from studies conducted at basin-wide or regional scale is devoid of plausibility. A local scale study of climate change impacts on hydrological extremes is thus more crucial to provide local water managers with the baseline knowledge and tool to assess

future risks associated with the local water resources and thereby draw a strategy for adaptation through faster policy implementation.

1.3 General and specific objectives

This thesis adopted the research philosophy outlined in the IPCC standard approach to the assessment of climate change impacts[2]. That is, based on climate change scenario-driven 'impact approach', developed from the seven steps assessment framework of IPCC (1994). The approach aims to evaluate the likely impacts of climate change under a given scenario and to assess the need for adaptation and/or mitigation in order to alleviate the resulting vulnerability of climate change risks.

The main objective of the research was to improve understanding and estimation of the quantitative impacts of climate change on the frequency of hydrological extremes and water resources through a statistical downscaling approach of rainfall and a rainfall-runoff modeling at medium size catchment scale. The study is an attempt to fulfill the pragmatic information needs of water managers who are responsible for adaptation planning including tackling challenges related to practical engineering applications. The specific objectives of the study are listed as follow:

(i) Review of literatures related to impacts of climate change on water resources with particular attention to hydrological extremes.

(ii) Selection of a case for the study, and the collection, processing and assessment of the quality and adequacy of the data required for the study.

(iii) Carry out analysis on monotonic trend and variability (cycles) to establish any underlying observed significant changes in the long-term historical hydrometeorological extremes in precipitation, temperature and streamflows.

(iv) Assessment of the performance of climate models for the study area through a validation of simulated climate against the present or observed climate. In this case, the major climate variables considered were rainfall and temperature.

(v) Apply an innovative approach to derive future time series needed for hydrological modeling purpose. That is, the focus was to use statistical approach to downscale precipitation and temperature from several climate model runs and assess the associated impacts of climate change by comparing the downscaled precipitation and temperature with the observed.

(vi) Simulation of future streamflows through a rainfall-runoff model using downscaled variables as inputs. The focus was to compare the extremes

[2]The approach: 1. Define problem, 2. Select method, 3. Test method/sensitivity, 4. Select scenarios, 5. Assess bio-physical impacts, 6. Assess autonomous adjustments, 7. Evaluate adaptation strategies.

(high streamflows) of the simulated streamflow with the extremes of the control period in order to assess the possible influence of climate change on the streamflow regimes. This benchmark information is intended to inform local water managers of the possible risks associated with the water resources of the study area.

1.4 Research framework

The upper Nile basin was selected as the case study with specific focus on the Lake Victoria basin and its two medium-size river catchments (River Ruizi and Katonga). The research was based on a combination of statistical techniques and hydrological modeling using rainfall-runoff. Statistical techniques were used to understand the patterns of trends and changes in the past and recent climate of the study area. The presence of linear trends in the long-term hydrometeorological variables (e.g. rainfall, temperature and streamflow) was tested using Man-Kendall methods. Meanwhile, the inter-annual variability and changes in the past and recent climate was analysed based on empirical statistical approach. The emphasis was put on the identification of significant linear trends and significant inter-annual changes in the observed variables in order to provide possible evidence of the change in the observed climate. The impact modeling was entirely based on the outputs from several GCMs and a lumped conceptual model based on the VHM approach. For the outputs from climate models, the special report of emission scenarios, identified as A2, A1B and B1, were considered. The selection of the GCM runs completely employed in the study was based on a validation technique, which utilizes key statistical metrics. A non-parametric statistical downscaling technique was employed to derived local-scale future variables (rainfall and temperature) from the selected GCM runs. Because of the complex nature of rainfall, compared to temperature, emphasis was put on analysing the projected changes in rainfall extremes using special statistical technique, the extreme value analysis. The lumped conceptual (VHM) model was developed for each selected river catchment. The calibration and validation of the models were carried out in a manner that ensure that each model has a good proficiency in communicating with peaks during streamflow peaks simulation such that the projected peaks are gleamingly captured. Based on the flood frequency analysis, it was possible to provide information on how future peak streamflows for the Ruizi and Katonga catchments were likely to response to anthropogenic induced climate change based on the emissions scenarios A2, A1B and B1.

The results of the statistical trend analysis and the findings of the response of rainfall and streamflow extremes were then used to form an opinion on the likelihood of the impacts of climate change on the water resources in the Lake Victoria basin, upper Nile basin,.

1.5 Report structure

The thesis is assembled into ten chapters. The genesis chapter is the general introduction, which is this chapter. The chapter provides the definition of the hydrological risks associated with the looming global warming, the general and specific objectives of the study. In addition, an abridgment of the methodology (research framework) is also provided in the chapter. Chapter two provides a general overview of the literatures on climate change impacts assessment. That is, the current knowledge relevant to the research topic is provided. In chapter three, the description of the study area and the data processing procedure is presented. In the former, the hydroclimatology of the Nile basin, Lake Victoria basin and River Ruizi and Katonga catchments are described. While in the latter, climate model data processing procedure is described. In addition, all other data related information is discussed. In chapter four, linear and cyclic trends analysis, for selected hydrometeorological historical data sets are discussed. The chapter provides further information on the significant changes that were observed in the most recent and past climate of the study area.

In chapter five, the climate models are evaluated with respect to their skills and reliability to simulate the recent and current climate of the study area. The former determines the fate of the hydrological impact simulation. Further discussions on the inter-models performance comparison are provided in the chapter. Chapter six presents a statistical downscaling method of climate model runs to catchment scale. To improve on the perturbation approach for statistic downscaling of climate model runs to catchment scale, a rigorous analysis of an innovated non-parametric downscaling methodology for precipitation is described. The technique ensures that change in the wet spells is accounted for during the application of perturbation approach to downscale rainfall. Based on the downscaled precipitation and temperature, chapter seven makes an analysis of the impacts of climate change on rainfall and temperature with specific emphasis on rainfall extremes. In chapter eight, the construction of the rainfall-runoff models for River Ruizi and Katonga, based on the VHM approach, is presented. Based on the calibrated and validated models, the potential impacts of climate change on the hydrological regimes of the River Ruizi and Katonga is addressed in chapter nine. Special emphasis was put on the possible changes in the flood frequency and the seasonal mean streamflows. Finally, chapter ten provides an overall synopsis of this research including conclusive statements and recommendations. In addition, potential areas requiring further research are suggested in chapter ten.

The following terminologies have been used interchangeably: flow, streamflow and discharge; hydrological, hydroclimatic and hydrometeorological, baseline period and reference period, rainfall and precipitation.

CHAPTER 2

CLIMATE AND CLIMATE CHANGE

2.1 Introduction

Water resources planning has traditionally viewed climate as stationary a position that is increasingly indefensible given the verity that most hydraulic infrastructures can be in place for many decades, even centuries. Quantification of the future changes in hydrological extremes due to climate change because of the variation in anthropogenic forcing is a process that involves understanding a number of systems and concepts. These include the: (i) climate system, (ii) climate change, (iii) climate models, (iv) likelihood of vulnerability of water resources due to climate change and (v) climate change impacts assessment methodology and associated uncertainties. Furthermore, the relationship between the climate system and the hydrological system and how they interact and can be modelled, must be well understood. Information on the past and present climate is also undoubtedly essential in the climate change impacts assessment study. Knowledge on the states of the recent and present climate enables the future to be put into perspective. In addition, "digging out" and knowing what had been done on the subject matters shapes the direction of any response. For example, numerous literatures show that a number of scientific studies have been undertaken worldwide to assess impacts of climate change on water resources. Conventional approaches involve generating scenarios for daily or monthly hydroclimatic variables using climate model outputs then application to a water balance or hydrological model to investigate the consequences at a river catchment scale (e.g. Diaz-Nieto and Wilby, 2005). This chapter gives an overview of each of the different systems and concepts required to be understood prior to assessment of the impacts of climate change on water resources at catchment scale. Most of the concepts and methodologies discussed in this chapter were applied in most of the subsequent chapters.

2.2 Climate

2.2.1 Climate system

The World Meteorological Organization (WMO) defines climate as the "average weather", or the statistical description of the weather in terms of the mean and variability of relevant quantities over periods of several decades, typically three decades. The quantities are, most often, surface variables such as temperature, precipitation and wind. In a wider sense, "climate" is the description of the state of the climate system, hereafter defined. The climate

system consists of the following major components: (i) the atmosphere; (ii) the oceans; (iii) the terrestrial and marine biospheres; (iv) the cryosphere, which are sea ice, seasonal snow cover, mountain glaciers and continental scale ice sheets; and (vi) the land surface (Figure 2.2). These components interact with each other and through this collective interaction, the Earth's surface climate is defined. These interactions occur through the flows of energy in various forms such as the exchanges of water, flows of various other radiatively important trace gases commonly known as the green house gases (GHG), including carbon dioxide (CO_2), Nitrous oxide (N_2O), methane (CH4) and the halocarbons and cycling of nutrients. The climate system is powered by the input from solar energy, which is balanced by the emission of infrared ("heat") energy back to space. Solar energy is the ultimate driving force for the motion of the atmosphere and ocean, fluxes of heat and water, and biological activity. The components of the climate system influence the global and regional climate by: (i) influencing the composition of the Earth's atmosphere thereby modulating the absorption and transmission of solar energy and the emission of infrared energy back to space, (ii) altering the surface properties and the amount and nature of cloud cover, which have both regional and global effects on climate and (iii) redistributing heat horizontally and vertically from one region to another through atmospheric motions and ocean currents.

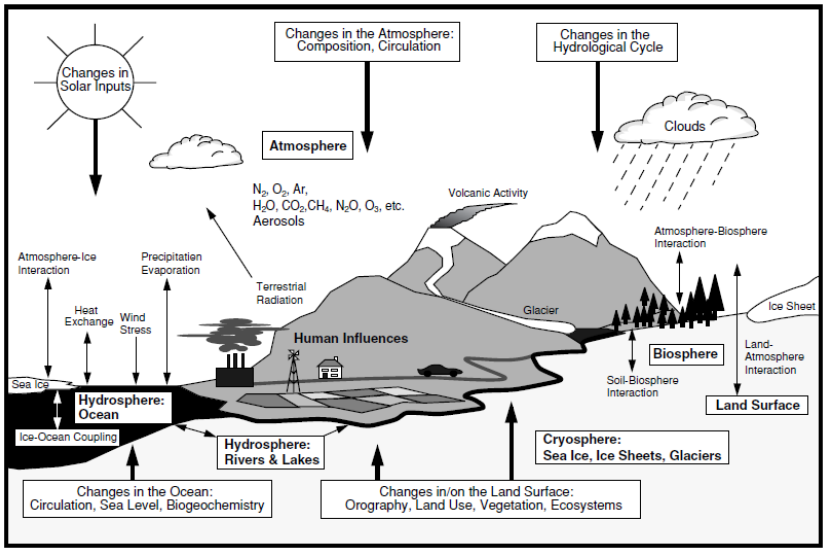

Figure 2.2 Schematic view of the components of the global climate system (bold), their processes and interactions (thin arrows) and some aspects that may change (bold arrows) (adopted from IPCC, 2001a).

In the natural state, the various flows between the climate system components are usually very close to being exactly balanced when averaged over periods of one to several decades. From one year to the other, there can be modest imbalances, which fluctuate in sign due to the natural variability of the

climate system. Human activities can affect the operation of climate processes and hence the natural balance of the climate system through persistent regional to global scale alterations in the composition of the Earth's atmosphere and in the properties of the land surface resulting into climate change (Hansen et al., 2005; Jacob et al., 2005).

2.2.2 Climate change and climate variability

Climate change is a difference over a period (with respect to a baseline or a reference period) and corresponds to a statistical significant trend of mean climate or its variability, persistent over a period of time that spans decades or more (IPCC, 2007). In weather terms, climate change is detected when the average weather parameters over the time interval of interest are significantly different from the climatic values of the same parameters, calculated over a precisely defined reference period. Measurements and studies of time series of meteorological parameters and of other indirect indices show that the climate is generally a variable in time characteristic of a place.

Reference period (Figure 2.3) is typically three decades long. That is, 30 years and 1961-1990 is often used as a climatological baseline period in climate change impact and adaptation assessments and to quantify the anomalies in the future. The period is of sufficient length to represent a given climate adequately and is commonly used to compare fluctuations in climate between one period and another (IPCC, 2001a). In general, IPCC (2001a) recommended a 30-year averaging period for a common definition of a reference or a baseline climate. Conventionally, the reference period differences (future climate minus baseline climate) are mainly used in climate or climate change studies. The differences are also often expressed as ratios (future climate/baseline climate) or percentage differences between periods. Although the IPCC (2001a) recommended a 30-year period as sufficient to measure climate and detect climate change, challenges in climate modeling and archiving of global climate data have forced the global community to consider a 20-year period as plausible for impacts assessment. This is because deviation from using a 20-year period from that of using a 30-year period is not very significant. A number of fixed time horizons in the future are considered in literatures, especially in the recent AR4 IPCC, e.g. the 2020s (2010-2039), 2050s (2040-2069) and 2080s (2070-2099). These are some of the future periods for which any assessment of climate change impacts can be related. In contrast to the adjustment in the future periods, the reference periods have also been adjusted and quite often several studies have adopted 1961-1980, 1971-1990 and 1981-2000. However, in the case where there are sufficient data, it has been strongly recommended that a 30-year period for the current (control) and a 30-year period for the future (scenario) climate be considered.

Climate variability is defined as a deviation from the overall trend or from a stationary state and refers to variations in the mean state and other statistics (such as standard deviations, the occurrence of extremes, etc.) of the climate on all temporal and spatial scales (Figure 2.3). Climate variability is typically a short-term fluctuation superimposed on top of the long-term climate change or trend (Barrow and Gachon, 2004). Cycles of high and low values of weather events (e.g. drought, floods, etc.) are not climate change unless prolonged over many decades. Low frequency variability refers to the phenomena such as the North Atlantic Oscillation (NAO) or El Niño, which occur at a decadal scale or longer period and the high frequency variability refers to the meteorological events and their distributions (e.g. frequency, duration and intensity) at yearly, seasonal or monthly timescales.

Detecting a climate change is the process of demonstrating that climate has changed in some defined statistical sense (Hegerl et al., 2007). Climate scientists argue that climate change may be due to internal processes and/or external forcings acting on the climate system. They further argue that some external influences such as the changes in the solar radiation and volcanism, occur naturally and contribute to the total natural variability of the climate system. Other external changes such as the change in the composition of the atmosphere that began with the industrial revolution are the result of human activity. This is what is referred to as the anthropogenic induced climate change.

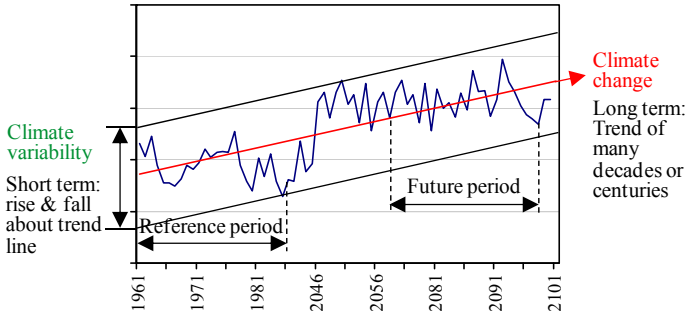

Figure 2.3 Graphical illustration of the climate change, climate variability and reference period concepts.

So far, there are no substantiated protestation to the verity that human activities, principally burning of fossil fuels and clearing of forests, have greatly intensified the natural greenhouse effect causing global warming and resulting in temperature increase by 0.74±0.18 over the last 100 years (Trenberth et al., 2007). Trenberth et al. (2007) further reports that the rate of warming over the last 50 years is almost double that over the last 100 years (0.13°C ± 0.03°C vs. 0.07°C ± 0.02°C per decade). Regardless of the authentic source of this phenomenon, climate change is one of the most contemporary environmental challenges we face in this century. The main

priority for the environmental research community is to gather all knowledge about climate change and what drives it and then predict its future impacts despite the different sources of uncertainty involved.

2.2.3 Climate change scenarios

An advanced way of attempting to project future climate and thereby assessing possible climate change impacts is the inevitable postulation of the possible states of future environment (climate) based on the current and past physical phenomena. The possible states of future climate are the so called climate change scenarios. However, some prominent scientific definitions of climate change scenario exist in literatures. Parry (2002) defined a climate change scenario as a coherent, internally consistent and plausible description of a possible future state of the world. Meanwhile, IPCC (2001a) defined a climate change scenario as a plausible future climate that has been constructed for explicit use in investigating the potential consequences of anthropogenic climate change. Climate change scenarios are a means of using common standards and thereby making common comparisons of research results. Nevertheless, climate change scenarios are the first step along the path to creating plausible representations of the future climate based on assumptions concerning future atmospheric composition and on the understanding of the effect of increased atmospheric concentrations of, for example, GHGs, particulates and other pollutants on the global climate.

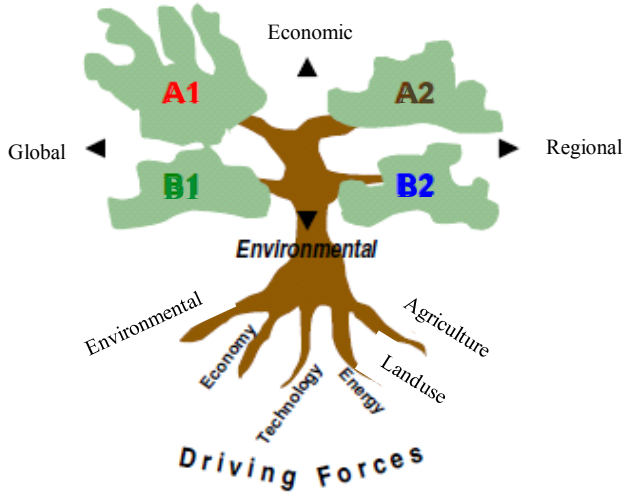

Figure 2.4 A schematic representation of the SRES scenario family. A1 and A2 scenario families have an economic focus than B1 and B2, which are more of environmental focus, whilst the focus of A1 and B1 is more global compared to the more regional A2 and B2.

Future emissions of GHGs and aerosols into the atmosphere depend very much on factors such as population and economic growth and energy use. For

its Third Assessment Report, the IPCC commissioned a Special Report on Emissions Scenarios (SRES) which developed about forty different emissions scenarios (Nakicenovic et al., 2000). The emissions scenarios are classified into four families based on a global or regional development focus, environmental or economic considerations (Figure 2.4). Of these forty emissions scenarios, six have been chosen as illustrative or marker scenarios: A1FI, A1B, A1T, A2, B1 and B2. Of these six marker scenarios, most global climate modelling groups completed climate change simulations using A2, A1B and B1 scenarios that were used for the AR4 IPCC, 2007.

Each scenario family follows a possible storyline about future evolution of demographic composition, economic development and technological progress of the human species (Nakicenovic et al., 2000). Recent publications about climate change impacts assessment have shown that SRES scenarios are, by far, the most commonly used because of its link to global reality (Figure 2.4).

2.2.4 Climate models

Climate models are based on well-established physical principles and have been demonstrated to reproduce observed features of recent climate and past climate changes reasonably well (e.g. Wang and Lau, 2006; Knutti et al., 2005; Knutti et al., 2002; Tebaldi and Knutti, 2007). The physical principles incorporate what is inherently known as the parameterization of the climate models using the climate variables to represent the climate system.

Today, different types of climate models are in force depending on their scope, construction and applications. A general circulation model or a Global Climate Model (GCM) is a mathematical description of parts or the whole climate system and we can have an Atmospheric General Circulation Model (AGCM), an Oceanic General Circulation Model (OGCM) or both coupled Atmosphere-Ocean General Circulation Model (AOGCM). Theoretically, the solution of such a mathematical problem would give the weather and climate state at any time moment. In practice, however, the problem is much more complicated. Thus, it is a common norm to adopt simplified descriptions of the climate system and work with them using the available processing power of appropriate computing equipment in order to perform calculations and obtain results of practical and operational significance. GCMs are considered the only credible tools currently available for simulating the response of the global climate system to increasing GHG concentrations. This is because GCMs are based on mathematical representations of atmosphere, ocean, ice cap and land surface processes and being based on physical laws and physically-based empirical relationships means that they are the only tool that estimates changes in global climate due to increased GHGs for a large number of climate variables in a physically-consistent manner (Takemura et al., 2006). Despite being a credible tool, there are limitations restricting the usefulness of GCM outputs because of the high cost of conducting simulation

experiments and their coarse spatial resolution (Takemura et al., 2005; Chen and Penner, 2005). Although GCMs accurately represent global climate, their simulations of the current regional climate are often inaccurate and they do not produce outputs on a geographic and temporal scale fine enough for many climate change impact assessments. In addition, a single GCM or even several GCMs may not represent the full range of potential climate changes in a region (Takemura et al., 2005). In the recent warm-start transient GCM experiments used in scenario construction, the following two types of experiments were undertaken: (i) the control simulation, where a constant atmospheric composition, representative of the present-day or pre-industrial times, is assumed the simulation of the observed climate over the historical period (e.g. 1861-1990), in which the atmospheric composition reflects the observed information (often referred to as the simulation of the 20th century climate and denoted at 20c3m) and (ii) the simulation of future climate, where the concentrations of the GHGs (and sulphate aerosols) associated with a particular emissions scenario are used. Both the control and future simulation results of GCM experiments (runs) are needed for use in the assessment of climate change impacts. The former is also very important is assessing the performance (consistency) of the GCMs in reproducing past and present climate and this often forms the first step in the climate change impact assessment (impact study) as it provides the means of selecting the reliable GCM runs from the several available runs to be used in impacts study.

2.3 Climate change impact assessment

2.3.1 General overview

Assessment of the future impacts of climate change on hydrology or water resources requires a methodology to estimate certain meteorological variables (e.g. rainfall, temperature, etc.) for the time period and the geographical area (e.g. river catchment) of interest. Two physical systems are inherently involved and these are the climate system and the hydrological system (Figure 2.5). In most cases, the estimates of the variables of the climate system are produced by a GCM with GHGs emissions forcing as inputs (Figure 2.5). Different climate models with different spatial resolutions can be used to obtain similar outputs but of different estimates. However, estimates (outputs) from GCM are not, generally, at an appropriate scale to be used directly for local scale or even regional hydrological impacts study. Instead, an interface is required to transform the outputs from the GCM to a scale, which is acceptably usable at the hydrological system scale (Figure 2.5). The hydrological system forcing variables, which are transformed outputs from GCM, can then be used in different hydrological models, typically of different resolutions as well, to obtain hydrological system outputs (Figure 2.5). Local scale impacts analysis also can be carried out on the transformed variables (hydrological system forcing variables) and/or on the hydrological system

outputs (Figure 2.5). In this way, the projected impacts of climate change on hydrology or water resources can be assessed.

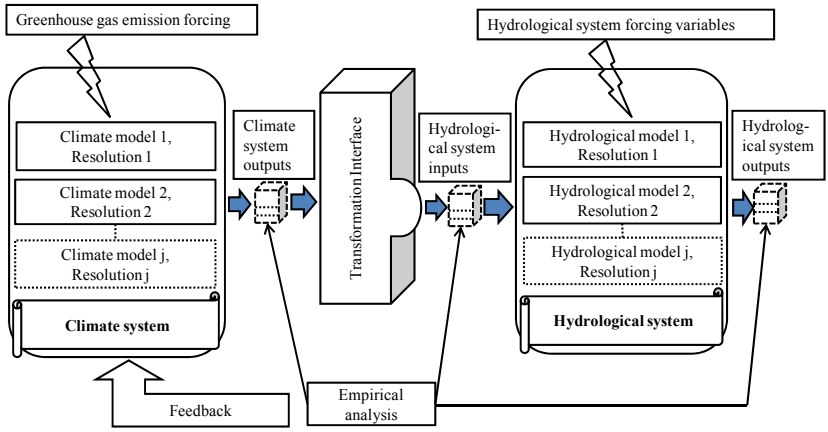

Figure 2.5 Aspects involved in the hydrological impacts assessment of climate change (adapted from Boukhris, 2008).

In specific terms, the main input variables (GCM outputs) required by most hydrological models are hydrometeorological variables. That is, rainfall and reference evapotranspiration (ET_o). ET_o are indirectly derived from variables such as temperature, wind speed, humidity and other solar variables (e.g. sunshine hours and solar radiation), which are also part of GCM outputs. There are some applications where the GCM scale can be sufficient for an impact assessment. Such is the situation for assessments that are global in scale. In all the other cases, a regional or local adaptation of the GCM data is inevitably required.

2.3.2 Reliability of climate models

Question often arises as to whether climate models mimic, in any way, the climate system or make sense. This is an important question, which needs to be addressed especially in a situation where impacts study is entirely dependent on the outputs from climate models. In weather prediction, forecasts are produced on a regular basis and evaluation of the outputs against what actually happens can be quickly carried out or verified. The climate predictions however are designed for many decades and for conditions without precise past analogues. One approach to gain confidence about a climate model for performing reliable simulations is to compare its results with known historical measurements or indirect evidence when records are missing. This is commonly known as the evaluation of the reliability or the performance of a climate model. In the current situations, where similar outputs from several climate models exist, model inter-comparison can be made by evaluating their skills against the same historical record.

Due to nonlinearities in the processes governing climate, the climate system response to perturbations depends, to some extent, on its basic state (Randall et al., 2007). Consequently, for models to predict future climatic conditions reliably, they must simulate the current climatic state with some degree of fidelity. Poor model skill in simulating present climate could indicate that certain physical processes have been misrepresented. The better a model simulates the complex spatial patterns and seasonal and diurnal cycles of present climate, the more reliable it is. Thus, when new models are constructed, considerable effort is devoted to evaluating their ability to simulate today's climate (e.g. Collins et al., 2006; Delworth et al., 2006).

Several climate model simulations are archived in public domains with the main objective of availing data for impact research. Due to limitations in assimilating data from all the climate models for impact assessment, climate model evaluation is used as a criterion for selecting the climate model runs, which better simulate the recent or present-day climate of the target study area. The 20c3m simulations that constitute a part of the Multi-Model Data (MMD), archived at the Programme for Climate Model Data and Inter-comparison (PCMDI) are currently being used for testing GCMs performance and their selection for impacts assessment.

A common practice in evaluating the performance of a climate model is to isolate the individual model components and test each independently from the others. The components of a climatic model usually tested in such an approach are the atmospheric, oceanic, sea ice and land-surface components. In hydrological impact assessment, precipitation and temperature are the key land-surface variables used in climate models performance and selection or testing.
Randall et al. (2007) showed that there is some evidence that the multi-model mean field is often in better agreement with observations than any of the fields simulated by each of the individual models. The multi-model averaging serves as a filter for biases of individual models and only retains errors that are generally pervasive. This information supports the continued reliance on a diversity of modelling approaches in projecting the future climate and provides some further interests in evaluating the multi-model mean results. This also suggests that the use of multi-models in hydrological impacts modelling could provide multi-model mean impact result, which is more reliable than the individual impacts results.

2.3.3 Downscaling of climate model runs

As stated in section 2.3.1, spatial and temporal scales used in the atmospheric studies considerably differ from those of hydrology where the basic unit, a river catchment, embraces quite a considerable range of finer scales. In order to match the discrepancy between GCMs and hydrological scales, techniques are required to transform (downscale) GCM outputs to the hydrological inputs

of appropriate scale. The choice of the technique for downscaling outputs from GCMs, needed for the assessment of hydrological climate change impacts, is dependent on the objective of the study. Downscaling can be dynamical, through the use of a Regional Climate Model (RCM) with GCM output as the boundary condition (Christensen et al., 2007) or statistical (empirical), through the use of large-scale predictors (Vidal and Wade, 2008; Fowler et al., 2007). In downscaling, the quality of the hydrometeorological variables from the GCM is improved increasing the resolution in time or in space or both. In some cases, only the climate change signals are required from the GCM outputs in order to derive the future time series based only on the observed variables (Carlsson et al., 2005; Willems and Vrac, 2011). Dynamic downscaling is one possibility through which estimate of changes in river discharges are carried out by using the outputs from RCMs directly to run the hydrological model. Due to inherent bias in the RCM outputs, it is often necessary to apply bias corrections to RCM outputs based on historical records.

The primary advantages of the dynamical downscaling approach are: (i) it is physically-based, (ii) it delivers meteorologically consistent variables and (iii) the downscaling results are provided for most climatic variables. The disadvantages are: (i) the approach requires expensive computational resources, (ii) the uncertainty and the non-uniqueness of the solution are often not taken into account, (iii) spatial and temporal resolutions of the RCMs are generally not sufficiently high given the hydrological requirements; in some cases further refinement (e.g. bias removal) or downscaling is required.

Statistical (or empirical) downscaling methods are based on local observations that are used to develop or estimate appropriate downscaling functions. In statistical downscaling, two different levels are considered which consist of the physically-based climate system level and the hydrological system level including the past record and the present situation. A link is searched between these two levels in order to establish statistical relationships between one or several large-scale climatic variables and local scale hydrometeorological variables. The main assumption made in statistical downscaling is that the statistical relationships between the large-scale and the local scale features remain the same even under a changing climate. The features under consideration are dubbed predictors and predictants. The predictors are the large-scale meteorological variables (e.g. temperature, air moisture) and are essentially the GCM outputs. In principle, any kind of variable can be used as predictor as long as it is reasonable to expect a correlation with the predictants. The predictants are the local scale variables to be downscaled (e.g. precipitation). Precipitation is the most important variable in hydrological modeling. The statistical downscaling methods can also be used to evaluate the statistical properties of the predictors and their correlations to the predictant.

The advantage of statistical downscaling over the dynamic downscaling is that the information can be generated at higher resolution and that uncertainties involved in the downscaling process can be accounted for. Furthermore, statistical downscaling can provide the possibility of focusing on hydrometeorological extremes specifically and the method is computationally cheaper. The major disadvantages of the statistical downscaling are that the application is restricted to the observed values; thus, only limited number of variables can be considered and it requires long and homogenous data series for the establishment and validation of the statistical relationships.

A statistical leaning downscaling approach, which has been commonly used in practice is dubbed "delta" or perturbation approach" (Middelkoop et al., 2001; Carlsson et al., 2005). The perturbation downscaling is the method used to transfer climate change signals from climate model outputs to the hydrological model system forcings. In perturbation downscaling, only differences in the most relevant climatic variables to hydrology, principally, rainfall and ET_o are extracted from the control simulations and the future simulations of the climate model and applied to respective observed variables for the reference period. The climate change signals are essentially relative changes derived as ratios or differences (perturbation factors or perturbations) from climate model control and future simulations.

The main advantages of the perturbation approach are: (i) it uses observed climate as a baseline as compared to the direct forcing approach where the RCM outputs are directly applied and (ii) it is stable and provides results that can be related to present conditions. The disadvantages of the perturbation approach are: (i) the use of the observed climate as a baseline implies the assumption of a no shift in the shape and type of the distribution of the hydrometeorological variables would substantially occur under future climate and (ii) in some cases, extremes are modified by the same factor as all other events.

Standard perturbation downscaling typically does not include changes in variability between climate model control and future simulations. In order to use more information from climate models, adjusted perturbation approach is more plausible. The main assumption behind the adjusted perturbation downscaling is that the bias in the control run is the same as the bias in the future run and they canceled out in the process of extracting climate change signals. The advantage of the adjusted perturbation approach is that it provides more direct representation of the climate model results and, thus, climate variability are more consistent with the climate model simulations. The disadvantages are that the approach is quite sensitive to the quality of the climate model simulations and the observed data and that it assumes a static bias correction that may not adequately represent future climate changes such

as changes in circulation. In addition, the approach only works well in non-arid and semi-arid regions.

2.4 Extreme value analysis

Assessment of hydrometeorological impacts of climate change is chiefly carried out to provide water manager with information associated with risks in water resources engineering planning and management practices. These risks are inherently those associated with extremes of meteorological variables (e.g. rainfall – too little or too much) resulting into hydrological extremes such as floods and droughts. This section discusses some elements of extreme value theory and provides a synoptic account of why extreme theory is important in the assessment of hydrological climate change impacts.

If a data set is assumed to be drawn from an unknown probability distribution, consisting of independently, identically distributed (iid) random variables then in the classical approach, it is possible to calculate several statistical functions of the data set and draw conclusions about the mean, dispersion, etc., values. In climate change impacts assessment a quantitative measure and description of the data set values lying in the extremes of the data distribution is of great interest. It is always classical to calculate absolute and mean extreme values such as minimum and maximum and provide an empirical estimation of the frequency of occurrence of events (e.g. storm events) resulting in such extreme values. Extreme value theory is one way to address this issue (e.g. Beirlant et al., 2004).

Consider a set of sorted iid observations $x_1 \geq x_2 \geq \ldots$ in the sample of the random variable X with a cumulative probability distribution $F(x)$. As was first shown by Fisher and Tippett (1928), referenced in Cunnane (1985), the probability distribution of the maximum observation x_1, after relocating and scaling can converge to a limited number of possible distributions as the sample size tends to infinity. These distributions are called Generalized Extreme Value (GEV) distributions with their cumulative probability given by (von Mises, 1954; Jenkinson, 1955):

$$F(x) = \begin{cases} \exp\left[-\left\{1-k\left(\dfrac{(x-\xi)}{\alpha}\right)\right\}^{\frac{1}{k}}\right], & k \neq 0 \\ \exp\left[-\exp\left\{-\left(\dfrac{(x-\xi)}{\alpha}\right)\right\}\right], & k = 0 \end{cases} \tag{3.1}$$

where x is bounded by $(\xi + \alpha/k)$ from above if $k > 0$ and from below if $k < 0$. ξ, α (> 0) and k are the location, scale and shape parameters, respectively. The shape parameter determines which type of extreme value distribution is represented. Type I GEV distribution (EV1), also known as the Gumbel

distribution, corresponds to $k = 0$. Type II GEV distribution (EV2), also known as the Fréchet distribution, corresponds to $k < 0$. Type III GEV distribution (EV3) corresponds to $k > 0$. Note that if X is said to be distributed EV3, $-X$ has a Weibull distribution. The Weibull distribution is often used in hydrology to analyze low river streamflows.

Pickands (1975) has further shown that if only values of an iid random variable, X, above a sufficiently high threshold, xt, are taken into consideration, the conditional distribution converges to the Generalized Pareto Distribution (GPD), $G(x)$, when xt tends to ∞. The cumulative distribution function of the GPD is given by:

$$G(x) = \begin{cases} 1-\left(1-\dfrac{k\,(x-xt)}{\alpha}\right)^{-1/k}, & k \neq 0 \\ 1-\exp\left(+\dfrac{(x-xt)}{\alpha}\right), & k = 0 \end{cases} \tag{3.2}$$

The GEV and GPD distributions are frequently used when analyzing data in the context of extreme value theory. In the case of hydrology, such data are often time series of hydrometeorological variables of hydrological importance such as precipitation or time series of hydrological variables (e.g. streamflows and water levels), depending on the needs of the analysis. It is worth noting that some of the earliest applications of the statistical theory of extreme values were to hydrology and to closely related problems in climatology. Many contributions to extreme value theory come from the collaboration of hydrologists with statisticians.

For practical applications, extreme value distributions require calibration to empirical extremes, which can be extracted from time series using independence criteria. Most common approaches are the annual maxima (AM) and the peak-over-threshold (POT) or partial duration series (PDS) methods. An overview of these methods can be found in Smith (1987), Hosking and Wallis (1987) and Madsen et al. (1997), among others. The POT/PDS method has relative advantages over the method of AM. When isolating annual maxima from a time series, a substantial amount of potentially useful information is discarded. The POT method utilizes only peaks above a specified threshold. This increases considerably the number of data for statistical processing but the threshold must be high enough relative to typical data set values (Naess et al., 2000) or to apply sufficiently high independence levels (Willems et al., 2007).

If the extreme value analysis is carried out for a range of aggregation levels or time scales, amplitude or Intensity-Duration-Frequency (IDF) relationships (curves), for rainfall, and Streamflow-Duration-Frequency (QDF) relationships, for discharge can be constructed. The respective relationships, which involve return periods result into IDF and QDF curves. In professional

practices, these curves (design curves) are needed for many water related engineering applications. It is noteworthy that in the constructions of the design curves it is assumed that the statistical properties of the historical data are representative of what could happen in the future. However, under a changing climate, the assumption of the stationarity of the statistical properties of extremes events may be null and void. In impacts assessment, the influence of climate change on extremes can be analysed by comparing IDF/QDF constructed from projected rainfall/streamflows with the observed rainfall/streamflows or their respective control. Thus, the vindication of the significance of extreme value theory in the climate change impacts assessment on hydrological extremes.

2.5 Uncertainties in climate change impact assessment

Albeit representing uncertainties in climate change impacts studies is a difficult challenge, the task of providing information about uncertainty in the climate change impacts assessment, whether qualitatively or quantitatively, is very important for the assimilation of the impact results by the decision making bodies.

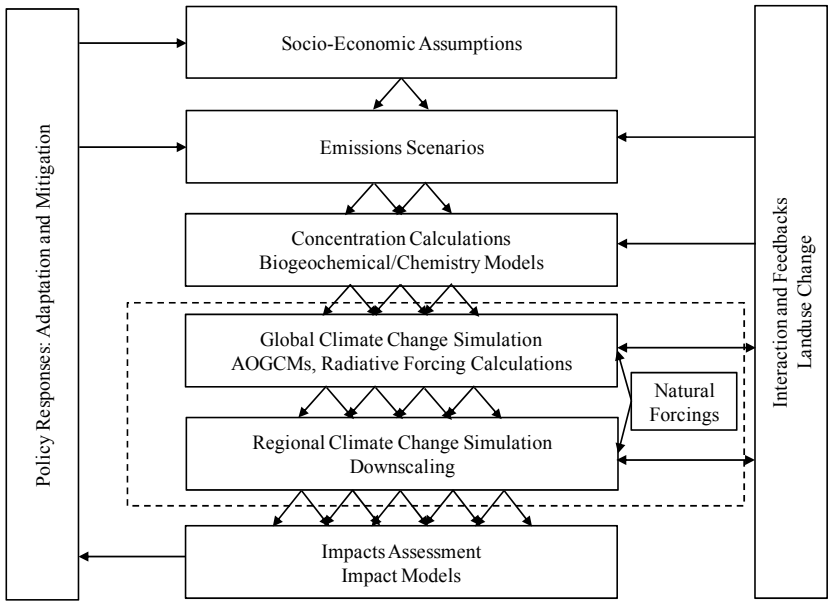

Figure 2.6 Cascade of uncertainties in the assessment of climate change impacts (Giorgi, 2005).

The modelling of the hydrologic impacts of climate change is generally a simple process: (a) define, calibrate and validate a model for the hydrological system using current climate data, (b) define climate change scenarios, (c) run the hydrological model under current and future conditions and (d) compare variables of interest. This “blue-print” process, however, might not lead to

useful results without explicit knowledge of what are the uncertainties involved. First, the definition of "uncertainty" is paramount. From a decision-making point-of-view, uncertainty can be defined, as "the gap between the available knowledge and the knowledge policymakers would need in order to make the best policy choice" (Walker et al., 2010). Refsgaard et al. (2007) and Klauer and Brown (2004) however define uncertainty as follows: "a person is uncertain if he or she lacks confidence about the specific outcomes of an event. The reasons for the lack of confidence might include a judgment of the information as incomplete, blurred, inaccurate, unreliable, inconclusive or potentially false". This is an inherently subjective perspective on uncertainty. Both Walker et al. (2010) and Refsgaard et al. (2007) relate their definitions of uncertainty to the satisfaction and awareness of the decision-maker. Therefore, the definition includes recognized ignorance ('known unknowns'), but generally excludes unrecognized ignorance ('unknown unknowns'). Irrespective of the different definitions of uncertainty, identification (as pointer) and description of the sources of uncertainty in impact assessment should be part of the impacts study process.

There are several sources of uncertainties in the modelling process and are present in the context of the impacts assessment (e.g. in the scenarios and climate data and projections used), and in each step of the assessment itself. They add up along the way, resulting in an 'uncertainty explosion' or 'cascade of uncertainty' (Figure 2.6). In the uncertainty cascade, two major "blocks" of uncertainty sources can be identified: (i) uncertainty in climate model - including scenarios and (ii) uncertainty in hydrological modelling.

2.5.1 Climate modelling uncertainties

Uncertainties of climate scenarios and GCM outputs are large and the ability of the GCMs to reproduce the present situation on a regional or catchment scale is low. The major source of uncertainties within the climate model is the structure of the climate model, which includes the initial and the boundary conditions and the parameters of the model. Generally, because the true climate system is highly complex, it is fundamentally impractical to describe all its processes in a climate model, irrespective of the complexity of the model. Choices have to be made on what processes to include, how to parameterize them and what pieces to neglect. On the one hand, what is relevant to include in a model should depend on the question of interest and a wide spectrum of models does exist, each suitable for specific applications. The process of selecting pieces to include in a model is inevitably and partly subjective based on expert knowledge and experience. Any uncertainty that is introduced by choices in the model design such as going beyond changing values of particular parameters is also encapsulated in structural uncertainty and would be hard to capture by changing parameters within a single model, irrespective of the range of parameters. Similar argument can be advanced to the type of grid, the resolution, truncation or the type of numerical methods

used to solve the equations. These numerical aspects are also part of the model structure, but sometimes considered separately from the physical aspects. Quantification of the uncertainty at climate model level is a complex and an *unlarable* (difficult) subject matter itself.

2.5.2 Hydrological modelling uncertainties

Hydrological model generally represents the physical processes of runoff production through mathematical, conceptual formulations. Although large simplifications have to be made, the resulting simulated time series is often satisfactory in reproducing observed streamflows. Albeit hydrological models often produce satisfactory results of observed streamflows, there are two main sources of uncertainties in the hydrological modelling: (i) the data and (ii) the model itself. Measurement of input data is always subject to uncertainties. Secondly, sampling from a short record rarely accounts for natural variability. Reducing errors in data can only be done by thorough checking of the climatic and hydrological input series and resampling techniques may allow evaluation of uncertainty resulting from short record. Like climate model, hydrological model also suffers from model structure uncertainty. Hydrological model structure is formed by a set of algorithms designed to describe the underlying hydrological processes. Modelling errors are assumed to be of the same order of magnitude under current and changed conditions when using the same model and can, thus, be ignored. Secondly, hydrological parameters form a huge source of uncertainties; it is assumed that the same set of parameters can be used for both current and changed hydrological simulations. Furthermore, scaling up hydrological model in space and time is an approximation of reality and not the exact reality. However, a hydrological unit (e.g. a river catchment) is less complex compared to a climate unit (regional or global).

2.5.3 Ensemble opportunity

Given the verity that uncertainty is a broad topic, which requires detailed analysis, the use of multi-models is an “ensemble opportunity” for providing quantitative information about uncertainty in the climate change impacts assessment. Several studies (e.g. Hagemann et al., 2004) have shown that - uncertainties among models are much higher than other sources of uncertainties (e.g. scenarios) and that the use of multi-models provides a simple but steadfast method of quantifying possible range of uncertainty in climate change projections and associated impacts (Fowler et al., 2007; Tebaldi and Knutti, 2007). Improvements in the performance of a multi-model mean over single models were also demonstrated when detecting and attributing greenhouse gas warming and sulphate cooling patterns in the observed climate record (Gillett et al., 2002).

There are, indeed, different ways to combine models. In most cases, the Bayesian methods (e.g. Robertson et al., 2004) or weighted averages, where

weights are determined by using the historical relationship between forecasts and observations (e.g. Krishnamurti et al., 2000), perform better than simple averages where each model is weighted equally. Intuitively, it makes perfect sense to put better performance scales to realistic models. The intricacy however is in the quantification of model skills and deriving model weights appropriately. Controversial results exist regarding the best way to combine model results even in the case where skill or performance can be calculated by comparing model predictions to observations. An equally weighted average of several coupled climate models is usually demonstrated to agree better with observations than any single model (Lambert and Boer, 2001). Multi-model projections for long-term climate change were used in AR4 IPCC, where unweighted multi-model means rather than individual model results were often presented as best conjecture projections.

CHAPTER 3

CASE STUDY AND DATA

3.1 Introduction

The case study is the River Nile basin with a focus on its upper catchbasin, Lake Victoria basin. The Nile represents a crucial resource for the economy of eastern and northeastern Africa. Agriculture, energy production and livelihood in the basin generally depend strongly on the River Nile. Any relevant information regarding possible impacts of climate change on the water resources of the River Nile is not only necessary but of critical importance for the water managers in the basin. Even though the River Nile basin can be considered as one hydrological unit, the geopolitical and transboundary nature brings in a complex dimension and an unlarable challenges. In a huge and complex river basin such as the River Nile, water resources are effectively managed at catchment or local scale and adaptation measures can quickly be taken at that scale. This means that climate change impacts assessment, in the River Nile basin, is much worthily carried out at a meso-catchment scale than at a macro-catchment scale in order to provide water managers with the baseline knowledge and tool to quickly assess future risks associated with water resources of the local catchment and thereby draw an immediate strategy for adaptation.

In this study, a two-in-one case was considered. That is, a case for the entire Lake Victoria basin and a case for two river catchments, Katonga and Ruizi, in the Lake Victoria basin. In the former, the impacts of climate change on hydrometeorological variables (e.g. rainfall and temperature) were assessed based on selected stations spatially located in different parts of the basin. Meanwhile in the latter, the impacts of climate change on the hydrological responses of River Katonga and River Ruizi were addressed.

On the data, the impact study made use of qualified observed and GCM data relevant for the case study. Observed hydrometeorological data used include streamflows, rainfall, maximum and minimum temperature and evaporation. The GCM data considered include rainfall, maximum and minimum temperature. This chapter therefore covers the discussions on the study area, the data, data processing and data qualification.

3.2 The River Nile basin

3.2.1 Hydroclimatology of the River Nile basin

The River Nile basin (Figure 3.1(a)) is situated between 8° S to 33° N and 20 °E to 42 °E covering an area of approximately 3,762,000 km² (Figure 3.1(b)). The climate is mainly tropical in the upstream parts of the basin arid and semi-arid in the downstream parts of the basin. The upper parts of the basin are mainly covered by mountainous plateau with a varying elevation from about 1100 to 2150 m a.m.s.l. The mean annual rainfall varies from more than 1200 mm, in the upstream parts, to less than 10 mm, in the downstream parts. The main rivers flowing across the basin are: Victoria Nile, Albert Nile, White Nile, Blue Nile, Sobat, Atbara, Jur and Main Nile, each with several tributaries forming up the Nile basin (Figure 3.1(b)). Recent attempts to assess the impacts of climate change on hydrology of the River Nile basin have targeted mainly the water balance (e.g. Beyene et al., 2010; Amy, 2006; Mohamed et al., 2005) which were carried out mainly on the downstream catchments outflows such as from the Blue and the White Nile.

3.2.2 The Lake Victoria basin

The Lake Victoria is the largest fresh water body in Africa and the second largest in the world. Lake Victoria water-body is geopolitical in nature, characterized by Kenya, Uganda and Tanzania with Rwanda and Burundi as key sources of the famous River Kagera, the major contributor to the lake. Lake Victoria is, on average, 68,800 km^2 and politically shared as follows: Kenya (6%), Uganda (43%) and Tanzania (51%). The Lake Victoria basin area in Uganda is 59,858 km^2 out of the total basin area of about 196,000 km^2 (Figure 3.1(c)). Lake Victoria stretches, approximately, 415 km from north to south between latitudes 0°30’ N and 3°12’ S and approximately 355 km from west to east between longitudes 31°37’ and 34°53’ E. It is situated at an altitude of about 1,130 m above sea level and has an estimated volume of about 2,750 km^2, and an average and maximum depth of 40 m and 80 m, respectively.

3.2.2.1 Climate of the Lake Victoria basin

The climate of the Lake Victoria basin is generally tropical humid, with temperatures values ranging from 15° C in the highlands to 28° C in the semi-arid areas. The mean annual rainfall varies from a minimum of about 886 mm to 2600 mm. The mean evaporative rate over the Lake is in the range 1100-2040 mm, which decreases with increasing altitude, but in some months exceeds rainfall.

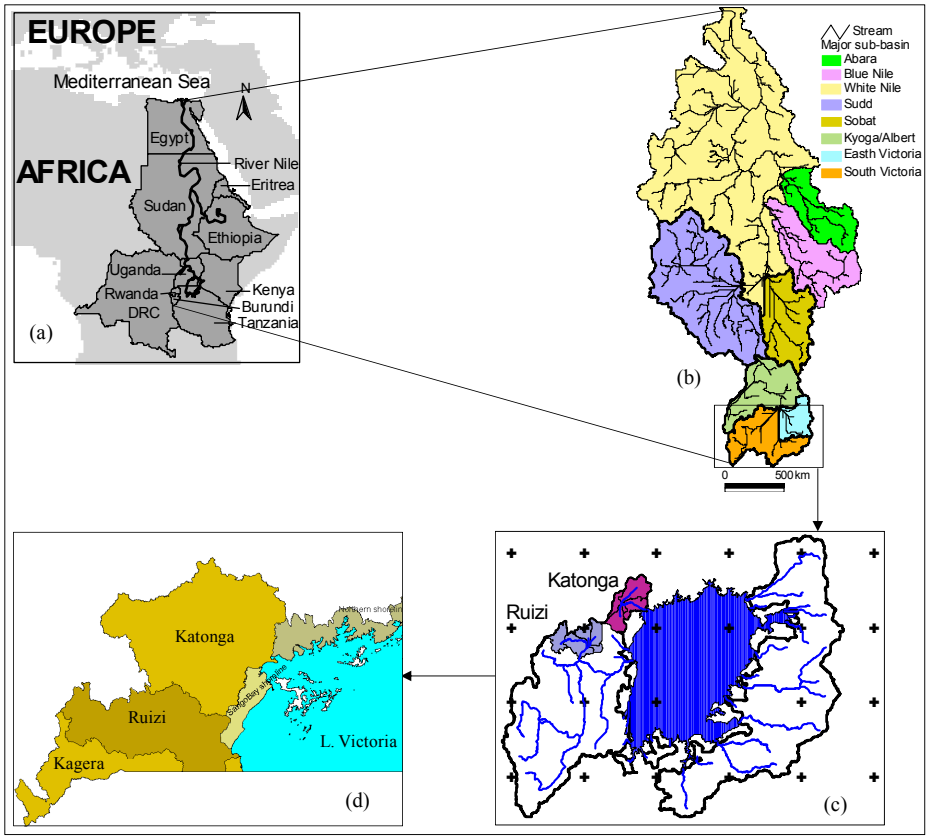

Figure 3.1 Location of the River Nile in Africa, the countries in which the Nile basin takes part (a), the major streams and major catchments of the River Nile (b), the Lake Victoria basin (c), the locations of the River Ruizi and Katonga catchments in Lake Victoria basin (c) and (d). The plus (+) signs, superimposed over the Lake Victoria basin (c) indicate the mean grid size of the GCMs used.

3.2.2.2 Catchments draining to the Lake Victoria basin

The major rivers draining into and forming up part of the Lake Victoria basin, based on geopolitical sources, are Mara, Kagera, Grumeti, Issanga, Mirongo, Mbalageti and Simiyu (Tnazania). The major rivers from the Kenya side are Nzoia, Yala, Nyando, Kibos, Sondu, Mawa, Migori, Kuja, Riaria and Miriu. From Uganda side the rivers are Katonga, Bukora and Ruizi (Figure 3.1(c)). River Ruizi is partly a tributary of River Kagera. River Kagera, being the single largest river flowing into the Lake Victoria and shared by Uganda, Rwanda, Burundi and Tanzania contributes about 33% inflows into the Lake Victoria. Rivers entering the Lake Victoria from Kenya side, which contains smallest portion of the Lake, contribute over 37% of its surface water inflows. About 86% of the total water input, however, is a contribution from precipitation, with evaporative losses accounting for approximately 80% of water leaving the lake. The Victoria Nile is the only surface outlet draining the Lake Victoria, with an average outflow of about 23.4 km^3 $year^{-1}$.

3.2.2.3 The Northwestern catchments of the Lake Victoria basin

The chief Ugandan river catchments that drain into the Lake Victoria are the River Ruizi and Katonga. The Uganda Government first introduced integrated Water Resources Management (IWRM) practices in the River Ruizi catchment. The foremost known anthropogenic environmental impacts on the two catchments are severe erosion, deforestation, conversion of wetlands into arable lands, low soil fertility, overgrazing and water pollution. The nexus to the environmental degradation and the waning water resources regimes of the river catchments is poverty and poor watershed management, respectively (Niringiye et al., 2010; MWE, 2011). One other environmental threat with unclear possible impacts on the catchments is the climate change postulate. The two rivers thus provide an opportunity for contribution (this study) towards the contemporary issue (assessment of climate change impacts) of the 21st century given the fact that such contribution is to date limited.

3.2.2.4 The River Ruizi catchment

The River Ruizi catchment, shown in Figure 3.1(d), located between 29°55' E 0°55' S and 30°55' 0°16' S, covers a total area of about 8,436 km^2; the altitude varies from 1,262 m a.s.l. at the outlet to about 2,165 m a.s.l. at the very northern part of the catchment. The average elevation is 1,517 m a.s.l. The central part of the catchment is very flat. The altitude, at a gauging station located at the intake for the new water-works at Mbarara, to the old gauging station at Ndeizha (where the river starts entering the mountainous area in the south), only increases by about 50 m, from 1390 to 1440 m a.s.l. The distance from the west to east is about 80 km whereas the distance from the north to south is approximately 70 km. This part of the catchment is dominated by wetlands, which have a major effect on the streamflow regimes in the catchment. The long-term instrumental mean streamflow, recorded at the Mbarara water works station and the downstream of the catchment as for the period 1970-2001 is about 3.8 m^3 s^{-1}. The mean annual rainfall, based on a data measured in the period 1950-2006, is about 800 mm.

3.2.2.5 The River Katonga catchment

The River Katonga catchment, shown in Figure 3.1(d), located between 31°30' E 0°22' S and 32°18' 0°42' N, covers a total area of about 13,930 km^2 and its flow is bifurcated continuously between the Lake Victoria and Lake George in the Western Rift. This is due to the verity that since the upwarping of the western side of the Lake Victoria basin, rivers crossing it have, in part, reversed their directions of surge. Thus, the swampy watershed now occurs on the River Katonga from which the river flows sluggishly in opposite directions. The greater part of River Katonga flows eastwards to Lake Victoria despite the fact that the angles of its tributaries suggest that it flows westwards throughout its course. The long term mean discharge, based on the data recorded in the period 1965-2006, is about 4.8 m^3 s^{-1}. The altitude in the catchment varies from 1110 m a.s.l to about 1500 m a.s.l. The topography of

the River Katonga catchment is generally flat, allowing satellite wetlands to predominate. The inflows from the River Katonga contribute about 0.8% of the total inflow into the Lake Victoria. The instrumental mean annual rainfall depths in the catchment based on a data recorded in the period 1950-2006 is about 1186 mm. This means that River Katonga catchment receives much rainfall than River Ruizi catchment. River Katonga originates from Lake Wamala (not shown).

3.3 The data and quality control

Among the research needs is the estimation, in quantitative terms, of the climate change impacts on future hydrometeorological extremes (e.g. extremes of rainfall and streamflows) and their management, which requires improvement. Progress in understanding this is conditioned on adequate availability of observed data addressing the challenges posed by projected climate change to freshwater resources and reversing the tendency of shrinking observation networks. Observed hydrometeorological data will globally continue to be limited both in quantity and quality. At global scale, a recent example of data-related difficulties (*unlarabilities*) is the continental runoff study by Gedney et al. (2006) and related discussion (Peel and McMahon, 2006) challenging the representativeness of the data set and the practice of runoff reconstruction. The lack of sufficient data, especially in the developing countries, is very notorious for stagnating the progress of crucial research. In the Lake Victoria basin the density of meteorological monitoring stations is very high but it is does not necessarily translate to data availability and quality. Some of the selected data stations are shown in Figure 3.2 Adequate and qualitative data are crucial for understanding observed changes and for the improvement of models, which can be used for future projections. The limitation of data makes it impractical to collect sufficient data on all hydrological variables required for catchment-scale studies. Even with the unlarability of data limitation, it is still necessary to use the available data to understand catchment response to certain hydrological events such as the catchment response to climate change.

Data used in this study included mainly observed hydrometeorological and climate model data. Data quality checks were, mainly carried out using graphical and statistical methods to ensure that only data with acceptable quality were employed. The correlation, double mass curve, hydrographs and visual inspections were the methods used to check the quality of the hydrometeorogical data used in this study. Details of data quality assessment are comprehensively given in WMO gudide to hydrological practices (1994). Two sets of observed hydrometeorological data were processed and used. The first set was from selected representative stations in the Lake Victoria basin (Figure 3.2) used to investigate observed changes in the basin's climate and for the possible impacts of climate change on rainfall and temperature. The second set of hydrometeorological data was those used for hydrological

modeling of the impacts of climate change on the streamflows of River Katonga and Ruizi (Figure 3.2).

3.3.1 Observed hydrometeorological data

Several observed hydrometeorological data collected[3] were mainly daily rainfall, maximum and minimum temperature, streamflows and pan evaporation. Some stations had data with longer records while others had data with shorter records. In addition, some stations had data with missing values while others had data with values assumed outliers. Only stations with data record of length longer than 30 years, for rainfall, and longer than 20 years, for streamflows and temperature were selected for the study. However, data from stations not fully utilized in the study were partially used to improved quality of data fully utilized in the study. First, the data were screened for homogeneity using double- and cumulative-mass curves and possible outliers that could be attributed to errors in transcribing the data. Apart from streamflows data, selected data with missing values were in-filled using a technique described in section 1.1.1.

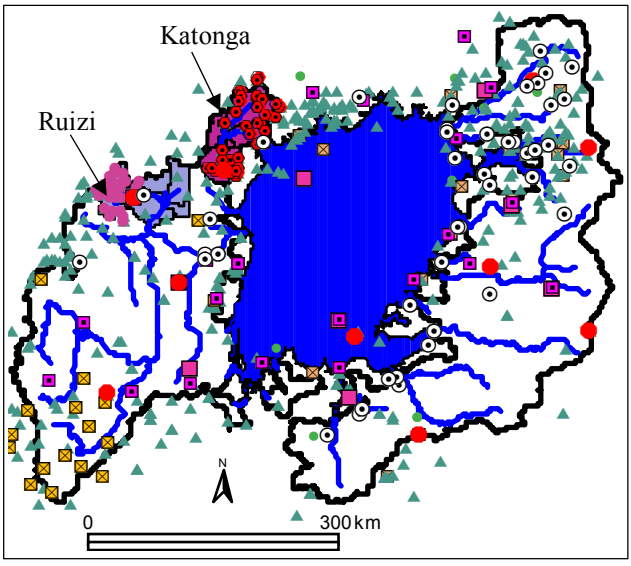

Figure 3.2 Hydrometeorological stations for streamflow (⊙), rainfall (▲, ●, ●, ●), temperature (■,■, ●) and evaporation (■) in the Lake Victoria basin including the River Ruizi and Katonga catchments. The data stations shown are those with at least 30 years of records. The stations marked with ● and ■ are the selected representative stations for rainfall and temperature, respectively, used for trend analysis.

[3] Sources of data: Ministry of Water and Environment (MWE), Uganda and the FRIEND/Nile project of UNESCO.

3.3.2 Hydrometeorological data quality improvements

According to World Meteorological Organization (WMO) data with missing records of up to 10% could be improved by interpolation technique. Thus, the method of Inversed Distance Weighting (IDW) (eq. 3.1), originally used by Shepard (1968), was applied to estimate missing data values for the data with some missing records. First, correlations between the data, to be used for estimating the missing records and the data whose records were to be estimated were measured at a monthly scale for the periods where both have data. Missing records of the target data, at daily time scale, were then estimated based on data having reasonably good correlation with it based on a search process using a simple Visual basic for Application (VBA) algorithm. There were no metrics used to measure reasonably good correlation but it was based on "sound" judgement and the data available and employed in the IDW metod. The IDW method (eq. 3.1) is based on the hypothesis that, for example, rainfall estimates at ungauged sites can be obtained as the linear or non-linear combinations of the values measured at a number of instrumented locations using the appropriate weights. The method is applied widely in spatial studies (e.g. Ware et al., 1991; Bartier and Keller, 1996; Miller 2005; Lu and Wong, 2008) and its function form is given by:

$$P = \frac{\sum_{i=1}^{N} (P_i / d_i)}{\sum_{i=1}^{N} (1/d_i)} \tag{3.1}$$

where P is the unknown climatic variable value (e.g. Rainfall)
P_i is the known variable value at station i and N is the total number of stations with known variable value
d_i is the weight assigned to variable value at station i (e.g. distance between station with unknown and known rainfall)

In this study, IDW was applied mainly to improve the quality of rainfall, temperature and evaporation data. The rainfall station data whose quality were improved include ten, 10, twenty, 20, and fourteen, 14 stations for the Lake Victoria basin, River Katonnga and Ruizi catchments, respectively (details in appendix A). For temperature and evaporation, a total of nine, 9, stations for the Lake Victoria basin case and four, 4, stations, each for Katonga and Ruizi catchments, were also quality assured. Furthermore, seven, 7, streamflow gauging stations (including one station, each for the River Katonga and Ruizi) were considered for quality improvements. Details of the loci and characteristics of the stations are also given in Appendix A. The discussions on the details of the properties of the data and other relevant information are given in the following subsections. Figure 3.2 shows spatial information of some of the data stations used in this study.

3.3.3 Reference evapotranspiration estimation

Estimation of the ET_o was carried out using three methods, the pan coefficient, K_p, (Allen et al., 2006), Hargreaves (Hargreaves et al., 1985) and the modified (FAO) Penman-Monteith (Allen et al., 2006; Adeboye, 2009). The pan coefficient method requires pan evaporation (E_p). The K_p method is strongly based on the type of pan used and the climatic conditions and suitable mainly for local conditions. However, pan evapotranspiration methods clearly reflect the shortcomings of predicting crop evapotranspiration from open water evaporation (Allen et al., 2006). The methods are susceptible to the microclimatic conditions under which the pans are operating and the rigour of station maintenance (Allen et al., 2006). The details of K_p values for different climatic conditions are given in FAO Irrigation and Drainage Paper No. 56. The ET_o estimate is related with K_p and E_p as

$$ET_o = K_{pan}\, E_{pan} \tag{3.2}$$

where ET_o reference evapotranspiration [mm day^{-1}],
K_{pan} is the pan coefficient [-],
E_{pan} is the pan evaporation [mm day^{-1}].

Hargreaves method was originally published by Hargreaves (1985) and adopted in Hargreaves and Samani (1985) and Allen et al. (2006). It requires mainly maximum and minimum temperature (T_{max} and T_{min}). This method behaves best for weekly or longer predictions although some accurate ET_o daily estimations have been reported in literature (Hargreaves and Allen, 2003). The massive comparison using daily weather data between Hargreaves equation and the American Society of Civil Engineers Penman–Monteith (ASCE PM) method, with the latter used as reference, was made by Itenfisu et al. (2003). The analysis used data from 49 sites in 16 states in USA and showed that the ratio between ASCE Penman–Monteith and Hargreaves ETo ranged from 1.43 to 0.79, with a mean of 1.06 and a standard deviation of 0.13. The Hargreaves equation tended to predict greater ET_o than ASCE PM when mean daily ET_o was low and vice versa. Besides, the Hargreaves equation is sensitive to sensible heat advection, so that, when advection is severe, it underestimates ET_o up to 25% for daily periods (Berengena and Gavilán, 2005). Despite its limitations, Hargreaves' method has shown reasonable ET_o results with a global validity (Allen et al., 2006) and is universally applicable, as it does not require the observed solar input. The model for the estimation of ET_o, using Hargreaves method is given by

$$ET_o = 0.0023.0.408.\left(T_{mean} + 17.8\right)\left(T_{max} - T_{min}\right)^{0.5} Ra \tag{3.3a}$$

where

$T_{mean} = \left(T_{max} + T_{min}\right)/2$, the average air temperature (°K)

R_a is the extraterrestrial radiation ($MJm^{-2}\,day^{-1}$), a function of location given by

$$R_a = 15.392 d_r \left(\omega_s \sin\phi \sin\delta + \cos\phi \cos\delta \sin\omega_s\right) \quad (3.3b)$$

where ϕ is the latitude of the location and d_r is the relative distance between the earth and the sun given by:

$$d_r = 1 + 0.033 \cos\left(\frac{2\pi J}{365}\right) \quad (3.3c)$$

where J is the Julian day to estimate incoming solar energy (Duffie and Beckman, 1980).

δ is the solar declination (radians) defined by:

$$\delta_r = 0.4093 \sin\left(\frac{2\pi J}{365} - 1.405\right) \quad (3.3d)$$

and ω_s is the sunset hour angle (radians) given by:

$$\omega_s = \cos^{-1}\left(-\tan\phi \tan\delta\right) \quad (3.3e)$$

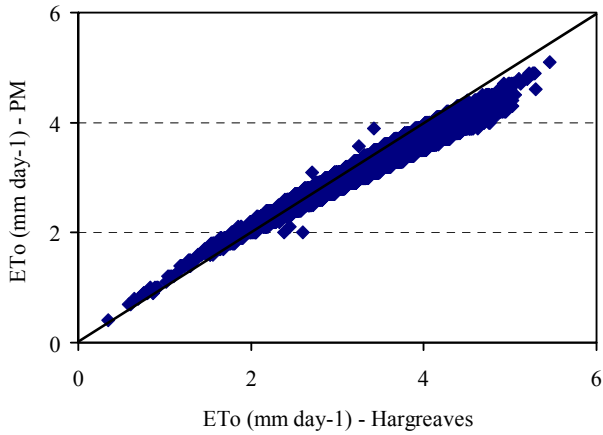

Figure 3.3 Comparison of the daily ET_o values estimated using FAO-PM and Hargreaves methods for an example data with records of 30 years.

The FAO Penmann-Monteith, FAO PM, method estimates ET_o based on several variables. The FAO PM method is recommended as the sole standard method (Allen et al., 2006). This also means that the accuracy of the ET_o results estimated using other methods can be evaluated based on the ET_o results estimated using FAO PM method. Allen et al. (2006) further notes that FAO PM is a method with strong likelihood of correctly predicting ET_o in a wide range of locations and climates and has provision for application in data-short situations. That is, where data are limited, the method allows estimate of ET_o to be based mainly on T_{max} and T_{min}, and few other locations

characteristics such as elevation and coordinates. FAO PM is a very popular method for estimating ET_o and further information on it can readily be found in literatures. The FAO PM equation is provided in Appendix B.6.

Due to data limitation, the Hargreaves method was mainly used for the the estimation of ET_o. However, to gain confidence on the results, comparison was made between the daily ET_o values estimated using FAO-PM (appendix A.18) and Hargreaves (e.q. 3.3a) methods for a station with relatively sufficient data. The results showed that the correlation between the daily ET_o time series values estimated using FAO-PM and Hargreaves methods is reasonably strong (Figure 3.3) with the correlation coefficient value of 0.96. This demonstrated that the difference between the results of the daily ET_o values estimated using the FAO-PM and Hargreaves methods for the current study area could be neglected.

3.3.4 Catchment rainfall and evapotranspiration estimations

The catchment variables such as areal rainfall and areal evapotranspiration were estimated based on Thiessen polygons method (Linsley et al., 1949; WMO, 1986). This is justifiable given the fact that the current study area is generally consist of fairly uniform topography and not a mountainous area. Based on the assumption that, for example, rain gauge measurements can reliably account for the "true point rainfall" after accounting for a number of possible errors (e.g. Sevruk, 1982; WMO, 1994 and Humphrey et al., 1997), the areal rainfall and the areal evapotranspiration estimates, over the River Katonga and Ruizi catchments, were computed based on point measurements. The catchment areal rainfall and the catchment evapotranspiration estimates were needed for hydrological modelling of streamflow. In addition, the catchment rainfall was also needed for the GCM performance assessment discussed in chapter 5. For the impacts analysis discussed in chapter 7, case point rainfall data were converted to areal values using ARF.

3.3.5 Properties of the hydrometeorological variables

The properties of rainfall for the selected stations in the Lake Victoria basin are shown in Figure 3.4 and also provided in Table A.1 of Appendix A. Figure 3.4 provides the long-term monthly mean of the rainfall data for the indicated locations. Table A.1 contains the long-term annual properties such as the mean, coefficient of variation and coefficient of skewness.

It can be seen from Figure 3.4 that two distinct seasons can be identified; the wet and dry seasons, with April and July as the wettest and driest months, respectively, for most locations. The characteristics of the rainfall for the region represented by stations (4), (5) and (6) may suggest that the climate of that region is one case of the types of climate of the Lake Victoria basin (Figure 3.4) because of the tendency of the rainfall to be of a uni-modal

nature. The only dry season occurs during the months of December-March. Similarly, the region represented by stations (2), (3), (7) and (10) may belong to another type of sub-climate of the Lake Victoria basin, consisting of two separate dry and wet seasons. The rainfall type in this region is clearly bi-modal ((Figure 3.4)) and occurs during the months of March-May and September-November. Furthermore, the southern region, represented by stations (1), (8) and (9), has longer dry season (June-September) compared to the same northwestern and western regions of the basin (Figure 3.4). This may also suggest that the southern parts of Lake Victoria basin belong to another different type of sub-climate.

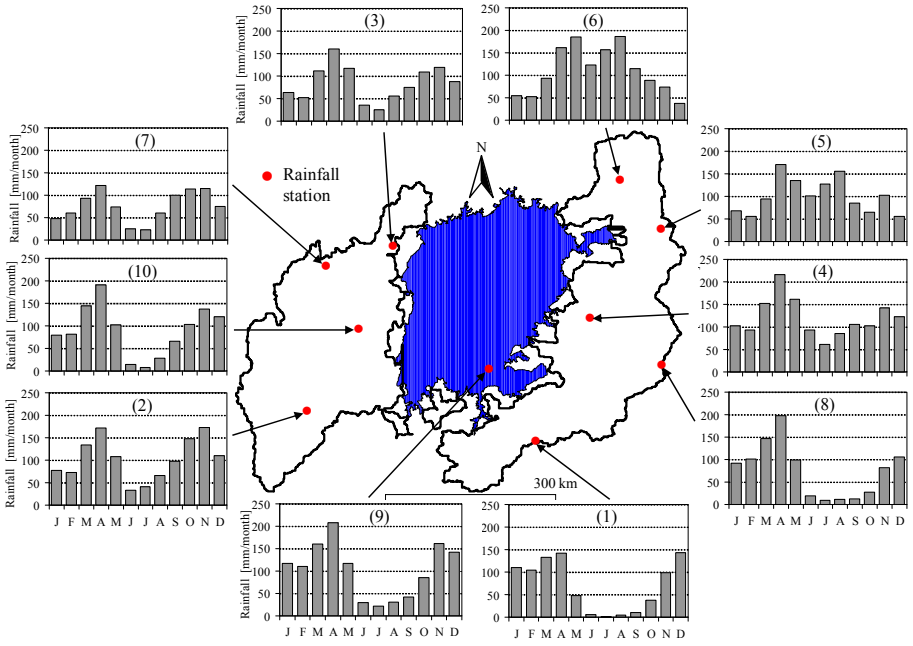

Figure 3.4 Long-term mean of the monthly rainfall volume for selected stations in the Lake Victoria basin.

The mean temperature properties for selected stations in the Lake Victoria basin are shown in Figure 3.5 and in Table A.2 of appendix A. Unlike mean annual rainfall, mean annual temperature over the Lake Victoria basin does not vary as much.

River Katonga and Ruizi catchments, being a subset of Lake Victoria catchments, consist of rainfall and temperature characteristics (Tables A4-6 of Appendix A) which are similar to that for the western and northwestern regions of the Lake Victoria basin. Relative to the River Ruizi catchment, Katonga is a wetter and swampy catchment, and the mean annual rainfall is about 18% (220 mm) higher than that of the River Ruizi catchment.

The hydrographs of the streamflow time series for the respective selected gauging station for the River Katonga and Ruizi are given in Figure 3.6. During screening, it was noted that the streamflow data for the River Katonga for the period 1981 to 1997 (Figure 3.6(a)) have many missing values and this was taken into consideration during the course of the study.

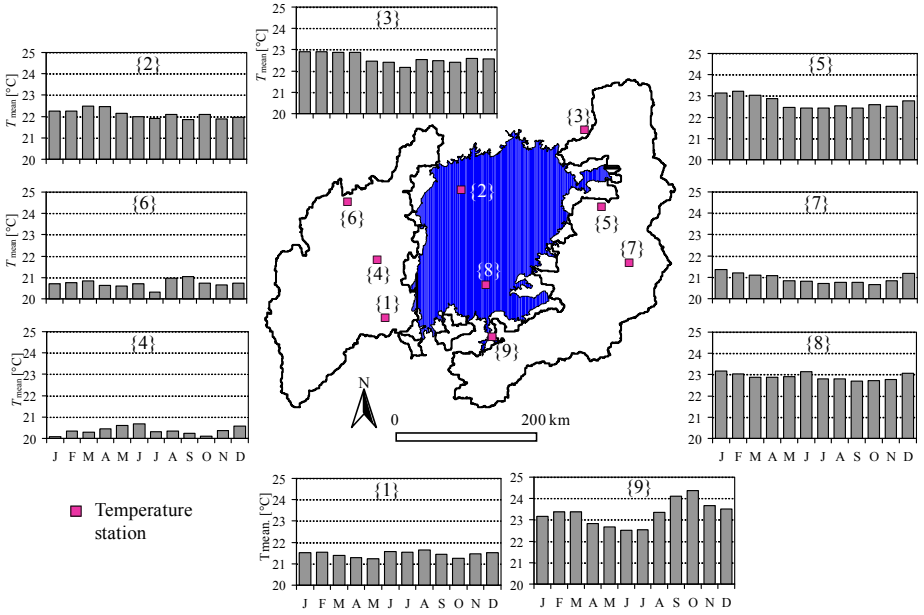

Figure 3.5 Long-term mean of the monthly mean temperature for selected stations in the Lake Victoria basin.

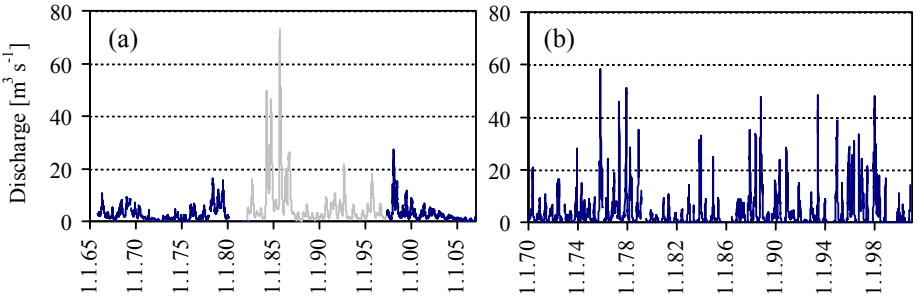

Figure 3.6 Daily hydrographs for: (a) the River Katonga, and (b) River Ruizi

3.3.6 Overview of the GCM data

The GCM data used in this study were principally daily precipitation and maximum and minimum surface air temperature for the relevant grids covering the areas of interest. The data were obtained from the PCMDI database[4]. The data were used for the AR4 IPCC, 2007. There are however

[4] The website for PCMDI database is "http://www2-pcmdi.llnl.gov/esg_data_portal", last accessed 13 June 2011.

several public domain databases from which one can obtain either observed climate data and/or climate model data. The choice of the domain is dependent on the purpose for which the climate data is required, the spatial coverage of the data, the temporal resolution, user interest, data completeness, and access. The GCM data (available as daily atmospheric variables) are the only high-resolution climate model data available for the study area. The details of the models and the scenarios, for which the GCM data were downloaded and processed, are given in Tables A.7 and Table A.8 of Appendix A.

The GCM data are coded (e.g., netcdf[a] format) and some have quality problems (e.g., error in naming of files, some precipitation values being negatives). The data were processed and quality assured using a cross-pollination of techniques, experiences and tools. For example, CDO (Schulzweida & Kornblueh, 2011) is a powerful tool for manipulating grid data of different formats. In addition, many other climate data processing tools such as the NCDF can be annexed to MATLAB (MathWorks Inc., 2008) and are very instrumental in climate model data decoding.

[a] Recent standardization efforts have resulted in adopting Network Common Data Form (netCDF or ncdf) by many standard bodies to archive data of huge volume. The format is noted as ".nc" c.f. ".txt".

CHAPTER 4

TREND INVESTIGATION

4.1 Introduction

Investigating changes in observed hydrometeorological data for a given provides information on the features of the recent and past climate. Such investigation is the process of demonstrating that the changes have occurred in some defined statistical sense and may lead to provision of the reason for the observed changes. In most cases, detecting changes in observed hydrometeorological data is done through statistical analysis of the relevant time series. Through statistical analysis, quantitative assessments of the time series can identify different patterns of change. A change in the times series may occur abruptly (step change) or gradually (trend) or may take a cyclic form (cycle) or a combination of trend and cycle with intermittent step jump (Shahin et al., 1993). Such change may affect the overall long-term statistical properties of the time series such as the mean, median, variance or any other aspects of the time series. Understanding changes in time series is very crucial for general water resources planning and other practical applications such as adaptive engineering designs and may also situate the aspect of the near future climate into context.

Trend exists in a time series data set if there is a significant correlation between the observations and time. In hydrological time series, linear trend, for example, is normally introduced through natural or artificial changes. Periodicities in natural time series are usually due to the astronomical cycles such as the earth's rotation around the sun or any other cyclic climatic phenomenon such as the ENSO[5] (El Niño/La Niña-Southern Oscillation). Persistence is the tendency for the magnitude of an event to be dependent on the magnitude of the previous event(s).

The focal tenet of trend analysis is to detect trends, cycles and shifts in hydrometeorological time series and to describe possible generating processes underlying a given sequence of observations. The most sustained, non-parametric traditional methods, among others, for detecting monotonic trends in time series are the Mann-Kendall (MK) and Spearman's rho (SR) test methods. These methods have for long been applied to many hydrological and climatological situations. For instance, several studies (e.g. Alexander et al., 2006; Machiwal and Madan, 2008; Chen et al. 2007; Pujol et al., 2007;

[5] El Nino phenomenon is the large-scale warming of surface waters of the Pacific Ocean every 3-6 years, which usually lasts for 9-12 months but may continue for up to 18 months, which dramatically affects the weather worldwide.

Sneyers, 1990; Yazdani et al., 2011; Machiwal and Jha, 2008; López-Moreno, 2007; Hipel and McLeod, 1994; Hamed, 2008) have applied these tests to detect significant changes in precipitation and streamflow. The powers of the MK and the SR tests for detecting linear trends in time series have rigorously been examined by Yue et al. (2002a). The study demonstrated that the power of the tests is an increasing function of the slope of trend, sample size, and pre-assigned significance level. They further stated that there is little basis for choosing either MK in preference to SR test or vice versa because both tests provide identical results in the absence of autocorrelation. In addition to monotonic trend, one other crucial form of change in a time series is the periodicity or cycle, which defines the change in the annual and decadal variability of a time series. A number of studies (e.g. Blanckaert and Willems 2006; de Jongh et al., 2006; Machiwal and Madan, 2008; de Jongh et al., 2011) have applied either spectral or harmonic analysis to detect periodicity in time series. Meanwhile, Ntegeka & Willems (2008) applied empirical quantile analysis to detect periodicity in long-term rainfall data for Uccle station in Belgium. The main conclusion by Ntegeka & Willems (2008) was that the periodic high extremes temporal clustering highlights the difficulty of attributing ‘‘change’’ in climate series to anthropogenically induced global warming.

Previous studies show that trends and cycles analysis for rainfall and streamflow extremes in the Lake Victoria basin have not been examined extensively. Most studies aimed mainly at trends in the mean rainfall temporal variability (e.g. Kizza et al., 2009; Nyenzi, 1990; Ogallo, 1989). Kizza et al. (2009) examined trends in mean annual and seasonal rainfall using MK for several stations in the Lake Victoria basin. They derived most of the precipitation data from monthly values. The results showed that positive trend in the annual rainfall predominate. Among the rainfall stations selected, significant trends were manifested in those, which are located in the northern part of the basin, albeit the pattern finding was not conclusive. The study further concludes that the 1960s represents a significant upward jump in the basin rainfall and that, on the seasonal rainfall; the short rains tend to have more trends than the long rains. A study by Ogallo (1979) showed that most of the annual rainfall series in the region were mainly of an oscillatory characteristic with no significant trend. Ogallo (1989) used monthly records from over 90 stations in East Africa to study the dominant spatial and temporal modes of seasonal variation using rotated principal component analysis for the period 1922–1983. In particular, he showed that the Lake Victoria region has a distinctive rainfall regime in East Africa as a whole. Such kinds of study, though, have long not been updated. The preceding discussions intuitively show that most studies of trends on the hydrometeorological time series for the Lake Victoria basin had focused mainly on the mean annual or seasonal rainfall amount only and not much attention was paid to extremes, which are antecedents of disastrous events

(e.g. floods, droughts). In addition, change in climate is mainly manifested in extreme meteorological events. Thus, this chapter aims to carry out trend analysis on the extremes of hydrometeorological time series.

In this study, the methods of the MK test for monotonic trend and quantile perturbation were employed to investigate trends in rainfall, streamflow and T_{max} and T_{min} extremes of the hydrological time series for selected monitoring stations in the Lake Victoria basin. Application of the MK allows the establishment of the existence of long-term significant linear trends in the observed extremes. The quantile perturbation method is used to establish the existence of significant changes in the variability of the observed extremes. Assessing trends in precipitation and temperature concurrently allows statements to be made about the drivers of some of these trends, given the fact that the occurrence of rainfall resonates well with the changes in temperature across much of the region. It is important to note that the results of trend analysis are often used to understand changes in observed extremes as well as application to rivers infrastructure designs.

4.2 Extraction of extreme indices

Several categories of extreme indices can be extracted from climatic variables. Details of such categories of the extreme indices can be found in Alexander et al. (2006). This study considered absolute indices for daily rainfall, streamflows, T_{max} and T_{min} values. Absolute indices represent maximum (max) or minimum (min) values within a season or year (Alexander et al., 2006). For the trend test using the MK method, the annual max (AM) daily rainfall, T_{max} and min daily $T_{min,}$ as well as the AM daily streamflows were extracted as the absolute extreme indices required for the trend analysis. For the trend analysis using quantile perturbation method, flexibility exists in the use of the number of extreme events required per year. That is, optional selection of extreme absolute indices above a given threshold (Ntegeka and Willems, 2008) is possible if the available data is of a resolution of daily or higher. The optional selection of the extreme absolute indices is related to the POT approach (Willems et al., 2007) which assumed total statistical independency and allows for more absolute values of the extremes in a year to be used in the analysis of the changes in the time series variability. Data for some representative hydrometeorological stations in the Lake Victoria basin were considered for the trend analysis. These were data from ten (10), Nine (9) and seven (7) stations for rainfall, temperature and streamflows, respectively, spatially distributed over the study area (see chapter 3, section 3.3).

4.3 Monotonic trends in the hydrometeorological extremes

4.3.1 The Mann-Kendall test

The MK method for trend testing is a non-parametric (distribution free) approach. That is, the method does not require any assumption about the form of the distribution the data is derived from; e.g. there is no need to assume that the data are normally distributed. However, the prerequisite of the test is that the data are iid. The main benefit of the non-parametric statistical tests, compared to parametric statistical tests, is that the data need not to conform to any particular distribution and are thought to be more suitable for the non-normally distributed and censored data, which are frequently encountered in the extremes of hydrometeorological time series.

The details of the procedure for trend test using the MK are described in Appendix B.1. The null hypothesis, H_0, is that there is no trend in the data and the trend test statistic, S, is evaluated for significance based on a bootstrapping resampling technique. The bootstrapping (see section 3.5) helps to circumvent the need for stern adherence of the data to the test assumptions.

For the extreme time series, which violated the assumption of a no serial correlation, the method proposed by Yue & Wang (2004) was applied. Yue et al. (2002b) demonstrated that the existence of serial correlation alters the variance of the MK statistic. In order to ameliorate the effect of autocorrelation, Yue & Wang (2004) proposed a method in which the variance of S is modified by the use of an effective sample size. The details of how the MK variance is modified are given in appendix B.2.

4.3.2 Statistical significance of a monotonic trend

In order to curtail the effect of the test assumptions (e.g. form and constancy of the distribution, independence) on the linear trend test results, a bootstrap sampling technique was applied to compute the significance levels of the MK test statistic, S, for linear trend. The advantages of resampling are that it is a flexible method that can be adapted to a wide range of types of data, including autocorrelated or seasonal data and is also very useful for testing hydrological data because they require relatively few assumptions to be made about the data, yet they are also quite powerful tests (Kundzewicz, 2004). The bootstrap resampling method is often preferred where a test is looking for change in variance (Kundzewicz, 2004).

In the bootstrap resampling method, the original time series is sampled with replacement to furnish a new time series that has the same number of values as the original time series but may contain more than one of some values in the original time series and none of the other values (Kundzewicz, 2004;

Efron and Tibshirani, 1998; WMO, 2000; Davidson and Hinkley 1997). The approach assumes that if no trend exists, under H_o, then shuffling the data should not significantly change the gradient. The data are shuffled many times and after each shuffle, the test statistic of the generated series is recalculated. The test statistic of the original time series is then compared with that of the generated data to determine the significance level. If the test statistic of each of the generated time series is estimated as S_j and $S_1 \leq S_2 \leq \ldots \leq S_K$, for MK, and the original test statistic is S_0 and $S_1 \leq S_0 \leq S_{j+1}$, the probability value, p, of the test statistic being less or equal to S_0 under H_0 is approximated as

$$p = \frac{j}{N} \tag{4.1}$$

where N is the number of times a series is resampled. If large values of S indicate departure from H_0, the significance level is estimated from

$$2\min(p, 1-p)*100\% \tag{4.2}$$

A critical issue to address when using resampling methods is the number of samples that should be generated, which depends on the level of significance required and on the degree of change seen in the data. Usually, a more accurate estimate of the significance is achieved with more samples. On the other hand, when using permutation testing, all permutations ($n!$ where n is the series length) could be generated. These are typically too many. However, 100-2,000 samples are usually recommended as sufficient. In this study, 1,000 samples were used. For example, if the test statistic value of the original data is greater than the 950th highest test statistic value from 1000 replicates, H_0 is rejected at $\alpha = 0.05$ (i.e., a linear trend is detected, with a 5% chance that this linear trend is incorrectly detected). Therefore, the critical test statistic values for significance levels of $\alpha = 0.1$, $\alpha = 0.05$, and $\alpha = 0.01$, are the 90th, 95th and 99th percentile values, respectively, of the test statistic values from the resampled time series.

4.4 Results and discussions on monotonic trends

4.4.1 Extremes of rainfall

Table 4.1 contains results for the MK trend test on the rainfall extremes. Column (1) of Table 4.1 provides the station identifier, ID, of each of the selected rainfall stations and the numbers embraced after the IDs using parentheses, ( ), are the numbers indicated in Figure 3.4, which also show the spatial loci of the selected stations in the study area. The actual record length, n, the ratio between n and effective record length, n^*, n/n^*, the mean, coefficient of variation, C_v, coefficient of skewness, C_s, and coefficient of kurtosis, C_K, of the rainfall extremes, are presented in columns (2)–(7). For normally distributed random time series, its C_s and C_K should be equal to 0 and 3, respectively. It is evident from Table 4.1 that the rainfall extremes of 9

out of the 10 rainfall stations are positively skewed and in all likelihood poorly described by a normal distribution.

The lag-1 serial correlation coefficient, r_1, and its upper and lower limits of the confidence interval at the significant level of 0.05 of the two-tailed test for the autocorrelation on the rainfall extremes, are contained in columns (8)–(10), respectively. If the value of r_1 falls outside the upper and lower values of the confidence interval, the effect of the lag-1 serial correlation is significant, otherwise it is negligible. It can be seen that 8 out of the 10 extreme rainfall series sets are not significantly serially-correlated at the significant level of 0.05. Hence, the application of the MK trend test to these stations without considering serial correlation is valid. The magnitude of the gradient (slope) of the trend was estimated using the method proposed by Theil (1950) and Sen (1968) (Appendix B.3). The value of the slope is contained in column (11) and is hereafter, referred to as Sen's slope. The Sen's slope, b, divided by the mean of the extremes is contained in column (12), which is termed a unit slope. The values of the Sen's slope of all the time series are positive, which is an indication of the likelihood of an increasing trend of the rainfall extremes for the study area. Visual exploration of Figure 4.1 also shows that the magnitude of the values of the Sen's slope, indicated in Table 4.1, reflects the gradual tendency of the linear trends.

Table 4.1 Basic properties and the *P*-values of the rainfall extremes for 10 selected rainfall stations in the Lake Victoria basin.

Station (no.)	n	n/n^*	Mean	C_V	C_S	C_K	Correlation			Slope, b		*P*-value		*P*-value (R)	
							r_1	Limits		(mm/d/year)	(per year)	P	P^*	$P_{\alpha=0.05}$	$P_{\alpha=0.1}$
								Upper	Lower		(11)/(4)				
(1)	(2)	(3)	(4)	(5)	(6)	(7)	(8)	(9)	(10)	(11)	(12)	(13)	(14)	(15)	(16)
9333005 (1)	79	1.271	65.3	0.303	1.029	1.936	0.121	0.201	-0.226	0.0198	0.000302	0.572	0.564	0.973	0.954
10149 (2)	64	1.395	69.7	0.558	2.813	10.028	0.168	0.232	-0.267	0.2756	0.003956	**0.976**	0.952	0.975	0.956
9031026 (3)	57	1.311	67.1	0.331	0.984	0.813	0.137	0.235	-0.276	0.4167	0.006212	**0.985**	0.972	0.975	0.948
9134008 (4)	79	1.497	61.6	0.298	0.985	1.172	0.201	0.205	-0.230	0.2536	0.004113	0.999	**0.996**	0.975	0.952
9035127 (5)	45	1.352	61.1	0.444	3.593	16.521	0.153	0.225	-0.270	0.3762	0.006161	0.995	**0.988**	0.976	0.953
8935076 (6)	45	1.651	57.0	0.267	-0.133	-1.013	0.251	0.275	-0.320	0.5000	0.008769	1.000	**0.995**	0.980	0.957
9030003 (7)	87	3.365	56.7	0.298	1.452	2.905	**0.548**	0.191	-0.214	0.1095	0.001932	0.976	0.860	0.978	0.949
9235000 (8)	63	1.394	61.6	0.360	2.005	6.998	0.167	0.215	-0.247	0.2042	0.003313	**0.957**	0.919	0.973	0.956
9233008 (9)	58	2.505	82.0	0.342	1.193	1.904	**0.437**	0.234	-0.269	0.0611	0.000745	0.639	0.589	0.978	0.954
9131028 (10)	47	1.386	61.5	0.286	0.608	-0.164	0.165	0.260	-0.302	0.0092	0.000149	0.551	0.543	0.976	0.952

The mean cross-correlation of the cross-correlation coefficients (also see Yue and Wang, 2002) among the 10 rainfall stations is 0.0235. The mean cross-correlation value (0.0235), compared to the mean values of the upper (0.0576) and the lower (0.0001) limits of the 95% confident limits, implies that the cross-correlation among the sites could be ignored. Thus, there is some evidence that the upward trends may not be due to chance alone. In other words, given the available data, the rainfall extremes in the Lake Victoria region for the past 5-8 decades have generally been experiencing an upward trend, irrespective of the significance of the linear trend.

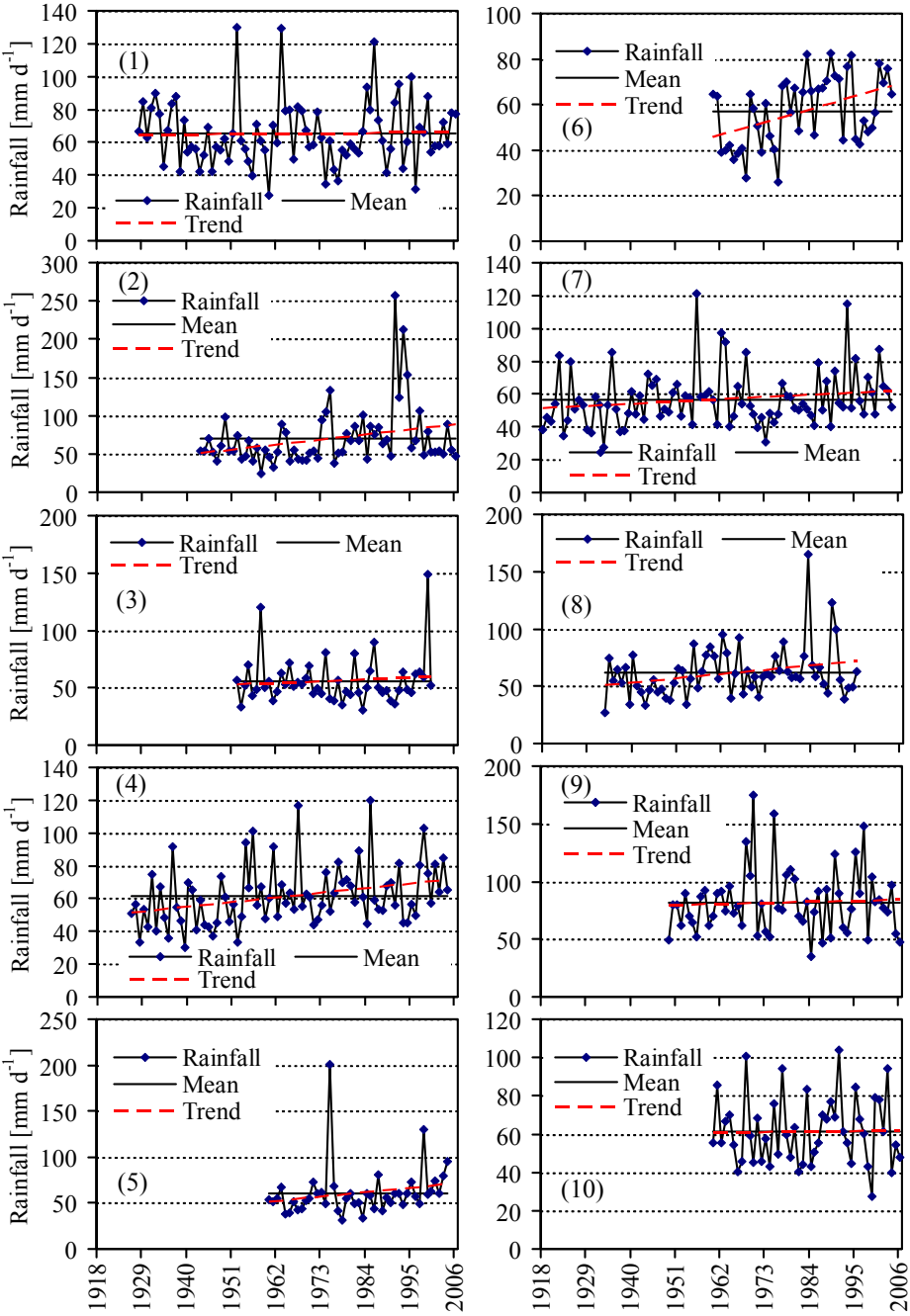

Figure 4.1 Time series plots of the daily AM rainfall for selected rainfall stations in the Lake Victoria basin.

The probability values, *P*-values, of the MK *S*, estimated from the original data before correcting for lag-1 autocorrelation, *P*, and after correcting for lag-1 autocorrelation, *P**, are indicated in columns (13)–(14). The *P*-values of

the upper quartiles of the replicates of the data corresponding to 95% confident interval, $P_{\alpha = 0.05}$, and 90% confident interval, $P_{\alpha = 0.1}$, are indicated in columns (15)–(16) of Table 4.1. As stated before, it is important to recap that the presence of statistically significant autocorrelation can have an impact on the significance of the linear trend tests (Yue and Wang, 2004; Villarini and Smith, 2010). As reported by Cox and Stuart (1955), "positive serial correlation among the observations would increase the chance of significant answer even in the absence of a trend."

The modification of the MK variance by a correction factor, n/n^*, before evaluating for the significance of trend, was, thus, to account for the effect the significant serial correlation on the trend test results, especially for stations (7) and (9) (Table 4.1). Comparison of values of P and P^*, in columns (13)–(14), shows that the effect of significant positive autocorrelation can influence the rejection of the null hypothesis, H_0, and indeed vindicates the need for autocorrelation correction. It can, also, be seen from Table 4.1 that the rainfall extremes series showed existence of linear trends which are statistically significant at $\alpha = 0.1$, S(0.1), for station (8) and S(0.05) for stations (2), (3), (4), (5) and (6). Although the values of the Sen's slope for all the extreme rainfall series sets considered are positive, the existence of monotonic trends for stations (1), (7), (9) and (10) is not statistically significant at any of the indicated significant levels, NS(0.1, 0.05). Thus, 60% of the extreme rainfall series showed significant positive (increasing) trend. The visual satisfaction of the magnitude of the inclination between the mean-line (continuous line) and the approximate linear trend-line (dash line), indicated in Figure 4.1, is an important complement to the test results. Given that there is an apparent nexus between the magnitude of the Sen's unit slope and the significant answer, the Sen's unit slope may provide evidence for significant answer if other influences are negligible.

4.4.2 Extremes of T_{max}

Table 4.2 provides results for the MK trend test on the AM daily T_{max} (T_{max} extremes). The definitions of the notations indicated in each of the columns of Table 4.2 are similar to the ones provided in section 4.4.1 for Table 4.1. The ID numbers embraced by parentheses, { }, are shown in Figure 4.2, which also indicate the spatial loci of the selected temperature stations in the study area. It is evident from Table 4.2 that all the T_{max} extreme series are positively skewed and in all likelihood poorly described by a normal distribution. Table 4.2 shows that 8 out of the 9 T_{max} extreme series are significantly serially correlated at the significant level of 0.05. Irrespective of the level of the significance of the autocorrelation, useful trend test results, however, were obtained after correcting for the effect of autocorrelation. Column (11)–(12) of Table 4.2 provides the values of the Sen's slope and their unit values. The magnitude of the slope for station {7} is naught, which is an indication that there is no linear trend at all in the available data for station {7}. The

magnitudes of the values of the slope demonstrated by stations {3}, {5} and {6} are negative and those for stations {1}, {2}, {4}, {8} and {9} are positive. Visual analysis of Figure 4.2 also reflects the gradual tendency revealed by the values of the Sen's slope.

Table 4.2 Basic properties and the *P*-values of the T_{max} extremes of 9 selected temperature stations in the Lake Victoria basin.

Station (no.)	n (years)	n/n^*	Mean (°C)	C_V	C_S	C_K	Correlation			Slope, b		*P*-value		*P*-value (R)	
							r_1	Limits		(°C/year)	(per year)	P	P^*	$P_{\alpha=0.05}$	$P_{\alpha=0.1}$
								Upper	Lower		(11)/(4)				
(1)	(2)	(3)	(4)	(5)	(6)	(7)	(8)	(9)	(10)	(11)	(12)	(13)	(14)	(15)	(16)
9231011 {1}	33	2.3	31.5	0.077	1.503	1.671	0.405	0.286	-0.347	0.1000	0.0032	0.999	**0.979**	0.975	0.948
9032010 {2}	36	19.0	32.3	0.067	0.669	3.041	0.937	0.269	-0.325	0.0706	0.0022	0.997	0.736	0.973	0.946
8934140 {3}	31	5.0	34.4	0.050	0.898	1.453	0.692	0.278	-0.343	-0.1000	-0.0029	0.000	0.047	0.973	0.947
9232027 {4}	32	3.9	29.5	0.053	0.086	0.635	0.613	0.313	-0.375	0.0526	0.0018	0.968	0.825	0.971	0.946
60462 {5}	34	1.2	33.7	0.063	1.174	1.274	0.096	0.301	-0.360	-0.0160	-0.0005	0.334	0.348	0.978	0.956
9030000 {6}	30	1.9	30.2	0.055	1.009	1.175	0.333	0.293	-0.359	-0.0414	-0.0014	0.255	0.318	0.969	0.946
6070 {7}	39	27.8	32.9	0.056	2.553	8.142	0.972	0.244	-0.295	0.0000	0.0000	0.558	0.511	0.971	0.945
9132002 {8}	39	28.8	33.4	0.074	0.797	0.236	0.975	0.278	-0.329	0.0913	0.0027	0.996	0.690	0.972	0.944
9233044 {9}	37	28.3	35.0	0.044	1.514	3.061	0.977	0.276	-0.330	0.0625	0.0018	1.000	0.747	0.977	0.949

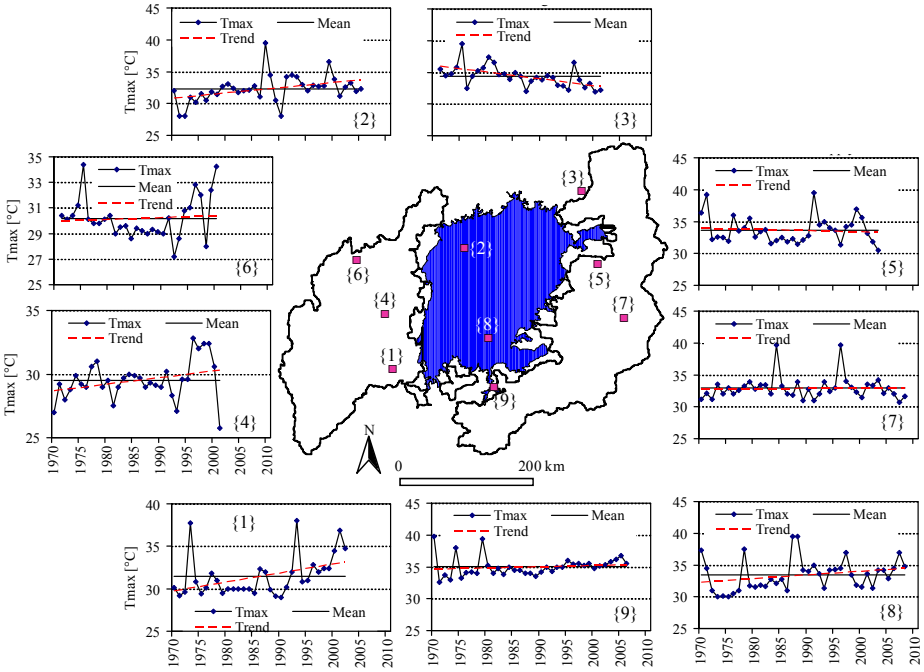

Figure 4.2 Time series plots of the AM of T_{max} for selected temperature stations in the Lake Victoria basin.

The mean cross-correlation of the cross-correlation coefficients among the 9 T_{max} stations is 0.0251. The corresponding mean values of the upper and the lower limits of the 95% confident limits are 0.1160 and 0.00013, respectively. This evidence implies that the cross-correlation among the sites could be

neglected as well. Thus, the evidence of increasing and decreasing linear trend may not be due to chance alone. Visual analysis of Figure 4.2 also shows that the T_{max} extreme series for stations {5} and {6} have tendencies of decreasing trends. A more critical visual inspection of chart for stations {1}, {4}, {6} and {9} in Figure 4.2 reveals that albeit the approximate linear trend-line indicates an increasing trend, the path of a decreasing trend appears to have been abruptly altered by the T_{max} extremes experienced in the recent decade (1990s). It can be seen from Table 4.2 that the T_{max} extremes series showed existence of linear trends, which are S(0.) for station {1} only. The linear trends identified in T_{max} extremes series for all other stations are not statistically significant at any of the indicated significant levels. Although the values of the Sen's slope for 5 out 9 T_{max} and 3 out of 9 extremes series are positive and negative, respectively, the existence of monotonic trend for only one station, {1}, is S(0.05). Thus, only about 10% of the extreme T_{max} series considered showed significant increasing linear trends.

4.4.3 Extremes of T_{min}

Table 4.3 provides results for the MK trend test on the annual minimum daily T_{min} (T_{min} extremes). The notations indicated in each of the columns were defined in section 4.4.1. The IDs for the T_{min} stations are similar to that of the T_{max} (Figure 4.3). It can be seen that the values of the C_v for the T_{min} extremes are much higher than the corresponding values for the T_{max} extremes. This is an indication that the amplitude of the variation of the T_{min} extremes is higher than that of the T_{max} extremes. It is also evident from Table 4.3 that the T_{min} extreme series for 4 and 5 stations are positively and negatively skewed, respectively. All the T_{min} extremes series are poorly described by a normal distribution and can not be assumed to follow a normal distribution.

Table 4.3 Basic properties and the *P*-values of the T_{min} extremes for 9 selected temperature stations in the Lake Victoria basin.

Station (no.)	*n*	*n*/*n**	Mean	C_V	C_S	C_K	Correlation			Slope, *b*		*P*-value		*P*-value (R)	
	(years)		(°C)				r_1	Limits		(°C/year)	(per year)				
								Upper	Lower		(11)/(4)	*P*	*P**	$P_{\alpha=0.05}$	$P_{\alpha=0.1}$
(1)	(2)	(3)	(4)	(5)	(6)	(7)	(8)	(9)	(10)	(11)	(12)	(13)	(14)	(15)	(16)
9231011 {1}	31	2.3	13.0	0.105	-0.254	0.054	0.405	0.306	-0.371	0.05240	0.00403	0.947	0.857	0.970	0.947
9032010 {2}	23	1.7	12.7	0.109	0.367	0.470	0.272	0.337	-0.424	0.00000	0.00000	0.604	0.580	0.962	0.940
8934140 {3}	30	4.9	12.0	0.143	0.191	2.871	0.683	0.291	-0.357	0.11436	0.00954	1.000	**0.964**	0.976	0.950
9232027 {4}	31	2.8	12.4	0.092	-0.012	0.511	0.488	0.305	-0.369	0.04473	0.00361	0.992	0.924	0.970	0.937
60462 {5}	37	27.7	12.8	0.119	0.416	-0.041	0.975	0.299	-0.353	0.00769	0.00060	0.672	0.534	0.977	0.950
9030000 {6}	31	2.7	12.4	0.089	-0.853	-0.150	0.482	0.322	-0.386	0.00000	0.00000	0.373	0.423	0.974	0.949
6070 {7}	35	14.5	10.1	0.177	-0.716	-0.461	0.905	0.287	-0.344	0.13280	0.01321	1.000	0.902	0.974	0.947
9132002 {8}	32	2.1	14.0	0.113	-0.693	1.226	0.376	0.290	-0.352	0.06667	0.00476	0.996	**0.967**	0.974	0.948
9233044 {9}	35	21.9	12.5	0.098	0.148	-0.193	0.955	0.295	-0.352	0.06594	0.00529	0.995	0.711	0.971	0.937

The magnitudes of the slope for stations {2} and {6} are naught, which is an indication that there is no linear trend in the available data. All other stations showed evidence of positive slope. Visual inspection of Figure 4.3 also reflects the gradual tendency revealed by the values of the Sen's slope

indicated in Table 4.3. The mean cross-correlation of the cross-correlation coefficients among the 9 T_{max} stations is 0.0253. The corresponding mean values of the upper and the lower limits of the 95% confident limits are 0.1255 and 0.00014, respectively. The low values of the correlation among the stations show that the cross-correlation among the sites could be neglected. Thus, the evidence of increasing linear trend, demonstrated by all the T_{min} extremes, may not be due to chance alone. Visual inspection of Figure 4.3 shows that the strong increase in the T_{max} extremes in the 1990s is demonstrated by all the T_{min} stations, except for station {6}. It can further be seen from Table 4.3 that the existence of linear trend in the T_{min} extremes of stations {3} and {8} are S(0.1). However, visual inspection of Figure 4.3 gives the impression that station {7} has steeper linear trend than that for station {3} and {8}. Indeed, the Sen's slope for {7} is greater than that of {3} and {8}. Thus, insignificant trend in T_{min} extremes for station {7} can only be explained by the value of its r_1, which is much higher than that for stations {3} and {8}. Generally, the results showed that about 20% of the selected nine T_{min} extremes series demonstrated significant increasing trends. Nevertheless, positive trend is evident in 7 of all the T_{min} extreme series studied. Significant increasing trend in the T_{min} extremes for station {3} and that of rainfall extremes (Table 4.3), and a positive decreasing trend in the T_{max} extremes for station {3} apparently demonstrates the physical nexus among the variables.

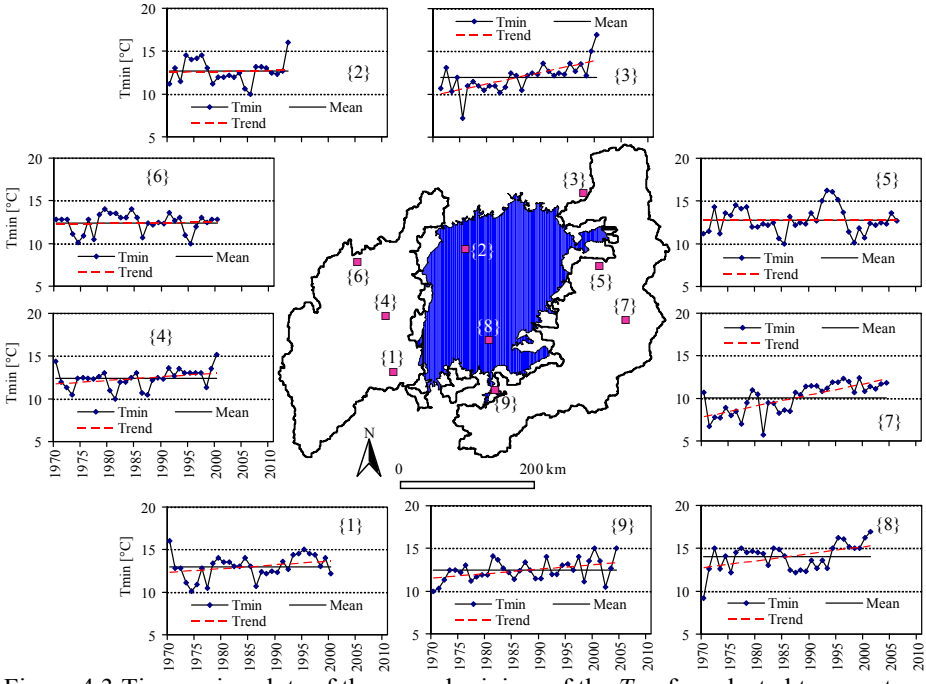

Figure 4.3 Time series plots of the annual minima of the T_{min} for selected temperature stations in the Lake Victoria basin.

4.4.4 Extremes of streamflows

Table 4.4 provides results for the MK trend test on the AM streamflows (streamflow extremes) for seven selected streamflow stations. The definitions of the notations contained in columns (1)–(16) were provided in 4.4.1. Table 4.4 shows that the streamflow extremes of 5 out of the 7 selected stations are positively skewed and are more variable than rainfall and temperature (T_{max} and T_{min}) extremes. This means that, other than rainfall, the influence of the other factors also controlling the changes in the variability of the streamflow extremes can not be ignored. The streamflow extremes can also not be assumed to follow a normal distribution.

Table 4.4 Basic properties and *P*-values of the streamflow extremes for 7 selected streamflow stations in the Lake Victoria basin.

Station (no.)	n	n/n^*	Mean	C_V	C_S	C_K	Correlation			Slope, b		*P*-value		*P*-value (R)	
	(years)		($m^3 s^{-1}$)				r_1	Limits		(m^3/s/year)	(per year)	P	P^*	$P_{\alpha=0.05}$	$P_{\alpha=0.1}$
								Upper	Lower		(11)/(4)				
(1)	(2)	(3)	(4)	(5)	(6)	(7)	(8)	(9)	(10)	(11)	(12)	(13)	(14)	(15)	(16)
112022 [1]	28	1.8	202.9	0.283	-0.417	-0.566	0.289	0.316	-0.388	1.646	0.008	0.861	0.793	0.978	0.947
81248 [2]	45	16.4	22.3	0.430	0.338	-0.555	0.910	0.263	-0.307	0.118	0.005	0.792	0.580	0.968	0.945
81259 [3]	42	17.3	10.4	1.054	2.550	7.008	0.920	0.261	-0.309	0.013	0.001	0.577	0.519	0.976	0.951
104172 [4]	39	8.0	177.4	0.421	0.835	0.022	0.800	0.264	-0.315	0.875	0.005	0.856	0.647	0.973	0.946
1EF02 [5]	51	36.4	376.4	0.477	1.333	1.227	0.978	0.247	-0.286	2.032	0.005	0.967	0.620	0.980	0.956
81224 [6]	31	14.4	25.5	0.567	0.653	-0.672	0.910	0.300	-0.365	0.120	0.005	0.718	0.561	0.976	0.950
1AH01 [7]	43	12.6	56.1	0.176	-0.525	-0.495	0.878	0.251	-0.297	0.512	0.009	1.000	0.913	0.972	0.947

The streamflow extremes of the selected series are all significantly-serially correlated at the significant level of 0.05. Hence, the correction for the effect of serial correlation is vindicated for the MK test. Table 4.4 shows that the values of the slope for all the extreme streamflow series are positive, indicating that the data have tendencies of increasing trend. The values of the Sen's unit slope of all the selected stations are comparable to that of the unit slope values for the extreme series of rainfall and temperature having significant trends. However, the P^* values indicate that no significant linear trend exist in the extreme streamflow series at the significant level of 0.05 or 0.01. Failure of the MK test to detect significant trends in the streamflow extremes is probably due to the higher values of the coefficient of variation and the differences in the distributions (and skewness) of the extremes for stations [5] and [7]. Yue et al. (2002a) noted that the power of the MK almost decreases exponentially with increase in the value of coefficient of variation of the data. The dependent of the MK power on a number of factors, especially on the site's statistical properties such as the skewness, which vary depending on the variable being analyse could have impacted on the existence of significant trends in extreme flow series. Visual inspection of Figure 4.4 shows that the linear trends in the streamflow extremes are less amplified except for stations [1], [4] and [7].

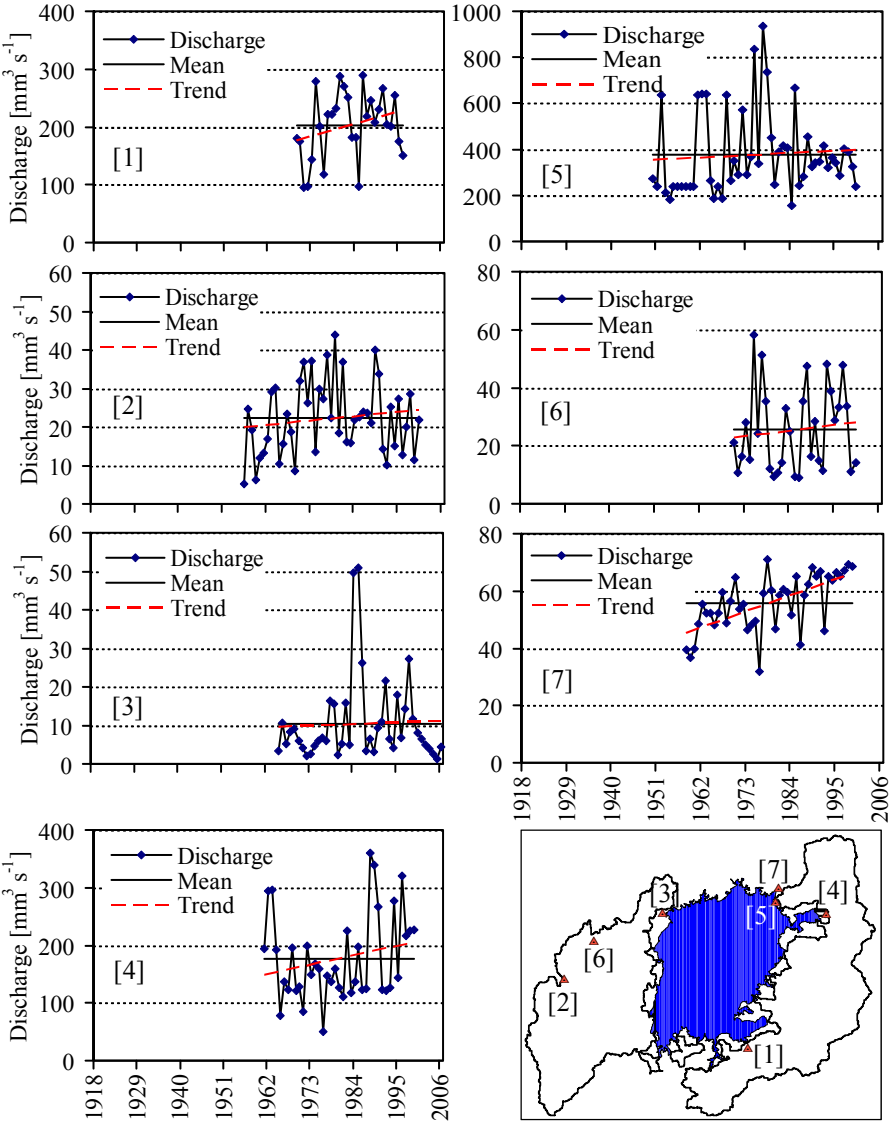

Figure 4.4 Time series plots of the AM of the mean daily streamflows for selected streamflow stations in the Lake Victoria basin. The bottom-right figure indicates the locations of the gauging stations in the Lake Victoria basin.

4.4.5 Practical significance versus statistical significance

Yue et al. (2002a) discussed the relationship between the statistical and practical significance; they noted that a statistically significant trend may not necessarily be practically significant and vice versa. In addition, they further argued that adequately large samples will definitely reveal any change, irrespective of the magnitude of change, with a statistical test but the result may not render any help practically. Similarly, small samples of a given time

series may not demonstrate any statistical change, but the amplitude of the change could be practically very significant.

Consider, for example, the values of the unit slope for the streamflow and rainfall extremes presented in column (12) of Table 4.4 and in column (12) of Table 4.1, respectively. Although the values of the slope for all the rainfall extreme series are positive, only 6 out of the 10 rainfall stations demonstrated statistically significant upward trend. The trend in the streamflow extreme series for station (1) is not statistically significant and the visual inspection of the chart representing station (1) in Figure 4.1 can reveal that there is little evidence of trend in the data. Over a 50-year period, for example, the slope yields an increase in the mean AM rainfall of 65.3 mm/day by about 1 mm/day or 1.5%. From a practical perspective, the estimated change is within the sampling error of the rainfall measurement and does appears, given the available data, not as being of practical importance. Similarly, the unit slope of trend for station (7) can yield 5.5 mm/day or 9.7% of the mean of 56.7 mm/day over a 50-year period. This is also within the sampling error. Furthermore, over a 50-year period, the unit slope of trend of magnitude 0.006212 per year for station (3) can yield 20.9 mm/day or 31.1% in the mean of 67.1 mm/day. This is both statistically and practically significant and may not be ignored assuming no possible reversal in the linear trend.

Trends in the extreme streamflow series of stations [1], [5] and [7] are not statistically significant. Figure 4.4 clearly shows the tendency of increasing trend in the streamflow extreme series. Table 4.4 shows that the streamflow extremes of stations [5] and [7] have values of the unit slope of 0.00540 and 0.00912, respectively. Over a 30-year period, for example, the respective slope yields an increase of 60.9 $m^3 s^{-1}$ or 16.2% and 15.4 $m^3 s^{-1}$ or 27.4% of their mean of 376.4 $m^3 s^{-1}$ and 56.1 $m^3 s^{-1}$, respectively. Similarly, over a 28-year period, the slope of station [1] yields an increase in the mean of the extreme streamflow of 202.9 $m^3 s^{-1}$ by 46.1 $m^3 s^{-1}$ or 22.7%. These changes in the mean values of the streamflow extremes could be practically significant and need not to be ignored despite the fact that significant trends were not demonstrated in the streamflow extremes.

Yue et al. (2002a) noted that beside detecting the existence of statistically significant change in the past or recent climate (hydrometeorological time series) it is important to take heed to provide information to the engineer in charge of a water resources engineering project on the current attributes of, for example, the streamflow (e.g. AM and minimum, mean). However, even if the test shows a significant trend with a slope of practical importance, the engineer will only be vindicated in changing his assumption regarding the magnitude of the flow characteristic only if the change is permanent for the life of the project. Permanent change in streamflow characteristics is mainly attributed to change in climate and this can be reflected in the trends in

temperature and rainfall. Despite the fact that no significant trend was detected in selected extreme streamflows, in general, the identified trends appear to resonate fairly well with that of extreme series of rainfall and that of temperature. This is important for attributing the influence of observed climate extremes on the streamflow extremes.

4.5 Conclusions on monotonic trends

The MK test was applied to detect the existence of statistical significance linear trends in the extreme time series for daily rainfall, streamflow and maximum and minimum temperatures for selected stations in the Lake Victoria basin. The record lengths of the selected stations vary from 47-87, 28-51, 31-39, and 23-37 years for rainfall, streamflow, maximum temperature and minimum temperature, respectively. The data records of most of the stations date up to 2006. The magnitude of the gradient of the linear trend was estimated by Sen's slope estimation technique to enable the evaluation of the practical significance versus statistical significance. In general, the presence of positive linear trend was eminent in the extremes series of all the variables.

For rainfall extremes, all the selected stations demonstrated increasing trend of positive slope, indicating that the evidence of increase in the observed rainfall extremes in the study area is eminent. Of the 10 selected stations, 6 demonstrated the presence of significant positive trend. Thus, given the available data, the rainfall extremes in the Lake Victoria basin, for the past 4-8 decades, had had a general upward trend. Given the fact that the study used relatively longer records of rainfall series, the presence of significant upward trend in the extremes fairly demonstrates the trend in the climate of the recent decades in the Lake Victoria basin.

Of the 9 selected stations, for maximum daily temperature, 7 demonstrated the present of increasing trend while 2 demonstrated the evidence of decreasing trend. The existence of statistically significant increasing trend was exhibited by only 1 station. All the 3 stations, with negative slope, were not statistically significant. For daily minimum temperature, the presence of increasing trends was demonstrated in 7 out of 9 stations. 2 stations had stationary slope. Significant positive trend was demonstrated only in two stations. Irrespective of the significance of the trend, an upward trend is thus more demonstrated in the annual extremes for minimum daily temperature than that for maximum daily temperature.

The evidence of the presence of increasing trend in the streamflow extremes of all the 7 selected streamflow stations was demonstrated by positive slope. No significant trend however was detected in all the 7 streamflow extreme series. Given that statistically significant trend does not necessarily imply trend of practical significance and vice versa, in overall, 6 of the 7 streamflow

stations with statistically insignificant upward trend have values of slope with practical importance.

Changes in climate are relatively eminent in the changes in extreme events even with a relatively small climate changes (Meehl et al., 2007). Furthermore, climate change may be perceived most through the manifestation of extremes (Trenberth et al., 2007) and detecting trend in extremes through statistical analysis may put the changes that occurred in the recent decades into perspective. With these statements, we can conclude that there is some evidence of change in the climate of the Lake Victoria basin as demonstrated by the presence of linear trends in the long-term hydrometeorological extremes.

4.6 Variability of hydrometeorological extremes

4.6.1 Quantile perturbation

The quantile perturbation method for analysing the changes in the variability (cyclic trend) (QPMtc) of hydrometeorological extremes investigates the historic changes in ranked extremes (Ntegeka & Willems, 2008). The approach amalgamates aspects of the frequency analysis practiced in extreme value analysis, and perturbation used in climate change impact studies. The technique is analogous to the frequency-perturbation approach applied as one of the methods for deriving climate change scenarios from historical series using information from climate models runs (Willems and Vrac, 2011; Mpelasoka and Chiew, 2009). For the climate change impacts analysis, instead of applying one factor to the whole range of values and all the time scales, different factors can be derived and applied to the time series based on the ranked values of the time series. The change factors (perturbations) are ratios or differences of two similarly ranked values obtained from the future (climate model scenarios) and the observed (climate model control) time series. The quintessence of QPMtc, however, is solely based on historical time series and given the fact that perturbation is a relative change it necessitates two series. For the climate-model based approach, one of the series is taken as the reference or baseline series while the other is a future scenario series. In the QPMtc, one of the series is derived from the long-term historical time series, while the other series is taken from a particular block (subseries) of interest or where the change is being investigated. Given a particular block of series of B_L-years, one of the series contains the actual extremes within the block while the other series is derived from the distribution of the original long-term historical time series to obtain a reference series. The extreme values within each block are ranked in order to relate them to return periods of B_L/i, where i is the rank of each extreme value. The ranking ensures that the extreme values correspond to the quantiles $q(B_L)$, $q(B_L/2)$, …, $q(B_L/i)$, where $q(B_L/i)$ is the quantile corresponding to return

period B_L/i years. If N_L is the total record length of the extreme time series under consideration or the reference series, similarly, $Q(N_L)$, $Q(N_L/2)$, …, $Q(N_L/i)$ are the quantiles corresponding to N_L, $N_L/2$, …, N_L/i years return periods, respectively. It can be noticed that the return periods B_L, $B_L/2$, …, do not, obligatorily, coincide with the empirical return periods of N_L, $QN_L/2$, …, years and in such cases, the $Q(N_L/i)$ values are obtained by linearly interpolating from the boundary values in the extreme series before $q(B_L/i)$ is compared with the interpolated value, $Q(N_L/i)$.

4.6.1.1 Application to quantitative time series

Changes that occur in quantitative hydrometeorological variables such as rainfall, evapotranspiration and streamflows can be compared in terms of ratios. Thus, changes in the extremes can be derived as ratios of similarly ranked quantiles as $q(B_L) / Q(N_L)$, $q(B_L/2) / Q(N_L/2)$, ... $q(B_L/i) / Q(N_L/i)$.

Figure 4.5(a) illustrates the estimation of the first three values in the reference series for an example rainfall dataset (Station (7) in Figure 4.1) for B_L = 10 years. The curve contains all the selected extremes in the dataset for a reference period (1961-1990) of 30 years. Using linear interpolation, estimates of the reference series for a particular given block can be obtained. Based on a sliding window technique, a similar procedure is followed for all the other sets of blocks of series when estimating the reference series.

Note also that for each 'window slide', the number of perturbations is equivalent to the block length (size) and cannot exhibit the temporal nature of the changes in the extremes. In order to reveal the temporal variability of the perturbations, an average perturbation value for each block of years is estimated from all the block perturbations centered in the block. Similarly, it is also possible to obtain the average of the reference time series, which if multiplied by the average perturbation gives the value of the average of all the extremes for the given block.

Figure 4.5(b) illustrates the temporal evolution of perturbation over time; the equivalent in percentage change is shown in Figure 4.5(c). Figure 4.5(d) illustrates the temporal evolution of the mean of the reference and that of the actual extremes series. Given the value of the percentage change, %P, perturbation (P) can be obtained as 1+ (%P)/100. The procedure described above was repeated for all the selected rainfall stations in order to analyze changes in rainfall extremes over the study area. Similarly, the same methodology was applied to streamflow extremes for all the selected streamflow stations. The anomalies of the extreme time series can be seen as a series of quantile perturbations above a certain return period. The average quantile perturbation calculation assumes that above a certain exceedance probability, the perturbations are constant and this can be proved by explicitly

calculating the slope of the block perturbations and comparing it with the bootstrapped 95% confidence interval (Ntegeka, 2011).

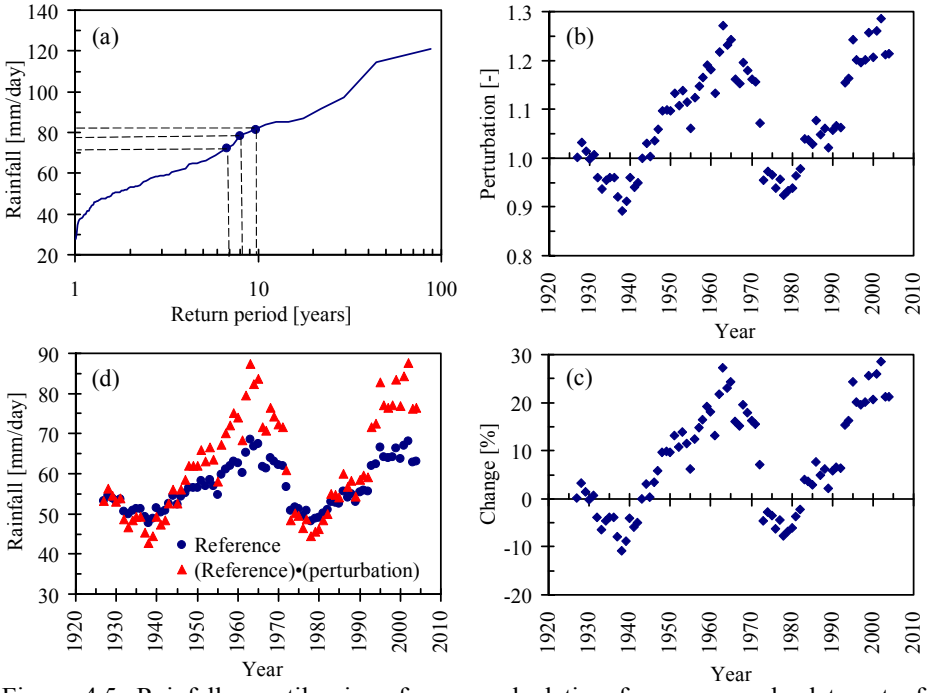

Figure 4.5. Rainfall quantiles in reference calculation for an example data set of rainfall intensities (a), evolution of the estimated changes in the extreme time series: (b) perturbations, (c) percentage change, (d) reference series and actual extremes.

In the work of Ntegeka and Willems (2008), QPMtc was only applied to quantitative variables such as rainfall, evapotranspiration and streamflows. However, the technique can also be applied to qualitative variable such as temperature in the same way but may requires that the temperature data are in absolute units.

4.6.1.2 Confidence interval and sensitivity of the block length

The temporal evolution of perturbation can reveal whether the most recent changes in the climate of the study area can be considered statistically significant in contrast with the natural temporal variability or reference period. Identification of statistically significant cyclic trends enables an assessment of the likelihood of climate change effects during the previous decades. Using bootstrapping technique (section 4.3.2) the confidence interval is also estimated and superimposed on the perturbation plot. Based on visual exploration, it is possible to spot out periods that depict significant deviations under the null hypothesis of no change or if perturbations are not significantly different from unity (Figure 4.5(b)).

The QPMtc is however sensitive to block length considered and to capture a meaningful change, varying a block length between 5-15 years is sufficient to check the persistence of perturbation and hence identification of clustering or systematic changes of the extremes in a given period. The choice of the block length may also depend on the objective of the study. In this study, a block length of 10 years was used for rainfall and streamflow data.

4.6.1.3 Application to other data

Application of QPMtc to qualitative climatic variable such as temperature requires a new definition of perturbation. Since perturbation is a relative change, perturbation for temperature can be defined as the arithmetic difference of two temperature values with similar return period obtained from the ranked series of the block series under consideration and the reference series obtained from the original series. Note that the temperature values may need to be in absolute units, Kelvin (K), to simplify the arithmetic calculation, which involves ranking of the temperature extreme series. However, the results can be displayed in degree centigrade (°C) (Figure 4.6).

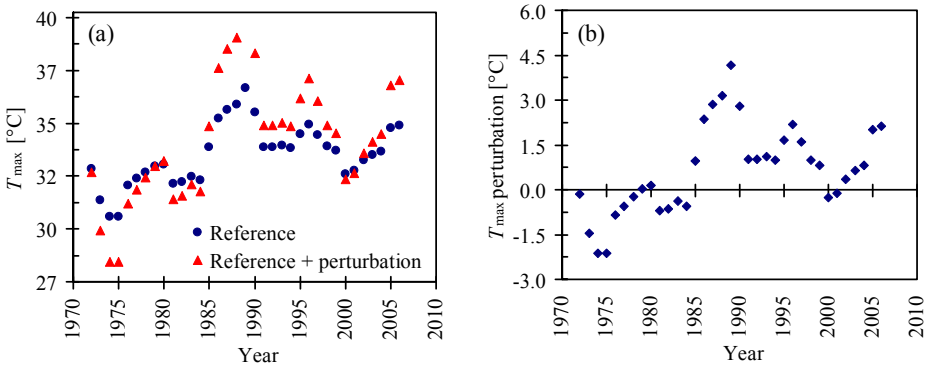

Figure 4.6(a) Temperature changes in reference calculation for an example data set of maximum temperature, before and after perturbation, (b) evolution of the estimated maximum temperature perturbation in extreme time series.

4.6.2 Comparison of trends in rainfall and temperature extremes

In order to unearth the links between change in rainfall extremes and temperature extremes, perturbations of rainfall and that of temperature (T_{max} and T_{min}) were compared. Given that each of the selected temperature stations does not necessarily come from the respective same locations as that for the selected rainfall stations, the average perturbations were compared. The topography of the Lake Victoria basin is fairly homogeneous and making the use of average value provides a fairly consolidated result. To obtain the average perturbation for rainfall for a given year, for example, the values of rainfall perturbations for all the selected rainfall stations were considered. The average perturbations for all the other years were obtained in a similar way but for the data with common periods. The average perturbations for T_{max} and

T_{min} (temperature) were also calculated in the same way as that of the rainfall. Comparison of the average perturbations was made in two ways. In the first case, the values of the normalized average perturbations for rainfall and temperature were compared in the same chart. Normalization of the average perturbations was done by their respective mean value. In the second case, the correlations between the average perturbations of rainfall and that of corresponding temperature were calculated. To this extent, it was possible to compare the perturbations of rainfall and temperature. In the second case, the influence of temperature change on rainfall extremes was determined by considering the average perturbation of rainfall per unit average temperature perturbation. That is, change in rainfall per unit change in temperature was calculated for each year and for the data with common periods.

4.6.3 The influence of sunspots on the trends in rainfall extremes

Historical record showed that the Lake Victoria water levels rose during every peak of about 11-year sunspot[6] cycle since the late 19th century (Stager et al., 2005). While in Stager et al. (2007), it is reported that "peaks in the ~11-year sunspot cycle were accompanied by the Lake Victoria water level maxima throughout the 20th century, due to the occurrence of positive rainfall anomalies ~1 year before solar maxima". They further argued that if the Sun-rainfall relationship persists in the future, sunspot cycles could be used for long-term prediction of precipitation anomalies and associated outbreaks of insect-borne disease in much of East Africa. This information may need to be validated base on the perspective of rainfall extremes.

An attempt to establish how the changes in sunspot maxima influence the changes in rainfall extremes is, herein, made. Application of QPMtc was extended to sunspot series and the correlation between the perturbations of sunspot maxima and that of rainfall extremes was established. That is, the average perturbations of rainfall were compared to that of sunspot in a similar way the perturbations of rainfall and temperature extremes were compared.

4.7 Discussions on the variability of hydrometeorological extremes

4.7.1 Rainfall extremes

Figure 4.7 shows plots of percentage change (perturbation) for rainfall extremes together with the 95% confidence interval versus the year. Note that the reference perturbation represents the long-term expected rainfall extremes in the block periods following the total length of observed record. In addition, the reference provides the basis for testing the null hypothesis that the

[6] Sunspots are seen as "small" dark spots on the surface of the sun. They are easy to observe and count if the sunlight is strongly filtered. The collection of sunspot numbers is mainly done by the International Sunspot Count, Brussels. The data are available freely in public domains.

perturbations are not statistically significant from 1. Figure 4.7 also shows the locations of the rainfall stations for which the charts are related. The numbers in parentheses, ( ), are the IDs for the rainfall stations defined already in section 4.4.1. Perturbations of rainfall extremes for selected rainfall stations show some outstanding features of the observed rainfall characteristics in the Lake Victoria basin for the recent climate. It can be seen from Figure 4.7 that during the 1990s, the average perturbations for all the selected stations fall outside the 95% confidence limits. This means that the null hypothesis is rejected at the significant level of 0.05. That is, 1990s experienced some dramatic high rainfall extremes over and above the expected natural variability.

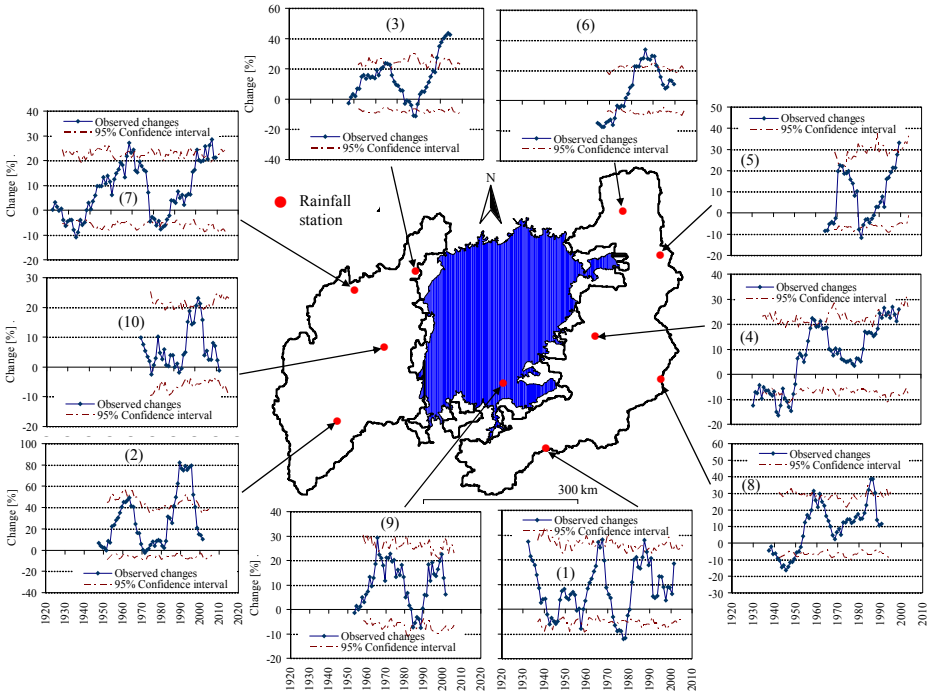

Figure 4.7 Estimates of the average percentage change in the extreme quantiles of the daily rainfall using a 10-year blocks, together with the 95% confidence interval for selected rainfall stations in the Lake Victoria basin.

During the 1960s, the rainfall extremes of all the others stations, apart from stations (6) and (10) whose records begin just after the 1960s, were significantly high (Figure 4.7). Further visual inspection of Figure 4.7 also reveals that, given some of the selected stations, the 1940s and the 1970s received significant low rainfall extremes. However, it should be noted that the significant increase in the rainfall extremes observed in the 1960s (up to ~ 10–20%) is less than that observed in 1990s (up to ~10–60%). Similarly, the significant low rainfall extremes observed in the 1940s (up to ~20%) is much higher than that observed in the 1970s (up to ~ 10%). This implies that the

tendency for the rainfall extremes to shift towards positive change (high extremes) is evident. It is important to note that, in the Lake Victoria basin, significant increase and decrease in the rainfall extremes appear to occur after every cycle (high and low) of about 32 years, given the data.

4.7.2 Streamflow extremes

Figure 4.8 shows estimates of the percentage change (perturbation) for the streamflow extremes together with that of the 95% confidence interval. Apart from other stations, stations [3], [4], and [7] show some significant change in the streamflow extremes for the 1990s and statistically significant decrease for the 1970s. This is consistent with the anomalies for rainfall extremes.

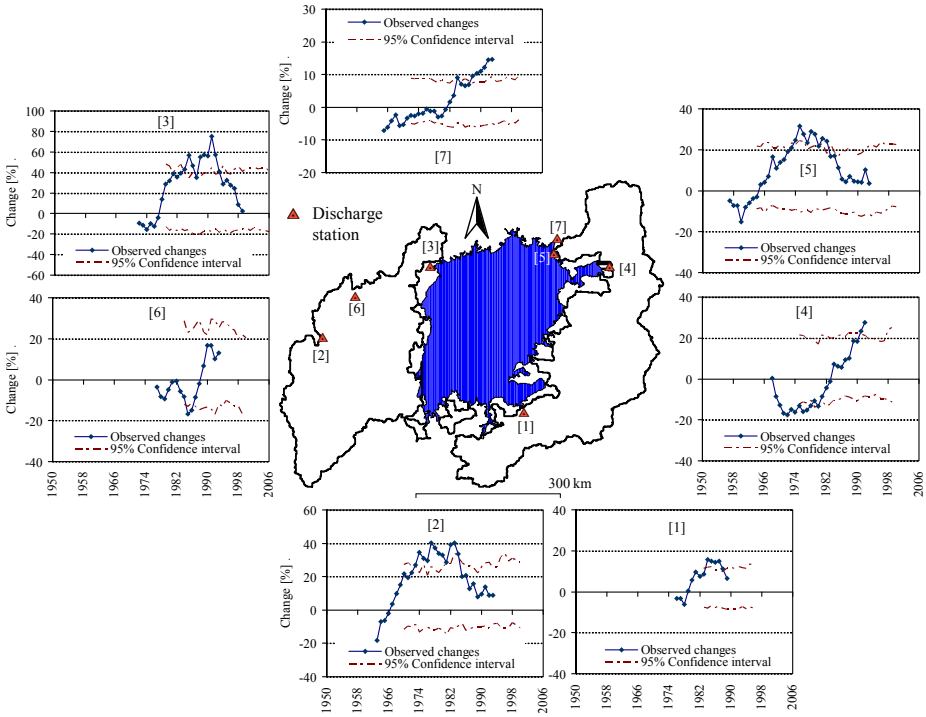

Figure 4.8 Estimates of the average percentage change in the extreme quantiles of the daily streamflow using a 10-year blocks, together with the 95% confidence interval for selected minimum temperature stations in the Lake Victoria basin.

The mean cross correlation of the cross-correlation coefficients among the 3 streamflow stations is 0.105 and the upper and low limits of the 95% confidence interval of the two-tail *t*-test for correlation are 0.0943 and 0.0001. That is, the spatial correlations among the three stations are statistically significant and the change pattern in the observed streamflow extremes for the 1990s and 1970s might be due to chance. Other factors, other than the primary factor of rainfall, also significantly influence the catchment response to hydrological extremes (e.g. Githui et al, 2009; McDonnell, 2009; Elferta, and

Bormann, 2010). This makes trend investigation on streamflow time series, in most cases, inconclusive.

4.7.3 Change correlations

Figure 4.9(a)-(c) shows plots of perturbations for temperature (T_{max} and T_{min}) and rainfall for all the stations. It can be seen from Figure 4.9(a)-(b) that the perturbations for the T_{max} and T_{min} show that the anomalies for the 1990s were indeed higher than for the other periods. However, the perturbations for T_{min} for the different stations are more consistent for most of the periods than that for the T_{max}. Figure 4.9(c) shows that perturbations for rainfall for the different rainfall stations are generally consistent for the 1940s, 1960s, 1970s and 1990s. The high and low cycles in temperature appear to be of shorter cycle length (in years) than that for rainfall. Consistency in the change in rainfall and temperature extremes for the prominent periods (e.g. 10960s and 1990s) reveals correlation in the change in rainfall and temperature. Figure 4.9(d) shows the relative change in perturbations for rainfall, temperature (T_{max} and T_{min}) and sunspot maxima.

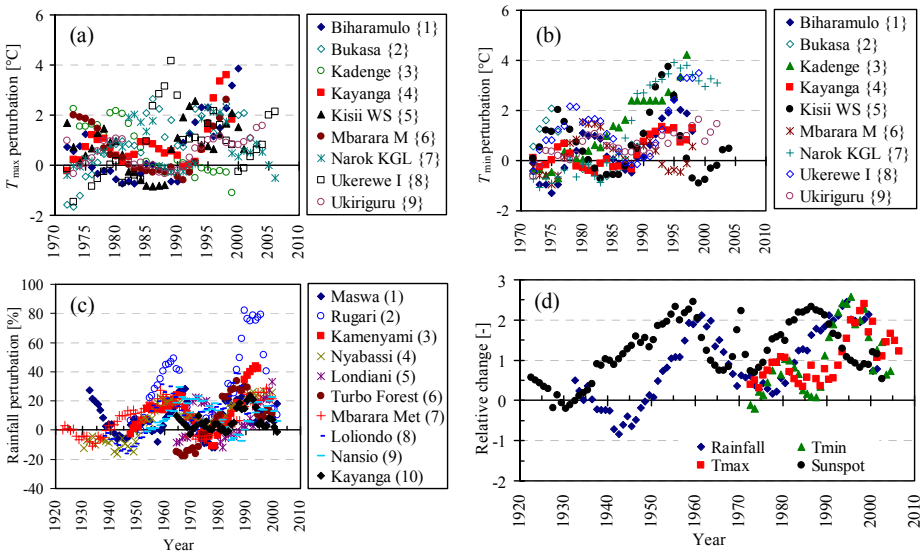

Figure 4.9 Change in the extremes for: (a) T_{max}, (b) T_{min} and (c) rainfall, (d) comparison of the relative (normalized) change among the different variables.

One very common feature in Figure 4.9(d) is the similarity in the magnitude of the relative perturbation. In addition, the periodicity of the perturbation for sunspot and that of rainfall appear to resonate in some similar way from the 1950s to 1970s. It can also be seen that an apparent negative correlation between the temperature perturbations and that for the sunspot maxima is very prominent for the 1980s to 2000s. These relationships mean that an increase in the temperature extremes is a manifestation of a decrease in the Sunspot maxima. A better indicator for the correlations in the perturbations between

rainfall and temperature, and between rainfall and sunspot can be revealed by the respective correlation values. Table 4.5 contains the values of the ranked correlation coefficient obtained between the perturbations of rainfall extremes and that of temperature, and between the perturbations of rainfall extremes and that of sunspot maxima for the indicated periods.

Table 4.5 Correlations between the change in the extremes of rainfall and temperature, and rainfall and sunspot.

	T_{max}	T_{min}	Sunspot
Period	1970-2006	1970-2006	1940-2006
Correlation [-]	0.38	0.68	0.31

It can be seen that the value of the correlation coefficient (0.68) for the correlation between perturbation of rainfall and that for T_{min} is higher than that between rainfall and T_{max} and that between rainfall and sunspot maxima. This means that there is a stronger correlation between daily rainfall extreme and the minimum of the T_{min} than that between daily rainfall extreme and T_{max}. The relationship between change in rainfall extremes and sunspot maxima is weak. Figure 4.10(a) shows the plots of change in rainfall extremes per unit change in temperature. In addition, Figure 4.10(b) shows plots of change in rainfall extreme per unit change in sunspot maxima.

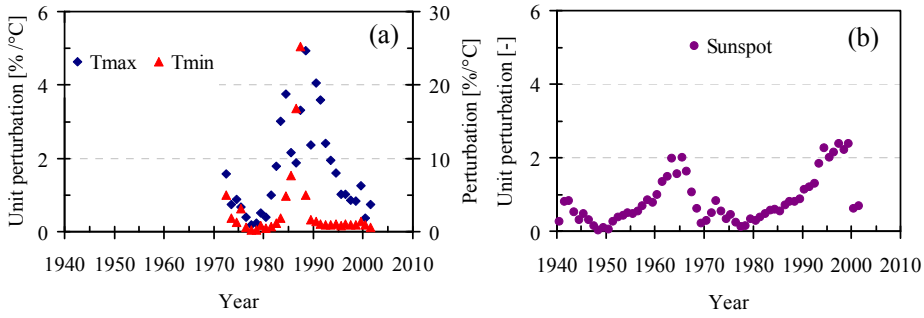

Figure 4.10 Change in the rainfall extremes per unit change in: (a) temperature (T_{max} and T_{min}), (b) sunspot maxima. The left and right ordinates in (a) are for T_{max} and T_{min}, respectively.

In Figure 4.10(a), the primary and the secondary ordinates are for T_{max} and T_{min}, respectively. It can be seen that the change in the extreme of T_{min} by 1°C causes the rainfall extreme to change by higher percentage (up to 25%) than the change in the extreme of T_{max} for the observed period 1970-2006. Figure 4.10 (b) shows that, given the available data, change in the sunspot maxima cannot cause rainfall extremes to change by more than 3%.

4.7.4 Conclusions on the variability of hydrometeorological extremes

Analysis of the change in variability (cyclic trend) of the hydrometeorological variables provides an opportunity for situating the characteristics of the observed changes into climate change and variability perspectives. The robust nature of the methodology used in the analysis, the empirical quantile perturbation, provides the possibility of the identification of significant temporal changes. The cyclic flaunts of the results is a very good way of providing information on the amplitudes of the temporal changes in the observed hydrometeorological extremes and probable evidence on the direction of change in climate as compared to the reference climate. In addition, the methodology also allows the comparison of the changes in the extremes of one variable with that of another variable. That is, it was possible to compare relative change in rainfall extremes with the relative changes in the daily maximum temperature as well as that of sunspot.

The statistically significant anomalies in the rainfall extremes for the recent decades are evidences of a more intensification of rainfall in the recent past observed in the 1990s compared to 1960s. The block occurrence of rainfall extremes in time is an evidence of the fact that wet decades tend to follow by dry decades leading to some kind of clustering of extremes (Ntegeka and Willems, 2008). Given the available data, the emergence of high and low extremes, in time, as evidenced in rainfall extremes, is an approximate cycle of about 32 years for the climate of the Lake Victoria basin.

Changes in maximum and minimum temperature extremes tend to resonate fairly well with the changes in the rainfall extremes. This change resonance was also evidence in sunspot. A unit change in minimum daily temperature causes a much higher change in rainfall extreme than a unit change in maximum temperature. A unit change in sunspot maxima causes insignificant change in rainfall extremes. There is a stronger correlation between change in rainfall extremes and that of minimum temperature, compared to that maximum temperature and that of sunspot maxima. This suggests that the change in minimum temperature is a better indicator for change in rainfall extremes for the Lake Victoria basin.

CHAPTER 5

CLIMATE MODEL RUNS EVALUATION

5.1 Introduction

The credibility of a GCM to predict future climate heavily depends on its ability to reproduce current and past climate; either for a particular region and/or for the globe. A compelling case is the ability of the GCM not only to predict the average climate conditions but also the variability in hydro-climatic variables (Katz, 1992). Regardless of the result, the model can be viewed critically in order to better understand the reasons of good or unrealistic predictions. In weather prediction, forecasts are produced on a regular basis and verification against what actually happens can quickly be performed. In contrast, climate predictions are designed for much longer periods (e.g. many decades) and for conditions without precise past analogues. One direct way to gain confidence about the performance a model for such predictions is to compare its predictions with known historical measurements or indirect evidence when records are missing. Results of climate model simulations are needed in impact analysis but for simulation to be considered reliable, the outcomes should fulfill some quality criteria (Christensen et al., 2007). Simulation of climate for the periods for which data are available and to acceptable accuracy is one of the most important qualities of a reliable climate model. The difficulty, here, is in determining what is acceptable or reasonable. Statistical metrics can be used to define the quality criteria and acceptability for a reasonable simulation. Although the field of statistics has played a relatively minor role in the development of GCM concept, its importance in validating the models is indispensable.

Due to the nonlinear character of the weather and climate evolution, the precision with which the actual climate must be represented by model simulations is simply unknown. Despite the weak relation between certain measures of the models to simulate correctly the climatology and the precise prediction of future climate revealed by some studies (Randall et al., 2007, Houghton et al., 2001), it still remains unclear what are the minimum criteria a model should meet to be considered a reliable prediction tool.

The model-testing phase has many aspects. Climate model must first be tested at system level; that is running the full model, including all components and comparing the results with observations. However, because of the model complexity, the problems are often *unlarable* to trace back to their source. This suggests a modular testing procedure:- instead of comparing the full model results at system level with the observations, one can proceed to test the model at component level, that is, isolate the individual model

components and test each independently from the others. This is a common practice in model testing. The components of a climate model usually tested in such an approach are the atmospheric, oceanic, sea ice and land-surface components (Emori et al., 2005). Despite the former, evaluating a climate model's performance at catchment scale would require archiving all observed variables at a central point and performing a testing exercise. This is impractical as data availability, storage and computational requirements can impose a notorious constraint. Thus, model evaluation is based on the objective and specific variables such as precipitation, temperature, etc. are used.

Statistics of errors, biases, correlations and trends, etc., have been used to quantify statistical inconsistencies between the model simulations and the historical time series (e.g. Christensen et al., 2007; Emori et al., 2005; Katz 1992; Nyeko-Ogiramoi et al., 2010). This approach can satisfy mean statistics of the considered variables. In this chapter, a range of statistical metrics, in combination with quantile/frequency analysis techniques are used to evaluate the performance of AR4 GCMs for simulating rainfall and temperature. The evaluation is based on several GCM runs for a grid covering the River Katonga catchment in the Lake Victoria basin (Figure 3.1). The grid covers twenty and four rainfall and temperature stations, respectively (Tables A.5 and A.4 in Appendix A). Models with poor performance are assessed based on their strengths and limitations in reproducing the observed climate.

5.2 Data scaling

The GCMs provide area-averaged gridded data and this means that for the evaluation purpose the rainfall values measured at a point, for example, requires scaling if areal rainfall measurement is not available. By scaling the point rainfall intensity, one can account for the expected systematic difference between the point rainfall and the grid averaged GCM rainfall. Point rainfall can be scaled to area-averaged rainfall by either applying areal reduction factor (ARF) (Svensson and Jones, 2010) or by spatial interpolation of point rainfalls using the technique such as the Thiessen polygon method. The points (measurement locations) under consideration should all fall within the GCM grid boundary. Thiessen polygon method was used in this study because of the uniformity in the topography of the study area. Temperature variability over the study area is low and a simple average technique was used to obtain mean temperature from the data measured at the selected temperature points. The climate models (Tables A.7 of Appendix A) were evaluated against the observed data for the River Katonga catchment (see Figure 3.1 for the location and Appendix A.4-5 for the data information).

5.3 Climate model runs evaluation methods

5.3.1 Absolute bias

Bias is the difference between an estimator value (GCM control run) and the value being estimated (observation). For a time series an average bias provide the mean bias needed for evaluation purposes. Let $(X_p)_i$ be the estimates of the time series for the p^{th} GCM, $p \in \{1,\ldots, M\}$, and let Y_i be the corresponding time series for observation. M is the number of the estimates. The mean bias between the estimator and the observation can be calculated as follows. The series $(X_p)_i$ and Y_i can also be aggregated to produce new time series $(X_p)^k$ and Y^k, $k \in \{1,\ldots,K\}$, e.g. $K = 12$ at monthly scale, or $K =$ the number of years at annual scale. From the new time series, the mean bias, B_p, is given by

$$E_p = \sqrt{\frac{1}{K}\sum\left((X_p)^k - Y^k\right)^2} \tag{5.1}$$

where the summation goes over all the months, seasons or years under consideration. If B_p is divided by the sample mean of Y^k, we can obtain relative mean bias (*NME*). *NME* is a unitless quantity and can be used to evaluate the GCM simulation skill for a given observed variable such as temperature and rainfall. The value B_p provides a measure of how close the estimate is to the observation and can easily be converted and presented in percentage. If B_p or the *NME* value is small enough, the estimate is said to approximate the observation. Thus, good performing GCMs are those with B_p or *NME* values which are, for example, within the sample error of the observation (e.g. ± twice the observed standard deviation (Stdev) or coefficient of variation) or close to naught. It is assumed that uncertainty bounds, of twice the standard deviation, well approximate a 95% confidence interval under a further assumption of normality of the time series.

5.3.2 Frequency distribution

Ability of a GCM to reproduce, for example, rainfall extremes (intensities or frequencies) can be unraveled by comparing its estimates (simulations) distribution with that of the corresponding observation based on the corresponding similar rainfall events. In order to do this, frequency distribution plots (quantile versus return period) of the model's simulations can be compared to that of the observation on the same charts. Let the ranked series of Y^k be Y_j^k, where $j = 1, 2, \ldots, n$ and n is the number of months or years. Similarly, let the ranked series of $(X_p)^k$ be $(X_p)_j^k$. The empirical return period, (T_j), for each quantile, in the ranked series, using Weibull plotting position, can be calculated as

$$T_j = \frac{n}{j+1} \tag{5.2}$$

A frequency distribution curve is the plots of the distribution values versus return periods, T_j. A good performing model is that with the frequency distribution curve close to that of the observation for all range of events. A perfect model would have its frequency distribution overlapping that of the observation.

5.3.3 Quantile bias

Quantile relative bias, $(B_p)_{j,}$ is the difference between the estimator value and that of the observation with similar rank (exceedance probability or return period) and can be calculated as follows:

$$(B_p)_j = \left\{(X_p)_j^k - Y_j^k\right\} / Y_j^k \tag{5.3}$$

where $j = 1,\ldots, n$ and for $p = 1,\ldots, M$.
Equation (5.3) indicates that any event can be considered for comparison without necessarily taking into account the whole distribution. To take this advantage, the bias for heavy rainfall events was computed and evaluated. In addition to quantile bias, event frequent biases were also computed and the events considered were the mean wet- and dry days in each month.

5.3.4 Ensemble bias

Ensemble mean bias is the average value of the mean bias for all the estimators (models). Similarly, an ensemble quantile bias can be obtained as the average value of all the models' mean quantile bias. In other words, a single estimator (ensemble run) can be obtained from all the estimators. This ensemble run, which is a series of average values, can be compared to the observation by using any measure. For example, a distribution plot of the ensemble run can be compared with the distribution of the observation. In this way, it is possible to establish if an ensemble run closely approximate the observation than any of the individual member of the ensemble vice versa.

5.3.5 Inconsistent projection

Although there is no scientific consensus on the future climate (the future being unknown), model intercomparison can also be done by considering the change each model is projecting. If we assume that consensus among models can provide clue for the future state of climate, a model that projects a change that is uniquely different from that of the other models can be considered inconsistent if it were inconsistent with the observation (Nyeko-Ogiramoi, et al., 2010). Projected change can be measured by comparing the model control and the projection itself. The differences in the future projections (controls

and projections) if combined with the differences in the current simulation (controls and observation) can enhance the understanding of the effects of the model bias on the future projections. Additionally, it checks for the robustness in future projections. If the model inter-comparison reveals that models differ significantly, the future projections are not robust.

5.4 Results and discussions on climate model runs evaluation

5.4.1 Annual absolute bias

Figure 5.1 shows the annual bias for 48 and 49 GCM runs for rainfall and daily mean temperature, respectively. A simulation period of 40 years (1961-2000) for rainfall and 30 years for temperature (1971-2000) were considered for the performance assessment. It can be seen that, for the study area, most of the runs are positively biased for rainfall and negatively biased for temperature.

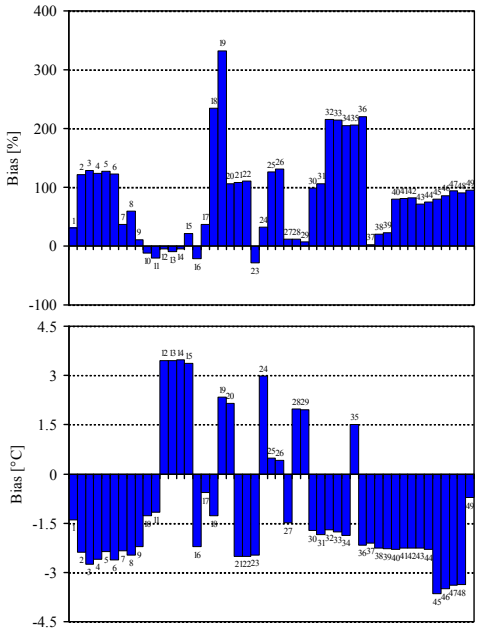

Figure 5.1 Annual bias of the GCM runs for precipitation (top) and temperature (bottom).

In addition, Figure 5.1 can also reveal that the bias values of 16 GCM runs for rainfall are more than twofold (B_p > 100%) the value of the observation. This implies that about 40% of the GCM runs are very poor and most GCM runs overestimate rainfall over the study area. In contrast, the temperature bias values for most the GCM runs are over 1.5°C of that of the observed mean daily temperature. Furthermore, it can be seen from Figure 5.1 that models that overestimate rainfall tend to under estimate temperature. This signifies

that the parameterization of most of the GCMs makes them positively and negatively biased for rainfall and temperature, respectively for the study area. Figure 5.1 shows that the models E-R and E-H, with over 300% bias, seem to stand out as the worst performing models for simulating rainfall over the study area. For temperature, the models MK3.5 and PCM1, with the bias values of over 3°C, are the worst performing models for simulating temperature over the study area. Furthermore, poor performing models for rainfall are FGOALS1.0-g, CGCM2.3.2a, ECHAM5, CCSM3.0, PCM1, CGCM3.1(T47) and CM4. For temperature poor performing models are FGOALS1.0-g , PCM1, MK3.0 and CGCM3.1(T47). The models marked with "*" in Table A.7 (Appendix A) are the most biased with respect to rainfall and temperature over the Lake Victoria basin. The discussions on the criteria used for screening out the models whose predictions are highly inconsistent with observation are made in section 5.4.5.

5.4.2 Monthly absolute bias

For a model to be considered a good performance, its simulation results should be consistent with that of the observation across different aggregation levels.

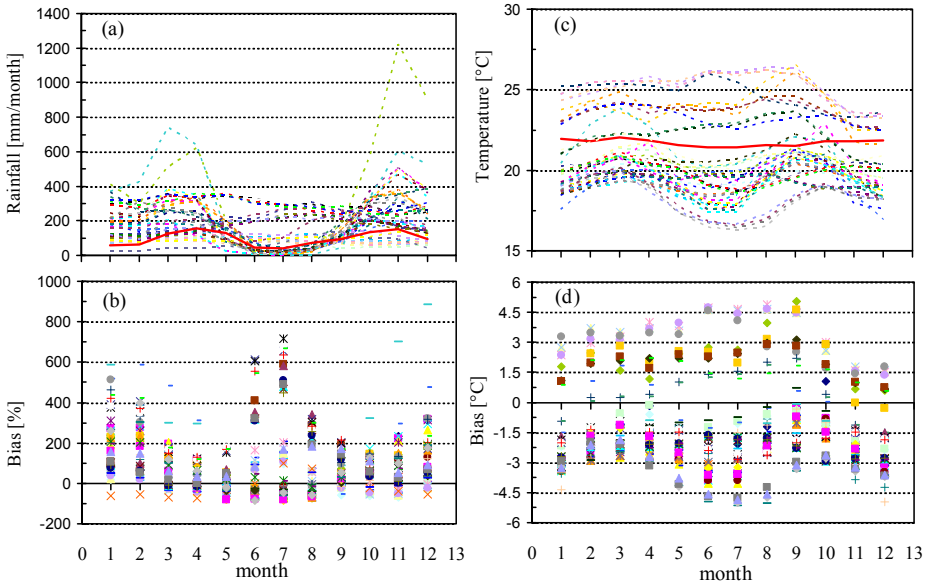

Figure 5.2 Monthly performance (top) and monthly bias (bottom) for precipitation and temperature. The continuous thick lines in (a) and (c) are for the observation and the dash lines are for the different GCM runs. The bias for each month for the different GCM runs are represented by the different markers.

Model performance at monthly aggregation is important because it also provides information that can be translated into seasonal performance. Thus, the bias values were calculated at monthly scale. Figure 5.2 provides the

models' variable values (dash lines) and that of the observation (continuous thick line) and bias at monthly aggregation. It can be seen that, for rainfall, the plots for most model runs are above that of the observation (Figure 5.2(a)). For temperature, the plots for most of the models are below the observation (Figure 5.2(c)). For the months of December-February and June-August, the values of the bias for most of the models are higher compared to that of the other months (Figure 5.2(b)). This implies that the models overestimate the monthly rainfall for the dry seasons than the wet seasons. Similarly, the models' bias values, for temperature, tend to be higher for the dry months than the wet months (Figure 5.2(d)). Furthermore, most models underestimate temperature and few models overestimate temperature.

5.4.3 Event bias

Evaluating the GCM runs with respect to certain rainfall events such as heavy rainfall events enables an assessment of the GCM skills in simulating extremes of rainfall. The occurrence of heavy rainfall events is often associated with the frequency of wet– and dry day events. Thus, the ability of the GCMs to simulate well the proportions of wet- and dry days, in a rainfall time series is significant for their reliability in predicting extremes.

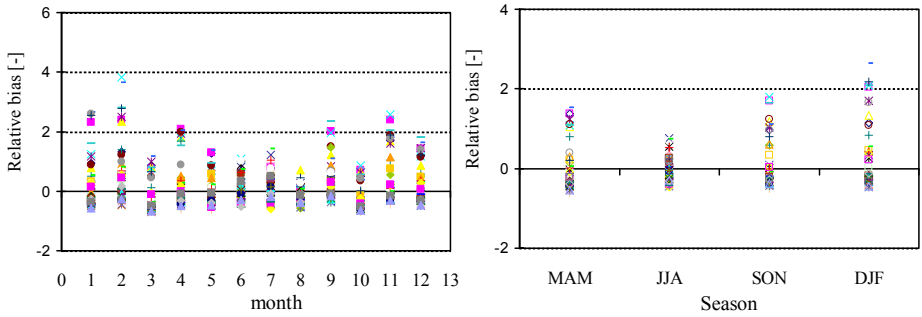

Figure 5.3 Heavy events performance (relative bias) of the GCM runs for the monthly (left) and seasonal rainfall (right).

Figure 5.3 shows the *NME* for the heavy rainfall events (quantile) for the monthly and seasonal daily rainfall. Heavy events, in this context, are the top 5% rainfall events in a ranked daily series. It can be seen that the values of *NME* are mainly within 2 and -0.6 for the monthly case and are within 1.7 and 0.4 for the seasonal case. The values of the relative mean bias for most of the models are huge because it is expected that *NME* be very close to zero for the simulations to be considered good. The GCMs simulations for the seasonal rainfall events are better than that of monthly. Figure 5.4 shows the models' performance on the simulation of wet day and dry day monthly frequency for rainfall. A wet day is defined as the day with rainfall intensity greater than 1 mm. Thus, a day with rainfall intensity less than or equal to 1 is considered dry. It can be seen from Figure 5.4(a) that for the dry months, most of the

GCMs simulated more wet days than the actual wet days represented in the observation. Similarly, most of the GCMs simulated less dry days than the actual dry days in the observation. The wet day frequency bias values for the dry months are generally higher for the dry seasons than that for the wet seasons (Figure 5.4(b)). Similarly, the values of the dry day frequency bias for the wet seasons are, on average, higher than that for the dry seasons (Figure 5.4(d)).

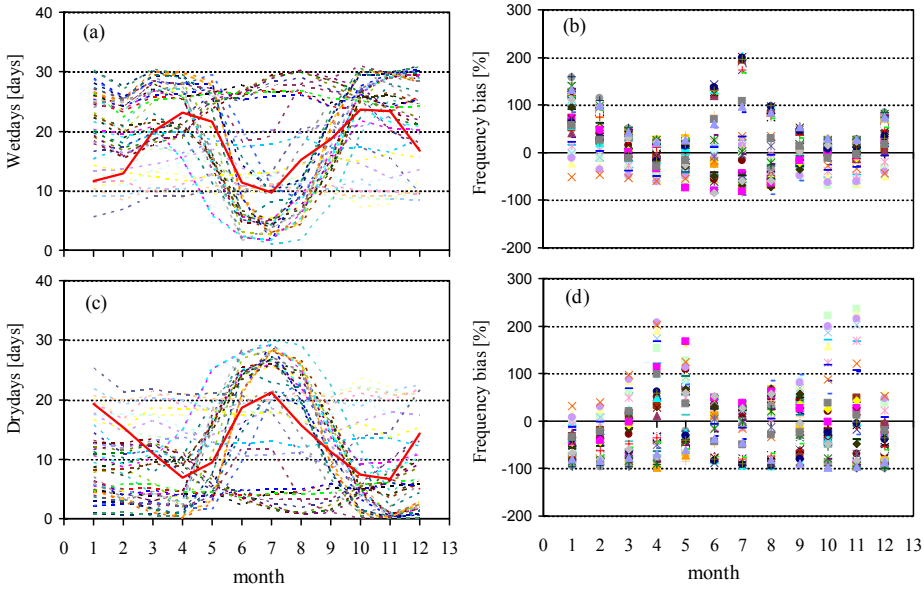

Figure 5.4 Monthly frequency performance of the GCM runs for the wet days (a)-(b) and dry days (c)-(d). The dash lines in (a) and (c) are for the different GCM runs and the continuous line is for the observation. The different markers in each month, in the charts on the right column, represent the different GCM runs.

Important implications can be derived from the GCMs performance on the frequency of wet- and dry day events. First, the overestimation of the heavy rainfall events is a result of the wetness in the GCM for the dry season. Secondly, the consistency in the bias values for most GCMs indicates that its parameterization were similar. Thirdly, the inconsistency in the bias values for some of the GCMs indicates that some parameterization were omitted, oversimplified or included in them, which were not omitted, oversimplified or included in the other GCMs.

5.4.4 Frequency distribution

Figure 5.5 shows the daily frequency distribution for the GCM runs and that of the observation, for the months of January and April. The results for two months, only, are provided to illustrative the typical frequency distribution needed to evaluate GCM runs against observation. In addition, the results for the dry and that for the wet seasons are assumed to be represented by that of

January and April, respectively. It can be seen from Figure 5.5 that the frequency distribution plots reveal the GCM ability to simulate rainfall quantiles for all the different rainfall events (return periods). Most of the GCMs overestimate the meek, medium and heavy rainfall events. The frequency distribution plots of few runs, however, agree with that of the observation.

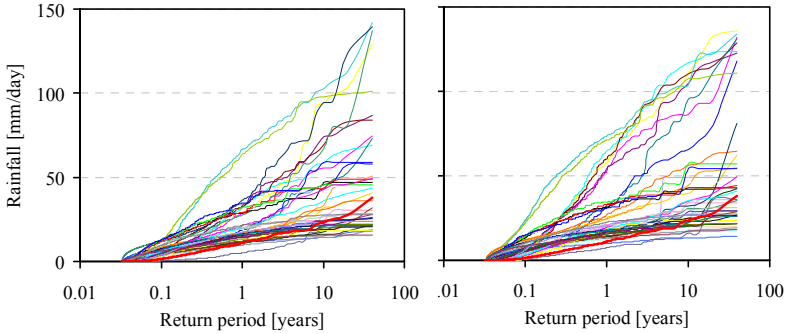

Figure 5.5 Frequency distribution of the rainfall for the month of January (left) and April (right). The thin lines are for the several models and the thick line (red) is for the observation.

It can further be seen from Figure 5.5 that some GCM runs are, in fact, outliers in their respective totality. Most GCM runs do not reproduce frequency events with return periods less than 1.2 years while a good number of GCM runs approximate well the frequency events with return periods greater than 1.2 years. That is, the model runs' distribution plots are either far away from or near to that of the observation. For example, the model runs with distribution plots far away from that of the observation are E-R, E-H, CGCM2.3.2a, CGCM3.1(T47), CGCM3.1(T463), PCM1, CM4 and FGOALS-g1.0.

5.4.5 Selection of climate model runs

It is often preferable to use average results for the selection of the good performing models. A standard method for selecting models is on the basis of their ability to accurately represent current climate. The mean bias (*NME*) was the statistical indicator used to identify good performing models in an objective way. The models with *NME* values greater than twice the coefficient of variation of the observed time series (2*ObsC_V) were considered to have exhibited poor performance. As stated earlier, the consideration of 2*ObsC_V as an objective criterion for model selection was based on the assumption that it approximates the 95% confidence interval under a further assumption of the data being normally distributed. To obtain the mean bias value for each model, the average of the mean bias values for all its available runs were taken (Table 5.1). The *NME* value of the models marked with "*" (Table 5.1) are greater than 2*100*ObsC_{Vr} for rainfall and 2*ObsC_{Vt} for temperature;

where ObsC_{Vr} and ObsC_{Vt} are the coefficients of variation for the observed rainfall and temperature, respectively. Additional model selection criterion was to eliminate models whose projections are inconsistent with those of other models (i.e., outlier models). To achieve this, visual inspections of the charts presented in previous sections were made. The models used in the impact assessment also included those that were considered inconsistent with other models or poor performance (e.g. CGCM3.1(T47), CGCM3.1(T63)) in order to evaluate if such models would project inconsistent results. It was established that such models were projecting disparate results (Chapter 7).

Table 5.1 Ranks of the good and poor performing models based on the mean bias statistic as compared to twice the value of the coefficient of variation of the observation (rainfall and temperature). Rank 1 is for the model with the lowest mean bias value among the considered models.

Rainfall						Temperature					
Rank	Model	Bias (%)	Rank	Model	Bias (%)	Rank	Model	Bias (°C)	Rank	Model	Bias (°C)
1	MIROC3.2(hires)	2.88	12	CGCM3.1(T63)	36.74	1	CM4	0.41	12	E-H*	2.14
2	MK3.5	4.59	13	CCSM3.0*	71.37	2	CM2.1	0.57	13	CM2.0*	2.22
3	ECHO-G	7.18	14	PCM1*	85.53	3	HADGEM1	0.71	14	CCSM3.0*	2.26
4	MK3.0	11.83	15	HADCM3*	95.09	4	MK3.0	1.17	15	E-R*	2.33
5	MIROC3.2(medres)	20.80	16	ECHAM5*	99.12	5	AOM	1.26	16	CGCM3.1(T63)*	2.35
6	CM2.0	21.45	17	FGOALS1.0-g*	106.46	6	BCM2.0	1.39	17	CGCM3(T47)*	2.36
7	CM2.1	21.52	18	CGCM3.1(T47)*	121.48	7	ECHO-G	1.49	18	FGOALS1.0-g*	2.46
8	BCM2.0	28.80	19	CM4*	126.46	8	MIROC3.2(hires)	1.52	19	CM3*	2.48
9	ECHAM4	30.56	20	CGCM2.3.2a*	205.07	9	CGCM2.3.2a	1.71	20	ECHAM4*	2.98
10	CM3.0	31.74	21	E.R*	234.93	10	ECHAM5	1.96	21	MK3.5*	3.37
11	AOM	36.56	22	E.H*	332.10	11	MIROC3.2(medres)*	2.11	22	PCM1*	3.37

5.4.6 Ensemble reliability

The model bias (uncertainty) is reduced when the mean of the values of the simulation variation for all the models are considered and compared with the observation. Figure 5.6(a) shows ensemble mean bias for rainfall and temperature and it is further apparent that the models are positively biased for rainfall and negatively biased for temperature. It can be seen that the bias completely varies with month. For rainfall, the mean of the ensemble mean bias of 40%, for June-August and 170%, for October-November, compared to the ensemble member mean bias of -60% to ca. 700%, if the bias values of all the models are individually considered (Figure 5.6), indicates that the mean of the ensemble values closely approximate observation. Similarly, for temperature, the mean bias of -4.8°C to 4.7°C for the ensemble members, compared to -0.5°C to ca. -2.25°C for the ensemble, gives a conclusion similar to that provided for rainfall. It can thus be deduced that if models with extreme bias are winnowed out, the mean of the values of the ensemble closely approximate the variable values of the observation, hence a substantial reduction in bias. In other words, the ensemble mean value can be more reliable than the individual member. The skeptics of climate models, who say, I quote, “the claim that anthropogenic CO_2 is responsible for the current warming of Earth’s climate is scientifically insupportable because climate

models are unreliable" (Frank, 2008), also do belief that the ensemble average concept is more reliable.

It is imperative to compare the simulation performance of the GCMs for simulating rainfall and temperature. In order to do this, the relative mean monthly bias for rainfall was compared with that of temperature. Figure 5.6 (b) shows that the monthly relative mean bias for temperature resonates about naught compared to that of rainfall. The implication is that the bias for temperature for each month is smaller than that of rainfall. Thus, the simulation ability of GCM for temperature is better than that for rainfall.

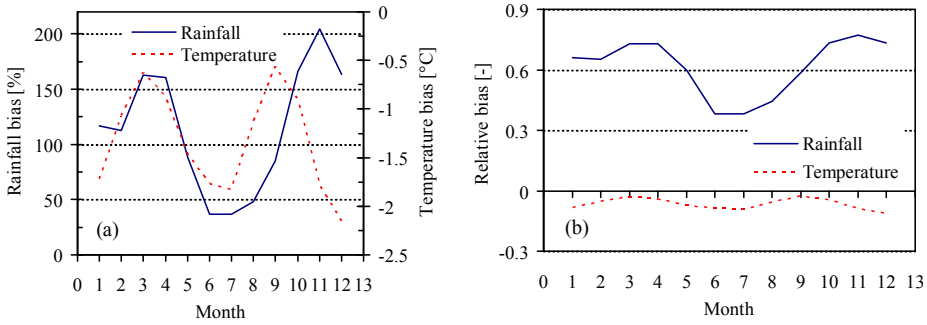

Figure 5.6 Ensemble bias (a) and simulation strength (relative bias) for the rainfall and temperature.

5.5 Conclusions on climate model runs evaluation

Assessment of the performance of the AR4 GCMs to reproduce rainfall and temperature, based on their simulation runs for the 20th century (20c3m), has been performed for the Lake Victoria basin. Statistical performance indicators were mainly used. The findings demonstrate the abilities and the limitations of the climate models to simulate past and current climate. It is unraveled that the climate models generally overestimate rainfall and underestimate temperature over the Lake Victoria basin. The annual monthly pattern, both for the intensity and frequency, however, matches that of the observation and is better for rainfall than temperature. The patterns for the wet- and dry frequency are well represented in the GCMs than for the intensity. Nevertheless, the mean temperature is better simulated than the rainfall intensity (or volume).

The bias in the GCMs cannot be ignored; especially regarding their selection and application to climate change impact assessment. First, models that are extremely biased can be sieved out of impact assessment simply because its simulation ability for the current and past climate is also extremely unrealistic. Secondly, the bias in the GCMs means that it is inappropriate to use their outputs directly for climate change impact assessment at local scale. Furthermore, Christensen et al. (2008) noted that significantly biased models

for the current and past climate have potential to transfer significant bias into the future projections. However, because the patterns in the current and past climate seem to be well represented in the GCM, its pattern prediction (or signal) may be reliable. Thus, the need to remove the bias directly, through bias removal technique or indirectly through downscaling, is vindicated.

The model internal parameterization seems to play a bigger role in their simulation skills than the scales of construction (e.g. spatial). Generally, there was no evidence in the evaluation results to suggest that higher spatial resolution models perform better than lower spatial resolution models. This is because of the fact that the model with the highest spatial resolution (CCSM3.0), among the models considered for evaluation, did not prove its ability to be better than some models with lower spatial resolutions (e.g. CM4 and ECHO-G). If a run of a GCM is extremely poor, all its other runs also tend to be poor and vice versa. Similarity in both the frequency and quantile bias among most of the GCM runs suggests that the differences in the internal parameterization may not be very big.

Conventionally, GCMs are most often assessed for the historical performance alone. However, for a more robust impact assessment, the inter-comparison of the future projections is also vital (Nyeko-Ogiramoi, et al., 2010). This is because models that have good ability in estimating the observed rainfall may not necessarily produce robust predictions (close to or in the same direction as the other models). Models that perform well for historical periods but are projecting disparate future changes should be examined further for performance. It is likely that because, for example, rainfall is an intermittent variable, the complex climate system may introduce inconsistencies for the future climate. Disqualifying a model from further analysis because it is inconsistent with other models is vindicated only if further examination shows a previously overlooked bias against the observed data. The inter-comparison of the projections aims to increase the confidence in the GCM projections while eliminating spurious projections. In addition, the differences in the future projections (controls and projections) if combined with the differences in the current simulation (controls and observation) can enhance the understanding of the effects of the model bias on the future projections.

Evaluation studies are valuable as they identify the weaknesses and spot the models whose performance is questionable. The inconsistencies of the AR4 GCMs with the observation over the Lake Victoria basin suggest further tasks for the climate model scientist. That is, further improvements of the GCMs construction are necessary to increase on the confidence for the assimilation of their outputs. However, the performance of climate model is regional or catchment based and should be treated as such; the conclusions of performance are mainly valid for the studied area.

CHAPTER 6

STATISTICAL DOWNSCALING OF CLIMATE MODEL RUNS

6.1 Introduction

Assessment of climate change impacts on hydrometeorological variables, such as rainfall and temperature at regional or local (catchment) scale, requires projected future time series. One of the common sources of such future times series are GCM runs. However, direct use of GCM runs may not be appropriate for climate change impacts assessment at catchment scale because the scales in GCMs are not at par with the scale at catchment level. For example, if the magnitude of the biases in rainfall and temperature is very high, there is a tendency for the impact signals in the GCM to be amplified under very wet and dry conditions (Christensen et al., 2008). Thus, the need for circumventing the biases in or downscaling the GCM runs. Once projected future time series such as rainfall and temperature are derived through downscaling, they can, either be assessed for impacts by comparing them with the observed or used as inputs into a rainfall-runoff model in order to obtain future streamflows time series. The latter can be compared with the present day control streamflows; hence, impacts on streamflows can be assessed. Therefore, methods are needed to downscale or remove bias from GCM outputs and the results should be appropriate for use at local scale.

Downscaling can be dynamical, through the use of an RCM with GCM as the boundary condition (e.g. Christensen et al., 2007) or through statistical (empirical) methods conditioned on large-scale predictors (e.g. Fowler et al., 2007). In most cases outputs from RCM are also biased and biased removal (e.g. Piani et al., 2010) is often employed. Often, bias removal involves some form of transfer function derived from the observed and simulated cumulative distribution functions (e.g. Ines and Hansen, 2006). This method is given a wide range of nomenclatures in literature such as statistical downscaling, quantile mapping, histogram equalizing and rank matching among others. In applying a hind-cast-derived correction to simulations of projected climate, it is assumed that the correction still holds for the projected climate. This is a non-trivial assumption (Trenberth et al., 2003). However, the assumption is more plausible provided the transfer function between the raw and the corrected RCM output is robust. In many regions of the world (e.g. Africa) data limitation will continue to be a major constraint for the calibration of the RCMs (Anyah and Semazzib, 2007; Christensen et al., 2007) and the use of other methods is sought. Bias correction is sometimes applied to GCM data (e.g. Ines & Hansen, 2006).

In a statistical regression method a purely statistical relation is sought between a model field that is well-represented on the large-scale (predictor), e.g., sea-level pressure or the height of the 500 hPa level, and the local quantity of interest (predictant), e.g., precipitation or temperature (Benestad et al., 2008). Assuming that the relation still holds in a changed climate, the changes of the large-scale circulation directly translate into the local changes that are of interest. Note that the predictant needs not be a variable of the global model, but can be anything related to climate. The great advantage of the statistical method is that it is easy and computationally simple. Nevertheless, (long) time series of both the predictor and the predictant are needed to calibrate the regression model. While the first requirement is usually not a problem, the second limits the applicability of the method to a limited number of places and to surface variables only.

The "delta" downscaling technique uses the concept of change factors (multiplicative or additive) extracted from the climate models and applied to observed series. The former has been tested by several researchers (e.g. Diaz-Nieto and Wilby, 2005; Lenderink et al., 2007). The traditional delta technique applies the changes to a time series without considering the variability of the time series. The technique assumes that relative changes obtained from the climate models are more representative than the absolute ones. Furthermore, it is assumed that the biases in the control (present) simulations are similar to the biases in the future simulations. Thus, the temporal structure of the derived time series is maintained. With significant changes in the variability of time series under climate change the delta method may not be suitable. The earlier attempts to improve on the approach included examining various scenarios (Prudhomme et al., 2002), and applying quantile scaling techniques (Harrold and Jones, 2003) to account for the variability in the time series. Olsson et al. (2009) and Willems and Vrac (2011) demonstrated that deriving future time series that considers changes in extremes is possible through the use of exceedance probabilities. This approach ensures that there is increased variability in heavy rainfall amounts compared to meek rainfall events. This approach is simple, robust and can be applied to any set of data without worrying about the length of a previous record. However, the omission of other changes such as wet spells, which has strong synchrony with the extremes, in precipitation downscaling makes the approach further faulty. Accounting for change in wet spells can improve precipitation downscaling and impact(s) results focusing on extremes.

Previous studies have used and compared different downscaling techniques and have concluded that the choice of the method is dependent on the nature of the study and that more research is needed to improve on available downscaling techniques (Fowler et al., 2007). The tenet of this chapter is centered on the quantile perturbation technique because it properly accounts for the downscaling of extremes and thus correctly enables the assessment of

the impact of climate change on extremes of hydrometeorological variable such as precipitation. Improvement of the technique is here suggested and applied to data from catchments in a tropical climate.

6.2 Synchrony between wet extremes and wet spells

Analysis of projected changes in climate by Meehl et al. (2007) showed that the type, frequency and intensity of extreme events are expected to change even with relatively small mean climate changes. Meehl et al. (2007) noted that in a warmer world, precipitation tends to be concentrated into more intense events, with longer periods of light precipitation in between. Thus, intense and heavy downpours would be interspersed with longer relatively dry periods. Furthermore, Meehl et al. (2007) noted that wet extremes are projected to be more severe where mean precipitation is expected to increase and dry extremes are projected to become more severe in areas where mean precipitation is projected to decrease. In concert with the results of projected increased extremes of intense precipitation, even if the wind strength of storms in a future climate did not change, there would be an increase in rainfall intensity (Meehl et al., 2007). Kharin and Zwiers (2005) and Barnett et al. (2006) noted also that the increase in extreme events might be perceived most through the impacts of extremes. The implications are that changes in wet extremes are, quite often, associated with longer wet spells. The need to consider the characteristics of the wet spells is paramount in improving the precipitation downscaling techniques that employ the quantile perturbation approach. Thus, this chapter mainly explores the technique of employing the characteristics of wet spells in and for the improvement of the quantile perturbation approach for downscaling precipitation.

6.3 Perturbations

In this chapter, perturbation is referred to as any change that can be obtained from the GCM scenario and control runs or the observed time series. That is, the properties (or statistics) of the GCM control run (series) are compared with those of the GCM future series to obtain changes (perturbations) that are projected under the different climate change scenarios. Note that changes that occur in quantitative hydrometeorological variables, such as rainfall and evapotranspiration, can be obtained in many forms (e.g., ratios, percentage, difference). Meanwhile changes that occur in qualitative meteorological variable such as temperature can mainly be derived as differences. Different perturbations, for rainfall and temperature time series, can be extracted and analysed based on the different months or seasons and for different GCMs. In the context of this study, emphasis is put on analysing perturbations for daily rainfall because it is an essential variable of climate, which is needed for hydrological impacts of climate change. The main principle behind perturbation is that several perturbations can be isolated or extracted from GCM paired (control and scenarios) data at different aggregation levels and

can be analysed for their respective properties. In the subsequent sections, perturbations for rainfall are analysed for daily rainfall for each month. The results are presented mainly for the months of January and April for typical illustrations. This is because of the fact that January and April are considered representative of dry season (dry months) and wet season (wet months), respectively, of the climate of the case study. For temperature, an example of the perturbation for maximum daily temperature (T_{max}) is given. Lastly, a nonparametric methodology for the downscaling of the GCM time series to local scale forms the last sections of this chapter.

6.3.1 Rainfall perturbations

6.3.1.1 Rainfall wet-day quantile perturbations

Derivation and analysis of rainfall perturbation can be performed for rainfall time series at different time scale. However, in this case, the focus is on the daily time scale and the perturbations were derived by considering daily rainfall time series for each month, separately. In other words, the time series for each month for all the considered years are pooled together before perturbations are derived. Perturbations are derived only for the wet-day frequency of the rainfall series.

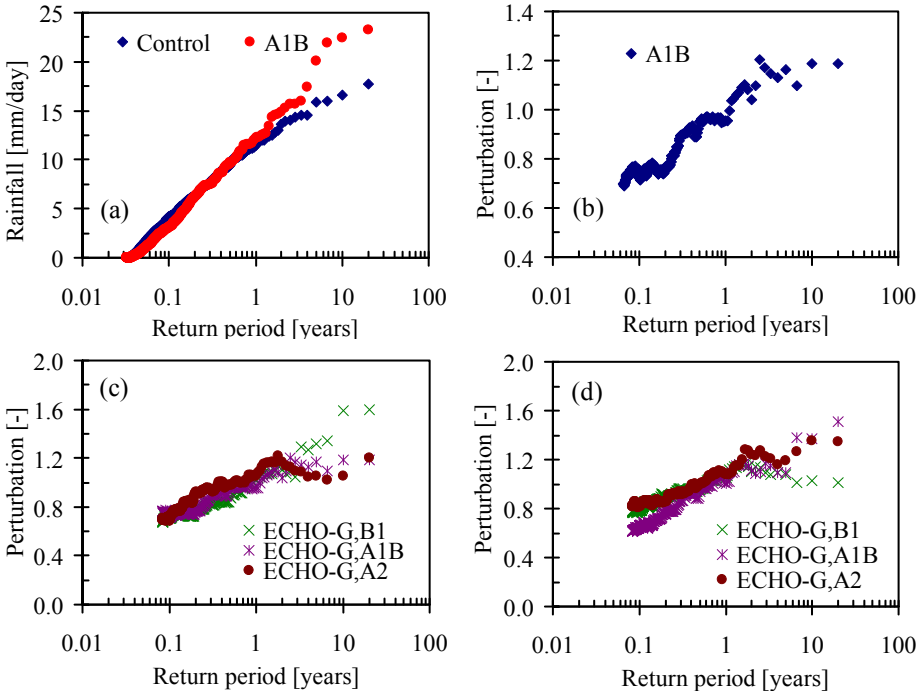

Figure 6.1 Distributions for January rainfall for the control and scenario (A1B, 2050s) (a), and the corresponding perturbations (b), and 3 scenarios (B1, A1B, A2) for the 2050s (c), and 2090s (d). The control and scenarios are for one GCM (ECHO-G) to

illustrate the typical perturbations for the two periods. The results are for the GCM data extracted from a grid over the River Katonga catchment.

The definition of a wet day is given in the next section. If $q_{s1} \geq q_{s2} \geq q_{s3} \ldots q_{sn}$ represent the scenario quantiles and $q_{c1} \geq q_{c2} \geq q_{c3} \ldots q_{qn}$ represent the control quantiles, quantile perturbations are derived as q_{si} / q_{ci}, for $i = 1, 2, 3, \ldots n$. In the case where n in scenario and control are not the same, interpolation is used exceedance probability based on exceedance probability. That is, perturbations can be derived as $P_p = Q_{s,p} / Q_{c,p}$, where P_p is the perturbation corresponding to probability p, $Q_{s,p}$ the future scenario value (for the same probability p) and $Q_{c,p}$ the control value (also corresponding to probability p). The plot of quantile perturbations versus the return period (or exceedance probability) can reveal the effect of projected possible warming for the future.

Figure 6.1 shows an illustration of the January daily rainfall distributions for a 20-year period (Figure 6.1(a)) and the corresponding plot of perturbation versus return period (Figure 6.1(b)) for the control and the future periods. Perturbations for different scenarios and the corresponding plots for different future scenarios, projected for the periods 2050s (Figure 6.1(c)) and 2090s (Figure 6.1(d)), can similarly be obtained. Note that the daily rainfall distribution and the perturbation plots, provided in Figure 6.1, represent evolutional stages of rainfall perturbations analysis of an example of one GCM (ECHO)-G). Perturbations analysis for other GCMs can also be obtained and analysed in a similar.

6.3.1.2 Dependency of the rainfall wet-day quantile perturbations

The effects of climate change on the light and heavy rainfall events can be exposed by examining the perturbations plots. Such effects can be analyzed for different temporal scales such as daily, weekly, monthly and seasonal. For a tropical climate, where the interest of this study lies, the climate is characterized by mainly wet and dry seasons. However, it is important to note that for a given season, daily rainfall variations among the months can be very high. Thus, analysis of perturbations for daily rainfall series for each month is particularly important.

Figure 6.2((a) and (b)) shows plots of perturbations versus return period for the months of January and April, respectively, for the period 2050s. For January, the perturbations are generally greater than 1 for the heavy rainfall events (> 1 year). However, the perturbations are less than 1 for lighter rainfall events (< 0.2 years). The perturbations for the mean rainfall events are, fairly, constant (0.2-0.4 years). It is important to note that for some GCMs (models) the perturbations are less than 1 between 1.1-1.4 years return periods. This variation of the perturbations for the heavy, mean and light rainfall events has implications for the changes in the rainfall intensity and frequency. First, it is expected that given a rainfall intensity of a return period less than 1 year, the intensity is projected to decrease from the current to the

future. Secondly, given a rainfall above 1-year return period, the intensity is projected to increase from the current value to the future for the most heavy rainfall events.

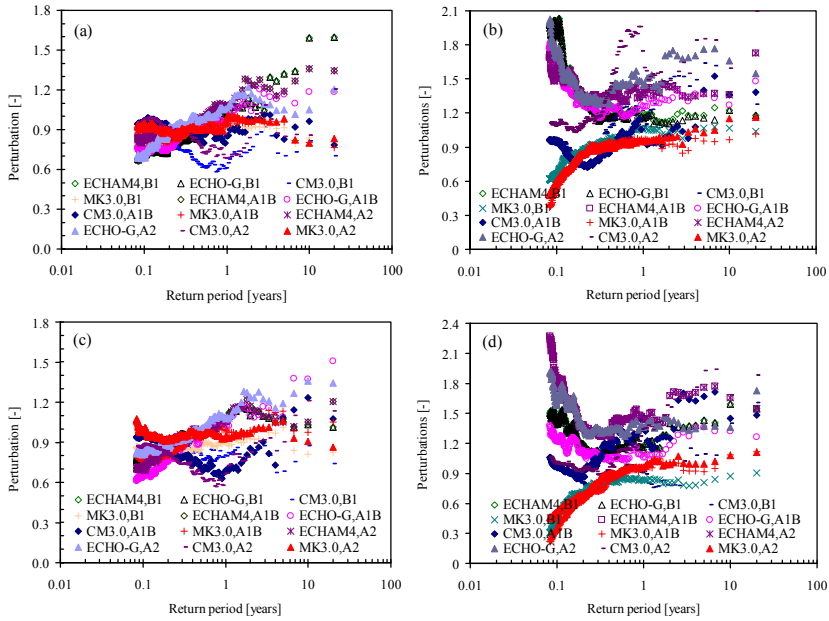

Figure 6.2 Perturbations for the daily rainfall: (a) January, 2050s, (b) April, 2050s, (c) January, 2090s and (d) April, 2090s. The perturbations are for 4 GCMs to illustrate the typical perturbations for a relatively dry month (January) and a relatively wet month (April). The results are for the GCM data extracted from a grid over the River Katonga catchment.

In the latter case, the rainfall intensity for the medium heavy rainfall events is expected to decrease as projected by some GCMs. Thus, for the dry months, the dry days will become moderately dryer and the very wet days will become much wetter. In some cases, the frequency of such wetter events will increase. For the month of April (Figure 6.2(b)) the perturbations are dramatically higher than 1 for return periods less than 0.2. This is the case for 9 out of 12 selected GCM runs irrespective of the scenarios. For return periods less than 0.2 the perturbations are generally greater than 1 but increase with return period moderately. For three models perturbations are less than 1 for return periods less than 1 years.

The variation of the perturbations with return period for the month of April also has implication for the projected changes in the rainfall intensity and frequency. The rainfall events are expected to strongly increase compared to the current but with moderate increase in their frequencies. Thus, more wet days are projected for the wetter months and the rainfall intensity is projected to increase compared to the current. However, the projections by some models indicate that as the intensity and frequency of the heavy events strongly

increase and the magnitude of the mean rainfall events remains constant, the rainfall intensity and frequency of the light rainfall events is projected to decrease compared to the current. In the latter case, it means that less rainfall is projected (dry days becoming dryer) coupled with a decrease in frequency. It is noteworthy, however, that perturbations become very sensitive (very high factors) as the return period decreases and the lighter events for the control series tend to zero. This is particularly important to note because further discussions are made in section 6.6.1.1.

The differences in the variation of the perturbations for the low (B1), middle (A1B) and high (A2) scenarios, and for the two different future periods 2050s and 2090s can only be discerned by examining Figure 6.1(c) and (d) or isolating a case for a model from Figure 6.2. For return periods < 1.1 years, the differences in the magnitude of the perturbations among the scenarios are not very eminent and are consistent for both the 2050s and 2090s. However, for a return period > 1.1 years, the perturbations are eminently different for low, middle and high scenarios and inconsistent for both the 2050s and 2090s. If many models are compared (Figure 6.2), the differences in the variation of the perturbations for the low, middle and high scenarios become trivial and the intermodal variation becomes fundamental. An important point to note is that perturbations are very sensitive when light rainfall events of very low return periods are considered. That is, the values of the perturbations can be dramatically low or large for meek rainfall events with intensity close to naught. In the latter case, it is recommended to derive perturbations while considering only the days above a certain-carefully-selected threshold intensity value or particularly wet days, which buffers the sensitivity of the perturbations.

6.3.1.3 Wet days and wet-day frequency perturbation

Schmidli & Frei (2005) defined wet days as the annual count of days with daily precipitation greater than or equal to a certain threshold precipitation value (e.g. ≥ 1 mm). In contrast, dry days are defined as the annual count of days with daily precipitation less than a certain threshold precipitation value (e.g. < 1 mm). Thus, wet days of a given month can be defined as the monthly count of days with daily precipitation greater than or equal to a certain threshold precipitation value (e.g. ≥ 1 mm or ≥ 0.1 mm). Given the fact that the frequency and intensity of precipitation are projected to change, as learned from the perturbations of rainfall intensity, wet days are also projected to change and it is possible to obtain a wet-day frequency perturbation and analyze its variation for the different scenarios and models. Thus, the monthly wet-day frequency perturbation is simply referred to as wet-day perturbation.

The wet-day perturbation is calculated as the ratio of the projected (scenario) total number of wet days to the corresponding total number of wet days in the control period and can be calculated as follows:

Let $(X_p)_{i,m}$ be the model daily time series of a given month, m, corresponding to the control of the p^{th} GCM, $p \in \{1,\ldots,M\}$, M is the number of control simulations or the GCMs, and let $(Z_{p,s})_{i,m}$ be the model time series for the projected scenario, s, $s \in \{1, \ldots, W\}$, where W is the total number of projected scenarios, for $i = 1, 2,\ldots, n$, and for month $m = 1, 2, \ldots, 12$. Note that n is the total number of years of the model simulations. If, $t_{c,m}$ is the threshold rainfall intensity for a given month, m, the wet-days perturbation is given by

$$\Delta d_{p(m)} = 100 * \left(\frac{d_{p(s,m)} - d_{p(c,m)}}{d_{p(c,m)}} \right) \tag{6.1}$$

where, $\Delta d_{p(m)}$ is the projected percentage change in wet days for a given month, m, $d_{p(s,m)}$ and $d_{p(c,m)}$ are the respective total number of wet days with intensity $> t_{c,m}$ in scenarios and control. Note that the control and future periods considered are 1971-1990 (control) and 2045-2065 (2050s) and 2081-2100 (2090s), respectively. Thus, $n = 20$ years.

Figure 6.3 shows the wet-day perturbations for 16 GCM runs for high, middle, and low scenarios, A2, A1B and B1, and for two different projected future periods (e.g. A2, 2050s for Figure 6.3(a)). For the months of January-May, the wet-day perturbations are generally greater than 1 but are less than 2. In contrast, the wet-day perturbations are also generally greater than 1 for the months of October-December but are greater than 2 for some models. Meanwhile, for the months of June-September the wet-day perturbations are generally less than 1. It can further be seen from Figure 6.3 that the perturbations for the months of April-May and October-November are relatively higher for the months where perturbation values are greater than 1. In addition, for the months where perturbations are less than 1, its values, for the months of June-August are relatively lower. Note that the wetter months are April, May, October and November; and the drier months are mainly June-August. Thus, the implications of the differences in the perturbations for the different months are that the wet days, in the wet and dry seasons, are projected to increase and decrease, respectively, in the future. The increase in the wet days will vary with the high, middle, and low scenarios. The high scenario (Figure 6.3(a) and (d)) reveals more increase in wet days than middle scenario (Figure 6.3(b) and (e)); and middle scenario (Figure 6.3(c) and (f)) reveals more increase in wet days than for the low scenario. If the charts in the left column (for 2050s) and the ones in the right column (2090s) of Figure 6.3 are compared, it can be seen that the increase and decrease in the wet days for the wet and dry seasons, respectively, are projected to be relatively higher for the 2090s than for the 2050s.

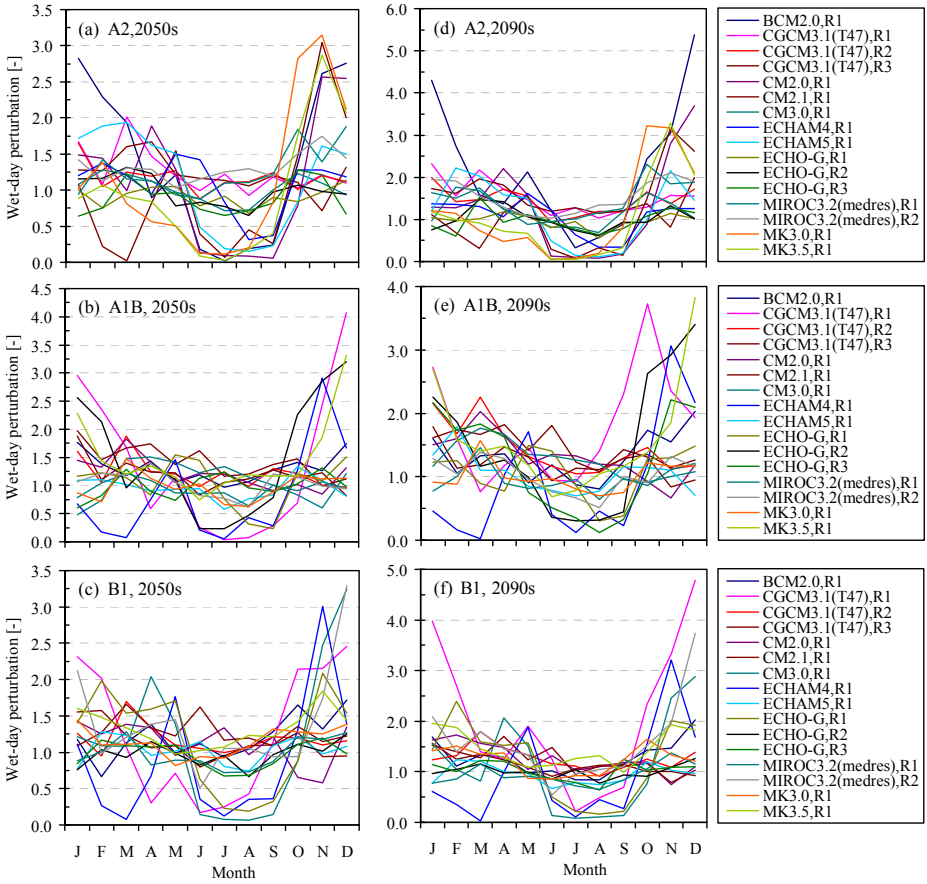

Figure 6.3 Typical monthly wet-day perturbations for the GCM runs calculated for a grid over the River Katonga catchment.

6.3.1.4 Wet spells and mean wet-spell length perturbation

A wet spell is defined as the number of consecutive wet days in a time series in which precipitation intensity exceeds a certain threshold precipitation value (Lall et al., 1996). The length of a wet spell is measured in days. Wet spells are considered one of the most important indicators of extreme precipitation indices. The basic indices of wet spells include, but are not limited to: (1) the maximum number of consecutive wet days in which the total precipitation is greater than or equal to a certain amount, and (2) the mean wet-spell length, which is the average length of the wet spells in a month, season or year (Schmidli & Frei, 2005). These indices represent characteristics of the duration of consecutive wet-day sequences (Schmidli & Frei, 2005). The latter is particularly of interest to this study.

Analysis of the projected changes in wet spells provides insight into how the future rainy days, as projected by the climate models, will be like. As established in the analysis of the wet-day perturbations that the wet days are

projected to change, it is important to assess how the increase in the wet days, for example, affects the mean wet-spell length. Study by Yue-Cong and Barry (2010) on how climate change may influence the demand for water in the future, under the different climate change scenarios, showed that changes in wet spells would have significant implications for water supply.

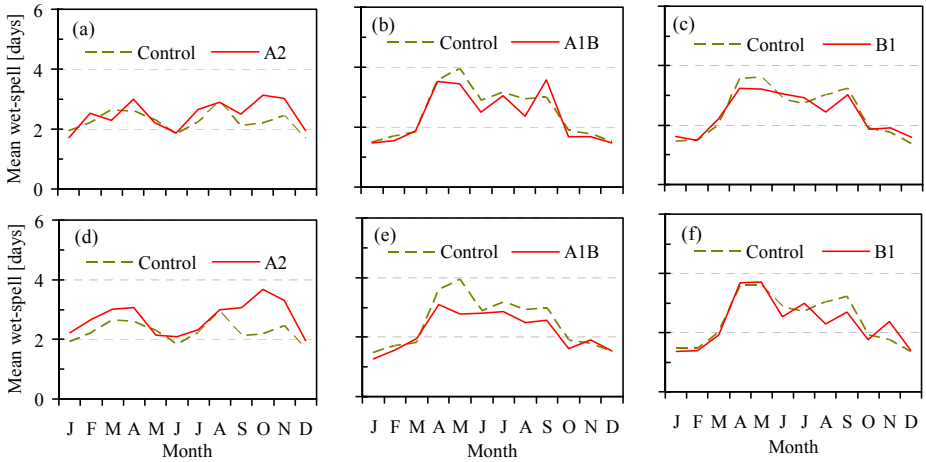

Figure 6.4 Typical monthly mean wet-spell length for the rainfall data of a GCM (MIROC3.2(medres),R1) run calculated for a grid over the River Katonga catchment for the 2050s (a)-(c), and 2090s (d)-(f).

Given GCM runs (control and scenarios), and if 1 mm/day is the threshold precipitation that defines a wet day in the control run ($t_{c,m}$), the mean wet spell length for a given month can be obtained. Similarly, the corresponding mean wet spell length for the scenario can also be calculated based on $t_{c,m}$. This procedure can be repeated for all the months, scenarios and considered GCMs. Figure 6.4 shows an example from one GCM run under the high, middle and low scenarios for the periods 2050s and 2090s to illustrate the typical mean wet spell lengths in the control and scenario runs. It can be seen that under the high scenario (2050s), the mean wet spell length for the months of January and March is projected to decrease with respect to the present whereas for the months of February, April, July and September-December, it is projected to increase (Figure 6.4(a)). Figure 6.4(d) shows that the increase in the mean wet spell length for the months of March-April and September-November will be relatively higher. The implications are that the increase in mean wet spell length for the wet months is probably a manifestation of longer wet spells under the high scenario. In addition, the increase in the mean wet spell length in the 2090s will be higher than that in the 2050s under the high scenario. Under the middle scenario (Figure 6.4(b) and (e)), the plots for the scenario run lie below that of the control run for both the 2050s and 2090s mainly for the very dry (June-August) and very wet (April-May) months. This implies that the GCM run generally projects a decrease in the mean wet spell lengths for both the very dry and very wet months with a relatively no change

for the other months. The model, under the low scenarios, however, projected little change (Figure 6.4(c) and (f)).

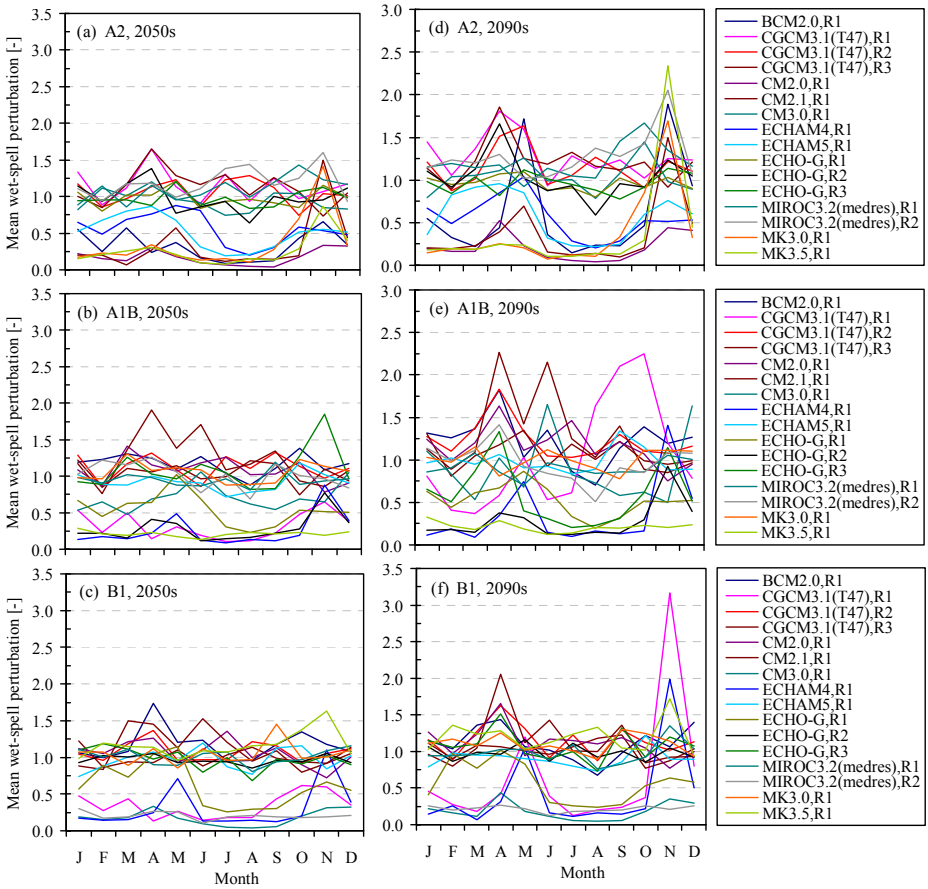

Figure 6.5 Typical monthly mean wet-spell perturbations obtained from the daily rainfall of 16 GCM runs extracted from a grid over the River catchment.

Perturbation of mean wet spell is calculated as the ratio of the mean wet spell for the scenarios series to that of the control and can easily be represented in terms of percentage. If $w_{p(s,m)}$ and $w_{p(c,m)}$ is the mean wet spell for scenario and control series, respectively, given by

$$\rho_{p(m)} = \left(\frac{w_{p(s,m)}}{w_{p(c,m)}} \right) \tag{6.2}$$

where $\rho_{p(m)}$ is the mean wet spell perturbation and the equivalent percentage change is given by

$$\Delta\rho_{p(m)} = 100 * \left(\frac{w_{p(s,m)} - w_{p(c,m)}}{w_{p(c,m)}} \right) \tag{6.3}$$

Figure 6.5 shows monthly mean wet-spell perturbations of 16 model runs under high, middle and low scenarios for two different future periods. It can be seen that there is a "band of plots" with the mean wet-spell perturbation that resonates around 1, with some completely below 1 and others (for the month of November) willowing out (Figure 6.5(a)). A similar pattern for the former can be seen in Figure 6.5(d) but with a shift in the upper "band of plots". Figure 6.5(d)-(f) further shows that for models with mean wet-spell perturbations of less than 1, the mean wet-spell perturbations are generally less than 0.5 for most models except for the months of May and November. Similarly, Figure 6.5(d)-(f) also shows that for the models with mean wet-spell perturbations greater than 1, the mean wet-spell perturbations generally fall in the range 1-1.25 except for the months of April and November. Figure 6.5(a)-(f) also reveals that the mean wet-spell perturbations for the months of February and August are less than 1 for most models. It can also be seen that the "depression" in the plots for the models with the mean wet-spell perturbation of less than 1 is eminent for the months of June-September.

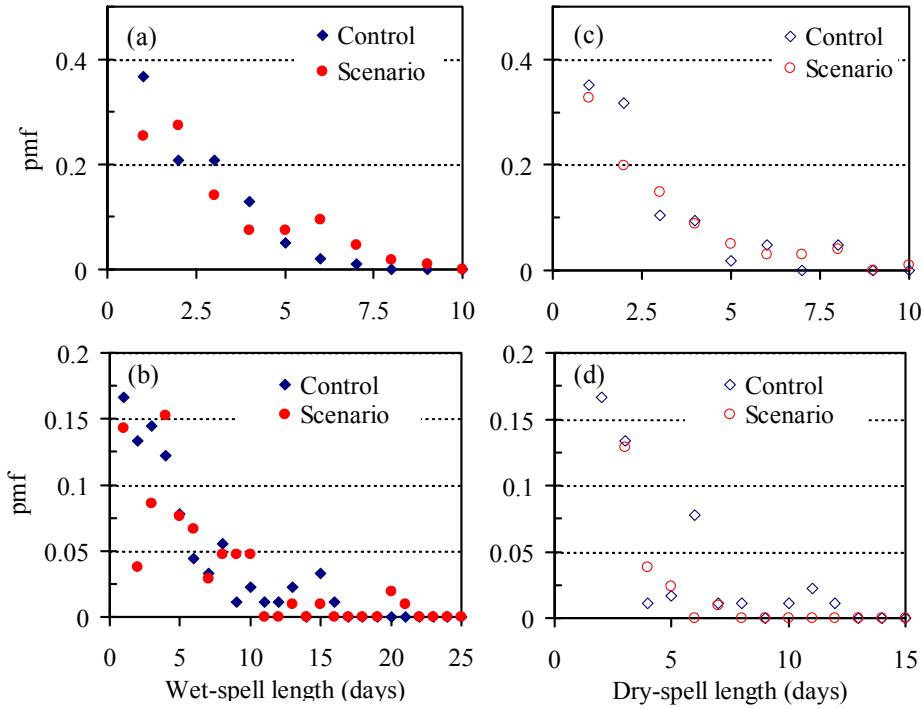

Figure 6.6 Typical distributions for: (a)-(b) wet spells, (c)-(d) dry spells for (a) and (c) January, and (b) and (d) April for an example data set for a GCM run (CGCM3.1(T47),R2) under the A2 scenarios, 2090s, extracted for a grid over the River Katonga catchment.

The preceding discussions have implications for the changes in the wet and dry spells. First, the mean wet spell for the wet seasons is projected to increase and the wet spells for the wetter months will increase more than that

for the less wet months. Secondly, for dry season where the mean wet spell is projected to decrease, the wet spells in the drier months will decrease more than that in the less dry ones. Furthermore, the change in the mean wet spell implies that the distributions of both the wet- and dry spells will alter. Figure 6.6 shows the distributions of the wet/dry spell lengths for the months of January and April. The ordinates and the abscissa of the plots (Figure 6.6) represent the relative frequency (pmf) and the days, respectively. It can be seen that the proportion of wet spells with length of one day is projected to reduce and the proportion of wet spells of length of 2 days will dominate (Figure 6.6(a)). Meanwhile, the proportions of the wet spells of length 2-3 days will reduce in the future. The wet spells of length greater than 4 days are projected to increase. The implication of the latter is that increase in the frequency of longer rainy days may be linked to river flooding.

Figure 6.6(c) shows that, generally, the proportion of the dry spells will reduce for the dry months. Figure 6.6(c) shows that the proportions of wet spells of lengths between 3-10 days will increase and this means that the current longer wet spells are projected to be longer. For both the dry and wet months, the wet spells of length between 4-10 days are projected to increase. Thus, the frequency of the wet and dry days are projected to increase and reduce, respectively. Furthermore, the increase in the mean wet spell length may be a manifestation of the increase in the wet spells with longer lengths.

6.3.1.5 Mean rainfall wet-day intensity perturbation

The perturbation of mean intensity for the wet days is obtained by comparing those for the scenarios and control runs. Figure 6.7 shows the percentage change in the monthly mean daily rainfall intensity of 16 model runs for the high, middle and low scenarios for two different future periods. Figure 6.7 shows that the percentage change in the monthly mean daily rainfall intensity for January-May and October-December will generally increase as compared to the control run. The increase is projected to be within 5%. However, the projections for some models are above 5% especially for the months of November and December. The increase in the monthly mean daily rainfall intensity for the months of January, March, October and December will relatively be higher than that of the other months whose monthly mean daily rainfall intensity are projected to increase.

Changes in the monthly mean daily rainfall imply that the mean volume of the rainfall received in a month will change but the change is projected to be little. The projection for the increase in the mean rainfall intensity for the wet months is higher, compared to drier months. The mean rainfall intensity for the dry months is, however projected not to change much from the current state. Figure 6.7 may suggest that the change in each category of rainfall events are suppressed if the mixtures of different events such as the meek, medium and heavy are pooled together and their mean change is considered.

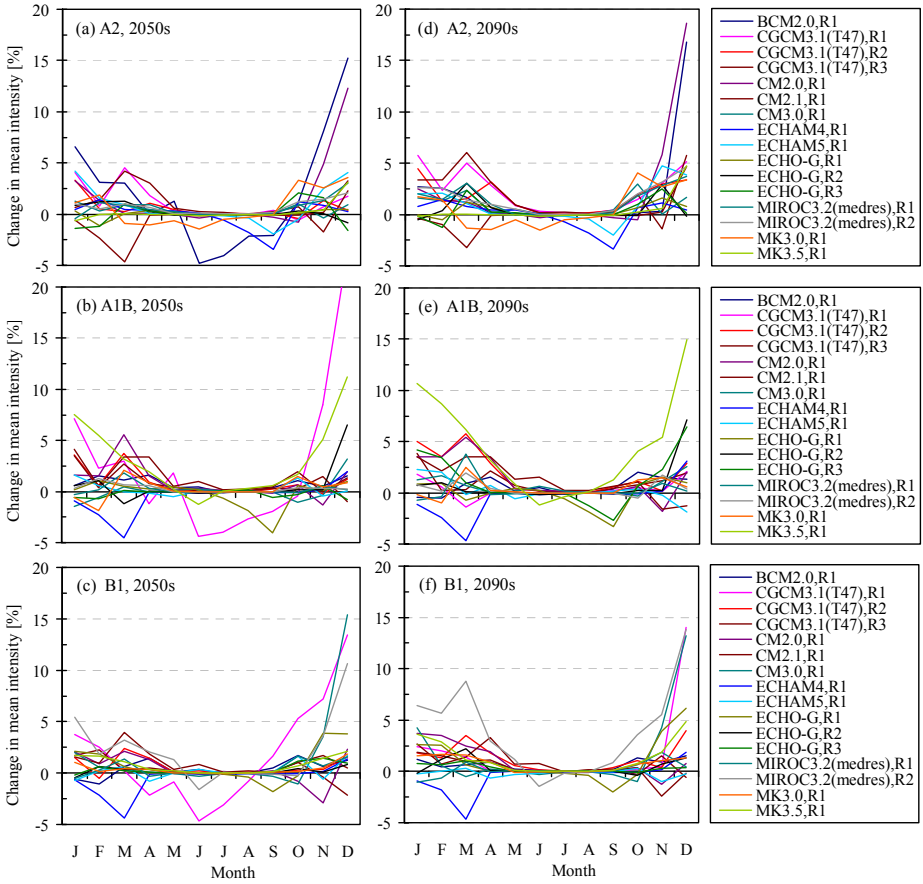

Figure 6.7 Typical monthly perturbation of the mean of the daily rainfall wet day intensity for 16 GCM runs extracted for a grid over the River Katonga catchment.

6.3.1.6 Perturbation of the C_v of rainfall wet-day intensity

Figure 6.8 shows the percentage change in the coefficient of variation, C_v, of the monthly daily rainfall intensity for the wet days as projected by 16 model runs under the high, middle and low scenarios for two different future periods. C_v is a measure of the variability from the mean value and for the current subject matter, it indicates the change in the variability of the daily rainfall from the monthly mean daily value. Figure 6.8(a)-(c) shows that for a future warmer world (A2 scenario), the change in C_V is projected to be in the range -50–+500%.

For the middle scenarios the projected change in C_V is in the range -50–+300% and for the future cooler world (B1 scenario), the change in C_v is projected to be in the range -50–+400%. Figure 6.8(d)-(f) however shows that the ranges of change in the C_V for the high, middle and low scenarios are -50–+300%, -50–+250% and -50–+300%, respectively. The difference in the range of the change in C_v for the periods 2050s and 2090s is thus appear not to be significant. Furthermore, it can be seen from Figure 6.8 that the change

in C_v is within -50% and 100% for the months of October-May. Thus, the change in the variability of the monthly daily rainfall is projected to be higher for the dry season (June-September) than the wet season (October to May).

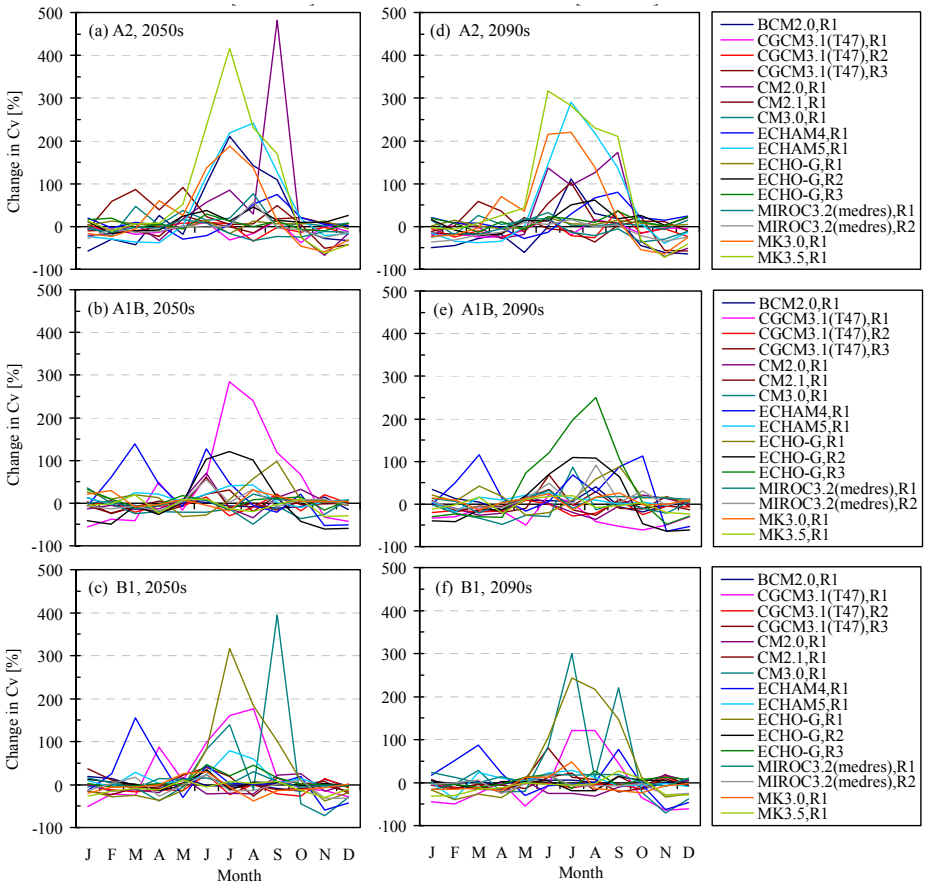

Figure 6.8 Typical monthly perturbations of the C_v of the daily rainfall wet-day intensity for 16 GCM runs extracted for a grid over the River Katonga catchment.

6.3.2 Temperature perturbation

Perturbations of temperature can be calculated as the difference between the values of the scenario and control runs with same exceedance probability. Note that in order to obtain realistic perturbations of temperature, the units of the temperature data may need to be in degree Kelvin (°K). The GCMs temperature data however are in units of °K. The absolute zero temperature equivalent in different units are 0°K = -273.15 centigrade (°C) = -459.67 Fahrenheit degrees (°F). If T is the temperature value in °K, the equivalent in °C is (T -273.15). Thus, after the derivation of the temperature perturbations, which have the same units as the units of the temperature itself, the results can be converted or presented in degree centigrade or Celsius (°C) where necessary. Figure 6.9 shows plots for the change in the mean of the T_{max} for

the classical illustration only. Some researchers have described such plots (Figure 6.9) as "spaghetti" like because it is difficult to discern prominent features among the plots; perhaps "grasshopper" terms is appropriate. It is apparent that the change in temperature for the 2090s is higher than that for the 2050s.

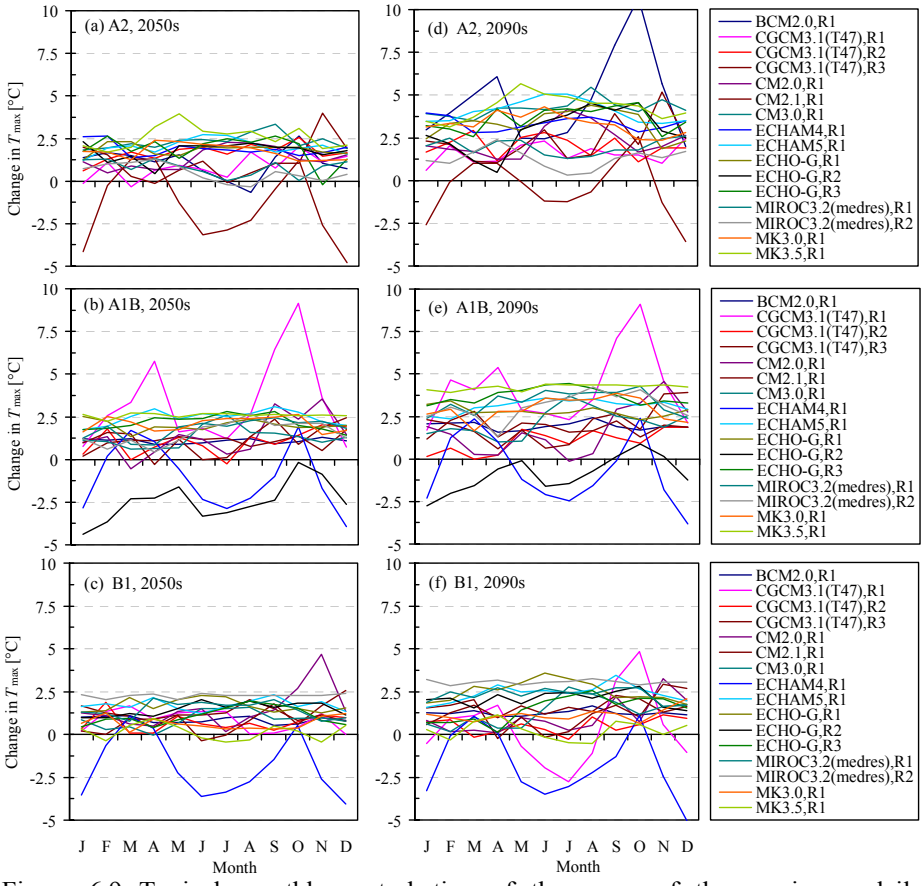

Figure 6.9 Typical monthly perturbation of the mean of the maximum daily temperature for 16 GCM runs extracted for a grid over the River Katonga catchment.

Given the available model, the 2050s projection change in T_{max} is within 0-2.5°C. Similarly, for the 2090s, the projected change in T_{max} is within 0-5°C. If the change in the monthly mean of the T_{max} is compared with that of the mean rainfall intensity for the same month (e.g., March), a unit increase in the monthly mean T_{max} produces about 2% increase in the monthly mean of the wet-day rainfall intensity. This temperature–rainfall change relationship is important because the two variables interact in a physical way.

6.4 Climate change signals

The changes (perturbations) extracted from the GCM control and scenario runs such as rainfall intensity, wet-day, mean wet spell length, mean and C_v of the daily rainfall for each month are referred to as climate change signals (CCS). If we assume that the bias in the control run runs is similar to the bias in the scenario runs then CCS are bias-free. The transfer of the CCS to observed time series (OS) at local scale would thus produce perturbed observed series (POS) which have similar statistical properties as the projected future time series. In the context of this study, we refer to the process of transferring the CCS to OS as a nonparametric statistical downscaling of GCM runs based on adaptive perturbation approach. The procedure for transferring the climate change signals is discussed in section 6.6.

6.5 Conclusions on perturbations and climate change signals

The change (perturbation) between GCM scenario and control runs provides useful information on climate change signals in the hydrometeorological time series. Such climate change signals, if carefully extracted, can provide substantial preliminary information on climate change impacts at local scale. A methodology that can transfer CCS to OS at local scale with minimum error margins would constitute an important nonparametric statistical downscaling of GCM runs. The resulting downscaled time series can be used in hydrological climate change impacts at local scale.

6.6 Perturbation approach to statistical downscaling

The CCS, considered important for capturing change can be transferred to OS using perturbation approach without explicit assumption of the underlying distribution to obtain POS. A number of nonparametric approaches are used in stochastic hydrology to generate weather variables (Lall, 1995). An approach is considered nonparametric if (1) it is capable of approximating a large number of target functions, (2) it is "local" in that estimates of the target function at a point use only observations located within some small neighborhood of the point and (3) no prior assumptions are made as to the overall functional form of the target function. In the perturbation approach, some CCS are used to perturb OS to obtain POS such that the other CCS are used for validation of POS. Once POS is obtained and validated, it can be employed in climate change impacts assessment at local scale.

6.6.1 Downscaling of rainfall

In the downscaling of the daily rainfall time series, two CCS are considered: (1) the wet-day rainfall intensity perturbations, and (2) mean wet-spell length perturbations, as the most important signals to transfer to OS. The mean and the coefficient of variation of the wet-spell rainfall intensity, the mean wet-

spell length and the distribution of the wet spells are the statistics used in the validation of POS. In the following sections, we discuss how each of the selected signals (CCS) is transferred to observed series and validated.

6.6.1.1 Wet-day climate change signals

The wet-day intensity perturbations (perturbation factors) are calculated based on the procedure described in section 6.3.1.1. However, a methodology for choosing a threshold intensity value that defines a wet day in the GCM control series (CS) is revised by involving OS. Let t_o be the threshold wet day rainfall intensity selected to define a wet-day for OS. The corresponding wet day rainfall intensity value for CS, t_c, is the value that makes the number of wet days in the OS equals the number of wet days in the CS provided CS is positively biased. If CS is negatively biased, the value of t_c is taken to be the same as t_o. This is to ensure that all the properties of the wet days in OS, POS, CS and scenarios series are correctly estimated and to eschew "chaos" from wet-day intensity perturbations with low return periods. For example, if the GCM is positively biased and t_o = 1 mm, $t_c > t_o$ (e.g. t_c = 8.2 mm). Thus, all the properties of the wet days in both the CS and the GCM scenario series (SS) are calculated by considering the value of t_c. Figure 6.10 shows an example of the threshold wet-day intensity values for 16 different CS for all the months as compared to t_o = 0.1 mm of an observed time series. It can be seen that the CS can be highly biased positively with, for example, 0.1 mm daily rainfall for the month of December in observed time series simulated as 16 mm by the GCM (ECHAM5).

The values of the wet-day intensity for the OS are ranked and the exceedance probability of each data point is calculated based on its rank number. Similarly, the values of the wet-days intensity for SS are ranked and the exceedance probability of each data point is calculated based on its rank number. Perturbation is therefore the ratio of the wet-day intensity for SS to that of the CS with same probability. Note that if the SS has more wet days than the control run, the exceedance probability points are also more than that of the CS and OS. Thus, the perturbations of the extra wet-day intensity values of the SS are obtained by interpolating over the wet-day intensity values of CS. The perturbations are then applied to the wet-day intensity of the OS to obtain POS. In the case where more wet days are projected by the SS the extra wet-day perturbations are also applied to the wet-day intensity values interpolated over wet-day intensity values of OS. Note that this methodology ensures that the extra wet-days (projected increase in wet-days) are added during the application of perturbation factors to OS. If the GCM projects a decrease in the number of wet days then the wet-day intensity perturbations are only applied to the OS based on exceedance probability "equation" and the extra wet days in OS are converted to dry days. Figure 6.11(a) and (b) shows the wet-day intensity before and after application of perturbations, respectively. The procedure described above was carried out for

each month but for all the years of the time series records. The POS is then resorted to enable transfer of CCS for the mean wet spell length. The properties or the statistics of the resulting POS are compared with the statistics of the OS to obtain climate change signal at local scale (CSL).

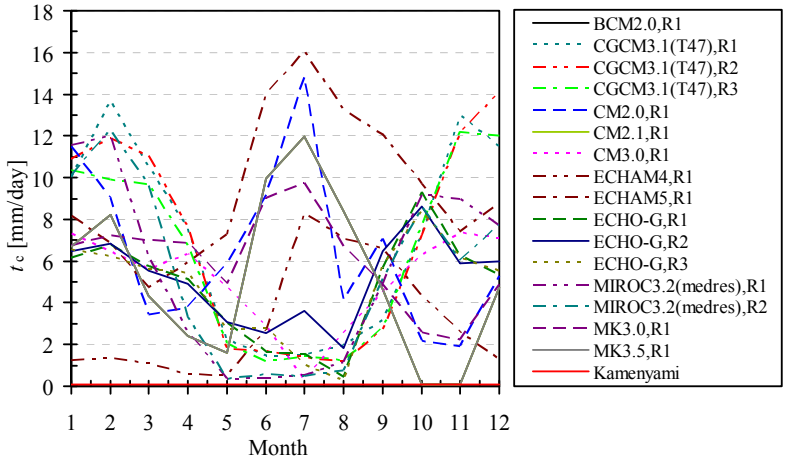

Figure 6.10 Typical threshold for monthly wet-days daily intensity for different CS compared to t_o = 0.1 mm for an observed time series (Kamenyami) for a GCM grid over the River Katonga catchment.

6.6.1.2 Wet-spell climate change signal

The transfer of the mean wet-spell length perturbation is only considered after the perturbations of the wet-day intensity. The wet spells to be adjusted are those in POS. There are only two cases of change to be considered in the mean wet spell length: an increase or a decrease in the mean wet spell. In the case of an increase in the mean wet-spell, each of the wet spells in POS greater than their mean value is adjusted by the mean wet-spell perturbation. That is, each of the wet spells in POS greater than their mean value is extended by giving it additional wet days. The value(s) of the wet-days intensity to be added, in order to extend a wet spell, is/are obtained through a non-parametric resampling technique using kernel density estimates (Lall et al., 1996) described in section 6.6.1.3. For the case of a decrease in the mean wet spell, each of the wet spells in POS greater than their mean value is reduced by the mean wet-spell perturbation. The reduction of each of the wet spells with length greater than their mean value is carried out by extending the dry spells bounding the target wet spell. That is, extra wet days in the target wet spell are converted into dry days by removing the required number of wet days located at the ends of the wet spell and replacing them with dry days. The statistics of POS are calculated and compared with the statistics of OS to obtain adjusted climate change signal at local scale (CSLa). CSLa is validated against CCS and if the error margins are small enough, the modified POS (POSa) is the downscaled GCM run, which represents the projected time series at the local scale. Note that the wet days to be added are considered

days with missing value(s) and is/are added at the ends of the target spells in a proportional way. That is, the wet and dry spells are assumed independent and no transition to the same spell is possible.

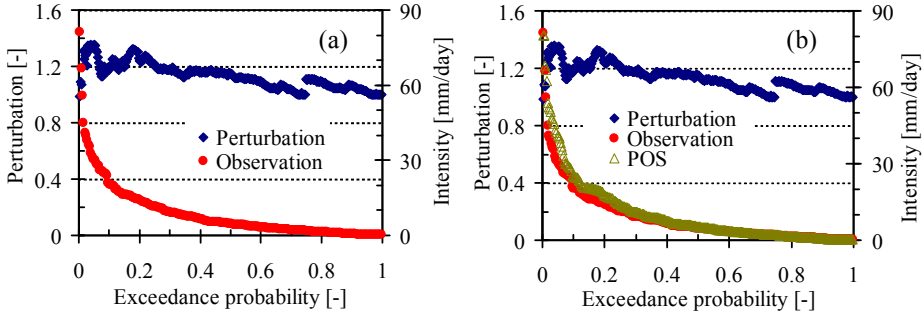

Figure 6.11 Typical wet-day daily rainfall intensity for the OS before (a), and after (b), the application of the perturbations. The OS is the areal rainfall data over the River Katonga catchment and the GCM data is also extracted from a grid superimposed on the River Katonga catchment.

The application of wet-spell perturbation to OS, in downscaling GCM runs, is similar to the nonparametric approach used for generating weather variables in which the wet/dry spell approach is used. There are two major advantages of considering perturbation of wet spells in the perturbation approach for downscaling GCM runs. First, compared to other perturbation (or change factor) approaches (e.g., Olsson et al., 2009; Willems and Vrac, 2011; Ntegeka, 2011), the rainfall wet and dry spell structures in the OS and the change in the mean of the OS wet spell lengths as projected by GCM are both considered concurrently. Secondly, the distributions of the wet and dry spells can easily be validated against that of the GCM. That is, the distribution of the spell signal can be validated graphically. However, as noted by Lall et al. (1996) the justification of the independence between the wet and dry spell lengths at short time scales is difficult. Nevertheless, the data are allowed to inform the wet-spell perturbation process to ensure that very long wet spells separated by a very short dry spell are not merged.

6.6.1.3 Kernel density estimation method

Probability density function (PDF) estimation is of major concern in areas such as hydrology. In parametric density estimation, the assumption is that the random variable (data) are drawn from a specific density model. The model parameters are then fitted to the data. Unfortunately, in many cases an a priori choice of the PDF model is not suited since it might provide a false representation of the true PDF. Kernel density estimation is a robust non-parametric way of estimating the PDF of a random variable. The technique does not assume any functional form of the PDF and allows its shape to be entirely determined from the data. It is a fundamental data smoothing process where inferences about the population are made based only on a finite data

sample. Kernel density estimates (k.d.e) are closely related to histograms with the former having several advantages. A comprehensive overview of the nonparametric density estimation techniques can be found in Izenman (1991). The paper by Lall et al. (1995) presents a comprehensive nonparametric approach to a stochastic model for generating daily precipitation based on k.d.e. The salient features of the model were the consideration of the alternating wet and dry spells of a daily rainfall structure within the wet spells. k.d.e were espoused as effective methods for recovering univariate, multivariate (conditional), discrete and/or continuous probability densities that were directly required from the histogram record. In Lall et al. (1996), kernel density estimators of the continuous and discrete variables were critically reviewed and tested with various data sets. The k.d.e methods have garnered favours for generating weather time series for various applications with Rajagopalan et al. (1997) and Rajagopalan and Lall (1999) expanding the methods to "*k*-nearest neighbours resampling". Lall et al. (1996) stated that sampling from k.d.e compared to sampling from the empirical distribution of the data itself lead to a reduced variance of the popular Monte Carlo design. The aim here is to take advantage of the flexibility and robustness of the kernel density estimator for daily rainfall to generate daily precipitation from which it can be resampled to extent the wet spells in POS.

The continuous, univariate PDF of interest is the $f(p)$, the PDF of daily precipitation in which the data set is composed of n_p days of daily rainfall values, p_i, for the wet-day rainfall intensity of a given wet spell in a month. A logarithmic transform of the rainfall data prior to density estimation is often attractive because it can provide an automatic degree of adaptability of the bandwidth selection (Lall et al., 1996). The resulting k.d.e is written as

$$\hat{f}(p) = \frac{1}{n}\sum_{i=1}^{n}\frac{1}{hp}K\left(\frac{\log(p)-\log(p_i)}{h}\right) \tag{6.4}$$

where h is the bandwidth of the log-transform data, $K(\ )$ the kernel density function. The paper by Sheather and Jones (1991) provides a recursive method of selection of the bandwidth, h. The target distribution from POS can be constructed using the k.d.e. Lall et al. (1996) provides some useful examples of kernel density estimators for both the continuous and discrete random variables. One such kernel density estimator is $K(t) = 0.75(1 - t^2)$ for $t = (x - x_i)/h$, for a random variable X. The normal kernel ($K(x) = h^{-1}\phi((x - x_i))/h)$) is a robust estimator and is often recommended for use when dealing with real-valued random variables that tend to cluster around a single mean value and was used in this study. ϕ is the standard normal density function. Once the k.d.e is constructed using PQS, it is possible to generate a random number, x, that follows the estimated distribution.

The kernel estimation procedure is discussed as follows: Consider the original POS (p_i, $i = 1, .., n$) from which the kernel density that depends on p, and h

was constructed using kernel function $K(\ )$. To generate a random number X that follows the estimated distribution, do the following: (1) Sample a random integer j uniformly between 1 and n. That is, identify the POS data to perturb. (2) Generate a random variate R from the probability density corresponding to the kernel function $K(\ )$ (e.g., $K(r) = h^{-1}\phi((r - r_i)/h)$). This reinforces the notion that the k.d.e is formed as a convolution of local densities centered at each data point and that the generated sequence will constitute a smooth bootstrap of the data. Lall et al. (1996) further noted that any of a number of standard procedures (e.g., based on order statistics or rejection) fro sampling from a density may be used to generate R from the density $K()$.

6.6.1.4 The overall flow chart for the downscaling method

The downscaling process applied in this study involves the following seven steps. (1) Choose from OS the threshold rainfall intensity that defines a wet day and obtain from CS the corresponding rainfall intensity value that defines a wet day in CS and SS. Select and calculate the CCS from CS and SS needed to perturb OS. (2) Calculate the wet-day intensity perturbations from CS and SS by considering rainfall quantiles with same exceedance probability. Note that the exceedance probability is calculated based only on the wet-day component of the time series. If there are more wet days in SS than in CS, the additional quantiles for CS are obtained by interpolation over its ranked series. (3) Modify each of the OS quantiles by the intensity perturbation to obtain POS. Note that additional wet days are added through interpolating over OS for additional quantiles and are modified by the extra perturbation factors obtained in step (2). (4) Calculate CSL and validate them against CCS obtained in step (1). (5) Transfer the mean wet-spell length perturbation through extending or reducing the length of each of the wet spells greater than their mean value. Use k.d.e (e.g., normal kernel) to generate intensity values from which you can sample to extend the required wet spells. (6) Calculate the new CSL after the application of the wet-spell length perturbation (CSLa) and validate it against CCS. If the respective error between CSLa and CCS is small enough, the final POS is POSa (POS modified by wet-spell perturbation); if not, repeat steps (5)–(6). (7) Examine the distributions of the wet spells graphically for visual satisfaction.

6.6.1.5 Validation of the results

The key aspect in the wet-spell technique of the perturbation approach for downscaling GCM runs to local scale is the validation of the climate change signals. Four important characteristics of a rainfall time series for deriving climate change signals needed for the validation of the results are: (i) mean wet-days daily intensity, (ii) mean monthly volume of the wet-day intensity, (iii) mean wet spell length and (iv) coefficient of variation of the wet-day intensity. This section presents an example of one GCM to illustrate the typical validation result. Figure 6.12 shows the validation results for the selected climate change signals. The perturbation represents the change or

ratio of the time series feature between the control and target scenario series for the different months. The plots represented by continuous, dot and dash lines are for CCS (*x*SS/CS), CSL (*x*POS/OS) and CSLa (*x*POSa/*x*OS), respectively, where *x* represents the time series feature or statistic under consideration.

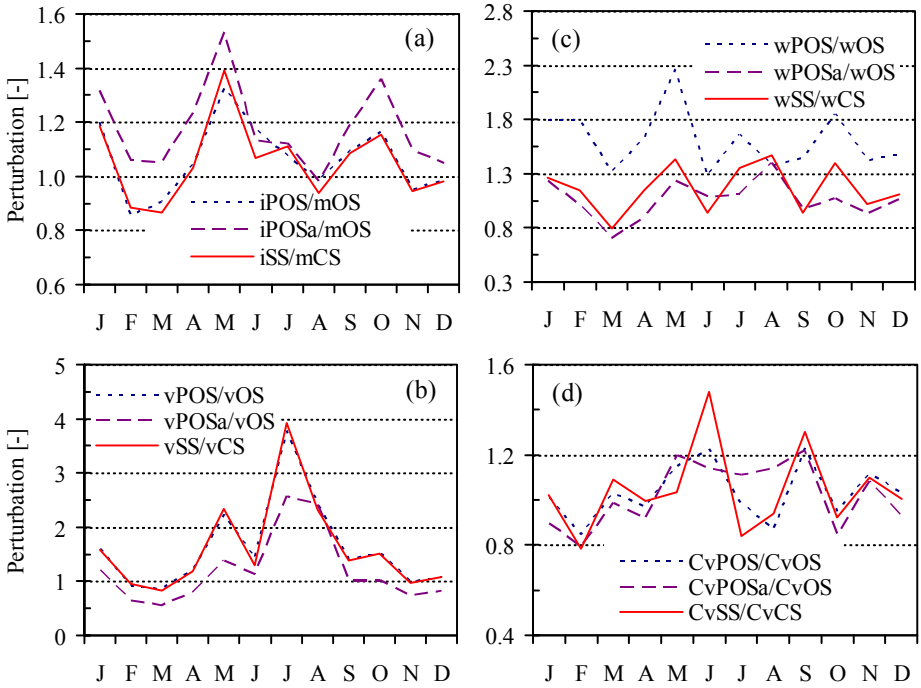

Figure 6.12 Typical validation results for the climate change signals: (a) mean wet-day daily rainfall intensity, (b) monthly mean volume for the wet-day rainfall intensity, (c) mean wet spell length, (d) coefficient of variation for the wet-day daily rainfall intensity for an example GCM run (CGCM3.1(T47), R2). The results are for the data extracted from a GCM grid over the River Ruizi catchment.

The time series features, $x = i, v, w, C_v$, represent intensity, volume, mean wet spell length and coefficient of variation, respectively. It can be seen that application of wet-day intensity and wet-days frequency perturbations to OS can perfectly transfer the CCS for intensity and volume (Figure 6.12(a)-(b)). In addition, the change in variability (C_v) is also well transferred simply by applying the wet-day intensity and wet-day frequency perturbations (Figure 6.12(d)). However, the transfer of the wet-day intensity and wet-day frequency perturbations alone does not "honor" in any way the CCS for the wet spells, except or perhaps by chance (Figure 6.12(c)).

Figure 6.12(a) and (c) reveals that the transfer of the wet-day intensity and wet-day frequency perturbations alone to OS results in perturbed observed series which has "inflated" value of the mean wet-spell length above the one projected by the climate model. Figure 6.12(a)-(b) indicate that adjustment of

POS series to reflect change in the spells, as projected by the model, results in reduction of the volume of the time series, especially in the case where the model projected decrease in the mean wet-spell. However, the reduction in the mean wet-spell is an indication that the mean wet-days intensity will increase (Figure 6.12(a)). In general, Figure 6.12 shows that the mean wet spell length is projected to reduce but the intensity of the rainfall will increase. The latter is projected to influence the change in the variability of the intensity and volume of the rainfall for the very dry months or season (June-August).

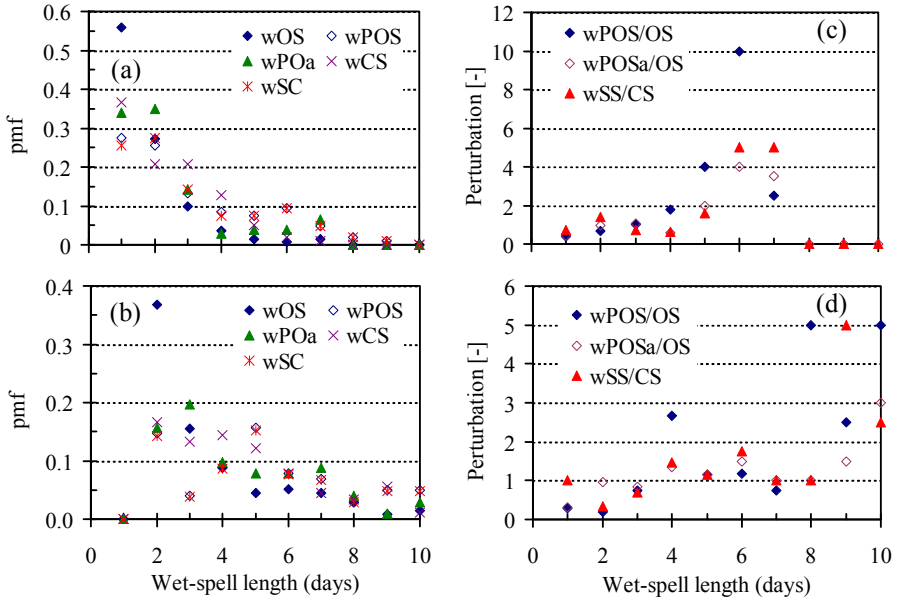

Figure 6.13 Typical validation results for the wet spells distribution: (a)-(b) January (b)-(c) April for an example GCM run (CGCM3.1(T47), R2). The results are for the data extracted from a GCM grid over the River Katonga catchment.

(a) Distribution of wet spells

From the preceding section, it is clear that the model projected an increase in the mean wet-day intensity and mean monthly volume. Furthermore, a balanced increase and decrease in the mean wet spell length for the dry and the wet months, respectively, are projected. However, what does this mean for the frequency of wet spells and intensity distribution. Figure 6.13(a)-(b) shows the distribution of the wet spells for the months of January and April. The ordinate represents the relative frequency or the proportion of the wet spell of a given length (between 1-10 days) in that month for a period of 20 years. Figure 6.13 (c)-(d) show the change in the distribution of the wet spells. From Figure 6.13(c)-(d), it can be seen that application of the perturbation for the mean wet spell length substantially improves the distribution of the wet spells in POS to follow the expected shape. Furthermore, it can be seen from Figure 6.13 that there are more wet spell events with length less than 3 days for the month of January compared to April, which has less wet spell events

of length less than 3 days. The wet spells with length between 3-5 days dominate the wet spell events for the month of April. Figure 6.13 shows that the proportions of wet spells of length 5-7 for January and 4-7 days for April, are projected to increase for both the months of January and April. Taking into account that intensity is projected to increase, the increase in longer wet spells has implications for the land areas with very high runoff coefficient and poor drainage. The longer wet spells events are more likely to results in river flooding than shorter ones. Note that, albeit the changes in the distribution of the wet spells of several other GCM runs were analyzed for both the 2050s and 2090s, and for different observed data, the results presented here are not in any way exhaustive.

(b) Distribution of rainfall series

Figure 6.14 shows the distribution versus return period for the daily rainfall of eight different months. Generally, it can be seen that the rainfall intensity with lower exceedance probability are projected to increase more than those with higher exceedance probability. In addition, it can also be seen from Figure 6.14 that generally, the intensity of POSa with exceedance probability between 0.08 and 0.1 will not change so much from that of OS. However, from Figure 6.14(b), (f) and (h), it can be seen that the distribution of the POS for the mean rainfall events are above those of OS. This implies that application of the rainfall intensity and wet-day frequency perturbations alone without explicitly considering the perturbation for the mean wet spell length results in an overestimation of the mean rainfall events (also see Figure 6.1). Consider Figure 6.14(b)-(c) and given an exceedance probability value less than 0.08; projected distribution for POS and POSa lie above the distribution of the OS. Similarly, the distributions for POS and POSa lie below the distribution of OS for an exceedance probability value greater than 0.1. These changes imply that the values of the intensity for the mild and heavy rainfall events are projected to decrease and increase, respectively, for that month. Figure 6.14(f)-(h) also shows similar changes. Thus, the mean of the wet-day intensity will increase for the wet months, which is consistent with the results of the increase in the mean of the wet-day intensity provided in Figure 6.12(a). However, Figure 6.14(a) shows that the intensity for both the meek and heavy events will decrease. In contrast, Figure 6.14(e) shows that the intensity of both the meek and heavy events will increase.

Further more, Figure 6.14(d) shows that the intensity of the medium events and heavy events will decrease and increase, respectively. Thus, for the dry months, consistent change pattern is not eminent. Figure 6.15(a) shows the distribution for OS, POS and POS, whereas Figure 6.15(b) shows the original perturbations derived from the control and scenarios runs and those which are derived from observed and the downscaled time series for the month of January. The plots in Figure 6.15(a) can be compared with those for CS and SS (e.g. Figure 6.1(a)). Note that the result is for the same model and scenarios (ECHO-G). It can be seen that the distribution for OS and POSa

follow similar change pattern as the distribution for the CS and SS. This may suggest that Figure 6.12(a) gives a false impression of a perfect match when iPOS/mOS iSS/mCS are compared.

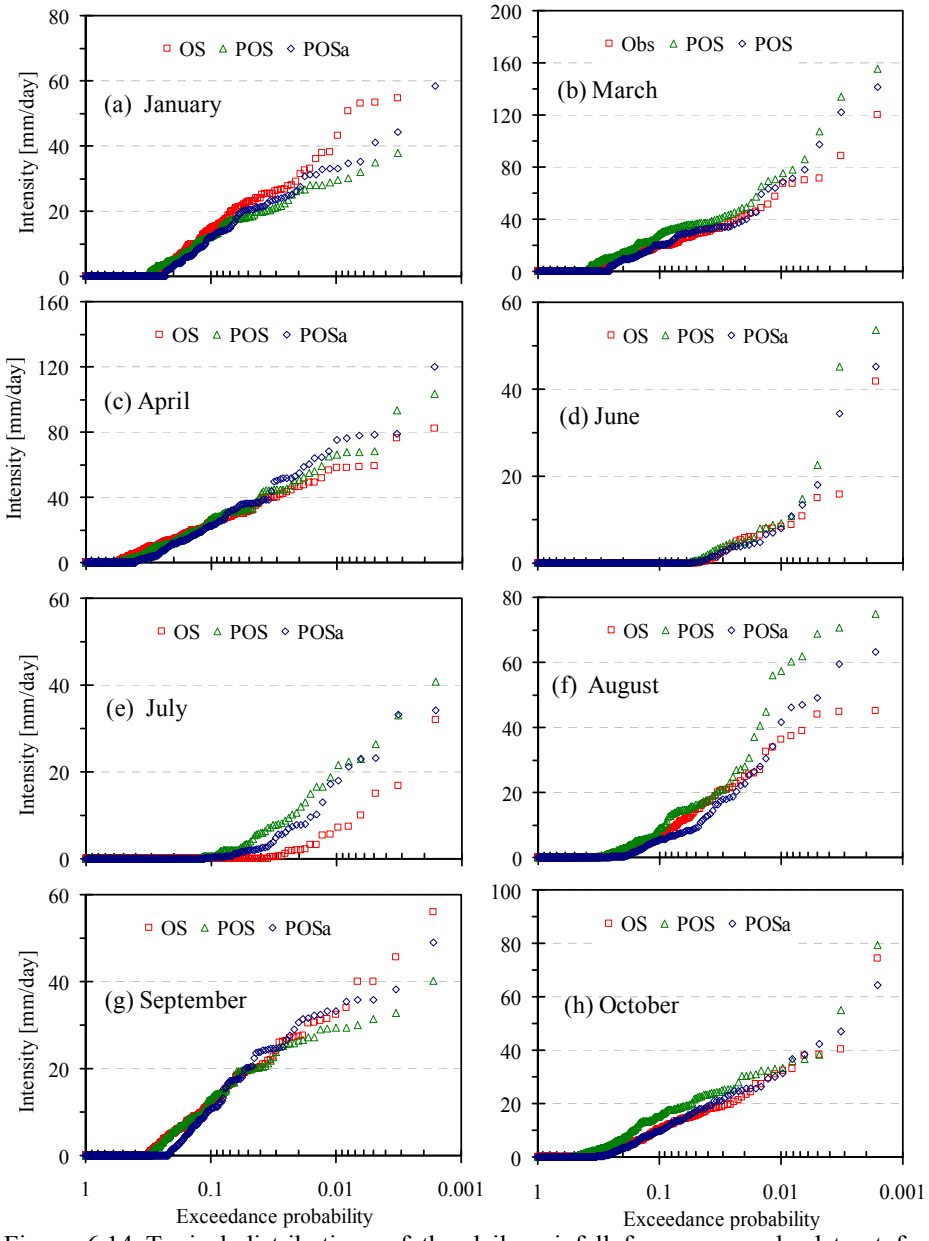

Figure 6.14 Typical distributions of the daily rainfall for an example dataset for different months for a GCM run (CGCM3.1(T47), R2). The results are for the data extracted from a GCM grid over the River Katonga catchment.

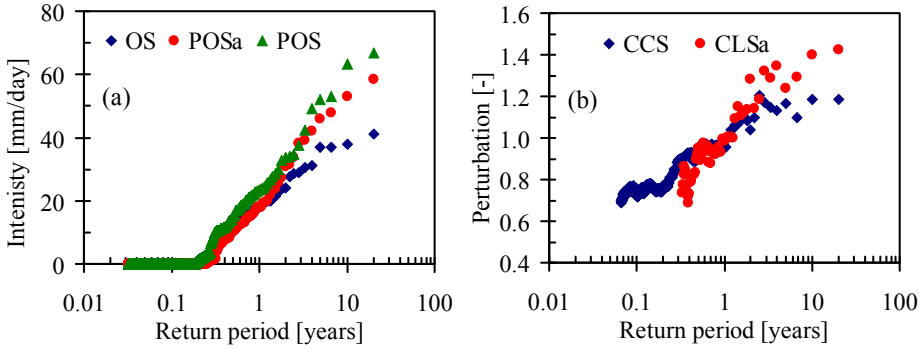

Figure 6.15 Classical distributions for the January daily rainfall (a), and perturbations (b) derived from the SS and CS (CCS) and from OS and POSa (CLSa). The results are for the data extracted from a GCM grid over the River Katonga catchment.

Figure 6.15(b) shows that the actual perturbations needed to be transferred to OS are not the same as those derived from CS and SS if the change in wet spells is to be considered. In the latter case, the perturbations for intensity with heavy rainfall events are actually higher and those for meek events are lower if the change in the wet spell is taken into account.

6.6.2 Downscaling of temperature

Temperature is a more stable time series than rainfall. This makes the derivation of temperature its perturbation much simpler. The change signal extracted from the temperature scenario and control runs is the temperature difference (perturbation). That is, the difference between the temperature scenario and control runs time series with same exceedance probability. In order to perturb the observation, each temperature perturbation was added to the observed temperature point with same exceedance probability. This process can be carried out for each month so that all the 12 months are perturbed in a similar way.

6.7 Conclusions on the downscaling of climate model runs

A non-parametric statistical downscaling of daily rainfall time series from GCM runs that uses a perturbation approach was formulated and applied. The core of the principle lies in the fact that climate change signals can be extracted from the GCM control and scenarios runs in an empirical way without explicit assumption of the underlying probability distribution and applied to the observed time series. The modified observed time series are the downscaled GCM results, which are plausible for climate change impact assessment at local scale. Among the important features of the rainfall time series are the wet spells, wet-day intensities, wet-day frequencies and coefficient of variation and are considered in the perturbation approach. If only wet-day intensity and wet-day frequency perturbations are considered, the resulting time series can still have similar signals of coefficient of

variation. However, it leads to an over estimate of the change in wet spells and intensity. Thus, the changes in the structure of both the dry and wet spells, which are very important temporal features of rainfall, are not captured in the perturbed series. Since hydrological models are very sensitive to rainfall, an overestimate of the change in the wet spells and rainfall intensity for different events may significantly affect the hydrological extremes in the hydrological impact assessment. In order to eschew and buffer these problems, changes in the wet spells need to be considered during the downscaling of rainfall using perturbation approach. One other advantage of considering the wet-spell change in the statistical downscaling of rainfall using perturbation approach is that the changes in the distribution of both the wet and dry spells can be validated through a graphical approach. In addition, the consideration of the wet spell in the perturbation approach preserves the changes in extremes of rainfall as projected by the climate model. Thus, hydrological impacts of climate change on extremes can appropriately be estimated given the fact that rainfall time series is an important input into hydrological model.

Variability of temperature at local catchment scale as compared to rainfall is low. Application of the quantile perturbation method to downscale temperature is carried out in a simple way, which was demonstrated to be adequate and appropriate.

CHAPTER 7

CHANGE IN RAINFALL EXTREMES AND TEMPERATURE

7.1 Introduction

In the previous chapter, we have seen that changes that may occur in the distribution of rainfall because of climate change are likely to affect rainfall extremes more than the mean rainfall events. As noted by Barnett et al. (2006) and Kharin and Zwiers (2005), the risks associated with increase in extreme events has far-reaching implications than that associated with increase in mean rainfall events. Extreme rainfall can have severe impacts on society. It afflicts the worst environmentally related tragedy, which contributes to loss of crops, valuable property and untold human misery. Adverse effects of extremes of rainfall are inform floods and droughts.

Modeling of extreme rainfall events is fundamental part of flood hazard estimation and is applied in many engineering applications such as urban drainage, dam design, farming and irrigation, etc. (Kunkel et al., 1999). In the case of river hydrology, the design of hydraulic systems whose design period is comparable to the time scale associated to the induced climate change has traditionally been based on statistical analysis of extreme events extracted from historical records. This is done based on the assumption that the intensity and frequency of past events is statistically representative of what could happen in the future. Under the influence of climate change, this assumption must be reconsidered to account for the expected changes in the extreme precipitation events (Grum et al., 2006). Thus, it is important to isolate the extremes from the overall rainfall distribution and assess how the projected climate change will affect the extremes for different aggregation levels or time spans over which the mean rainfall intensities are obtained. With the possible amplification of extremes by anthropogenic-induced climate change and the likely worrying projected situation, application of extreme value analysis to analyze rainfall extremes should be able to provide information that put the likely impacts into context. This chapter explores the possible implications of climate change on extreme events on the current study area with a focus on rainfall extremes. The downscaled variables, for selected stations in the current study area are utilized.

7.2 Types of extremes

In stochastic hydrology, the major types of rainfall extremes are the series of AM and the POT or PDS. The technique for extracting AM consists of sampling, for every single year (calendar or water year) of the rainfall time

series, the largest rainfall event (Figure 7.1(a)). When rainfall time series with high temporal resolution are available, the samples are close to real flask peaks. The main disadvantage of this technique is that it can sample events, which are not major extremes while other events of greater magnitude can de disregarded when occurring during a relatively wet year, if a great extreme had occurred. However, AM series are common in hydrological databases and the AM technique is very widely used (e.g. Robson and Reed, 1999), the approach being straightforward and based on a well-established concept. The second main automatic sampling technique, POT, aims to select all the highest independent extreme events recorded (Figure 7.1(b)). The POT consists in all rainfall peaks above a certain threshold (i.e. possibly several events in one year and none in another year) and provides a more complete description of extreme behaviour than AM series (Svensson et al., 2005). In generating a POT sample, it is important to ensure that the selected rainfall peaks are all independent, i.e. the sampling does not select two peaks, which relate to the same larger event mechanism. The details of the POT selection criteria, which results in nearly independent peaks, are described in the next chapter for reference. If the independence criteria are not robust enough, it is possible to sample rainfall peaks, which might result from the same event. The main disadvantage of the POT series is the absence of many long records in hydrological databases, while some rainfall records of the form of AM are sometimes accessible. Its main advantage is that it permits the capturing of all major events much more efficiently than the AM sampling. In particular, the use of POT series allows an estimate of the trend in the frequency (counts) of extremes rather than just their magnitude by calculating the number of POTs that occur each year and investigating the tendency in that series.

There are different types of POT samples or sets of extremes. Depending on the value chosen for the sampling threshold, it is possible to select more POT values than number of years of the original time series. When the threshold is such that exactly N peaks are selected for N years of record (often called POT1 sample), the sample is called Annual Exceedance Series, which is a special case of the POT series (Shaw, 1983). There is a direct link between the chosen threshold and the size of the peak sample: a high threshold will ensure that only the very high extreme events are selected but will lead to reduced sample size. This can be critical in particular for the catchments where the hydrological record length is short. On the other hand, lowering the threshold has the advantage of increasing the sample size and, thus, increasing confidence in the statistical analysis undertaken but may include events that would otherwise be considered as ‘middle-size peaks. In the previous chapter we have seen that for a relatively shorter record length of the GCM data (N = 20 years), significant changes in heavy rainfall events are eminent for events with return periods of approximately 2 years and more. Thus, in order to capture more extremes for impact analysis, it is reasonable to apply an appropriate threshold. Note that albeit the threshold is chosen decisively to

include more extremes for analysis, the selection varies with the aggregation scale.

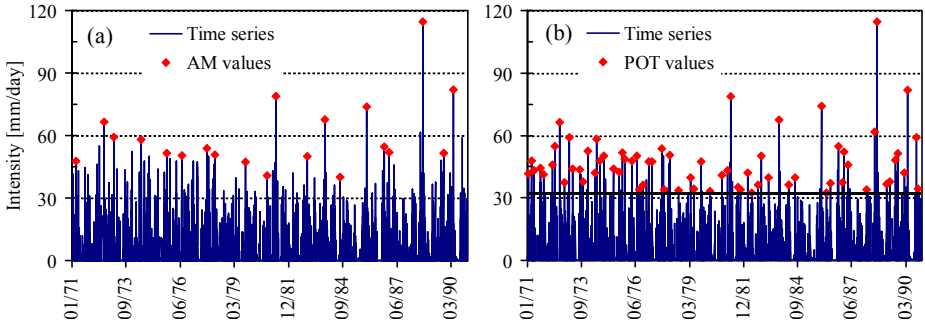

Figure 7.1 Illustration of the definition of (a) annual maxima (AM), and (b) Peak Over Threshold (POT) rainfall extremes. The continuous line across (b) indicates a position of a threshold of the daily rainfall intensity of slightly above 30 mm/day.

7.3 Aggregation scales and extraction of rainfall extremes

The time span over which a representative value of the rainfall intensity is considered constitutes the aggregation scale(s) or level(s) (AggL). The selection of an AggL is often based on the resolution of the data to be considered, the intended application and a common practice. In the current study, AggL of 1, 2, 3, 5, 7, 10, 30 and 90 days were considered. These are the common AggL used in practical applications. Apart from the daily time series, the series for the other AggL were obtained by a moving average technique (Willems, 2000). In the moving average technique, the series for a given AggL is obtained by taking the mean of each of the original time series values over the AggL span sequentially. For example, if x_i, …, x_n, is the daily rainfall series, for i = 1, 2, ..., n and l = 2, 3,…L, where n and L are, respectively, the total number of days in N years and the total number of AggL, the time series for AggL, l = *2*, for example, is $(x_1+x_2)/l$, $(x_2+x_3)/l$, $(x_3,+x_4)/l$,…, $(x_{n-1}+x_n)/l$. The series of all other AggL are got in a similar way in order to obtain L for different rainfall series.

Once the series for all the AggL are obtained the extreme series or the POT for each of the AggL can be extracted based on the POT selection principles. The technique above can be applied to an observation, which can be called observed POT (extremes). In a similar way, that for the model can also be obtained and can be called model (perturbed) extremes. Note that in the extraction of model POT, similar threshold for each AggL used for extracting observed POT is applied for extracting model POT. This is to ensure that both the observed and model extremes are given equal weighting. Thus, the impacts of climate change on the extremes can be assessed by comparing the observed extremes with perturbed extremes. This can be repeated for all the scenarios, models, periods under consideration, and for all locations of the case study. In this study, two methods were considered for comparing model

and observed POTs: (1) changes in the moments of peaks and (2) changes in the intensity-duration-frequency (IDF) relationship. The latter case, (2), requires technique for extreme value analysis, which was introduced in chapter 2. More details are, hereafter, given.

7.4 Extreme value distribution

Extreme Value (EV) theory forms the theoretical stochastic framework for estimation of extreme quantiles. It is a powerful and very robust framework for studying the tail behavior of a distribution. According to the Fisher–Tippett theorem (Fisher and Tippett, 1928) the block of maxima of a sequence iid random variables in the limit follows a Generalized Extreme Value (GEV) distribution. A parallel result to the GEV states that the excesses over a high threshold folow a Generalized Pareto (GPD) distribution (POT method). However, as noted in many studies (e.g. Engeland et al., 2005) hydrometeorological time series do not necessarily fulfill the basic requirements of EV theory as they are results of a complex dynamic physical process (e.g. for streamflow: daily streamflow data and their extremes are often auto-correlated and not iid). EV theory has shown to provide reasonable approximations in many hydrometeorological cases. However, there are five 3-parameter distributions for the study of extreme events (Sheng and Chun, 2002) and they include: GEV, GPD, Generalized logistic (GLO), 3-parameter Lognormal (LN3) and Pearson type 3 (P3) distributions. The selection of the best-fit distribution (from the five distributions) was based on the *L*-moment ratio diagram (Hosking & Wallis, 1993). The *L*-moment ratio diagram is used to compare the *L*-skewness (L-CS) -- *L*-kurtosis (L-CK) relations of different distributions and data samples. This gives a visual indication of which distribution may be expected to give a good fit to a data sample or samples. More details on *L*-moments and their ratios are provided in section **Error! Reference source not found.**. Figure 7.2 shows the *L*-moment ratio diagrams for the ten samples of rainfall extremes (POT series) for eight different AggL. The mean sample plot for each of the different AggL is generally close to the GEV theoretical curve (Figure 7.2). This implies that the POT sample series are best approximated by the GEV distribution.

7.4.1 Parameter calibration

Parameter estimation for analytical probability distributions based on empirical data is an important problem in engineering hydrometeorology. It is undoubtedly historical that it has been actively discussed and innovated, at least, in what regards the distributions of extreme values. The main issue is the fact that estimating extreme characteristics involves the extrapolation of distribution laws into the domain of events with small probabilities, in many cases, far beyond the range of available observational data. Theoretically, such estimates are of critical importance for practical applications. There are a number of approaches available for estimating the parameters of a

distribution. The methods of moments and maximal likelihood are such examples.

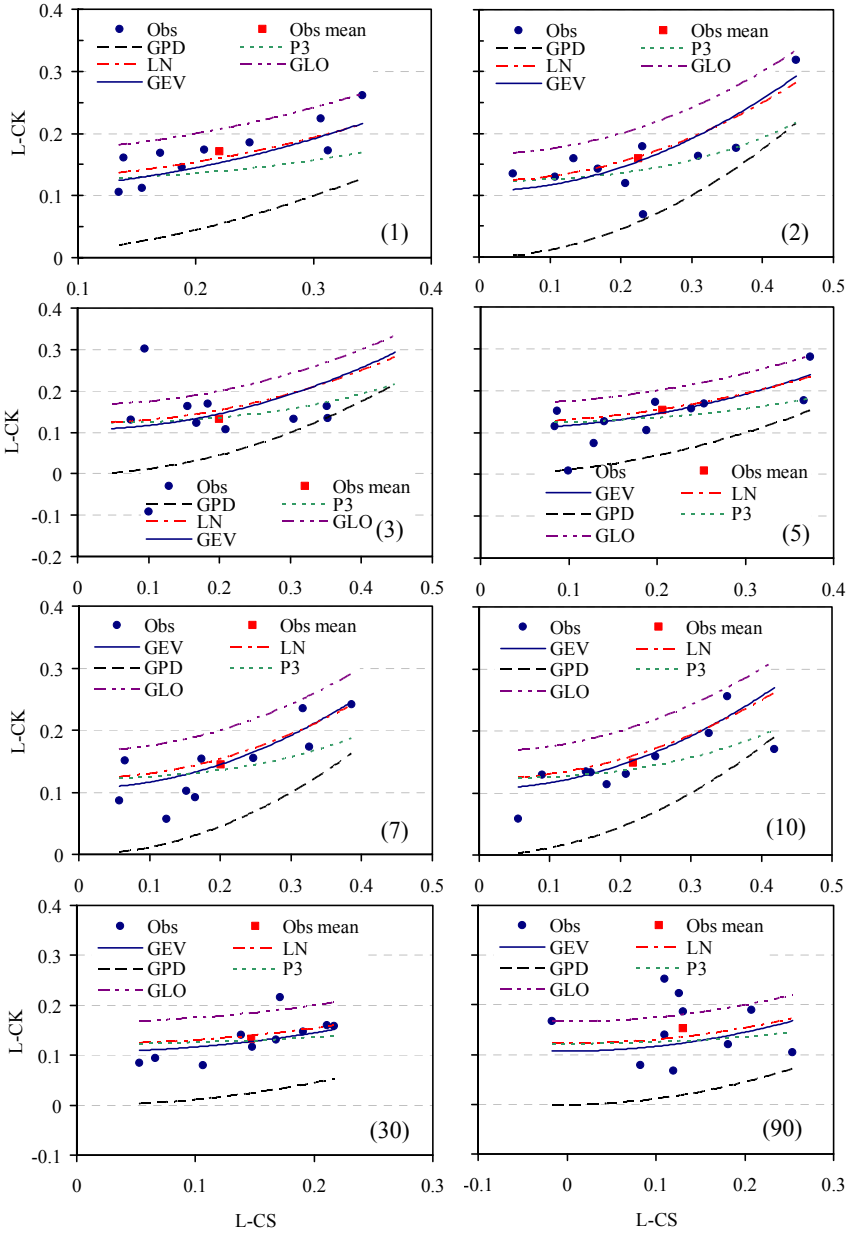

Figure 7.2 *L*-moment ratio diagrams used for the selection of the extreme value distribution needed to fit the rainfall extremes. The number embraced by ( ) on each chart is for the aggregation level of the rainfall data from which the rainfall extremes were extracted. The *L*-moment ratio (L-CK, L-CS) plots marked with ● and ■ are for the observed (Obs) and their mean (Obs mean), respectively for the rainfall extremes.

Their description can be found in textbooks on statistics, while some examples of their application to hdyrometeorological variables are found in literatures (e.g. Keefer and Verdini, 1993; Kitanidis and Lane, 1985). A considerable achievement of the late 20th century in statistical estimation was the method of *L*-moments proposed by Hosking (1990). The advantages of *L*-moments, as compared to ordinary distribution moments, are provided and shown in several studies (e.g. Hosking, 1990; Hosking and Wallis, 1997; Stedinger et al., 1993). First, *L*-moments always exist where the mean value exists for the probability distribution. This extends to the cases for which ordinary higher order moments may not exist as, for example, the third and fourth moments of GEV distribution with a heavy tail and the distribution shape parameter $k \leq 1/3$ and $k \leq -1/4$ do not exist. The second central moment for GEV distribution does not exist when the shape parameter $k \leq -0.5$. However, *L*-moments and their ratios exist in all ranges mentioned above. Secondly, unlike ordinary moments, only linear functions of sample values of the variable are used to estimate *L*-moments based on an observational series. The result is that the sample estimates of *L*-moments are unbiased and more effective; they are also less sensitive to random outliers and gross observational errors than the sample estimates based on ordinary moments. *L*-moments, as well as ordinary moments, are used as the first step in the distribution parameter estimation procedures based on available data. The second step of such procedure is to obtain the parameters based on *L*-moment estimates. This procedure is much more convenient than the maximum likelihood and the moments methods since it allows one to draw data on the shape of the distribution (based on *L*-moment estimates) and, as a rule, to obtain the parameters by relatively simple direct calculations. Given the lavish advantages of *L*-moment, it was chosen for the current study to fit the extreme series into the GEV distribution.

7.4.2 *L*-moments and their ratios

As a linear combination of Probability Weighted Moments (PWMs), defined by Greenwood et al. (1979), *L*-moments (l_i, i =1,2,3,4…) represent the location, dispersion (scale) and shape of the data sample similar to the conventional moments and can be calculated using equation (7.2). The *L*-coefficient of variation (L-CV), *L*-skewness (L-CS) and *L*-kurtosis (L-CK) are referred to as the second, third, and fourth order *L*-moment ratios, respectively. The first four sample *L*-moments, l_1 to l_4, of a given data sample (Hosking & Wallis, 1997; Greenwood et al., 1979) are used to obtain the *L*-moment ratios as follows:

$$t = l_2/l_1 = \text{L-CV},\ t_r = l_r/l_2\ (t_3 = \text{L-CS};\ t_4 = \text{L-CK}) \tag{7.1}$$

for r = 3, 4, respectively, independent of units of measurement, where

$$l_1 = b_0,\ l_2 = 2b_1 - b_0,\ l_3 = 6b_2 - 6b_1 + b_0,\ l_4 = 20b_3 - 30b_2 + 12b_1 - b_0 \tag{7.2}$$

$$b_0 = \frac{1}{n}\sum_{j=1}^{n} X_j \tag{7.3}$$

$$b_r = \frac{1}{n}\sum_{j=r+1}^{n} \frac{(j-1)(j-2)\ldots(j-r)}{(n-1)(n-2)\cdots(n-r)} X_j \tag{7.4}$$

are unbiased sample estimators (b_r) of PWMs and X_j is an ordered set of observations $x_1 \le x_2 \le x_3 \le \ldots \le x_n$. For most distributions, formulas for parameter estimation based on *L*-moments can be found in the appropriate literature in the explicit form. Thus, for the GEV distribution (Hosking et al., 1985), the parameters ξ, α, and k, are, explicitly, estimated by equating the first p sample *L*-moments estimates to the corresponding population as follows:

$$k \approx 7.8590c + 2.9554c^2 \tag{7.5}$$

$$c = \frac{2}{3+\tau_3} - \frac{\log 2}{\log 3} \tag{7.6}$$

$$\alpha = \frac{\lambda_2 k}{(1-2^{-k})\Gamma(1+k)} \tag{7.7}$$

$$\alpha = \lambda_1 - \alpha\left\{1-\Gamma(1+k)\right\}/k \tag{7.8}$$

where λ_1, λ_2, and τ_3, are estimated by l_1, l_2 and t_3, respectively. Calibration of the GEV was possible for both the observed and perturbed POT. This shows the possibility to compare several characteristics of the extremes of perturbed to that of observed extremes. Once the GEV distribution is calibrated, the extreme quantile corresponding to a givern return period T, (Q_T,) can be estimated using equation (7.9); where Gf_T is the extreme growth factor given by Q_T/M_p; M_p being the mean of the extremes or POT values.

$$Gf_T = \xi + (\alpha/k)\left[1-\left\{-\ln\left(1-\frac{1}{T}\right)\right\}^k\right] \tag{7.9}$$

7.5 Change in the rainfall extremes

7.5.1 Rainfall extreme quantiles

To assess the changes in the extreme quantiles, perturbations (a series of a ratio between the model peak and the observed peak with similar exceedance probability or return period), for a 1-day AggL, were plotted versus empirical return period. A value of perturbation greater than 1 indicates an increase in the rainfall extreme quantile in the future, meanwhile a value of the perturbation less than 1 indicates a decrease in the rainfall extreme quantile in the future. As an example, Figure 7.3 shows plots of perturbation versus return period for 10 selected stations under high scenario.

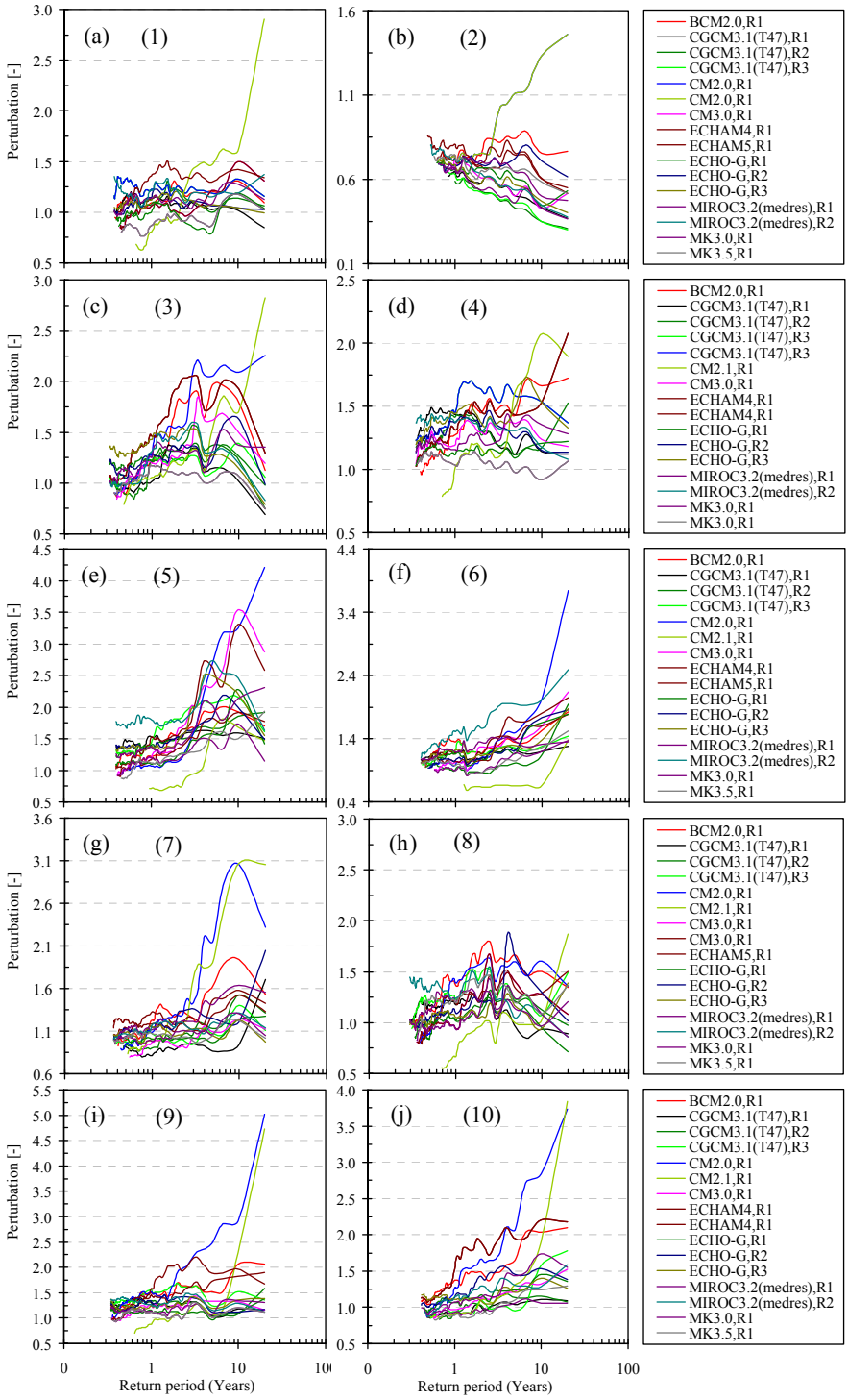

Figure 7.3 Typical changes in the distributions of the rainfall peaks (POT) for the A2 (2090s) scenario for the selected stations in the Lake Victoria basin.

The numbers (1)-(10) are the rainfall station identifier also indicated in Figure 7.5 indicating the locations of the selected rainfall stations. It is can be seen from Figure 7.3 that the perturbations are generally above 1 except for station (2), where perturbations are fairly constant for medium return periods for most models. This implies that the rainfall peaks for different return periods are projected to increase for most stations but are expected to decrease for station (2). Increase in the rainfall peaks for higher return periods is projected to be higher than that for the lower return periods. This also means that heavy extremes are projected to increase more that the lower extremes. As a further example, Figure 7.3(c), (e) and (g) shows that the perturbation increases with increase in return period from about 1.1 to 10 years then decrease with increase in return period. This is the case where heavy rainfall extremes are projected not to increase more that the less heavy extremes. In addition, Figure 7.3(b) shows that perturbations are below 1 for almost all the models except for run 1 of CM2.0 and strongly decreases with increase in return period. This implies that the rainfall peaks for location (2) are projected to decrease strongly.

7.5.2 Ensemble mean change in the rainfall extremes

In Figure 7.3, the variation in perturbations of rainfall peaks with return period under A2 scenario for several model runs is shown. Consistency among models is generally eminent but some differences exist. The differences in projection by the models indicate apparent uncertainty involved. The use of ensemble provides a simple but some useful method of quantifying the possible range of uncertainty in climate change projections and associated impacts (Fowler et al., 2007; Tebaldi and Knutti, 2007). However, the case can present too much information if the results for the other scenarios, and for the two future periods (2050s and 2090s) are also presented in the same way. In order to solidify information and provide uncertainly range base on scenario, an ensemble mean value was considered. That is, the average of the perturbations for all the model runs, at each return period, is obtained for each scenario. Plots of the ensemble mean perturbations versus return period, for all the scenarios, can be presented on the same chart. Figure 7.4 shows an ensemble mean results for the perturbations of rainfall peaks for all the scenarios. The numbers (1)-(10) are the stations' IDs indicated in Figure 7.5. It can be seen that perturbations are generally fairly constant for medium extreme events but significantly vary with return periods for very heavy and less heavy extremes for both 2050s and 2090s. This means that very heavy and meek extreme events are expected to change significantly as compared to the medium extremes. Generally, high scenario perturbations are higher than that for the middle and low scenarios, except for station (6). This is expected and is trivial.

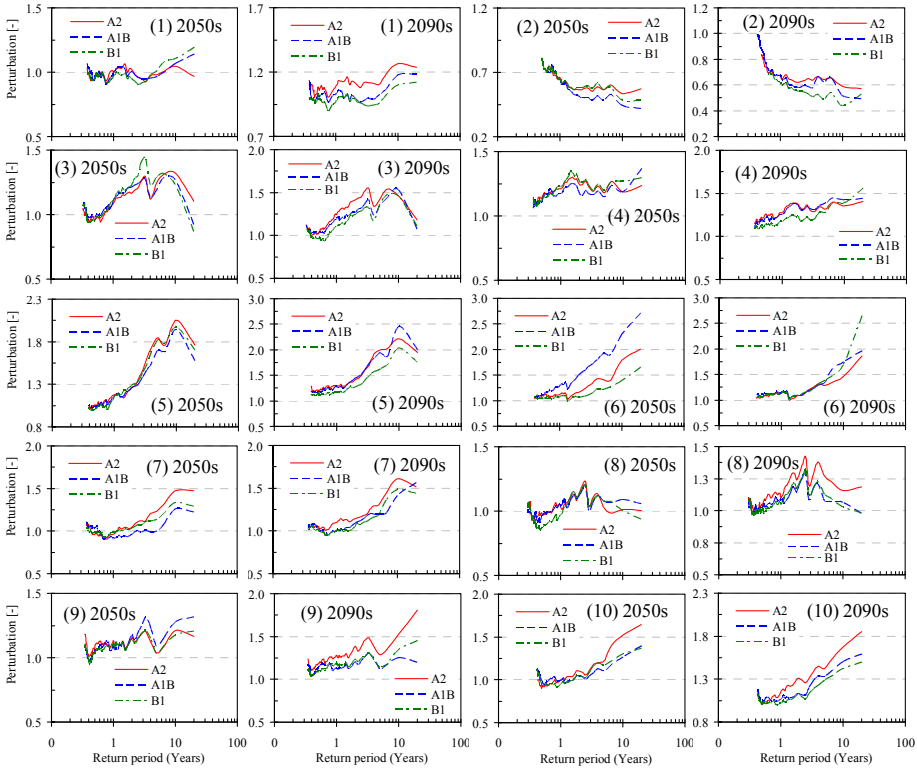

Figure 7.4 Ensemble mean for the changes in the distributions of the rainfall peaks (POT) for the selected stations in the Lake Victoria basin.

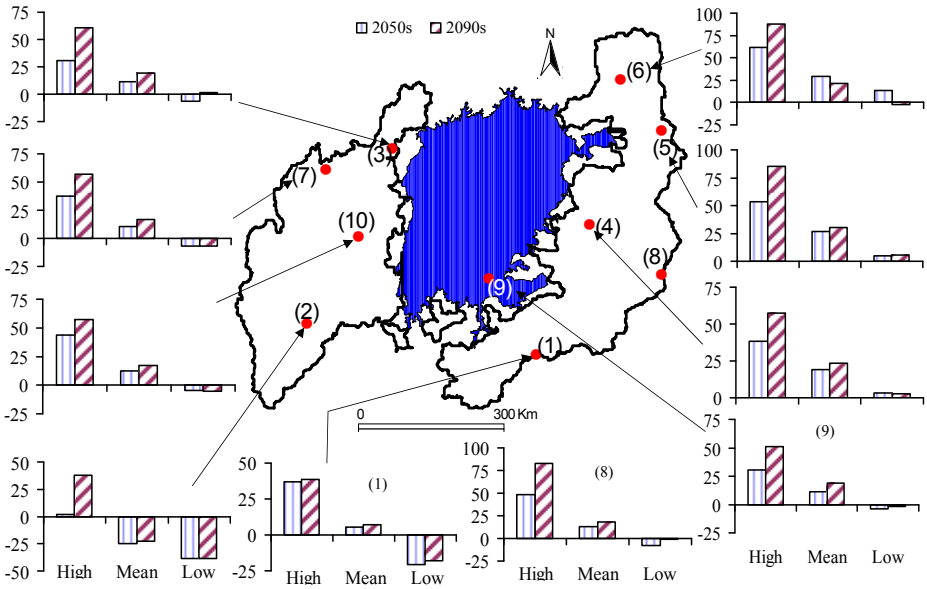

Figure 7.5 Percentage change in the mean of the rainfall extremes and locations of selected rainfall stations in the Lake Victoria basin.

For station (1), (4), (8) and (9) perturbations are fairly constant for the medium rainfall extreme events indicating that extremes of different categories will change by similar factors. For station (2), perturbations are less than 1 for all the scenarios and strongly decrease with increase in return period for both the 2090s and 2050s. Change in extremes demonstrated by station (2) is an explicit case of a strong decrease in rainfall extreme quantile with increase in return period. For all other stations, it can be seen that perturbations will generally increase with increase in return periods. This implies that, given the selected stations, the rainfall extremes are generally projected to increase for most parts of the Lake Victoria region except for the southern and western parts.

7.5.3 Change in the mean of the rainfall extremes

Mean statistic provides useful measure of the central tendency of a given data. The first moment of the rainfall peaks is, thus, very crucial among the statistics of extremes as it provides information on the location of the rainfall extremes. Change in the location of the rainfall extremes is demonstrated by the perturbation of the mean of the extremes and can be shown for each AggL. Figure 7.6 shows plots of perturbation versus AggL for different model runs, and the periods 2050s and 2090s of an example station (7). It can be seen that, for all the selected model runs and all the scenarios, the perturbations are greater than 1, except for 1-day AggL. Few model runs project slight decrease in the mean of the 1-day AggL rainfall peaks. Perturbation increases with increase in AggL of up to 30 days then a relative slight decrease for AggL of 90 days. This means that changes in the mean of the extremes for higher AggL will be higher than that for lower AggL. Figure 7.6 presents a case for one station but similar information regarding the change in the location of rainfall extremes for the other stations may also be required. Table 7.1 provides perturbations for rainfall peaks for different selected rainfall stations. The numbers embraced in parentheses are the station IDs, which are shown in Figure 7.5 for loci references. A value of perturbation of 1 indicates no change in the mean of the rainfall peaks. A value of perturbation greater and less than 1 indicates an increase and a decrease, respectively, in the value of the mean of the rainfall peaks. Perturbations labelled as “High” and “Low” are the “highest” and Lowest values, respectively, of the perturbations from the available model runs.

Perturbation labelled as “Average” is the ensemble mean. Given the selected runs, the perturbation provides the range of uncertainty for the change in the mean of the rainfall peaks. It can be seen from Table 7.1 that, generally, the ensemble mean perturbation, for each of the scenarios and for the two future periods is greater than 1. The implication for the change in the mean of the rainfall peaks is apparent; an increase in the mean of rainfall peaks is projected. Table 7.1 provides useful information about the change in the mean

of the rainfall peaks. However, a more solid information may be required which Table 7.1 cannot provide directly.

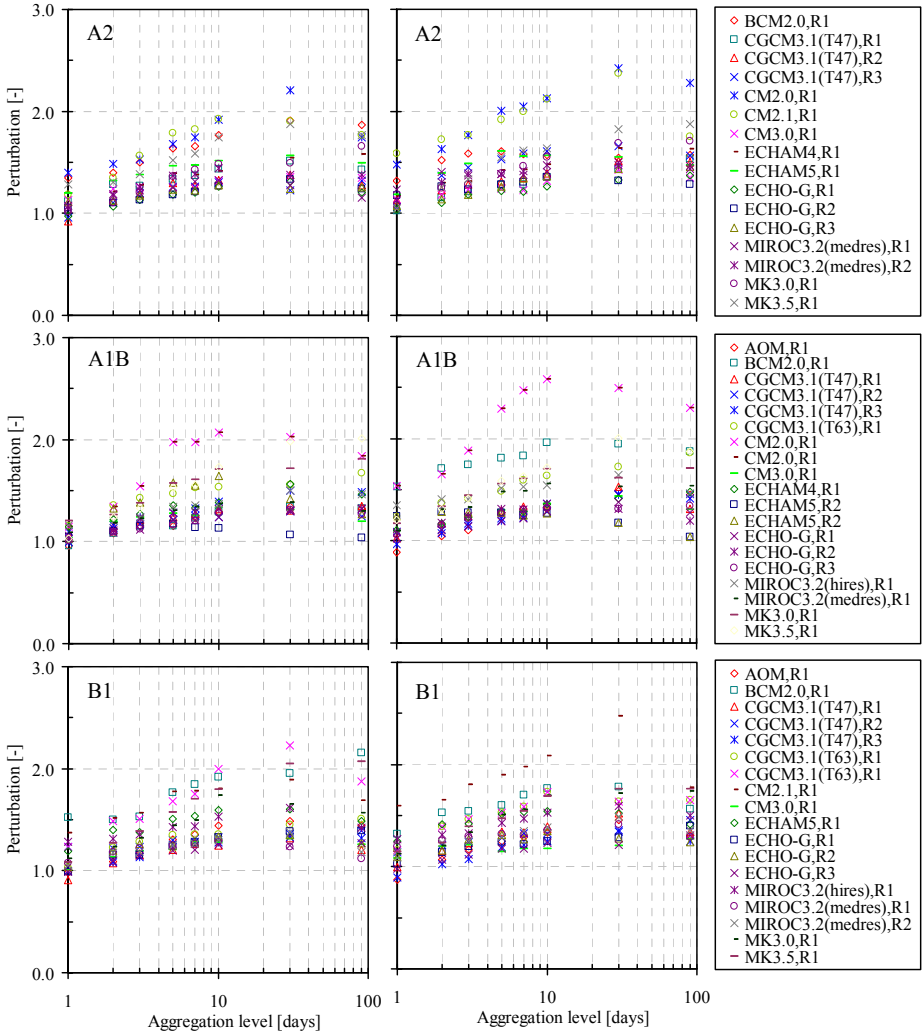

Figure 7.6 Typical change in the mean of the rainfall peaks for the 2050s (left column) and 2090s (right column). Results are for the rainfall station (7) to illustrate the change in the mean rainfall extremes.

In order to provide the mean perturbations for each scenario, the mean of all the values of perturbation for the "High", "Average" and "Low", for each scenario and period were obtained. That is, the average of the perturbation values for "High" in A2, "High" in A1B and "High" in B1 was calculated to obtain the upper value of the range. Similarly, the average of the perturbation values for "Low" in A2, "Low" in A1B and "Low" in B1 was calculated to obtain the lower value. Finally, the average of the ensemble mean in A2, A1B and B1 was obtained. The values of the perturbations, in each range for 2050s

and 2090s for each station, were converted into percentage change. Figure 7.5 provides the summary of the possible percentage change in the rainfall extremes for the rainfall measured at the different locations in the current study.

Table 7.1 Tabulated perturbation values of the mean of the rainfall peaks.

Period	Scenario	Range	Station number									
			(1)	(2)	(3)	(4)	(5)	(6)	(7)	(8)	(9)	(10)
2050s	**A2**	High	1.354	1.017	1.232	1.330	1.437	1.676	1.399	1.352	1.292	1.460
		Average	1.044	0.757	1.106	1.197	1.271	1.247	1.126	1.112	1.105	1.143
		Low	0.911	0.620	0.989	1.059	1.090	1.059	0.925	0.935	0.984	0.980
	A1B	High	1.492	0.965	1.356	1.415	1.575	1.591	1.205	1.720	1.331	1.483
		Average	1.093	0.736	1.123	1.186	1.245	1.471	1.072	1.174	1.135	1.107
		Low	0.742	0.579	0.927	1.012	0.971	1.360	0.959	0.891	0.991	0.911
	B1	High	1.263	1.081	1.331	1.399	1.591	1.587	1.522	1.370	1.302	1.378
		Average	1.019	0.758	1.116	1.195	1.290	1.164	1.116	1.092	1.096	1.115
		Low	0.731	0.646	0.897	1.023	1.087	0.992	0.911	0.948	0.911	0.970
2090s	**A2**	High	1.399	1.040	1.484	1.470	1.612	1.380	1.585	1.459	1.768	1.606
		Average	1.118	0.780	1.224	1.235	1.327	1.178	1.179	1.234	1.244	1.196
		Low	0.974	0.615	1.066	1.090	1.171	0.937	1.026	1.089	1.055	0.993
	A1B	High	1.459	2.195	1.694	1.676	2.505	2.824	1.533	2.163	1.366	1.662
		Average	1.075	0.812	1.202	1.273	1.350	1.239	1.182	1.159	1.166	1.191
		Low	0.742	0.601	0.992	1.041	0.999	0.904	0.884	0.936	0.966	0.908
	B1	High	1.296	0.905	1.641	1.577	1.446	1.420	1.593	1.873	1.406	1.446
		Average	1.016	0.738	1.142	1.201	1.240	1.220	1.133	1.145	1.148	1.120
		Low	0.748	0.630	0.988	0.949	0.992	1.092	0.874	0.943	0.931	0.943

If the values of the mean percentage change, for both the two periods 2050s and 2090s are considered, it can be seen from Figure 7.5 that the mean of the rainfall peaks for stations (2) is expected to decrease by over 20% while for the rest of the other stations are expected to increase by at least 10%. The percentage change for Station (1) is under 10%, which is strongly related to that for station (2). Meanwhile the change in the mean of the rainfall peaks for stations (4), (5) and (6) are skewed towards stronger increase. Thus, it can be concluded that, in the Lake Victoria basin, the eastern parts will experience increase in rainfall extremes while the southern parts will experience decrease in rainfall extremes and other parts will experience little increase in the rainfall extremes. The study of trends (Chapter 4) also demonstrated some kind of strong spatial connections for the stations in the east, west and south of the Lake Victoria basin.

7.5.4 Change in the variability of the rainfall extremes

Presumptively, the most widely used single measure of variability is the coefficient of variation, C_v, and it is the standard deviation of a given data set divided by their mean. This type of statistic can be used at all time scales such that if rainfall extremes are analysed then a measure of long-term variability will result. Perturbation of C_v is the ratio of C_v for the projected daily rainfall extremes to that of the C_v for the observed daily rainfall extremes. Perturbation of C_v was calculated for each AggL and for all the selected

model runs. Plots of the perturbations of C_v versus AggL enabled visual analysis and interpretation of the change in variability of daily rainfall extremes in the current study. As an example, Figure 7.7 shows the plots of perturbation versus AggL (in days) for daily rainfall extremes of station (7). It can be seen that the perturbations are generally greater than 1, which is an indication that the variability of rainfall extremes will increase in the future. The tendency of the perturbation of C_v to increase with increase in AggL is not visually eminent. This indicates that, unlike change in the mean of the extremes, change in the variability of the extremes for rainfall of different duration will be similar but are more uncertain.

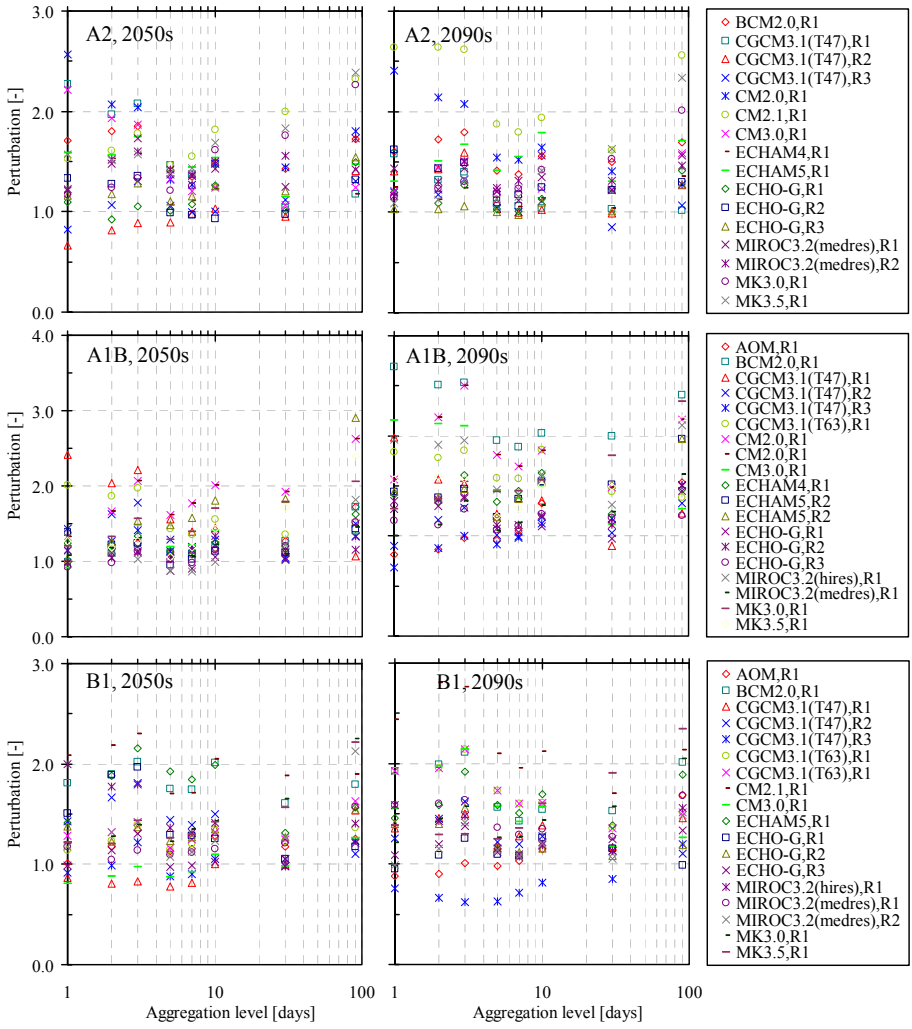

Figure 7.7 Typical change in the C_v of the daily rainfall peaks for different AggL illustrated by the rainfall station (7).

The intermodal variability of the results seems to overshadow the present of a more consistent change in the C_v for all the scenarios and for 2050s and 2090s. Note that the results for the perturbations of C_v, provided in Figure 7.7, are not representative of the results from other stations. A tabulated summary of the perturbations of C_v was obtained using the same procedure discussed in the previous section. Table 7.2 provides the range of percentage change for the C_v of the rainfall extremes for the different rainfall stations. The rainfall station (2) is the only one with projected percentage decrease in the variability of daily rainfall extremes is station (2). The values of the projected average percentage increase in C_v for stations (5) and (6) are relatively and exclusively higher. Recall that in chapter 4 it was also seen that the variability and trends in the observed extremes for these stations were also apparent.

The range of percentage change in C_v is wider compared to that of the mean of the rainfall extremes. For example, the range of percentage change in C_v for station (5) is +25 to +286% for the period 2090s. Similarly, for rainfall station (5), the range of percentage change in the mean of daily rainfall extremes is +5 to +85%. Thus, change in C_v will be much higher than the change in the mean of the daily rainfall extremes. Concisely, the variability of extremes daily rainfall will squarely increase under the influence of anthropogenic change.

Table 7.2 Tabulated perturbation values for the C_v of the rainfall extremes.

Period	Station number									
	(1)	(2)	(3)	(4)	(5)	(6)	(7)	(8)	(9)	(10)
2050s	83	24	74	88	177	167	135	47	82	192
	8	-37	17	21	84	69	35	5	20	57
	-42	-70	-14	-14	28	24	-21	-24	-8	1
2090s	102	44	148	152	286	280	159	52	138	183
	12	-34	30	33	89	64	45	5	31	66
	-36	-72	-19	-11	25	5	-17	-18	-4	-1

7.5.5 Change in the tail of the rainfall distribution

The shape of a tail of the distribution of daily rainfall extremes is modulated and characterised by the distribution extreme value index, γ. Shape parameter, k, is related with γ as $\gamma = -k$. γ is a measure of the tail "heaviness" of the distribution (Willems et al., 2007) and is also used to identify the class of the distribution of the extremes. That is, heavy tail is when $\gamma > 0$ or $k < 0$ (EVI), normal tail is when $\gamma = k = 0$ (EVII) and light tail is when $\gamma < 0$ or $k > 0$ (EVIII). To illustrate the tail behaviour using the distribution of the observed extreme quantiles, consider Figure 7.8. It shows plots of the distribution of observed extremes versus return period for the 10 stations, together with those of the model runs under A2 scenario of 2090s. The heavy tail behaviour means that the distribution of the daily rainfall extremes strongly increases with increase in return period (Figure 7.8(b), (e) and (g)).

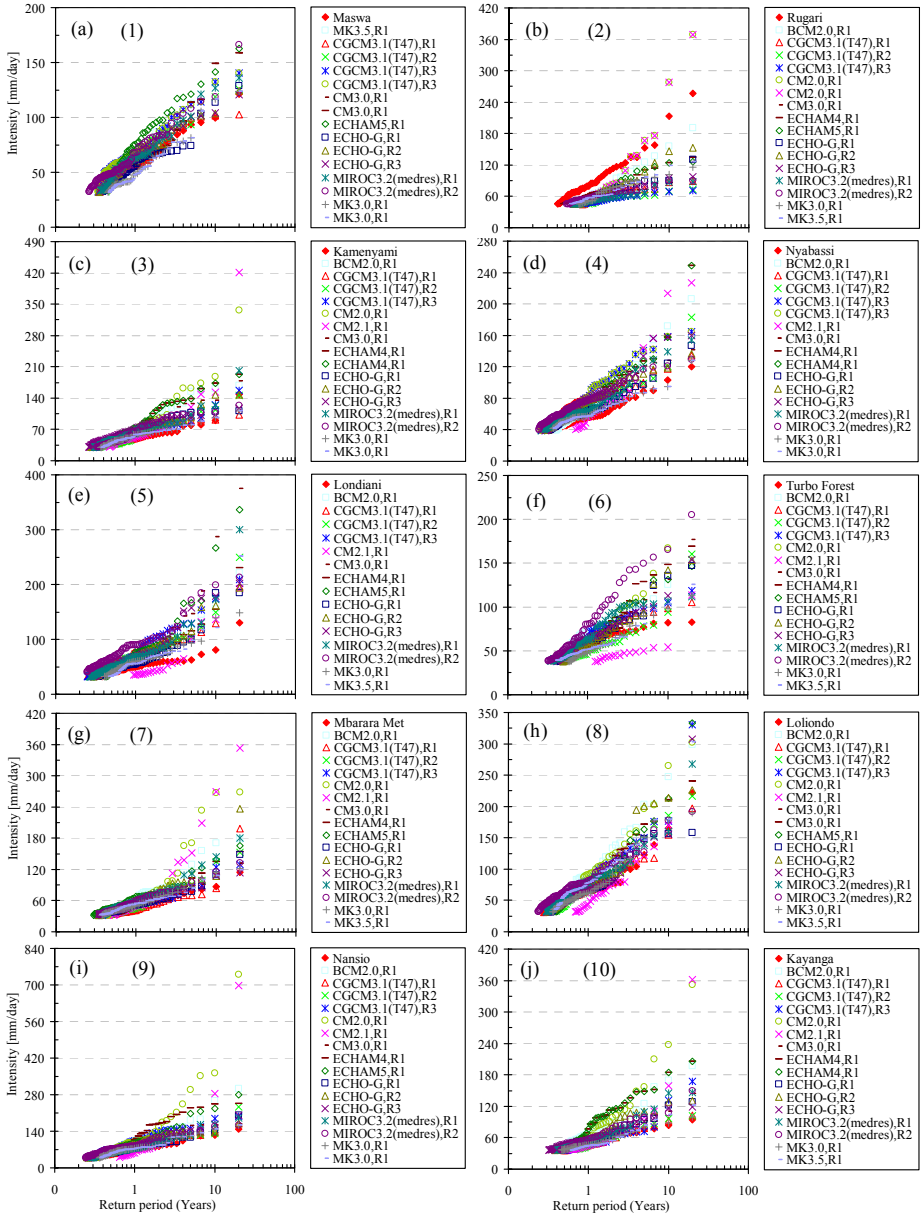

Figure 7.8 Typical distribution of the 1-day rainfall extremes for 10 different rainfall stations in the Lake Victoria basin, illustrated by the case of the A2 scenario. The number embraced in ( ) indicates the rainfall locations shown in Figure 7.5.

The normal tail behaviour means that the distribution of the rainfall extremes does not strongly increase with increase in return period (Figure 7.8(c) and (j)). The light tail behaviour is the case where the distribution of rainfall extremes increases with increase in return period up to a certain value then start decreasing with increase in return period (Figure 7.8(a), (f) and (h)). To date, change in *k* due to climate change influence will definitely agitate the

distribution tail behaviour or alter the extreme value distribution type of the daily rainfall peaks. For example, a change in k which results in a special case for $k = 0$ and $k = 1$ can yield, respectively, the exponential and uniform distribution.

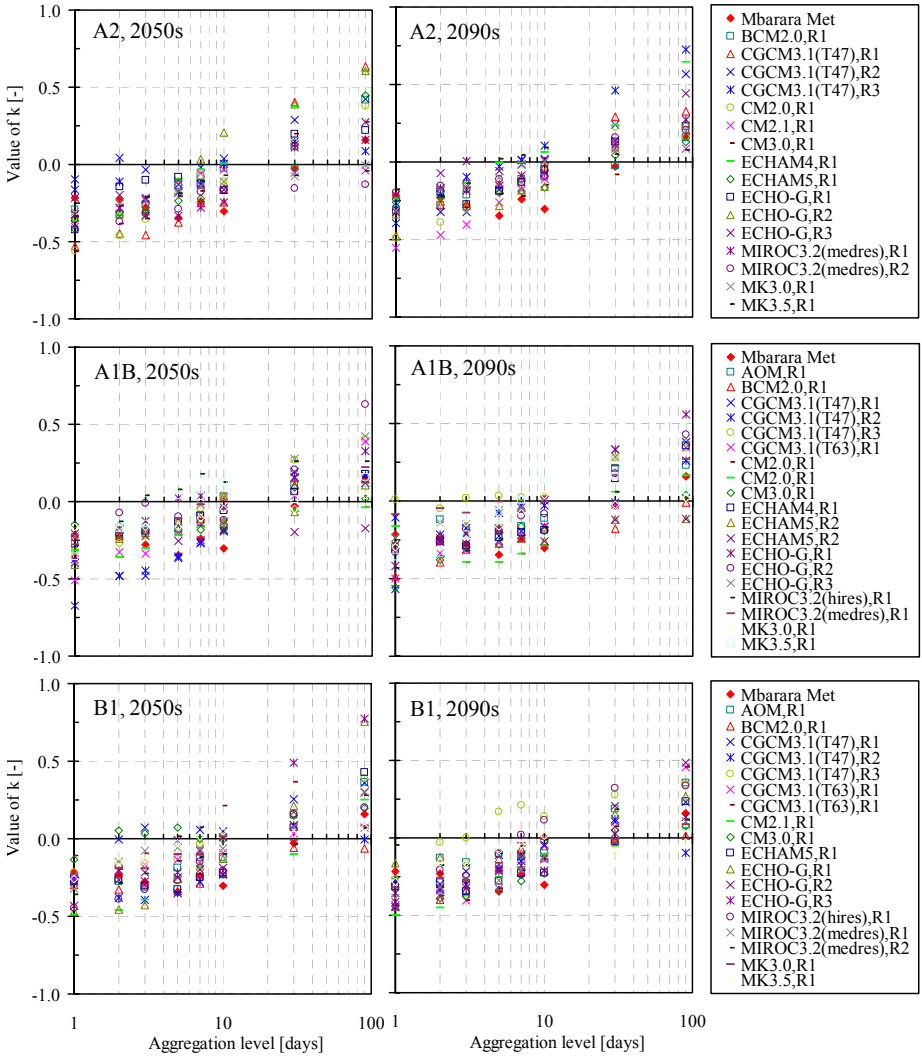

Figure 7.9 Typical changes in the rainfall extremes distribution shape parameter, k, for the GEV illustrated by the results of the data for rainfall station (7).

Following the preceding discussions, the impact of climate change on the rainfall extreme distribution tail can, thus, be detected by presumptively considering both the magnitude and the sign of the value of shape parameter, k, estimated for the model (perturbed) and observed. Figure 7.9 shows plots of shape parameter, k, versus AggL for different model runs together with that of the observation. It can be seen that for the observation, the values of k are well

below zero for AggL < 10 days, and $k > 0$ for AggL > 30 days. For an AggL of 30 days k is approximately close to naught. Thus, the distributions of the rainfall extremes for station (7) are poorly described by an EVI for AggL > 20 days.

Meanwhile for AggL < 20 days, the distributions of the rainfall extremes are well described by EVI. That is, the rainfall extremes are of heavy tail behaviour. With the influence of climate it can be seen that, under A2 and A1B of 2090s, the tendency for the value of k to shift towards naught is apparent for 2 days < AggL < 20 days. However, for 1-day rainfall extremes, most of the model runs project that k will be more negative. That is, the heavy tail behaviour will become much heavier.

Table 7.3 provides a synthesis of the values of k for all the 10 stations. If the average of the ensemble is considered, the magnitude of the values of k for stations (5), (6), (7) and (10) will increase, and for the other stations, the magnitude of the value of k will decrease. The implication is that, where the extremes are projected to increase, the very heavy rainfall extremes will increase very strongly than the less heavy rainfall extremes. In contrast, for the other stations, where rainfall extremes are projected to increase, the increase in the extreme quantiles with higher return periods will not strongly increase with increase in return period.

Table 7.3 Tabulated values of the ensemble mean of the shape parameter, k, of the GEV distribution for different scenarios and the 2050s and 2090s, and selected rainfall stations in the Lake Victoria basin.

Period	Scenario	Range	Station number									
			(1)	(2)	(3)	(4)	(5)	(6)	(7)	(8)	(9)	(10)
2050s	**A2**	High	0.133	0.012	-0.061	-0.093	-0.184	0.026	-0.094	-0.170	-0.069	-0.193
		Average	-0.102	-0.351	-0.267	-0.187	-0.367	-0.262	-0.357	-0.287	-0.187	-0.353
		Low	-0.231	-0.579	-0.496	-0.378	-0.556	-0.527	-0.560	-0.496	-0.445	-0.518
	A1B	High	0.023	0.117	-0.071	0.007	-0.164	-0.184	-0.150	0.088	-0.039	0.096
		Average	-0.159	-0.181	-0.232	-0.218	-0.367	-0.303	-0.326	-0.297	-0.243	-0.246
		Low	-0.468	-0.563	-0.399	-0.553	-0.573	-0.402	-0.672	-0.478	-0.489	-0.583
	B1	High	0.246	-0.074	-0.158	-0.044	-0.289	0.213	-0.112	-0.165	-0.045	-0.049
		Average	-0.179	-0.232	-0.236	-0.207	-0.368	-0.183	-0.299	-0.307	-0.209	-0.270
		Low	-0.396	-0.457	-0.286	-0.385	-0.523	-0.419	-0.488	-0.438	-0.355	-0.710
2090s	**A2**	High	0.033	0.231	-0.039	0.097	-0.172	-0.009	-0.180	-0.121	-0.075	-0.124
		Average	-0.166	-0.201	-0.242	-0.221	-0.353	-0.272	-0.318	-0.296	-0.232	-0.332
		Low	-0.458	-0.554	-0.555	-0.387	-0.660	-0.542	-0.552	-0.482	-0.624	-0.637
	A1B	High	0.078	0.672	-0.091	0.096	-0.196	-0.008	0.012	-0.168	-0.042	-0.046
		Average	-0.155	-0.155	-0.275	-0.211	-0.363	-0.204	-0.310	-0.293	-0.159	-0.284
		Low	-0.399	-0.478	-0.511	-0.509	-0.720	-0.672	-0.570	-0.454	-0.335	-0.507
	B1	High	-0.020	-0.097	0.224	-0.066	-0.239	-0.220	-0.050	-0.123	-0.102	0.017
		Average	-0.176	-0.319	-0.245	-0.264	-0.369	-0.349	-0.343	-0.270	-0.236	-0.300
		Low	-0.372	-0.663	-0.620	-0.569	-0.619	-0.587	-0.499	-0.437	-0.562	-0.483
		Observed	-0.175	-0.281	-0.252	-0.297	-0.173	-0.123	-0.218	-0.329	-0.221	-0.211

7.5.6 IDF relationships

The parameter/AggL relationships, together with the analytical description of the extreme value distribution, comprise the IDF curves. In traditional practice, IDF curves are developed using historical rainfall time series data. That is, extreme series of rainfall is fitted to a theoretical probability distribution from which rainfall intensities corresponding to particular durations and return period are obtained. In the use of such a procedure, an assumption is made that the historical extremes can be used to characterize the future extreme regimes. That is, the historical record is assumed to be stationary. This assumption may not be valid under the changing climatic conditions that may bring shifts in the magnitude and frequency of extreme rainfall. Such shifts in extreme rainfall at the local level demand new regulations for water infrastructure management as well as changes in design practices. For example, municipal water management infrastructure (sewers, storm water management ponds or detention basins, street curbs and gutters, catchbasins, swales, etc) designs are typically based on the use of local rainfall IDF curves.

7.5.6.1 Change in the IDF curves

Change in IDF curves is assessed by comparing the current and the projected IDF curves. Using the range of the AggL discussed in section 7.3, the theoretical extreme quantiles for return periods 2, 3, 5, 10, 20 and 50 years were estimated based on the calibrated distribution using equation (7.9). This was first done based on a given observed rainfall extremes. Given a model and a scenario, the model quantiles were similarly estimated. The empirical quantiles, obtained using interpolation technique was used to validate the accuracy of the fits. Note that the arbitrarily selected return periods correspond to acceptable risk levels and are the values commonly used in professional practice by many countries for specifying the extremes return period in hydraulic designs (Afshar et al., 1994). The impact of climate change on the IDF curve was then assessed by comparing the observed theoretical extreme quantiles with that of the model. The extent to which the IDF is shifted can be measured in different ways; e.g. by the perturbation of the theoretical quantiles for each corresponding AggL. That is, the ratio of observed quantile to that of the model with similar AggL. However, for visual satisfaction, the plots of observed and the model extreme quantiles versus AggL, for a given return period, can be obtained. This can be done for different models and a chart containing an observed IDF curve for a given return period and the IDF curve for each of the models can be constructed. From this chart, it is possible to draw conclusion on the possible shifts in the observed IDF curve due to climate change influence based on visualization only. Similar charts for the different scenarios and for the two future periods can be constructed. Figure 7.10 shows the IDF curves for the observed (station (5)) and that for the model runs for 10 years return period under the

different scenarios for 2050s and 2090s. It can be seen from Figure 7.10 that the shift in the observed IDF curve is upwards.

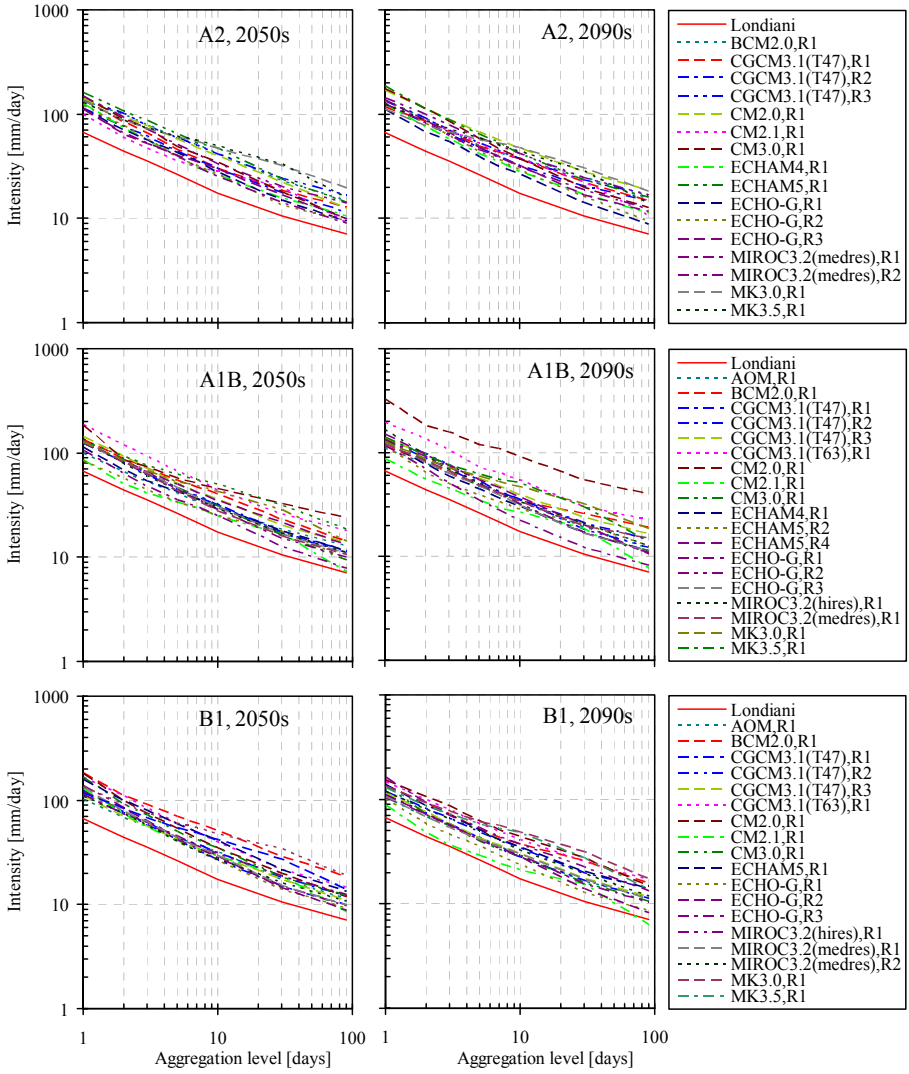

Figure 7.10 IDF curves for 10 years return period for the present (1971-1990) and different GCM runs under three different scenarios for the 2050s and 2090s. The results are for the data of the rainfall station (5) illustrating the typical upwards shifts in the present IDF curve as a consequence of climate change.

This shift is dramatic and can be quantified by obtaining the perturbation of the observed IDF. Albeit the differences in the shift in the IDF curve among the scenarios are not that very big, it is apparent that IDF curve for B1 for 2090s, compared to that of 2050s, is smaller. Like the IDF curves shown in Figure 7.10, Figure 7.11 also shows the IDF curves for 10 years return period but for station (2). In contrast, it can be seen that the shift in the observed IDF

is generally downwards. However, the shift is weaker than that of the upward shift for station (5). Apart from station (2), the IDF curves for all the other stations showed upwards shift (results not shown).

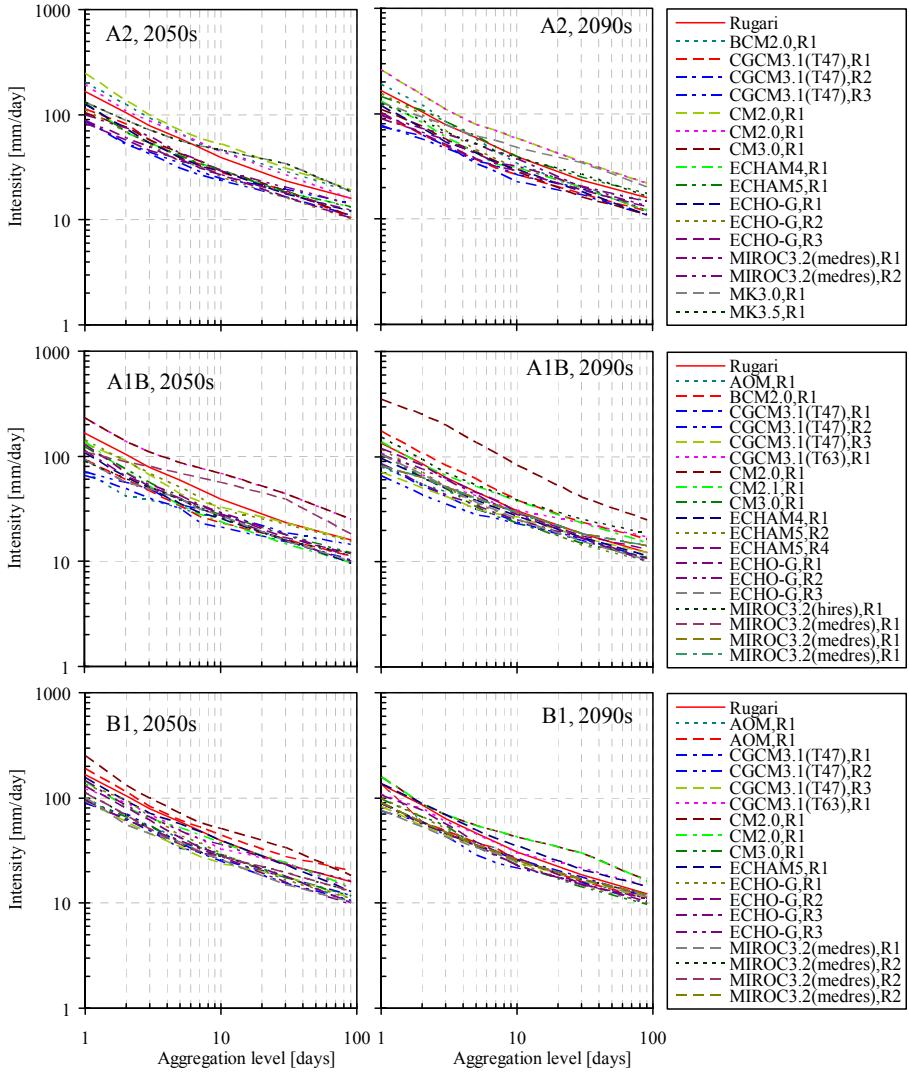

Figure 7.11 IDF curves for 10 years return period for the present (1971-1990) and different GCM runs, under three different scenarios for the 2050s and 2090s. The results are for the data of the rainfall station (2) illustrating the typical downwards shifts in the current IDF curve as a consequence of climate change.

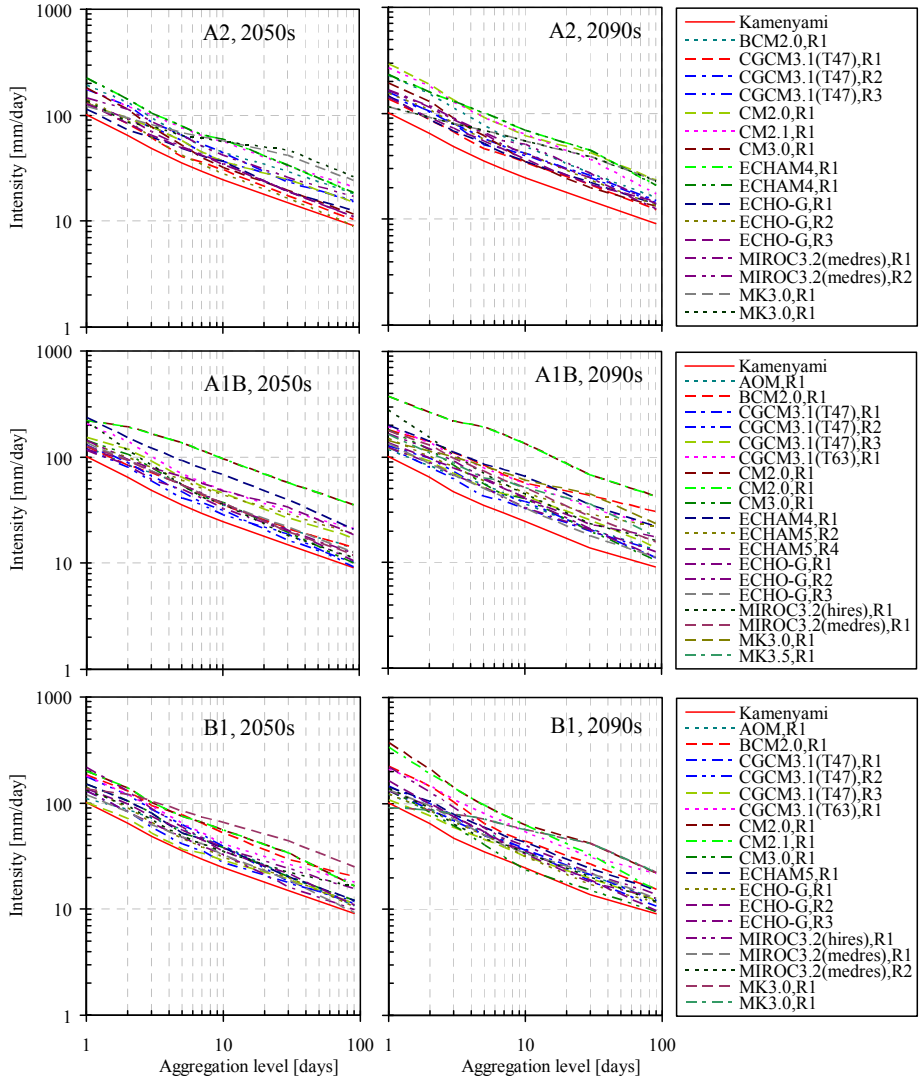

Figure 7.12 IDF curves for 50 years return period for the present (1971-1990) and different GCM runs under three different scenarios for the 2050s and 2090s. The results are for the data of the rainfall station (7) illustrating the typical upwards shifts in the current IDF curve as a consequence of climate change.

Change in the IDF curve is strongly related to the change in the mean of the rainfall extremes. Thus, given the perturbation of the mean of the rainfall extremes the observed IDF curve can easily be reconstructed. For example, the observed IDF curves in Figure 7.10 and Figure 7.11 can be reconstructed simply by applying the perturbations in Figure 7.3 or Table 7.1. This means that perturbation value greater than 1 will shift the IDF upwards and the perturbation value less than 1 will shift the IDF downwards.

The perturbation, however, is duration independent and this implies that the extreme quantiles for each AggL is assumed to change by the same amount. Such an assumption is valid because Figure 7.10 shows that the shift in the extreme quantiles for each AggL is proportionally correlated. Application of the high, mean and low perturbations to the observed IDF curve is, thus, able to produce a similar range of shift as that provided by several model runs.

The climate model runs used in this study provide data only for 20 years. This means that reconstruction of IDF curves for return period of more that 20 years requires extrapolation of data. Extrapolation was done by keeping the term M_p in equation (7.9) constant for the return periods greater than 20 years. Secondly, it is also not possible to validate the theoretical quantiles because the empirical extreme quantiles do not exist. However, it is still possible to compare the extreme quantiles extrapolated by observed extreme value distribution with those extrapolated by model extreme value distribution for return periods more than what the data provides.

Return period of 50 years was used to assess if the changes in the non-validated extreme quantiles were similar to that of the validated extreme quantiles. The results showed that the direction of shift in IDF curves for the corresponding station were similar to that for return periods less than or equal to 20 years. Figure 7.12 provides and example of the IDF curves for 50 years return period. It can be seen that the IDF curve are projected also to shift upwards.

7.6 Change in temperature

Change in temperature was examined by considering change in T_{max} and T_{min}. This change might be higher compared to mean temperature (King'uyu et al., 1999). At above day mean value, the mean monthly temperature variability is more significant for the region. Thus, the change in T_{max} and T_{min} was obtained at monthly scale. The difference between the observed temperature value and the corresponding model value (downscaled) provided the required change (perturbation) in temperature. The observed temperature represents the current climate.

Figure 7.13 shows the perturbations of T_{max} and T_{min} versus the month. The results are provided only for station {2} to illustrate the typical change in the T_{max} and T_{min} due to projected change in climate. For each month, each plot (the marker) represents a model run and the different plots (markers) are for the different model runs. The first, second and third rows are for scenarios A2, A1B and B1, respectively. Given the available model runs, it can be seen that, for T_{max} under A2 of 2050s (top left), for example, the projected change is in the range -4°C to 8°C. The change for the former but for 2090s, is within the range -2.5°C to 10°C. The projected change in T_{max} for 2050s as compared to that of 2090s is like a shift in T_{max} by +2°C. Change in T_{max} under A1B is

similar to that of A2. For B1 scenario, there is a slight difference, in which the range of change in T_{max} is -4°C to 6°C. The tendency for T_{min} to change in a similar way like T_{max} is also apparent. For example, the change in T_{min} under A2 and A1B of 2050s (Figure 7.13(g) and (h)) is in the range -3.5°C to about 9°C. Like the 2050s, the change for the 2090s (Figure 7.13(j) and (k)) is in the range -1.5°C to 9°C. Change in the T_{min} (Figure 7.13(i) and (l)) under B1 shows less increase as compared to A2 and A1B.

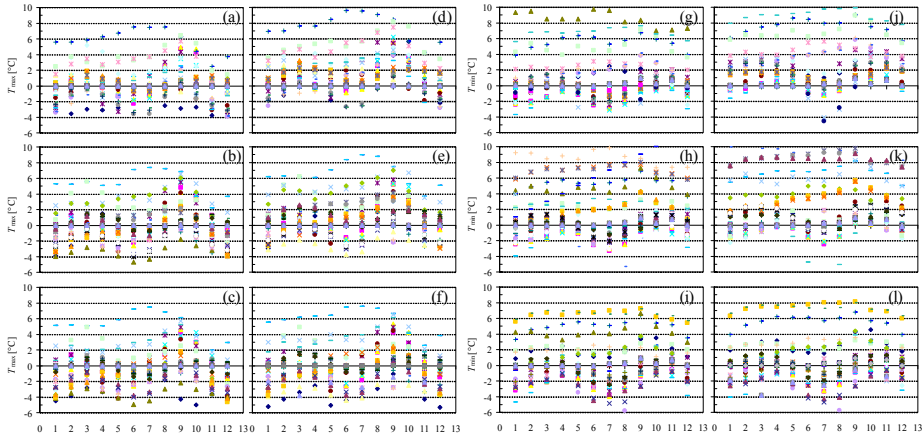

Figure 7.13 Perturbation for the monthly mean temperature (T_{max} and T_{min}) for the 2050s (a)-(f), and 2090s (a)-(l). The different markers in each month are for the different GCM runs. The results are for the data of the temperature station {2} illustrating the typical possible change in the mean monthly temperature in the Lake Victoria basin as a consequence of the influence of climate change.

The projected possible change in temperature indicates the lack of a clear and consistent change as demonstrated by the models. The possible change under the different scenarios is, however, consistent. The possible range of change is wider and indicates the uncertainty involved in the projection for possible change in temperature for the region, which is influenced by a number of systems. Particularly, for temperature, it is controlled by the recurrence of extreme values such as convective activities, ENSO, cloudiness, and above/below normal rainfall (King'uyu et al., 1999). The recurrences of extremes for the systems themselves also are not systematic. In addition, thermally induced mesoscale systems associated with orography and large Lake Victoria water body also introduce significant modifications to the large-scale flow over the region and if not well represented in the climate models, the resultant uncertainty is expected.

7.7 Conclusions on the change in rainfall extremes and temperature

The knowledge of the possible impacts of climate change on rainfall extremes provides useful and additional information for adaptation planning and management of water resources at local scale. Short of this knowledge, the

capacity of the local water resources manager to deal with adaptation to climate change becomes unquestionably limited. The study of the change in the rainfall extremes in the Lake Victoria basin, due to anthropogenic climate change, was carried out to provide benchmark information on the possible climate change impacts on rainfall extremes.

The change in rainfall extremes was assessed based on the principle of POT and extreme value analysis. Both change in rainfall and temperature was examined by comparing the present period and the future variable values. For rainfall, particular attention was paid to extremes while for temperature, the change in the monthly mean daily maximum and minimum temperature was considered.

With respect to rainfall, the findings indicate that possible increase in the magnitude of the rainfall extremes is projected. Based on emission scenarios A2, A1B and B1, the results revealed that rainfall extremes in the different parts of Lake Victoria basin are projected to change. For the western parts, consisting of Katonga, Ruizi, Bukora catchments and lower Kagera and some island catchments, the mean of the rainfall extremes are projected to increase by about 10% to 12% in the 2050s and 16% to 19% in the 2090s. The results further showed that the southwestern part of the basin would experience decrease in extremes by about 25% in the 2050s and 2090s. Furthermore, it was demonstrated that the eastern parts of the basin, consisting mainly of Nzoia, Yala, Mara and Nyando catchments would experience increase in rainfall extremes by about 13% to 29% in the 2050s and 18% to 31% in the 2090s. The rainfall extremes for the southern part of the basin are projected to increase with a relatively smaller percentage as compared to the western catchments.

The increase in rainfall extremes is projected for a range of durations and return periods. The magnitude of the heavier extreme events is projected to increase more than the less heavy rainfall extremes. This increase has major implications on the ways in which current (and future) water resources engineering planning is concerned, especially for river hydraulics and subsequently the municipal water management infrastructures.

The change in the monthly mean maximum and minimum temperature is projected to be more positive. The range of projected change in T_{max} is -4°C to 8°C and that for T_{min} is -4°C to 10°C. The tendency for the T_{min} to decrease in the drier months was eminent while the T_{max} is projected to increase more in the wetter months than in the dry months. The increase and decrease in T_{max} and T_{min}, respectively, would means an increase in difference between the T_{max} and T_{min} and thus an increase in evaporation.

CHAPTER 8

RAINFALL-RUNOFF MODEL DEVELOPMENT

8.1 Introduction

The development of a rainfall-runoff model for the simulation of a river catchment response involves the following: (1) defining its key components, (ii) preparation of its input variables, (iii) calibration and (iv) validation of the model. This procedure is often based on an existing hydrological model. The efforts needed during the development of the rainfall-runoff model depend mainly on the type and its input requirements. Several hydrological models exist, varying in nature, complexity and the purpose (Shoemaker et al., 1997). The selection of one or more of the models for a particular use is governed by numerous factors. Such factors include but are not limited to the objective for which the model is to be used, availability, the cost and expertise. Hydrological models, especially rainfall-runoff models, are widely used in understanding and quantifying the impacts of landuse change and to provide information that can be used in landuse decision-making (e.g. Fohrer et al., 2005). The contemporary wave of climate change has brought serious expansion in the application of hydrological models (e.g. Setegn et al., 2011; Baguis et al., 2010; Serrat-Capdevila et al., 2007; Chiew et al., 2007, 2009).

There are mainly two types of hydrological model commonly available in literatures. These are given nomenclatures such as conceptual and physically-based hydrological models. Physically-based hydrological models are based on the physics of the hydrological processes, which control catchment response, and use physically based equations to describe these processes. In physically-based hydrological model, a discretization or gridding of spatial and temporal coordinates is made and the solution is obtained at that level (Feyen, et al., 2000). A conceptual hydrological model describes essential features of a hydrological phenomenon and identifies the principal processes taking place. A complete conceptual hydrological model provides a: (1) definition of the phenomenon in terms of features recognizable by observations, analysis or validated simulations; (2) description of its life cycle in terms of appearance, size, intensity and accompanying weather; (3) statement of the controlling physical processes which enables the understanding of the factors that determine the mode and rate of evolution of the phenomenon; (4) specification of the key hydrological fields demonstrating the main processes; (5) guidance for predicted hydrological conditions or situations using the diagnostic and prognostic fields that best discriminate between development or non-development and (6) guidance for predicting displacement and evolution. Lumped conceptual type of models are

based on conceptual representations of the physical processes of the water flow lumped over the entire catchment area (Madsen, 2000). The parameters of such models cannot, in general, be obtained directly from measurable quantities of the catchment characteristics or estimated from a digital model of landuse for the catchment. Because the hydrological response is lumped as a unit, a lumped conceptual model requires less inputs compared to physically-based hydrological models. Thus, in an assessment of climate change impacts on the hydrology of a catchment where several climate models outputs are to be tested and utilized, a lumped conceptual model would be preferred. Thus, a lumped conceptual model was applied in this study.

The lumped conceptual hydrological model applied in this study is based on the generalized lumped conceptual and parsimonious model structure identification and calibration (VHM). The choice of the VHM was motivated by three factors: (1) its availability, (2) less input requirements matches well the data limitation of the study area, (3) it has the credibility of dealing with peak flows simulation as it has a component for the calibration of the peak flows, separately and (4) it is already tested for simulation of climate change impacts on hydrology of two catchments in the Nile basin (the focus area of this study) (Taye et al., 2011) with some plausibility in the results.

The calibration and validation of a rainfall-runoff model are often indispensable for its application. In a lumped concept, the calibration of the parameters of the model does not have, in most cases, a physical meaning and the parameterization is an optimization process not restricted to any physical boundaries (Sahoo et al., 2006). That is, the calibrated values of such model parameters are spatially averaged (e.g. Burnash, 1995) and cannot be derived from direct measurements. Nevertheless, lumped conceptual models have well proven record of accomplishment in terms of actual performance (Refsgaard, J. and Knudsen, 1996).

In the following sections, the components of the VHM is described, followed by its calibration and validation. Special emphasis was put on the performance of the model with respect to high flow peaks and streamflow constituents' simulation.

8.2 The VHM approach

The generalized lumped conceptual and parsimonious model structure identification and calibration is based on the procedure developed by Willems (2000b). Several pre-processing (using independent tools) steps are followed before the actual rainfall-runoff model component, in the VHM approach, is executed. The rainfall-runoff model component, in the VHM approach is also termed VHM, which is the simplified lumped conceptual hydrological model. The necessary input requirements are rainfall and potential evapotranspiration

(ET_o) lumped over the catchment. The hydrological or the rainfall-runoff (VHM) model is calibrated through a step-wise mode in which the time series preprocessing of the observed daily streamflows is considered very fundamental. The preprocessing permits the digital filtering of the historical streamflows into its constituents of hydrological sub-flows (quick flow, interflow and slow flow). In addition, it permits the selection of nearly independent quick and slow flow events and nearly independent high and low flow extremes from historical streamflows for the catchment (Willems, 2009). These constituents of hydrological sub-flows are very crucial for the calibration and validation of the model.

8.2.1 Extraction of high flows

Assessment of climate change impacts on water resources in which the focus is on hydrological extremes requires that the hydrological model exhibits a high proficiency in communicating with extremes (peak flows) during peak flow simulation periods. During calibration, therefore, the hydrological model needs to be well informed to capture peak flows such that the measure of calibration performance is considered good. This requires that the peak flows of the historical series are extracted a forefront. Extraction of flow peaks (POT) constitutes an important step in the VHM approach. Thus, a robust method for extracting peak flows needs to be employed. The techniques of subflows separation has been tested and employed in the field of hydrology (e.g. Chapman, 1999; Echardt, 2005). The objective is to separate total flow series into slow flow and quick flow periods. Willems (2009) provides a valuable method for digital filtering of total flow series into its said constituents. The principle in Willems (2009) is that the peak flows can be extracted from the total series based on the inter-event time, the inter-event low flow and the peak flow height criteria (Figure 8.1). Willems (2009) notes that two peak flow events are taken to be nearly independent if the following conditions are met:

(1) the time length, p, of the decreasing flank of the first event exceeds a certain time, k

$$p > k \tag{8.1}$$

(2) the discharge between the two events drops to a fraction lower than f of the peak flow

$$\frac{q_{\min}}{q_{\max}} < f \tag{8.2}$$

or close to baseflow

$$\frac{q_{\min} - q_{base}}{q_{\max}} < f \tag{8.3}$$

(3) the discharge increment $q_{max} - q_{min}$ has a minimum height q_{min}:

$$q_{max} - q_{min} > q_{lim} \tag{8.4}$$

The selection of the POT is based on the principle that a peak flow event can be considered as largely autonomous from the subsequence one, if the inter-event discharge reduces to a low flow condition or almost to the baseflow level. This is reasonable but on the condition that the quick flow components attributed to the peak flow events are within the independency proximity. In order to attain a near-baseflow state, p should be longer than the recession constants of the quick flow components.

The parameter k in (8.1) can be taken as equal to the recession constant of the quick flow or higher (e.g. two or three times the recession constant) if a stronger independence between subsequent flow events is to be attained. Note that the recession constant of a flow component is defined as that value which reaches a value lower than 37% of its peak value after a dry weather period longer than the recession constant (Nathan and McMahon, 1990). Note also that, since the inter-event periods are not always completely dry, criterion (2) is also significant. The fraction f is taken approximately to be the upper limit of the baseflow fraction in the peak flow. Depending on the accuracy of the baseflow filter results, small portion values of 5%, 10% or 15% are considered for f. Constraint (3) eliminates the noise from the low peaks. Parameter q_{lim} is considered an upper limit of the highest noise peaks or the high changes, which cannot be associated with quick flow events.

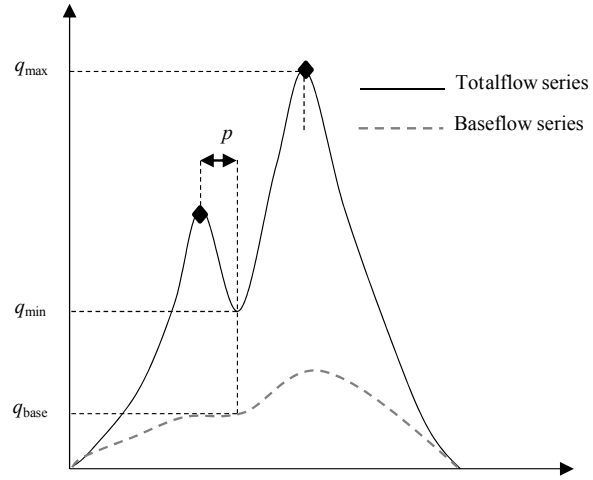

Figure 8.1 Parameters for the selection of nearly independent flow peaks from a river streamflow series. An illustrative diagram reproduced from Willems (2000b).

All significant peak events are extracted from the flow series using three criteria after which the peaks are assumed autonomous, i.e. iid, both physically and statistically. If the peak flow, q_{max}, is extracted and the interest is on low dip, the lowest flow dip is between two consecutive peaks (q_{max}) can

be determined and the time series divided in periods based on the time moments of these low flows. The series are then considered as PDS and form nearly independent quick flow hydrographs (Figure 8.2).

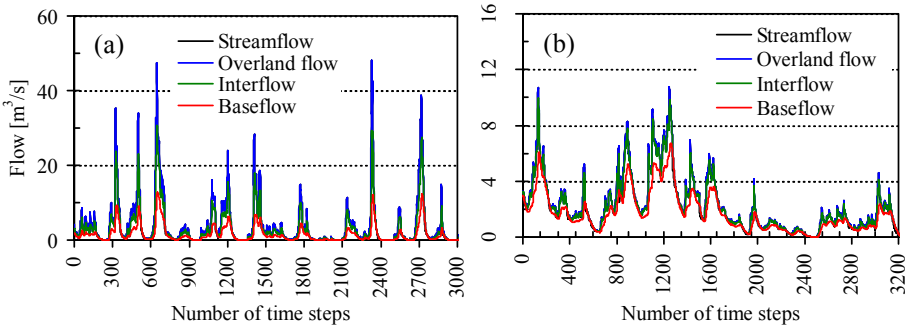

Figure 8.2 Digitally filtered constituents of the streamflows for the River Ruizi (a), and Katonga (b).

8.2.2 The VHM model structure

The key structural architectures of the VHM comprise the rainfall input, soil moisture storage, a groundwater storage and flow routing components (Figure 8.3). The components, together, represent or describe the rainfall-runoff process. The model is constructed after the disjointing of the historical series into quick flow and slow flows and in quick and slow flow events (Figure 8.2).

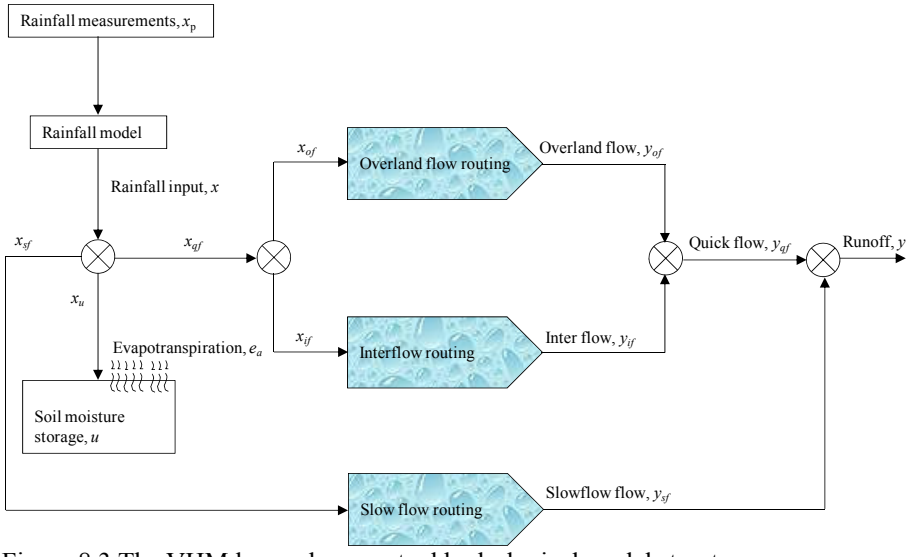

Figure 8.3 The VHM lumped conceptual hydrological model structure.

The initial separation shapes the calibration of the model. Analysis of the quick flows and slow flows time series enable the examination of the

hydrograph characteristics and event specific portions of the rainfall input, subflows and total flows are determined. They are used to isolate and calibrate the rainfall-runoff relationships, which converts rainfall depths to flow.

The rainfall input is assumed to be separated into different constituents based on the rainfall fractions f_{qf}, f_{sf}, f_u that contribute to quick flow, slow flow and soil moisture storage, respectively. The f_{qf} may further be divided into interflow, f_{if}, and overland flow, f_{of}, fractions (Figure 8.3). The time variation of these fractions is controlled by the relative soil moisture state, $u/u_{\max}$, where $u_{\max}$ is the maximum storage capacity and u the soil moisture content at a given time. If the soil moisture increases, the saturation increases and the infiltration decreases. Thus, the rainfall contribution to soil moisture, f_u, decreases with the increase in soil moisture content meanwhile f_{qf} increases. Willems (2000) further notes that the specific relationships are obtained in a databased means and take the forms given in equations (8.5)-(8.7) for both the River Katonga and Ruizi catchments.

$$f_u = c_{u,1} - \exp\left(c_{u,2} \left(\frac{u}{u_{\max}} \right)^{c_3} \right) \tag{8.5}$$

$$f_{of} = \exp\left(\left(c_{of,1} + c_{of,2} \frac{u}{u_{\max}} \right) + (c_{of,3} + c_{of,4} \ln r) \right) \tag{8.6}$$

$$f_{if} = \exp\left(\left(c_{if,1} + c_{if,2} \frac{u}{u_{\max}} \right) + (c_{if,3} + c_{if,4} \ln r) \right) \tag{8.7}$$

where $c_{u,1}$, $c_{u,2}$, $c_{of,1}$, $c_{of,2}$, $c_{of,3}$, $c_{of,4}$, $c_{if,1}$, $c_{if,2}$, $c_{if,3}$, $c_{if,4}$, are model coefficients and r is the cumulative rainfall depth during the antecedent periods. The first parts of (8.6) and (8.7) represent the model quick flow during the saturation level or saturation excess and the second parts represent the modelled quick flow if the rainfall depth is higher than the infiltration rate or infiltration excess. The rainfall fraction f_{sf} is estimated from

$$1 = f_{qf} + f_{sf} + f_u \tag{8.8}$$

The storage volume u is obtained from the respite rainfall after deducting the actual evapotranspiration, e_a, which is a function of the soil moisture storage and the potential evapotranspiration, e_p, given by

$$e_a = \begin{cases} \dfrac{u}{u_{evap}} & , \; u < u_{evap} \\ \text{else} & \\ e_a = e_p & \end{cases} \tag{8.9}$$

where u_{evap} is the threshold that fine-tunes the actual evapotranspiration. The rainfall depths are transformed into streamflows, y_{qf}, y_{of}, u_{if} and y_{sf} through the reservoir routing models. The routing of the subflows is modelled using a cascade of linear reservoirs principle with respective values of recession constant, k. These recession constants of the linear reservoir are k_{of}, k_{if} and k_{sf} for the overland flows, interflows and slow subflows, respectively.

8.3 Calibration and validation of the rainfall-runoff models

Hydrological model calibration is a search process for unknown optimal values of the target parameters and attainment of a better fit with the available hydrological data. A better model fit is usually attained by an objective criterion based on a numerical metric, often reported as a fraction or percentage. Calibration of a hydrologic model can be automatic or manual (e.g. Blasone et al., 2007; Madsen, 2000). Traditionally, calibration of hydrological models has been performed manually by trial-and-error parameter adjustment. The process of manual calibration, however, requires a high degree of expert knowledge of the model and the system and is characterized by subjectivity in the strategy employed to adjust the parameter values and in the criteria (mainly visual) used to judge the goodness-of-fit of the model simulation with the observation. Moreover, manual calibration is a very tedious and time-consuming task (Boyle et al., 2000; Madsen et al., 2002). However, the process allows the users to have a full control of the calibration process with a better understanding of the underlying principle. In a contemporary hydrological modelling, manual calibration is quite often substituted by automatic procedures, which have found widespread use in hydrology. The main advantages of automatic techniques are the speeding up of the calibration process, the reduced subjectivity involved in the calibration procedure and the availability of generic software that can be, relatively, easily linked to the model. Despite the availability of the various automatic calibration techniques, their applications are limited by computational constraints (Blasone et al., 2007).

Whether one employs automatic or manual calibration of a hydrological model, the objective is the model prediction equifinality. That is, calibration of rainfall-runoff models, with respect to local observational data, is used to improve model predictability. When model results match observed values of streamflow measurements, users have greater confidence in the reliability of

the model. Reliability of a model, thus, is assessed through a validation process, which is the post-testing of the calibrated model with a new but different set of observed data whose results can be verified using certain criteria.

In this study, a manual calibration methodology was employed to calibrate the VHM model. The VHM architectural environment provided in section 8.2.2 allows the users to have full control of the process and the calibration is based on the different components of the streamflows. That is, its step-wise calibration provides flexibility to calibrate the different constituents of the flows separately. The following section discusses the actual step followed and the procedure carried out to calibrate and validate the VHM model.

8.4 Rainfall-runoff model set up

The major input hydrometeorological variables into VHM model are the catchment rainfall and the catchment ET_o. For calibration and validation, ET_o was derived from pan evaporation data (type A pan) based on pan coefficient approach (Allen et al., 2006) discussed in chapter 3. Meanwhile, the catchment rainfall was obtained by application of Thiessen polygon method (Linsley et al., 1949) also discussed in chapter 3. The selection of the calibration and validation periods (Table 8.2) was based on the streamflow data availability and quality (see Chapter 3, section 3.3). In addition to the catchment rainfall and ET_o, the specification of the drainage area upstream of the selected streamflow station, was necessary. The constituents of the streamflows (baseflow, interflow and slowflow) also formed parts of the input requirements for calibration. Note that one streamflow station for each catchment, was considered in this study. Thus, calibration and validation was done at gauging station number 81224 for Ruizi catchment and at gauging station number 81259 for Katonga catchment (See appendix B). The respective drainage area upstream of the station 81224 (Katonga) and 81259 (Katonga) are 2070 km^2 and 6955 km^2. 6 and 8 years of data were processed and used for calibrating the VHM model for Ruizi and Katonga, respectively.

8.4.1 Calibration of the rainfall-runoff models

After model set up, VHM was calibrated in a stepwise manner. First, the storage water model was calibrated, in which the soil water moisture parameters are considered. In this case, the filtered baseflow is targeted for fitting based on the Nash-Sutcliff efficiency criterion (section 8.4.2). Secondly, the overland flow model was calibrated and the model parameters of interest were the coefficients, $C_{of,j}$, j = 1, 2, 3, 4 (eq. 8.6). For each adjustment of the coefficient, $C_{of,j}$, the model overland flow was checked against the filtered observed overland flow based on the Nash-Sutcliff efficiency criterion (section 8.4.2). Finally, the interflow model was calibrated by adjusting the parameters (coefficients), C_{if}, (eq. 8.7). For each adjustment

of the coefficient, C_{if}, the simulated interflow is checked against the filtered interflow also based on the Nash-Sutcliff efficiency criterion (section 8.4.2).

Table 8.1 Calibrated parameters for the rainfall-runoff (VHM) models

Ruizi								Katonga							
Soil moisture		Overland flow		Interflow		Flow routing		Soil moisture		Overland flow		Interflow		Flow routing	
u_{max}[mm]	280	$C_{of,1}$	0.92	$C_{if,1}$	-5.50	k_{sf}[h]	15	u_{max}[mm]	1950	$C_{of,1}$	0.93	$C_{if,1}$	-5.30	k_{sf}[h]	60
u_{evap}[mm]	91	$C_{of,2}$	0.99	$C_{if,2}$	2.80	k_{if}[h]	5	u_{evap}[mm]	101	$C_{of,2}$	0.99	$C_{if,2}$	2.80	k_{if}[h]	10
u_{ini}[mm]	50	$C_{of,3}$	-8.3	$C_{if,3}$	-0.55	k_{of}[h]	1	u_{ini}[mm]	60	$C_{of,3}$	-10.5	$C_{if,3}$	-0.55	k_{of}[h]	1
$C_{u,1}$	0.99	$C_{of,4}$	0.77	$C_{if,4}$	0.01			$C_{u,1}$	0.99	$C_{of,4}$	0.77	$C_{if,4}$	0.01		
$C_{u,2}$	0.13							$C_{u,2}$	0.12						

The routing of the simulated flow constituents, therefore, resulted into total flows, which were then compared with the observed total flows. Table 8.1 provides the optimum values of the different parameters used in the calibration. Note that the high value of u_{max} for the River Katonga catchment (Table 8.1) is a manifestation of the wetness of the catchment due to the presence of many small lowlands and wetlands.

8.4.2 Calibration performance criteria

Model performance criteria are ways in which the simulated streamflows can be evaluated against the observed streamflows in order to measure the fidelity and simulation skills of the calibrated model. Several of such criteria are available and the selection of one to be employed in the impact assessment is often based on the objective for which the model is calibrated. However, an indicator or statistic that gives the general assessment of a calibrated model is always necessary. The hydrograph of simulated streamflows is often the first graphical criterion used in assessing the model performance. Figure 8.4 shows the daily streamflow hydrographs for simulated and observed for the two catchments. It can be seen that the model underestimates peak flows in both cases.

The Nash-Sutcliffe coefficient of efficiency, *RE*, (Nash and Sutcliffe, 1970), described in appendix A.5, was used to evaluate the efficiency of the calibrated VHM model. A value of, $RE = 1$ indicates perfect fit between the simulated and observed streamflow. The values *RE* was 0.7 for Katonga, and 0.67 for Ruizi (Table 8.2). These values are within acceptable range of what is considered fairly good calibration according to the current sphere of hydrological modelling practice. Figure 8.5 shows graphical evaluation criteria for simulated peaks and water balance. In Figure 8.5(a) and (d), simulated and observed peak flows are compared after a Box-Cox (BC) transformation (Box and Cox, 1964). The BC transformation, rank-preserving transformation, is one of the power transforms, which is ubiquitously used in various fields to stabilize variance and make the data more normal distribution-like.

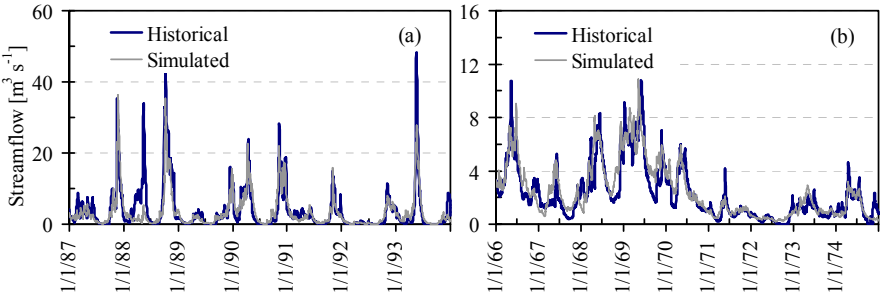

Figure 8.4 The hydrographs of the simulated (obtained during calibration) and observed streamflows for the River Ruizi (a), and Katonga (b).

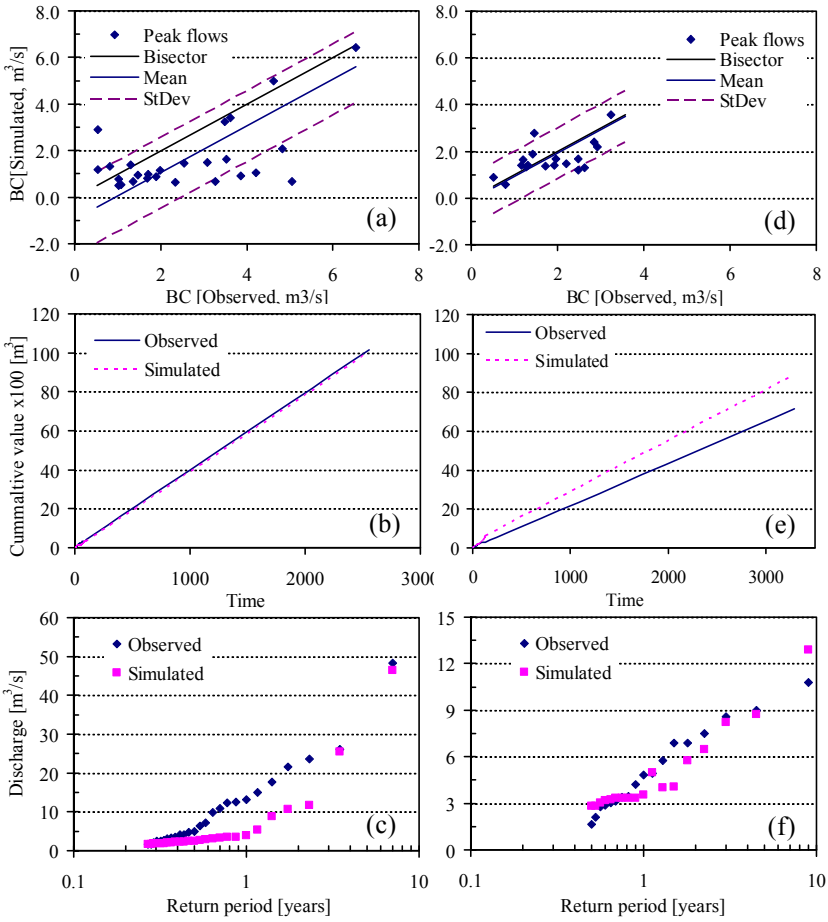

Figure 8.5 Comparison of the streamflow peaks and cumulative values of the simulated and observed streamflows during the model calibration: (a)-(c) River Ruizi, and (d)-(f) River Katonga.

For a good match between simulated and observed peaks, the peak plots are supposed to plot (fall) around the mean line and the mean line should be as close as possible to the bisector line. However, the peak plot that falls within

the limits of standard deviation (StDev) is considered to have a fairly good match. It can be seen that for the River Ruizi catchment (Figure 8.5(a)), the peak flows are generally underestimated; meanwhile for the River Katonga catchment (Figure 8.5(d)), the simulated peaks match the observed ones much better. This can further be seen from the distribution of simulated peak and observed streamflows for the River Ruizi (Figure 8.5(c)) and Katonga (Figure 8.5(f)) catchments. In both cases, the peaks corresponding to higher and lower return periods were well simulated.

Table 8.2 Calibration and validation periods and the associated values of the Nash-Sutcliff coefficient of efficiency, *RE* the Ruizi and Katonga rivers.

	Ruizi			Katonga		
	Calibration	Validation	Control	Calibration	Validation	Control
Period	1987-1993	1994-1997	1981-2000	1966-1974	1975-1979	1981-2000
RE	0.67	0.64		0.70	0.77	

The overall water balance discrepancy was -1.3% for the River Ruizi catchment and 20% for the River Katonga cathcment. Figure 8.5(b) and (e) shows the plots of cumulative value or the water balance discrepancy with the time. It can be seen that, albeit the *RE* for the River Ruizi catchment is lower than that of Katonga, its overall water balance was well replicated.

8.4.3 Validation of the rainfall-runoff models

Model validation, sometimes referred to as verification, is an evaluation of the capabilities of a calibrated model using different data set (Blasone, et al., 2007). In most cases, model validation is applied in the absence of site calibration data and limited validation data; it is possibly the most important step in the model building sequence. The data sets for the validation were taken from different data periods shown in Table 8.2. Indeed data limitations often impose calibration and validation constrains on hydrological modelling sequence (Refsgaard and Knudsen, 1996). Nevertheless, useful results can often be obtained from the limited available data (Stehr et al., 2008).

The criteria used to assess the calibration performance were also applied to assess evaluation performance. That is, the hydrographs, *RE*, water balance and the peak flow distribution plots were used. Figure 8.6 shows the hydrographs for the simulated and observed streamflows for the validation. It can be seen that for River Ruizi catchment (Figure 8.6(a)), the hydrographs of simulated matches well that of the observed for most parts of the period, except for the last year, 1997. For the River Katonga catchment (Figure 8.6(b)), simulated hydrograph appears to underestimate the peaks.

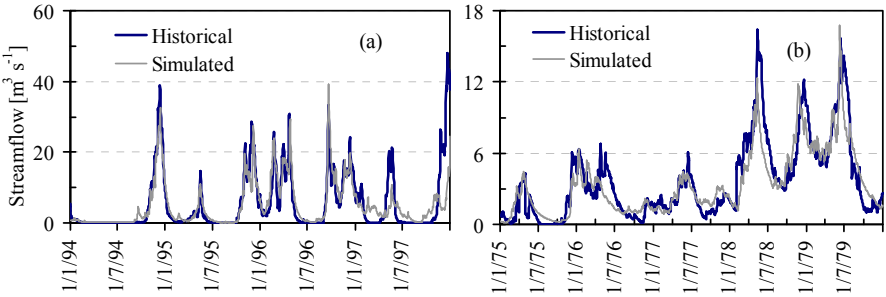

Figure 8.6 The hydrograph of the simulated streamflows, compared to the observed (historical), obtained during the validation: (a) River Ruizi and (b) River Katonga.

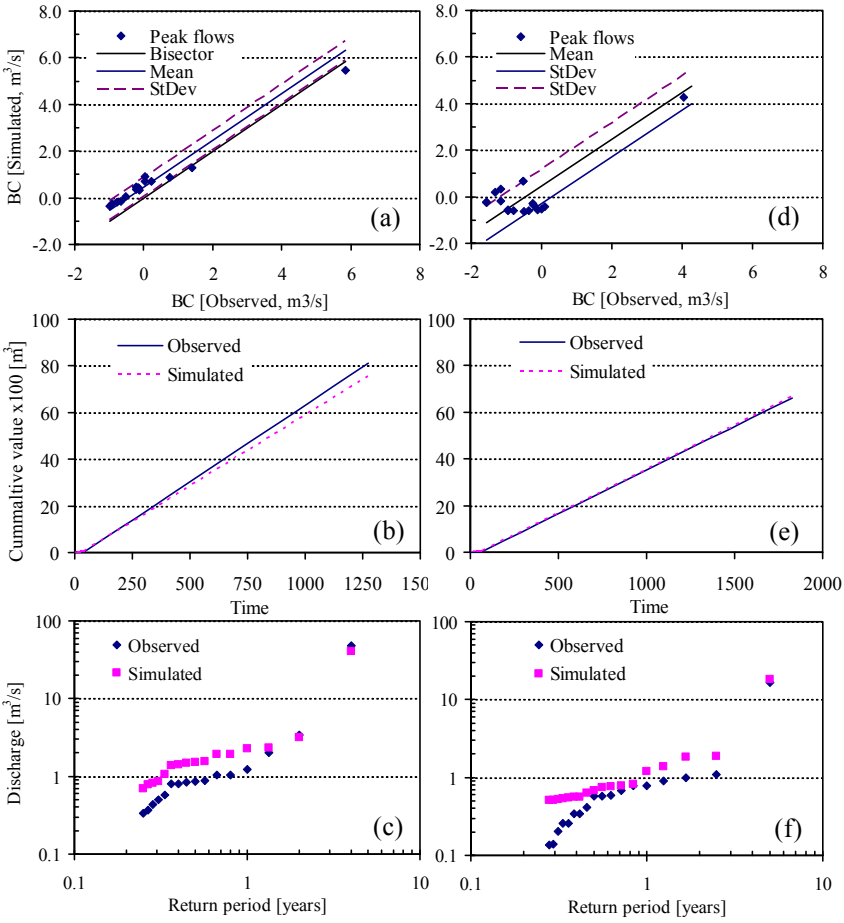

Figure 8.7 Comparison of the streamflow peaks and cumulative values of the simulated and observed streamflows during the model validation: (a)-(c) River Ruizi, and (d)-(f) River Katonga.

The water balance discrepancy was -6.9% and 1.1% for the River Ruizi and Katonga catchments, respectively. Figure 8.7(b) and Figure 8.7(e) also show that there is good agreement between the cumulative value, for the simulated

and that of the observed streamflow for both the two catchments. The BC plot for the River Ruizi catchment (Figure 8.7(a)) shows that most of the plot points are concentrated around the mean line and that the mean line is also close to the bisector line. The implication is that the model was fairly well informed to capture peak flows. However, evidence of overestimation of the peaks is apparent because the mean line is above the bisector line. The overestimation is mainly for the high flows with medium return periods (i.e. mean peak events) as can be seen from Figure 8.7(c). Similarly, Figure 8.7(d) also shows the model tendency to overestimate the high flow peaks with a little poor match for the high flow peaks having lower return periods. This is also evident in high flow peaks distribution (Figure 8.7(f)). The overall *RE* values for the model validation was 0.64 for the River Ruizi catchment and 0.77 for that of Katonga. These results reflect good fits between the simulated and observed streamflows for both the catchments.

8.5 Conclusions on the rainfall-runoff model development

The hydrological (rainfall-runoff) models for the River Ruizi and Katonga catchments were constructed based on a lumped conceptual principle using the VHM approach. Considerable efforts were put on the calibration and validation of the modles. The equifinality of calibration and validation of a hydrological model is the good representation of the catchment-response behaviour, irrespective of the method applied. The modelling purpose for which the model is calibrated and validated determines the sufficiency of the calibration and validation results. In this study, the VHM was calibrated and validated with the main objective of having a good proficiency in communicating with the high flow peaks during peaks simulation in order to increase confidence in the results of the impacts of climate change on the hydrological extremes. 6 and 8 years of data were used for the calibration of the models for the River Ruizi and Katonga cathcments, respectively. 4 and 5 years of data were used for validation of the models for the River Ruizi and Katonga catchments, respectively. Two strategies were employed for the calibration: (1) splitting of the observed streamflows into its constituents of baseflow, interflow and overland flow and calibrating the respective model separately, (2) selection of the nearly independent high peak flows, which were used during the model built up sequence. Both the calibration and validation efficiency were assessed based on the graphical and Nash-Sutcliffe statistical (*RE*) criteria. In the former, it was shown that the two catchments' high flow peaks could, fairly, well be simulated by VHM model. While for the latter, the results showed an overall efficiency measure of 0.67 and 0.70 for the River Ruizi and Katonga, respectively. The *RE* values for the validation were 0.64 and 0.77 for the River Ruizi and Katonga, respectively. Thus, the performance of the calibration and validation of the VHM models for the River Ruizi and Katonga catchments was well within acceptable level and was considered plausible for use in simulating the hydrological responses of the two catchments to anthropogenic climate change influence.

CHAPTER 9

HYDROLOGICAL CLIMATE CHANGE IMPACT

9.1 Introduction

Assessment of climate change impacts on hydrology of a catchment can appropriately be carried out through simulation of the hydrological conditions that shall prevail under the projected climatic states. Such a treatment is essential because of the fact that the hydrological response is a very complex process governed by a multitude of variables such as terrain, landuse, soil characteristics and the state of the moisture in the soil. The last element warrants a continuous time simulation to keep track of the changing moisture conditions.

A number of studies have reported on the use of both physically based and lumped conceptual models for the assessment of climate change impacts on the hydrology of a catchment (e.g. Chiew et al., 1995; 2009; Gosain et al., 2006; Andersen et al., 2006; Alcamo et al., 2007; Nóbrega et al., 2011). In most of the studies, the hydrological model is powered by the outputs from several climate models to provide runoff as outputs, which can then be analyzed for different impact interests. This is currently a widely accepted practice for better understanding of the possible impacts of climate change on the hydrological regimes. One of the key assumptions in the hydrological modeling of climate change impacts is that future landuse type will be similar to that of the current state and the resulting impacts is, purely, that from the climate change. However, some studies have incorporated landuse change scenarios within the hydrological scheme (Bronstert, 2002). In either case, the hydrological model needs to provide a robust physical basis in order for the results to be plausible. As noted by Kaspar (2004), the robustness of the hydrological model is very crucial in the estimation of the hydrological impacts of climate change.

Some relevant studies have been carried out with the aim of assessing the possible impacts of climate change on the hydrological regimes at local scale in the Nile basin. Githui et al. (2009) applied SWAT (a physically based hydrological model), powered by five climate model runs, to assess the impacts of climate change on the hydrological regimes of River Nzoia catchment under a basic assumption of no change in landuse type. They report that significant increase in streamflows may be expected because of the increase in the rainfall. Notter et al. (2007) also applied a physically based hydrological model (NRM3), driven by one climate model (ECHAM4) to a sub-catchment of Ewaso Ng'iro basin in Mt Elgon region. Their results

showed that the increase in the stream flow is projected to be dramatic. They further argued that the dramatic changes in the streamflows might have been a consequence of combining land use change with climate change scenarios. Setegn et al. (2011) also applied SWAT to assess the impact of climate change on the hydroclimatology of Lake Tana Basin, Ethiopia. They used 15 GCM runs under A2 scenario, and showed that statistically significant declines in annual streamflow for the period 2080-2100 are projected. Taye et al. (2011), in contrast, applied two lumped conceptual hydrological models, VHM and NAM model, to assess the impacts of climate change on low flows and high flows of River Nyando and Lake Tana catchments. Several GCM runs were used to power VHM and NAM. The results showed that the hydrological models project increase in runoff extremes for Nyando catchment towards the 2050s, while for Lake Tana catchment, unclear trend is projected for cumulative volumes as well as high flows and low flows.

From the preceding discussions, it is clear that apart from the uncertainties that are involved, the impacts of climate change on the hydrology of a given catchment will significantly be different even if the catchments are within the same basin. This is because of the fact that different catchments will response to climate change differently based on its internal dynamics influenced mainly by the type of catchment management. Albeit there are some relevant local studies on climate change impacts on high flows, the focus on flood frequency has not to captured much attention. In addition, an in-depth high flows frequency analysis for the current study is a subject matter, which has been seldom studied for climate change impacts. This chapter therefore deals with the impacts of climate change on the streamflows of the River Katonga and Ruizi catchments with a more in-depth analysis on high flow frequency.

9.2 Impact simulations

In the previous chapter, the rainfall-runoff model wasdeveloped for the simulation of the hydrological impacts of climate change. The model was principally used to simulate the future streamflows for the River Katonga and Ruizi catchments. The simulation of the future hydrologic state of a catchment is inherent in the projected catchment rainfall and ET_o. The projected catchment rainfall and ET_o are estimated from the selected and qualified GCM runs.

9.2.1 Projected catchment rainfall and ET_o

The projected catchment rainfall time series was obtained by downscaling the GCM runs based on the areal daily rainfall time series using the technique described in chapter 6. The projected catchment daily ET_o time series was indirectly derived from the downscaled T_{max} and T_{min} using the Heagreaves method for ET_o estimation (chapter 3). Estimation of the projected catchment rainfall and ET_o, for each GCM run, was done for scenarios A2, A1B and B1

and for the periods 2050s (2046-2065) and 2090s (2081-2100). At this stage, it was possible to assess the impacts of climate change on River Katonga and River Ruizi catchment rainfall and ET_o. The impacts of climate change on catchment rainfall and ET_o were also assessed based on the projections of the catchment rainfall and ET_o for the baseline period.

9.2.1.1 Change in rainfall and ET_o

Rainfall and ET_o play very important roles in the overall catchment water balance and are very synchronous. Understanding the changes in rainfall and ET_o provides preliminary information on the expected change in a catchment response. In some cases, changes in catchment response are predicted based on changes in ET_o and rainfall only using the "downward" principle (Sivapalan et al., 2003). In order to obtain the change (perturbation) in the catchment rainfall and ET_o, a baseline series for catchment rainfall and ET_o were computed based on the records of the measurements for the period 1981-2000. The ET_o for the baseline was estimated based on the FAO Penmann-Monteith (FAO PM) method for ET_o estimation (Appendix B.6). Application of the FAO PM to estimate the baseline ET_o was, in this case, because of the availability of some of the typical data.

The inter-annual mean seasonal catchment rainfall and ET_o values (mean seasonal estimates) were computed for both the baseline and the future periods. Using the mean seasonal estimates, the perturbations of the catchment rainfall and ET_o were computed as the respective ratios of the future value of the seasonal estimate to that of the baseline value of a given season. The perturbations were obtained as the ensemble average of the values of the perturbations of 15 GCM runs for scenario A2 and 17 GCM runs for scenarios A1B and B1 obtained from 13 GCMs. The use of the ensemble mean was to provide the average results of the projected change in the seasonal mean catchment rainfall and ET_o. Figure 9.1 shows the perturbation of the seasonal estimates for rainfall and ET_o. The different seasons are represented by MAM (March-May), JJA (June–August), SON (September–November) and DJF (December–February) (Figure 9.1). It can be seen from Figure 9.1 that the perturbations for ET_o (top) are generally, but slightly, greater than 1. For the River Katonga catchment (Figure 9.1(a)), for example, the perturbations for all the seasons resonate around 1. That is, an increase of about 3.5-4% (2050s-2090s) and 1.4-2.6% (2050s-2090s) is projected for MAM and JJA seasons, respectively. The implication is that for the River Katonga catchment, the seasonal mean ET_o, is projected not to change so much in the future as compred to the current record. For the River Ruizi catchment (Figure 9.1(b)), the ET_o perturbations for the seasons MAM, JJA and DJF are generally greater than 1. That is, an increase in ET_o of about 9.5-11.2% (2050s-2090s) and 7.7-9.7% (2050s-2090s) is projected for MAM and JJA seasons, respectively. Slight reduction, however, is projected for SON

and DJF seasons. The change in the ET_o for the River Ruizi is, thus, projected to be slightly higher than that of Katonga.

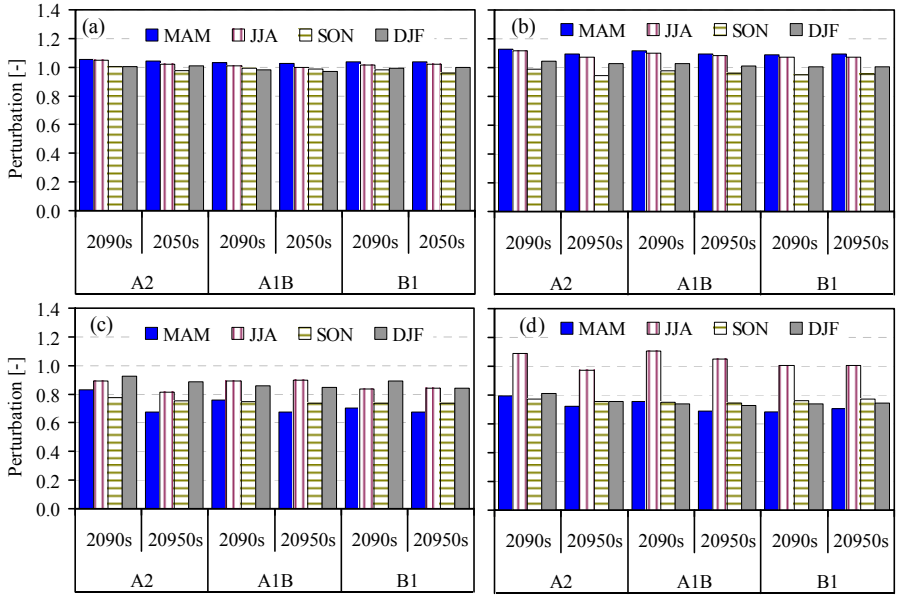

Figure 9.1 Change in the seasonal mean rainfall (bottom) and seasonal mean ET_o (top) for: (a) and (c) River Katonga, and (b) and (d) River Ruizi catchments. The results provided are for the mean of an ensemble of several GCM runs.

It should be noted that the change in evapotranspiration is strongly governed the changes in temperature and the humidity of the air (vapour pressure deficit) among other factors such as windspeed and net radiation. Thus, projected increase in ET_o for the seasons JJA and DJF reflects increase and decrease in temperature and humidity, respectively for the seasons.

In contrast to change in ET_o, the season mean catchment rainfall is projected to decrease (Figure 9.1 (c)-(d)). This is explained by the values of the perturbations, which are generally less than 1 (Figure 9.1 (c)-(d)) for both the River Katonga and Ruizi catchments. However, for the River Ruizi catchment (bottom right), the mean rainfall for the season JJA is projected to slightly increase. That is, an increase in rainfall is projected in the future by about 0.9-6.6% (2050s-2090s). For the River Katonga, the reduction in the seasonal mean catchment rainfall for SON will be higher than that of the other seasons in the 2090s, but in the 2050s, the seasonal mean catchment rainfall for MAM is projected to decrease more than that of the other seasons.

9.2.1.2 Relationship between change in rainfall and ET_o

Rainfall and ET_o are not absolutely independent variables because they are part of a physical system. Change that occurs within the physical system must be reflected proportionally in the rainfall and ET_o. In addition, ET_o is

indirectly estimated from direct outputs of GCM such as temperature. A realistic or meaningful change in ET_o, as compared to that of rainfall, vindicates the reliability of the GCMs. This is based on the assumption that the ensemble mean value is treated as though it is from a single GCM. Thus, the seasonal mean perturbations for rainfall and ET_o were correlated.

Figure 9.2 shows the correlations between the perturbations for the seasonal mean catchment ET_o and rainfall for MAM, JJA, SON and DJF seasons. Consider A1B and B1 scenarios for the River Katonga catchment (top), it can be seen that the correlation between the perturbation for ET_o and rainfall is negative for MAM and DJF seasons and positive fo SON and JJA seasons. JJA is a very dry season for the current study area and is a manifestation of an increase in temperature and a reduction in the humidity due to dryer air. For the River Ruizi catchment (bottom), a positive correlation between ET_o and Rainfall is apparent for JJA under A2 and A1B but a negative correlation for the season MAM. Furthermore, the tendency for negative correlation between ET_o and rainfall for MAM, SON and DJF is eminent, except for A2 and A1B, where the correlation for MAM, like for Katonga, is negative. The inconsistent correlation in the perturbations for the seasonal mean ET_o and rainfall, especially for MAM and JJA has some possible implications. First, it is a manifestation of the uncertainty in the GCMs, especially under the high scenarios, A2. Secondly, the increase in temperature accounts for the increase in ET_o in the case where there is a decrease in rainfall and humidity. That is, with the limited rainfall the increase in the ET_o is mainly temperature driven.

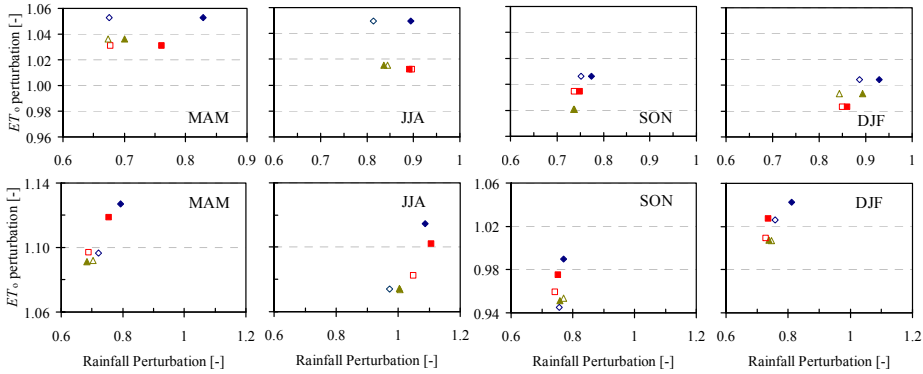

Figure 9.2 The relationship between the change in the seasonal mean ET_o and rainfall for the River Katonga (top) and Ruizi (bottom). The filled and non-filled makers are for the 2090s and 2050s, respectively. The diamond, square and triangle markers are for the scenarios A2, A1B and B1, respectively.

The irregular relationship between rainfall and ET_o (Figure 9.2) may not be anomalous because of the fact that the current state of the climate of the Lake Victoria basin, which the River Katonga and Ruizi catchments being integral parts, indicates that rainfall only exceeds ET_o by a factor of 0.1. In some months, ET_o exceeds rainfall, whereas outflow, from the lake, exceeds inflow

by a factor of 0.27 (Sewagudde, 2009). In addition, a change from 50% cloudiness to 30% can increase evaporation by about 30% (Yin and Nicholson, 1998). Thus, the influence of climate change may alter the current relationship between rainfall and evaporation significantly mainly due to increase in temperature.

9.2.2 Simulations of the future streamflows

After the estimation of projected catchment ET_o and rainfall time series, simulation of the future streamflows was carried out using the VHM model under scenarios A2, A1B and B1 for the 2050s and 2090s. The results of such simulations can be compared with the current streamflows. Simulated streamflows however cannot be compared directly with the observed streamflows obtained from the field measurements because of the bias in the hydrological model. One of the sources of the bias in the hydrological model stems from the fact that it is seldom possible to calibrate the hydrological model perfectly. Thus, a baseline period simulation was carried out to obtain the control streamflows. The period 1981-2000 was considered as the baseline to characterize the hydrological response (control streamflow) for that control period. The observed rainfall and ET_o estimated for that period were used as inputs into the VHM in order to realize the control streamflow.

9.2.2.1 Change in high flows

Understanding the change in high streamflows (flow peaks) is very crucial for the sustainable environmental management such as flood predictions and hydraulic (engineering) applications. The change in the magnitude of the flow peaks can be derived by comparing the peaks from the future streamflows (projected or future peaks) with that of the control (control peaks). First, the independence peaks, both for the future and control, for a 1-day duration were selected based on the selection criteria described in chapter 7, section 8.2.1. The ratio (perturbation) of future peak to that of the control with the same return period was computed for all the peaks. This was done for all the scenarios, GCM runs and the 2050s and 2090s. The perturbations of flow peaks provide information on its possible change in the future.

Figure 9.3 shows the perturbation of flow peak versus the return period (perturbation plot) for the different GCM runs. It can be seen that the perturbation plots for most of the GCM runs lie below the perturbation value of 1, except in some cases where the perturbations are above the value of 1. This means that the flow peaks, corresponding to different return periods are generally projected to decrease. Consider, for example, a case (A2, 2050s) for the River Katonga catchment (top left), the perturbation plots for two GCM runs are above 1 but with one of them being very high above 1. This indicates that the flow peaks corresponding to all the different return periods are projected to increase. Note that the perturbations for light peak flow events are higher than that for the mild and heavy peak flow events. In general,

perturbations are constant as return period increases, for the River Katonga peak flows. The implication is that the mild, medium and heavy peak flow events are projected to change by similar amounts. For the River Ruizi, catchment, the perturbation plots (last two columns on the right) for most of the selected models, are generally are less than 1 and for most of the return periods. Compared to that for Katonga, the perturbation, for the River Ruizi catchment strongly decreases with increase in return period. This means that a stronger change in the tail of the distribution of flow peaks, for the River Ruizi, is projected for both the 2050s and 2090s as compared to that of Katonga.

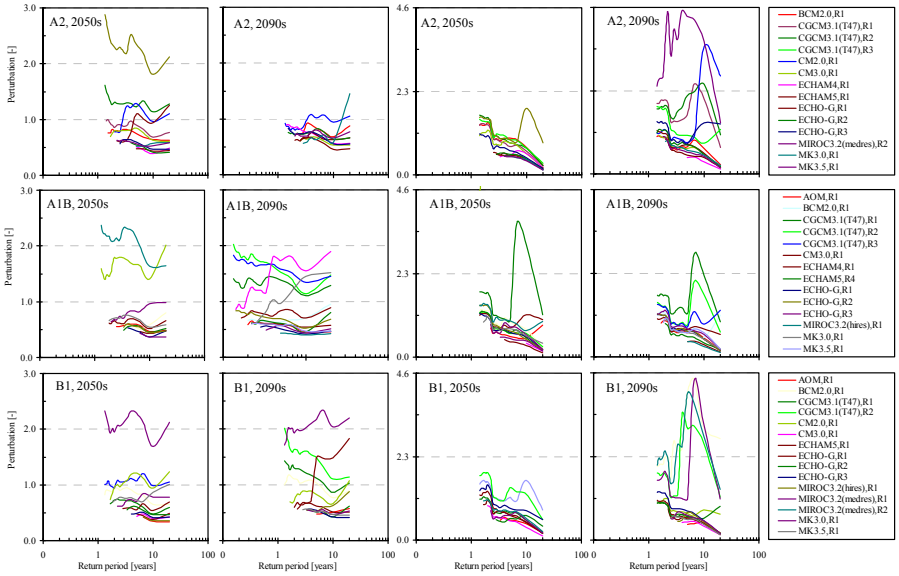

Figure 9.3 Perturbations of the streamflow peaks for the River Katonga (first and second column) and Ruizi (third and fourth column).

Albeit the flow peak perturbations for each of the selected GCM runs may be required to provide more information on possible change, Figure 9.3 shows that the information displayed may be seen as 'messy' and a more summarized analysis is required. To do that, an ensemble mean value of the perturbations for each scenario was obtained. Figure 9.4 provides the ensemble mean perturbation versus return period for the River Katonga (top) and Ruizi (bottom) catchments. The change under the high, middle and low scenarios is not very consistent. For both the River Katonga (Figure 9.4(a)-(b)) and Ruizi (Figure 9.4(c)-(d)) catchments, the tendency for the change under the A2 scenario to supersede A1B in the 2090s, as compared to that in the 2050s is apparent. It can also be seen that for both catchments, the perturbations corresponding to return periods greater tahn 10 years are less than 1, but are mainly greater than 1 for return periods less than 10 years. Between 2 and 10 years return periods, perturbations are fairly constant for all the scenarios. The implications are that the magnitudes of the mild flow peak

events are projected to increase and that of the medium events are projected not to change much. In addition, the magnitudes of the heavy flow peak events are projected to strongly decrease with increase in return period for the River Ruizi catchment but that for Katonga will not change much. In general, the magnitude of the streamflow peaks for most of the events in the future for both catchments are projected to decrease and that the occurrence of the heavy streamflow events will become less frequent.

In most practical applications, the mean of the flow peaks is more important than the individual values of the peaks because it provides information on their location. Thus, it is important to understand how the mean of the flow peaks are projected to change. The change can be obtained by simply taking the average of the perturbations of the flow peaks indicated in Figure 9.4.

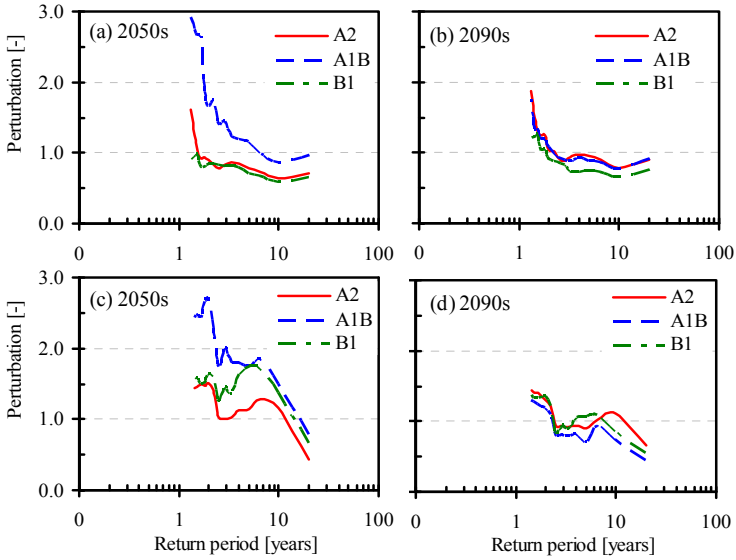

Figure 9.4 Ensemble average perturbations of the streamflow peaks for (a)-(b) the River Katonga and (c)-(d) Ruizi catchments.

Figure 9.5 contains plots of the mean of the flow peaks versus duration for both the control and the different selected GCM runs. Results for only one scenario, A2, are provided for illustration. It can be seen from the plots that for most GCM runs are below the control plots indicating that the mean of the flow peaks are projected to decrease. For the River Katonga catchment (top), it is likely that if the ensemble mean is considered, the plots would be close to the control, given the fact that the control plots appear to approximate the mean value of the multi GCM runs for the different durations. The implication is that for the River Katonga catchment, the mean of the flow peaks is projected not to change so much. That is, the future streamflow peaks will resonate around the present mean value. However, for the River Ruizi catchment (bottom), the case may not be similar to that of Katonga because

the plots of the mean of the flow peaks for some models are very high above the control. This kind of information provides an insight into the uncertainty involved in the climate change projection.

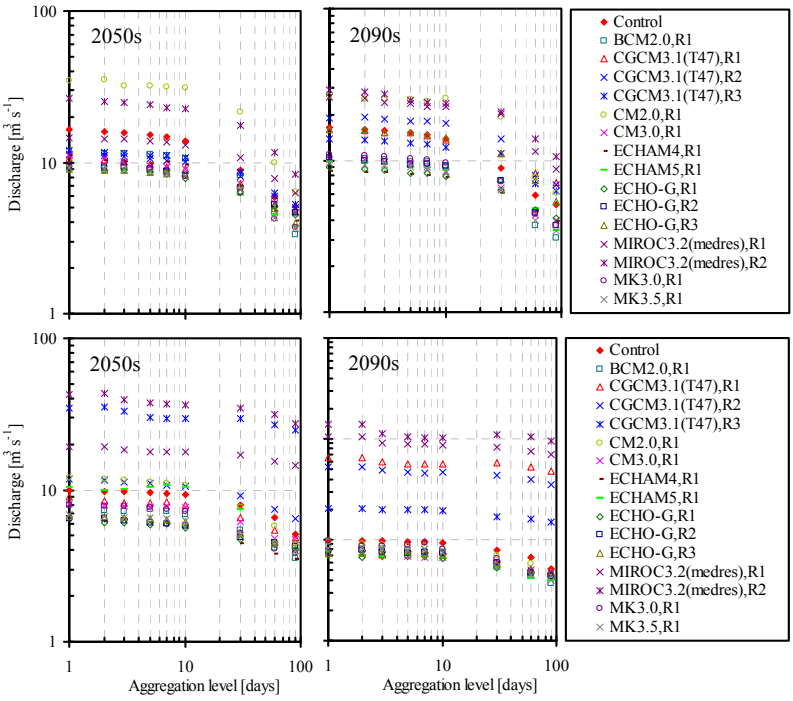

Figure 9.5 Perturbations of the mean of the streamflow peaks for different AggL and GCM runs for the River Ruizi (top) and Katonga (bottom) catchments. The results provided are for the A2 scenario only to illustrate the typical change in the streamflows as a result of climate change.

9.2.2.2 Change in flow-duration-frequency

In river engineering applications, such as the designs of culverts and other related hydraulic structures, the relationships between flow, duration and frequency (Flow-Duration-Frequency or QDF) are paramount. The third element of QDF, the return period, provides crucial information on the frequency of occurrence of a given flow. Such information is very important for the assessment of climate change impacts. Like IDF, QDF can be analysed based on EV theory, which forms the theoretical stochastic framework for the estimation of extreme quantiles. The parameter-QDF relationships, together with the analytical description of the extreme value distribution, for selected return periods, comprise the QDF curves. Information on the possible change in the QDF curves, because of the possible change in climate is significant for water resources engineering applications. To obtain such information, the flow peaks were fitted into GEV distribution and the QDF curves for the control and that of the GCM runs were compared to provide insights on the possible shifts in the observed QDF curves. The *L*-moment approach,

discussed in chapter 7, was used for the selection and fitting the GEV distribution to the flow peaks; the *L*-moment diagrams are shown in Figure 9.8.

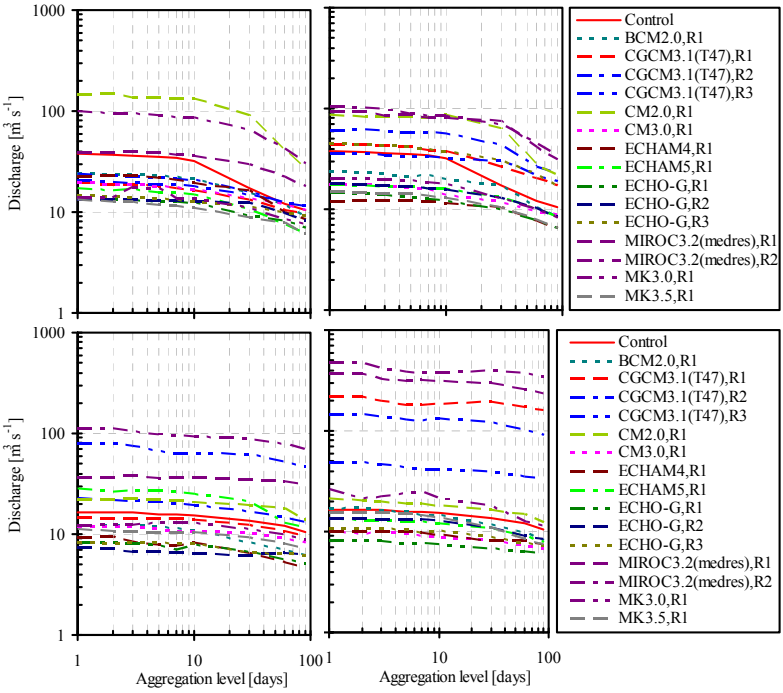

Figure 9.6 Flow-duration-frequency (QDF) curves for the observed and different GCM runs streamflows for the River Ruizi (top) and Katonga (bottom) catchments under different AggL. The results indicated are not exhaustive of all the scenarios; only A2 scenario for the 2050s (first column) and 2090s (right column) are provided to illustrative the possible shifts in the QDF as a consequence of climate change.

Figure 9.6 provides QDF curves for the control and for the different GCM runs under the high scenario only to illustrate the typical projected change in the QDF curves. It can be seen from Figure 9.6 that most of the GCM runs projected downward shifts for both the River Katonga (top) and Ruizi (bottom) catchments. Thus, it is apparent that the QDF curves in the future will significantly be different from the present-day ones. For the River Ruizi catchment the results for 3 (2050s) and 5 (2090s) GCM runs are inconsistent with the results of the other GCM runs. The GCM runs evaluated results (chapter 5) indicated that the same GCM runs are not candid with respect to the current climate. This may imply that the models, which are very biased and inconsistent with other models in simulating the present-day climate, are likely to be biased and inconsistent for the impact simulation as well.

The tail of the flow distribution is modulated by the shape parameter, *k*, of the extreme value distribution. Change in *k* is an indication of the change in the

tail of the streamflow distribution and is very important in extreme value analysis. The details of this subject were discussed in chapter 7. In this chapter, the case for the streamflows is illustrated. Change in the tail of the flow distribution is obtained by comparing the value of k for the control to that of the model. Figure 9.7 shows the plots of the values of k versus duration for the control and GCM runs. It can be seen that for Katonga (top), the values of k for the control are negative for all the durations; its magnitude being greater than 0.5 for durations less than 30 days and less than 0.5 for the duration greater than or equal to 30 days.

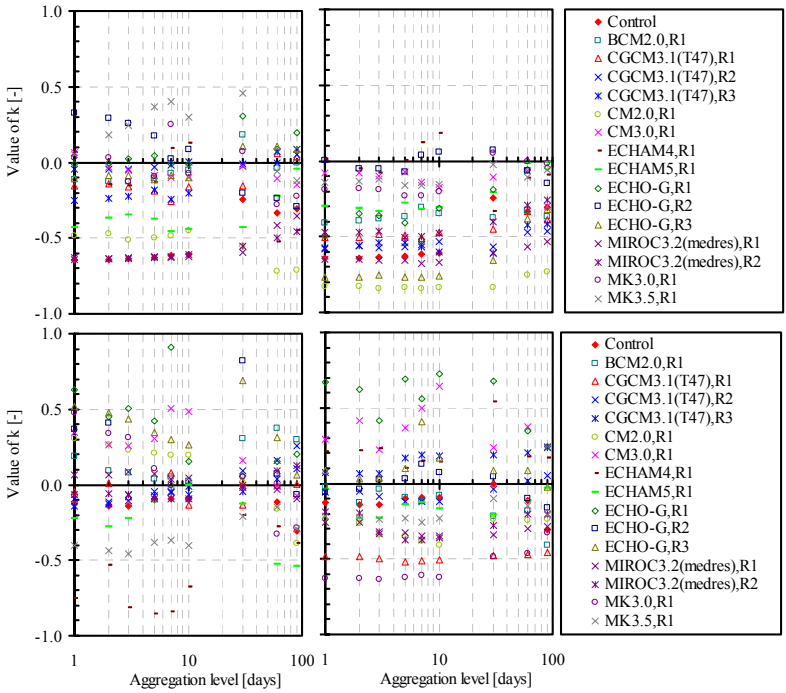

Figure 9.7 Values of the streamflow peaks distribution shape parameter, k, of the observed and different GCM runs for the River Ruizi (top) and Katonga (bottom) catchments for different AggL using GEV distribution. The results are only for scenario A2 for the periods 2050s (first column) and 2090s (right column) to illustrate the classical possible change in the tail of the streamflow extremes due to climate change.

For the River Katonga (top) catchments, the magnitude of k is projected to decrease below 0.5 in 2050s but the decrease is likely to be gained in 2090s. This implies that the tail of the distribution of the flow is projected to become less heavy compared to the control for the 2050s but the heavy behaviour will be regained in 2090s. For the River Ruizi catchment (bottom), the values of k for the control are generally less than 0.2 except for the duration of 90 days. Under climate change, the values of k are projected to become close to zero or positive in the 2050s but become negative again in the 2090s. A probable

change from the heavy to light tail behaviour in the 2050s is projected. A change from the light (2050s) to heavy tail behaviour in the 2090s is projected to be possible.

9.2.2.3 Change in flood frequency

(a) Flood frequency

Literally, flood is defined as an overflow of an expanse of water that submerges land or a temporary covering by water of land not normally covered by water. In rivers, floods can occur when flow exceeds the capacity of the river channel, particularly, at bends or meanders. In stochastic hydrology, floods may be defined as high flows with very low exceedance probabilities or very high return periods. Thus, flood frequency is the average interval between floods that have a flow of at least that flow or is the probable frequency of occurrence of a given flood. Strictly speaking, flood return period is the return period on the POT scale. However, there is an alternative definition based on AM series, which is used more widely in literatures. The AM return period is the average interval between years containing a flood of flow of at least that flow. The difference between the two definitions is only important at short return periods, less than about five years. AM is, thus, often referred to as AM flood (AMF) (Cigizoglu et al., 2004). The relationship between flood and return period is known as the flood frequency curve (FFC) and is described by an extreme value distribution (EVD). As stated in chapter 7, some known EVDs also used in flood frequency analysis are GEV, GPD, LN, P3 and GLO. The *L*-moment diagram (Hosking and Wallis, 1997), as already discussed in chapter 7, is a precious approach for fitting flood records to EVD and it has been widely applied in many related studies (e.g. Peel et al., 2001; Norbiato et al., 2007). In this study, the L-moment approach was also used in the analysis of the possible change in flood frequency.

The design of several civil structures, especially bridges, culverts, weirs, etc., is largely based on flood frequency curve. For example, a bridge or culvert would be designed to be able to convey a flood of a given flow without surcharging in a specified return period. Thus, in flood frequency analysis the goal is to estimate peak flows or flood magnitudes corresponding to any required mean reoccurrence interval. The concept is to fit to a historical flood record an EVD, which in turn is used to make inferences about the probability of occurrence of specific events. Direct statistical analysis such as at-site flood frequency analysis (Stedinger et al., 1993), which is done for data collected at a particular flow gauging station, and/or regional flood frequency analysis, which is done for data collected at various stations in a region of interest (Willems et al., 2005; Parida et al., 1998) are often used. In either case, the assumption is that the statistical properties of the historical flood data are representative of what could happen in the future. However, with the looming climate change, such an assumption is worrying. Furthermore, the

assumption of stationary approach to flood frequency analysis has prevailed in the hydrologic literature mainly due to (1) limited record, (2) the disciplinary boundaries limiting water resources engineers' knowledge of climatic processes and (3) the lack of a statistical tool set to analyze and represent extremes and make decisions under nonstationarity (Jain and Lall, 2000). The second point should not be a big issue in the current situation where interdisciplinary collaboration is possible. Under climate change, the statistical properties of floods are likely to change due to change in the flood frequency. For example, the extreme value frequency distribution currently used to describe past flood records may not necessarily be able to describe future floods anymore. Thus, the information on the changes in the flood frequency is important for many hydraulic planning purposes. With the availability of projected climate model data for the future, it is possible to validate the hypothesis of the non-stationarity in flood frequency.

(b) Flood frequency distribution

An *L*-moment diagram can be used to demonstrate that the EVD that currently well describes given flood records many not necessarily well describe future similar flood records. One might said it is obvious but it is not necessarily trivial and easy to demonstrate. In order to do this, the L-CS and L-CK, derived from AMF control series and that derived from AMF series for a given model run were represented on an *L*-moment diagram. The values of the L-CS and L-CK for all the models were also computed and added on the *L*-moment diagram. The corresponding theoretical values of the L-CS and L-CK for that of the five EVDs (stated above) were also obtained and superimposed on the same *L*-moment diagram. The resulting *L*-moment diagram contains the plots for the control, model runs and EDVs. The outcomes are such *L*-moment diagrams for all the scenarios and for the 2050s and 2090s. Figure 9.8 shows the *L*-moment diagrams for the River Katonga (Figure 9.8 (a)-(f)) and that for Ruizi (Figure 9.8 (g)-(l)) catchments for the 2050s and 2090s. For the River Katonga catchment, the plot for the control lies on that of the P3 distribution, while that for the River Ruizi catchment is close to the GLO distribution. This means that the AM of the control series for the River Katonga and Ruizi catchments are well described by P3 and GLO distributions, respectively. The plots for the models show that the P3 and GLO distributions are not necessarily the best distributions describing the AM of the different GCM runs. Consider a case of Figure 9.8(k) for the River Ruizi catchment, for example, the plot of the control lies on or near that of the GLO or GPD distribution. This means that the AMF for the control is well described by the GLO or GPD distribution. The plots for 4 models fall close or on the curve for GDP. The implication is that although the distribution of the AMF may change, it will still be described by GPD distribution. In contrast, the plots for 6 models fall on or close to the GEV (Figure 9.8(k)), meaning that the AMF of the 6 model runs are well described by the GEV distribution. That is, under climate change, the AM series for the River Ruizi

catchment will no longer be described by the GPD but by the GEV distribution.

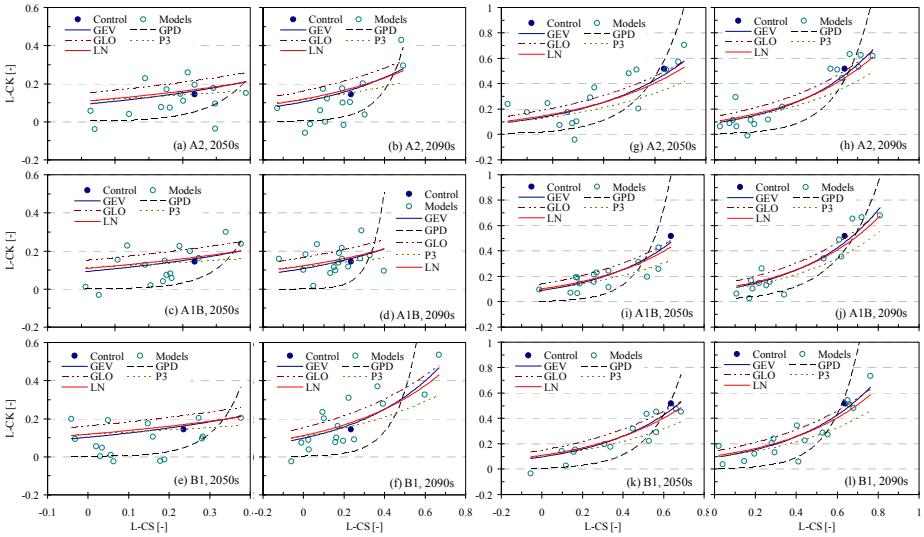

Figure 9.8 *L*-moment diagrams; constructed using the AM of the control series for the River Katonga (a)-(f), and Ruizi (g)-(l) catchments together with those for the different GCM runs (models) under the different scenarios for the 2050s and 2090s. The plots indicated by unfilled circle markers represent the different GCM runs.

Furthermore, the plots of two other GCM runs fall close or on the curve for the GLO distribution and the plots of two other GCM runs fall close or on LN distribution. This also means that under climate change, the AMF for the respective GCM runs are also well described by the GLO and LN distributions, respectively. The preceding analysis further demonstrates the uncertainty involved in predicting the EVD, which can best describe, for example, the future flood series. However, from Figure 9.8, it can be seen that, on average, the GEV and LN distributions appear to scuttle through the model plots for both the River Katonga and Ruizi catchments. In addition, the GPD distribution also appears to approximate well the plots with lower values of L-CK. Thus it is apparent that the statistical properties of the AMF of a given flow series will no longer be the same given climate change. Specifically, the extreme value distribution that well describes the AMF of given flow records may not necessarily describe the AMF of a similar flow data given the influence of climate change.

(c) Change in flood frequency distribution

The change in flood frequency distribution can be established by comparing the FFC for the model run to that of the control. This would mean constructing the FFC for each model using the EVD that best describes the AFM for that model run. However, on average, an EVD that approximate description of the AMF for the model and control may be nominated. In this

case, the GPD was selected based on Figure 9.8(b) and (e) to be used to construct the FFC for both the control and that of the model runs to illustrate the possible change in the FFC. The distribution was calibrated using the method of *L*-moment method described in chapter 7 and FFC was constructed based on equation (9.1). The GPD parameter estimation was based on the *L*-moment method (Hosking & Wallis, 1987).

Figure 9.9 shows FFC or plots of flood growth factor, Gf_T , versus return period, T, for the control and the model runs for the River Katonga (Figure 9.9(a)-(f)) and Ruizi (Figure 9.9(g)-(l)) catchments. It can be seen that the value of the Gf_T for the control (Katonga) does not increase strongly with increase in return period (normal tail behaviour) while that for the River Ruizi catchment strongly increases with increase in return period (heavy tail behaviour).

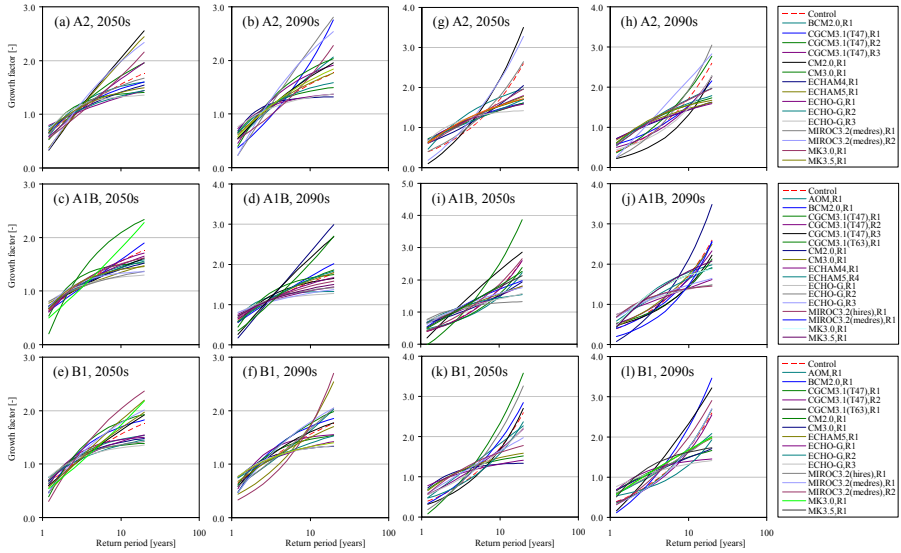

Figure 9.9 Flood frequency curves for the River Katonga (a)-(f), and Ruizi (g)-(l) for the different models under the different scenarios for the 2050s and 2090s. The dash line, in each chart, is for the control and the continuous lines are for the different GCM runs.

$$Gf_T = \xi + (\alpha / k)\left[1 - \left\{(1-F)\right\}^k\right] \tag{9.1}$$

$$T = \frac{1}{1-F} \tag{9.2}$$

where

Gf_T flood growth factor corresponding to return period, T

T return period

ξ , α, and k are location, scale and shape parameters

Growth factor, Gf_T, is the ratio between the design flood (flood corresponding to a give return period, T, and the mean of the AMF).

The plots under the A2 scenario (2050s and 2090s), for example, indicate that the normal tail behaviour will become light tail behaviour, while some model runs demonstrate the contrary to the latter (Figure 9.9(a)-(b)). Similar analysis can be provided for the other scenarios as well. For the River Ruizi catchment, the projections are more consistent among most of the model runs but the tendency for the heavy tail to remain heavy, under the A1B is apparent. Meanwhile, under the A2, the tendency to change from heavy to normal tail behaviour is also eminent.

In general, the flood frequency for both the River Katonga and Ruizi catchments will definitely change under climate change. Thus, it is no longer proper to assume stationarity in the statistics of the AM flow series or flood frequency. Some kind of climate change factor may be necessary during flood frequency curve construction intended for practical application. Climate change is not a myth and taking into consideration its possible influences on the flood (infrastructure) design may be worthy for ameliorating the likely flood risks.

9.2.2.4 Change in seasonal mean streamflows

Information on the periodic (e.g. annual, seasonal, etc.) characteristics of mean flow is crucial for management of water for various uses such as supply for drinking, irrigation, livestock, etc. Water managers may want to know the possible effects climate change is likely to impose on, for example, the seasonal mean streamflow. Such knowledge is crucial for adaptation planning to ensure sustainability of the current dwindling water resources. Information on the relationship between possible change in climate and the mean flow in a river is therefore not only a necessity but very valuable. The changes (perturbations) in the seasonal or annual mean streamflows can be obtained by comparing the model value with that of the control. In this study, the mean values of the AM and seasonal streamflows were considered.

Figure 9.10 shows the ensemble mean perturbations for the mean AM series for the Katonga and Ruizi rivers under the high (A2), middle (A1B) and low (B1) scenarios. It can be seen from Figure 9.10 that, for the River Katonga the perturbation for the high and middle scenarios are less than 1 and that of the low scenario is about 1.2 for the 2090s. Similarly, the perturbations for the 2050s, for all the scenarios are less than 1. The implication for the River Katonga is that the mean AM is projected to decrease in the 2050s but in 2090s, a slight gain to the present situation is expected under the low scenario. For the River Ruizi, a decrease in the mean of the AM is projected but the decrease will be stronger in the 2090s compared to that in the 2050s. In

general, a decrease in the mean of the MA for both the Katonga and Ruizi rivers is projected.

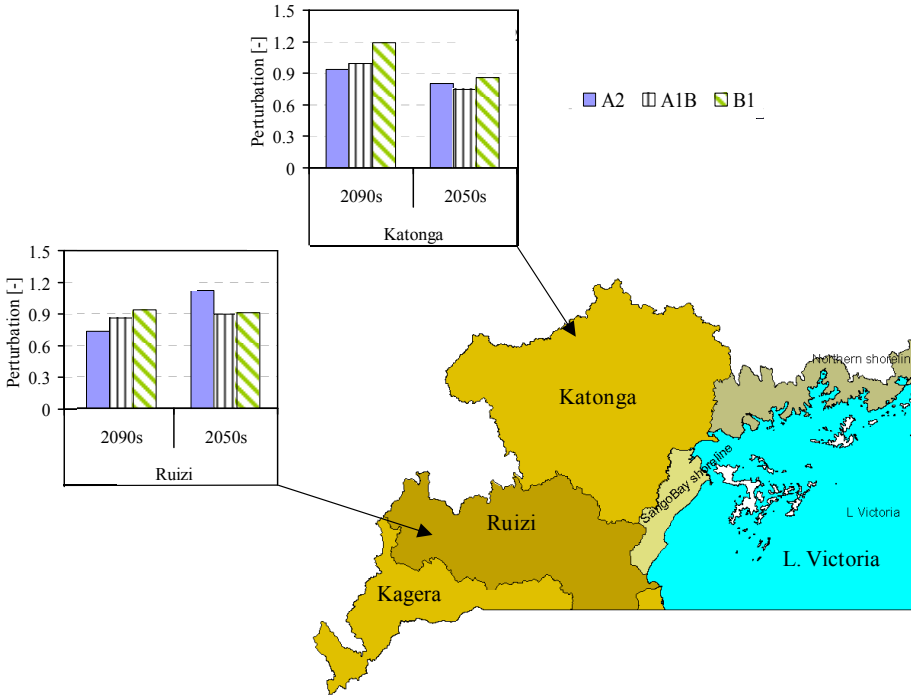

Figure 9.10 Change in the mean of the AM streamflows for the Ruizi and Katonga rivers.

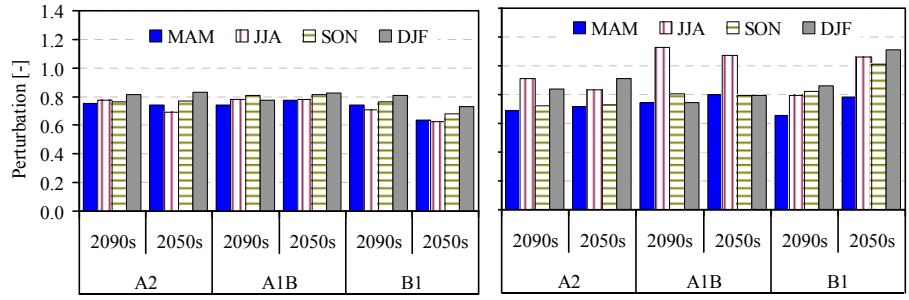

Figure 9.11 Change in the seasonal mean streamflows for Katonga (left), and Ruizi (right) rivers.

Figure 9.11 shows the perturbation for the seasonal mean flow (SMF) for the River Katonga and Ruizi in the 2090s and 2050s for the high, middle and low scenarios. Consider the case for Ruizi, for example, the perturbations for MAM and JJA seasons under the high scenario for the 2090s are about 0.69 and 0.72, respectively, and that for the 2050s are about 0.72 and 0.73, respectively. The corresponding perturbations for JJA and DJF are about 0.91 and 0.84, respectively. These perturbations are less than 1, implying that

under the high scenario for the 2090s, the SMF is projected to decrease stronger for the wet seasons than for the dry seasons. Perturbations for the JJA season under the A1B for both the 2090s and 2050s, and that for the JJA and DJF seasons under the B1 for 2050s are greater than 1. This demonstrates an increase in the SMF for the JJA season.

The change in the SMF for the River Katonga is more consistent almost across all seasons as compared to that of Ruizi. The mean perturbation is about 0.8 for the River Katonga, indicating that decrease in the SMF is by about 20% under the high and middle scenarios. While under the low scenario in the 2050s, the mean perturbation is projected to be below 0.8, indicating that the projected decrease in the SMF is more than 20%.
The inconsistent change between the projected SMF for the Katonga and Ruizi rivers may stem from the difference in type of their local climate. The climate for the River Ruizi catchment is drier than that of Katonga and this can be explained by their long-term mean monthly values of rainfall and ET_o (see chapter 3). In addition, the topography for the River Katonga catchment is flatter and consisting of many mainly lowlands than that of Ruizi. The dry characteristic makes River Ruizi catchment more vulnerable to climate change than Katonga albeit both demonstrated susceptibility to climate change.

9.3 Conclusions on hydrological climate change impacts

The hydrological response of the River Katonga and Ruizi catchments, in the Lake Victoria basin to possible change in climate, under different socioeconomic scenarios, has been examined. Prior to the assessment, the climate models were scrutinized for their reliability in reproducing observed climate for the study area. Models found fairly candid with respect to the observation were selected for use in the hydrological impact examination. The signals for climate change were extracted from the climate models based on the quantile perturbation approach and transferred to the local scale variables needed for driving the hydrological model. The hydrological model, a typical rainfall-runoff model, driven by climate model runs, was used to derive projected possible streamflows for the two catchments. The resulting streamflows were analysed using different statistical techniques, including flood frequency analysis, in order to unravel the possible changes that may characterize the future states of the water resources of the two catchments. The findings are not welcoming, especially with respect to rainfall and the flows in the rivers. However, the results are though characterized by uncertainty.

The estimated projected change in the evapotranspiration, ET_o, and rainfall for the River Katonga and Ruizi catchments is likely to underscore the integrity of the water balance of the catchments. Possible negative water balance deficits are projected in the future for the catchments, as compared to the

current state, and may severely affect the hydrologic responses of the catchments in addition to other constraints.

The magnitude and frequency of the flow extremes for the River Katonga and Ruizi catchments are significantly projected to change. The frequency of heavy extreme streamflow events are projected to reduce. The findings further showed that the flow-duration-frequency and the flood frequency relationships are projected to be affected. These may necessitate new and appropriate approaches to hydraulic designs. Water professionals may have to rethink on how to incorporate climate change elements into the current hydraulic design guidelines. Alternatively, the current design rules may be revised to incorporate higher safety level.

The change in seasonal mean flow is projected to decrease by about 20% for both the River Katonga and Ruizi and this may cause periodic shortfalls in the demands for water, such as for drinking, agriculture and ecological usages.

The current dwindling water resources of the River Ruizi and Katonga catchments (MWE, 2011) and the projected influence of climate change make the situation very worrying. This may necessitate some adaptive and austerity measures by the leading water agency in the Republic of Uganda to ensure sustainable management and utilization of the water resources of the two catchments.

CHAPTER 10

CONCLUSIONS AND RECOMMENDATIONS

10.1 Conclusions

This study was constituted to assess the impacts of climate change on the hydrological extremes and water resources in the Lake Victoria catchments, situated in the upper parts of the River Nile basin. The demand for and the execution of such assessment has grown due to the increasing availability of data for projected climate obtained through the use of climate models. The study was guided by four objectives. In the first objective, trends in the past and recent climate were examined in order to unravel the existence of significant changes that might have been observed in the recent climate. The second objective was to assess the reliability of the climate models' data for the climate change impacts study. The third objective was to downscale the climate model data to a scale, which was relevant for use at the local or catchment scale. Finally, the fourth objective was to unravel the possible change in the flows of the River Katonga and Ruizi catchments under the projected change in climate. Three socioeconomic scenarios defined by GHG emissions for the 2050s and 2090s were used. The findings were as follows:

Trends in the past and recent climate

The goal of the trend analysis was to determine the existence of significant linear trends and significant change over and above the natural variability in the recent and past climate, which could possibly be identified as the evidence of climate change. Data of 10, 9, and 7 rainfall, temperature and streamflows stations, respectively, were considered for the trend analysis. The detection of significant linear trends, in the annual extremes series, was carried out by applying the Man-Kendall test. Meanwhile, significant changes in the variability were analyzed using the quantile perturbation method. The results showed that significant positive trend was detected in the extremes of 4 out of the 10 selected rainfall stations. For temperature, significant positive trend was detected in the extremes of 1 and 2 stations for the T_{max} and T_{min} out of the 9 temperature stations. No significant trend was detected in the streamflow extremes of all the 7 selected stations. Linear trend test results for the streamflow showed a stationary tendency in the streamflow extremes for the western and southern catchments of the Lake Victoria catchments as compared to those for the eastern parts, which showed tendency for positive trend. The 1940s/1970s and 1960s/1990s demonstrated significant change in rainfall extremes below and above natural variability, respectively. The significant change, observed in the 1990s, was more intense than that

observed in the 1960s, and may provide evidence for anthropogenic induced change.

Reliability of climate models for the Lake Victoria basin

The candidness of the GCMs was assessed by evaluating several GCM control runs against the observed rainfall and temperature for a grid over the River Katonga catchment. The results showed that the climate models generally overestimate rainfall and underestimate temperature over the Lake Victoria basin. The GCM ability to simulate temperature is better than that for rainfall. The GCM prediction ability for the wet and dry rainfall frequency is better compared to rainfall intensity. The biases in the GCMs are significant and cannot be ignored. The bias removal techniques are vindicated and models that are extremely biased can be sieved out of impacts assessment. Models, which are very biased and inconsistent with other models in simulating the current climate are also likely to be inconsistent in projection.

Downscaling of the GCM runs to hydrological catchment scale

An empirical statistical downscaling, based on quantile perturbation approach, was formulated and applied to downscale rainfall. The concept behind the technique is based on the assumption that climate change signals are fairly free from bias because they are obtained from the control and scenarios, which are considered to contain similar bias. Thus, important climate change signals can be extracted from the GCM runs and applied to the observed time series in order to obtain the future time series. The climate change signals considered were the wet spells, rainfall frequency and intensity for different rainfall events. Earlier studies have only considered the latter two signals without explicit consideration of the former. The findings showed that omission of wet-spell consideration results in the future time series that overestimates change in the wet spells and intensity. Explicit consideration of climate change signals of wet spells significantly improve the accurately of climate change signals transfer for both the intensity and the wet spells.

Possible impacts of climate change on rainfall extremes

Change in rainfall extremes were investigated by comparing the observed with the perturbed extremes for 10 stations in the Lake Victoria basin. The results showed that for the eastern parts of the basin, the rainfall extremes are projected to increase by about 13-31%. The rainfall extremes for the western and southern parts of the basin are projected also to increase by 10-19%. In contrast, the rainfall extremes for the lower River Kagera catchment are projected to decrease by about 25% in the 2050s and 2090s. Significant change in the rainfall extremes has strong implications for hydraulic design practices as well as flood risks.

Potential impacts of climate change on water resources regimes

Two case studies were considered for the impacts of climate change on the water resources. That is, the River Katonga and Ruizi catchments, which are located on the western part of the Lake Victoria basin. Change in the catchment rainfall and evapotranspiration was investigated by comparing the observed and the projected ones. Projected evapotranspiration was indirectly derived from the downscaled maximum and minimum temperature. The findings indicated negative water balance deficits for both the catchments, as compared to the current state. The mean seasonal catchment rainfall for the River Katonga catchment is projected to decrease by about 10-20% while the evapotranspiration is projected to increase by about 1.4-3%. For the River Ruizi cathcment, the seasonal mean catchment rainfall is projected to decrease by about 15-23%. Like the River Katonga catchment, the evapotranspiration for Ruizi is projected to increase by about 2-11%. The projected change in the catchment evapotranspiration and rainfall for Katonga and Ruizi is likely to underscore the integrity of the water balance of the catchments.

The future streamflows were simulated by use of the rainfall-runoff models developed for the two catchments. The climate change impacts were assessed by comparing the future and control streamflows. Two major areas of change were considered: change in the high streamflows and that for the seasonal mean streamflows. The findings showed that moderate to high extreme events, including flood events (annual maximum streamflow) are projected to change differently. For both the River Katonga and Ruizi, the medium extreme flow events are projected to be similar to the current situation in the 2050s but will decrease in the 2090s. The intensity and frequency of the AMF series are projected to change differently as well. For the River Katonga, a decrease in the mean of the AMF by about 20% is projected for the 2050s but in the 2090s, a gain to the current state is projected. For the River Ruizi, a decrease is projected by about 5% in the 2050s and 15% in the 2090s. The possible change in the seasonal mean flow is projected to decrease by 20% and 15% for the Katonga and Ruizi rivers, respectively, which is proportional to the change in their respective MAF. Possible change in the projected streamflow has implications for the water resources planning and management, as well as ecosystem sustainability.

10.2 Recommendations

Water resources of a river catchment are very important for sustaining human and ecosystem survivals. Information regarding climate change and the eventual consequences on the water resources of a river catchment is crucial for adaptation planning and management. The potential change in the water resources of the River Katonga and Ruizi as a consequent of potential change in the climate of the future needs not to be ignored. The challenge and the unlarability in understating it and communicating the associated uncertainty to

policy makers is something well known. Adaptation to taking decision in an environment of uncertainty is recommended.

Water managers need to take keen interest on the information regarding the potential impacts of climate change on water resources. The following recommendations are geared towards the attention of the lead agency responsible for sustainable management of water resources for the study region. Key areas to pay attention to are: (1) the current practices regarding designs of hydraulic structures may need to be revisited. For example, the design guidelines may require modifications or reviews in light of the information presented in this research, (2) possible rational use of water from the rivers to ensure sustainability of ecological flows may be paramount, given projected possible change in flows for the River Katonga and Ruizi. (3) Extension of this kind of research to other river catchments, within the region to obtain a complete picture for the possible impacts of climate change on the current state of the water resources of the country may be very vital.

Potential areas for further research

Areas for potential research exist and are recommended for consideration in order to make refinement in the methodology involving use of global climate models outputs and hydrological models in climate change impacts study, especially under related situations. The following are recommended:

(1) The precipitation downscaling technique used in this study considered the change in the wet spells in which each wet spell is modified by the same climate change factor, change in the mean wet spell. Like intensity, where each quantile is modified by different factors, it would be interesting to conduct a research that allows each wet spell to be modified by separate factors. This would further improve the quantile perturbation technique involving the use of wet spells in downscaling precipitation from GCM runs needed for local scale impacts assessment. Once this is taken up, it can be evaluated against other methods such as the bias removal and that which uses the concept of predictors and predictants. A detailed climate change impacts analysis on the wet spells analysis may provide information, which can be relevant to farming.

(2) Validation of climate models will continue to be based on the focus of the study. For example, impact study focusing on water for agriculture would mainly focus on the criteria that are related to weekly, monthly or seasonal spells. Likewise, a hydrological assessment focusing on floods would be interested in criteria that identify GCMs, which well capture peaks of the target variables. In this study, the aim was to assess the performance of the GCM runs based on mean simulation at monthly, seasonal and annual scale including mean monthly wet and dry frequency. In addition, the GCMs ability to simulate, for example, the different rainfall events at daily scale was part of

the aim of the study. The former is a more general evaluation criterion, of course, not to eliminate as many models as possible but the latter is specifically geared towards rainfall events. A detailed study, which focuses on developing the candidness measures based on different applications, would provide important application-based criteria for comparing the GCMs.

(3) One potential area for further research is the uncertainty. Considerable efforts are being geared towards quantifying uncertainty at other levels such as the scenarios and climate models levels but not much at downscaling and hydrological model levels. In this study, an ensemble approach was used to define uncertainty range without attaching any confidence limits. This may not be appealing to policy makers. Quantification of uncertainty involving attachments of confidence intervals on the impact assessment results may improve on the acceptability of climate change impacts study results to policy makers.

(4) Hydrological response of a catchment is susceptible to changes in other factors such as landuse. This study assumed that future change in the landuse of the catchments is negligible as compared to the influence by climate change and only climate change factors were considered. This assumption, however, only filtered out the response of the catchment to climate change but ignored the contribution from the change in landuse. It would be vital also to combine the changes in climate and landuse in the hydrological impacts assessment.

(5) The trends in the extremes of the past and current climate were only assessed for some selected stations within the Lake Victoria basin. Extension of a similar kind of analysis to stations in other catchments within the region (e.g. the Uganda Water Management Zone) would provide valuable information regarding the trends in the climate of the country. It would further consolidate information needed for water policy improvements.

BIBLIOGRAPHY

Adeboye, O. B., Osunbitan, J. A., Adekalu, K. O. & Okunade D. A. (2009). Evaluation of FAO-56 Penman Monteith and temperature based models in estimating reference evapotranspiration using complete and limited data, application to Nigeria. *Agri. Eng. Inter. CIGR J.* **1291**(11), 1–25.

Alcamo, J., Flörke, M. & Märker, M. (2007). Future long-term changes in global water resources driven by socio-economic and climatic change. *Hydrol. Sci. J.* **52**(2), 247–275.

Alexander, L. V., Zhang, X., Peterson, T. C., Ceasar, J., Gleason, B., Klein Tank, A. M. G., Haylock, M., Collins, D., Trewin, B., Rahimzadeh, F., Tagipour, A., Rupa Kumar, K., Revadekar, J., Griffiths, G., Vincent, L., Stepenson, D. B., Burn, J., Aguilar, E., Brunet, M., Taylor, M., New, M., Zhai, P., Rusticucci, M., Vasquez-Aguirre, J. L.(2006). Global observed changes in daily climate extremes of temperature and precipitation. *J. Geophys. Res*. **111**, DO5109. DOI: 10.1029/2005JD006290.

Allen, R. G., Pereira, L. S., Raes, D. & Smith, M. (2006). Crop Evapotranspiration (guidelines for computing crop water requirements). *FAO irrigation and drainage paper 24*. *United Nations-Food and Agricultural Organization, Rome, 34*.

Amy, C. T. (2006). Assessing the impacts of climate change on river basin management: a new method with application to the Nile River. *A PhD dissertation, School of Civil and environmental Engineering, Georgia Institute of Technology, Georgia*.

Andersen, H. E., Kronvang, B., Larsen, S. E., Carl, C. H., Torben, S. J. & Rasmussen, E. K. (2006). Climate-change impacts on hydrology and nutrients in a Danish lowland river basin. *Sci. Total Environ*. **365**, 223–237.

Andersson, L., Wilk, J., Todd, M. C., Hughes, D. A., Earle, A., Kniveton, D., Layberry, R. & Savenije, H. H. G. (2006). Impact of climate change and development scenarios on flow patterns in the Okavango River. *J. Hydrol.* **331**, 43–57.

Anyah, R. O. & Semazzib, F. H. M. (2007). Variability of East African rainfall based on multiyear RegCM3 simulations. *Int. Jol. Climatol.* **27**, 357–371.

Arnell, N. W. (2004). Climate change and global water resources: SRES scenarios and socio-economic scenarios. *Global Environ. Change* **14**, 31–52.

Awange, J. L., Sharifi, A., Ogonda, G., Wickert, J., Grafarend, E. W. & Omulo, M. A. (2008). The Falling Lake Victoria water level: GRACE,

TRIMM and CHAMP satellite analysis of the Lake Basin. *Water Res. Manage*. **22**, 775–96.

Baguis, P., Roulin, E., Willems, P., & Ntegeka, V. (2010). Climate change scenarios for precipitation and potential evapotranspiration over central Belgium. *Theor. Appl. Climatol.* **99**, 273–286.

Barnett, D. N., Simon, J., Murphy, B. J. M., Sexton, D. M. H. & Webb, M., J. (2006). Quantifying uncertainty in changes in extreme event frequency in response to doubled CO2 using a large ensemble of GCM simulations. *Clim. Dyn*. **26**, 489–511.

Barnett, T. P., Adam, J. C. & Lettenmaier, D. P. (2005). Potential impacts of a warming climate on water availability in snowdominated regions. *Nature* **438**, 303–309.

Barnett, T. P., Malone, R., Pennell, W., Stammer, D., Semtner, B. & Washington, W. (2004). The effects of climate change on water resources in the West: introduction and overview. *Clim. Change* **62**, 1–11.

Barrow, E., B., Maxwell & Gachon, P. (eds.) (2004). Climate Variability and Change in Canada: Past, Present and Future, ACSD Science Assessment Series No. 2. *Meteorol. Service Canada*, *Environ. Canada, Toronto, Ontario*, 114.

Bartier, P. M. & Keller, C. P. (1996). Multivariate interpolation to incorporate thematic surface data using Inverse Distance Weighting (IDW). *Computers Geosci.* **22**(7), 195-799.

Bayley, G. V. & Hammersley, J. M. (1946). The effective number of independent observations in an autocorrelated time series. *J. Roy. Statist. Soc*. **8**(1B), 184–197.

Beirlant, J., Goegebeur, Y., Segers, J. & Teugels, J. (2004). *Statistics of extremes*: *theory and applications.* John Wiley & Sons Ltd.

Benestad, R. E., Hanssen-Bauer, I. & Chen, D. (2008). *Empirical-statistical downscaling*. World Scientific, Singapore, ISBN: 978-981-281-912-3.

Berengena, J. & Gavilán, P. (2005). Reference evapotranspiration estimation in a highly advective semiarid environment. J. Irrig. Drain. Eng. ASCE 131(2), 147–163.

Beyene, T., Lettenmaier, D. P., Kaba, P. (2010). Hydrologic impacts of climate change on the Nile River Basin: implications of the 2007 IPCC scenarios. *Climatic Change* **100**, 433–461, DOI: 10.1007/s10584-009-9693-0.

Blanckaert, J. & Willems, P. (2006). Statistical analysis of trends and cycles in long-term historical rainfall series at Uccle. The 7th *Int. workshop on precipitation in urban areas*, St. Moritz, Switzerland.

Blasone, R.-S., Madsen, H. & Rosbjerg, D. (2007). Parameter estimation in distributed hydrological modelling: comparison of global and local optimisation techniques. *Nordic Hydrol.* **38**(4–5), 451–476.

Bobba, A., Singh, V., Berndtsson, R. & Bengtsson, L. (2000). Numerical simulation of saltwater intrusion into Laccadive Island aquifers due to climate change. *J. Geol. Soc. India* **55**, 589–612.

Boko, M., Niang, I., Nyong, A., Vogel, C., Githeko, A., Medany, M., Osman-Elasha, B., Tabo, R. & Yanda, P. (2007). Africa. *Clim. Change*: Impacts, Adaptation and Vulnerability. *Contribution of Working Group II to the Fourth Assessment Report of the Intergovernmental Panel on Climate Change*, Parry, M. L., Canziani, O. F., Palutikof, J. P., Van Der Linden, P. J. & Hanson, C. E., Eds., Cambridge University Press, Cambridge, UK, 433-467.

Boukhris, O. E. F. (2008). Climate change impact on hydrological extremes along rivers in Flanders. *PhD desertation*, Katholieke Universiteit Leuven.

Box, G. E. P. & Cox, D. R. (1964). An analysis of transformation. *J. Royal Stat. Soc.* **SB**, 211-243.

Boyle, D. P., Gupta, H. V., & Sorooshian, S. (2000). Toward improved calibration of hydrologic models: Combining the strengths of manual and automatic methods. *Water Resour. Res*. **36**, 3663–3674.

Bronstert, A., Niehoff, D. & Bürger, G. (2002). Effects of climate and land-use change on storm runoff generation: present knowledge and modelling capabilities. *Hydrol. Process.* **2**, 509–529.

Burke, E. J., Brown, S. J. & Christidis, N. (2006). Modelling the recent evolution of global drought and projections for the 21st century with the Hadley Centre climate model. *J. Hydromet.* **7**, 1113–1125.

Burnash, R. J. C. (1995). The NWS river forecast system – catchment modeling. In: Singh, V.P. (Ed.). *Computer Models of Watershed Hydrology*. Water Resour. Pubs, Colorado, 311–366.

Carlsson, B., Graham, L. P., Andreasson, J. & Rosberg, J. (2005). Exploring the range of uncertainty in climate change impacts on runoff and hydropower for the Lulealven River. *15th Int. northern research basins symp. and workshop*, *29 Aug, 2005, Sweden*.

Carter, T. R., Jones, R. N., Lu, X., Bhadwal, S., Conde, C., Mearns, L. O., O'Neill, B. C., Rounsevell, M. D. A. & Zurek, M. B. (2007). New Assessment Methods and the Characterisation of Future Conditions. *Clim. Change 2007: Impacts, Adaptation and Vulnerability. Contribution of Working Group II to the Fourth Assessment Report of the Intergovernmental Panel on Climate Change,* M.L. Parry, O.F. Canziani, J.P. Palutikof, P.J. van der Linden and C.E. Hanson, Eds., Cambridge University Press, Cambridge, UK, 133-171.

Chapman, T. (1999). A comparison of algorithms for stream flow recession and baseflow separation. *Hydrol. Process.* **13**, 701-714.

Chen, H., Guo, S., Xu, C. & Singh, V. P. (2007). Historical temporal trends of hydro-climatic variables and runoff response to climate variability and their relevance in water resource management in the Hanjiang basin. *J. Hydrol*. **344**, 171–184.

Chen, Y. & Penner, J. E. (2005). Uncertainty analysis for estimates of the first indirect effect. *Atmos. Chem . Phys.* **5**, 2935–2948.

Chiew, F. H. S. (2007). Estimation of rainfall elasticity of streamflow in Australia. *Hydrol. Sci. J.* **51**(4), 613–625.

Christensen, J. H, Carter, T. R. & Rummukainen, M. (2007). Evaluating the performance and utility of regional climate models: the PRUDENCE Project. *Clim. Change,* DOI: 10.1007/s10584-006-9211-6

Christensen, J. H., Boberg, F., Christensen, O. B., Lucas-Picher, P. (2008). On the need for bias correction of regional climate change projections of temperature and precipitation. *Geophys. Res. Lett.* **35**(L20709), 6, DOI: 10.1029/2008GL035694.

Cigizoglu, H. K., Bayazit, M. & Önöz, B. (2004). Trends in the Maximum, Mean, and Low Flows of Turkish Rivers. *J. Hydrometeor*. **6**, 280–290.

Collins, M, Booth, B. B, Harris, G. R, Murphy, J. M, Sexton, D. M. H & Webb, M. J. (2006). *Clim. Dyn.* **27**, 127-147.

Cox, D. R. & Stuart, A. (1955). Some quick sign tests for trend in location and dispersion. *Biometrika* **42**, 80–95.

Cunnane, C. (1985). Factors affecting choice of distribution for flood series. *Hydrol. Sci. J.* **30**(1), 25-36.

Davidson, A. C. & Hinkley, D. V. (1997). *Bootstrap methods and their application*. Cambridge University Press, Cambridge, UK.

de Jong, R., de Bruin, S., de Wit, A., Schaepman, M. E. & Dent, D. L. (2011). Analysis of monotonic greening and browning trends from global NDVI time-series. *Remote Sens. Environ.* **115**, 692–702.

de Jongh, L. M., Verhoest, N. E. C. & de Troch, F. C. P. (2006). Analysis of a 105-year time series of precipitation observed at Uccle, Belgium. *Int. J. Climatol*. **26**, 2023–2039.

Delworth, T. L., Rosati, A., Stouffer, R. J., Dixon, K. W., Dunne, J., Findell, K., Ginoux, P., Gnanadesikan, A., Gordon, C. T., Griffies, S. M., Gudgel, R., Harrison, M. J., Held, I. M., Hemler, R. S., Horowitz, L. W., Klein, S. A., Knutson, T. R., Lin, S-J., Milly, P. C. D., Ramaswamy, V., Schwarzkopf, M. D., Sirutis, J. J., Stern, W. F., Spelman, M. J., Winton, M., Wittenberg, A. T. & Wyman, B., et al. (2006). GFDL's CM2 Global Coupled Climate Models. Part I: Formulation and simulation characteristics. *J. Clim.* **19**(5), 643-674.

Diaz-Nieto, J. & Wilby, R. L. (2005). A comparison of statistical downscaling and climate change factor methods: impacts on lowflows in the river thames, United Kingdom. *Clim. Change* **69**, 245–268.

Döll, P. & Flörke, M. (2005). Global-scale estimation of diffuse groundwater recharge. *Frankfurt Hydrol.* **3**, Institute of Physical Geography, Frankfurt University, Germany.

Duffie, J. A. & Beckman, W. A. (1980). *Solar Engineering of Thermal Processes*. John Wiley & Sons, New York.

Eckhardt, K. (2005). How to construct recursive digital filters for baseflow separation. *Hydrol. Process.* **19**, 507-515.

Efron, B. & Tibshirani, R. J. (1998). *An introduction to the Bootstrap*. Chapman & Hall, London, UK.

Elferta, S. & Bormann, H. (2010). Simulated impact of past and possible future land use changes on the hydrological response of the Northern German lowland 'Hunte' catchment. *J. Hydrol*. **383**(3-4), 245-255.

Emori, S., Hasegawa, A., Suzuki, T. & Dairaku, K. (2005). Validation, parameterization dependence, and future projection of daily precipitation simulated with a high-resolution atmospheric GCM. *Geophy. Res. Lett.* **32**(L06708), DOI: 10.1029/2004GL022306.

England, K., Hisdal, H. & Frigessi, A. (20045). Practical Extreme Value Modelling of hydrological Flood and Droughts: A case study. *Extreme* **7**, 2-30, DOI: 10.1007/s10687-004-4727-5.

Feyen, L., Vázquez, R., Christiaens, K., Sels, O. & Feyen, J. (2000). Application of a distributed physically-based hydrological model to a medium size catchment. *Hydrol. Earth Syst. Sci*. **4**(1), 47–63.

Fisher, R. A. & Tippett, L. H. C. (1928). Limiting forms of the frequency distribution of the largest or smallest member of a sample. *Math. Proc. Cambridge Phil. Soc.* **24**(2), DOI: 10.1017/S0305004100015681

Fohrer, N., Haverkamp, S. & Frede, H. G. (2005). Assessment of the effects of land use patterns on hydrologic landscape functions - Development of sustainable land use concepts for low mountain range areas. *Hydrol. Process.* **19**(3), 659-672.

Fowler, H. J., Blenkinsopa, S. & Tebaldib, C. (2007). Review: Linking climate change modelling to impacts studies: recent advances in downscaling techniques for hydrological modelling. *Int. J. Climatol*. **27**, 1547–1578.

Frank, P. (2008). A climate of Belief. In: Global Warming Debate. *Skeptic* **14**(1), 22-30

Gedney, N., Cox, P. M., Betts, R. A., Boucher, O., Huntingford, C. & Stott, P. A. (2006). Detection of a direct carbon dioxide effect in continental river runoff records. *Nature* **439**, 835–838.

Gillett, N. P., Zwiers, F. W., Weaver, A. J., Hegerl, G. C., Allen, M. R. & Stott, P. A. (2002). Detecting anthropogenic influence with a multi-model ensemble. *Geophys. Res. Lett.* **29**, 1970, DOI: 10.1029/2002GL015836.

Giorgi, F. (2005). Climate change prediction. *Clim. Change* **73**, 239-265.

Githui, F., Gitau, W., Mutua, F. & Bauwens, W. (2009). Climate change impact on SWAT simulated streamflow in western Kenya. *Int. J. Climatol.* **29**, 1823–1834.

Gosain, A. K., Rao, S. & Basuray, D. (2006). Climate change impact assessment on hydrology of Indian river basins. *Current Sci*. **90**(3), 346–353.

Greenwood, J. A., Landwehr, J. M., Matalas, N. C. & Wallis, J. R. (1979). Probability weighted moments: definition and relation to parameters of several distributions expressible in inverse form. *Water Resour. Res*. **15**(5), 1049-1054.

Grum, M., Jørgensen, A. T., Johansen, R. M. & Linde, J. J. (2006). The effect of climate change on urban drainage: an evaluation based on regional climate model simulations. *Water Sci. Technol*. **54** (6–7), 9–15.

Hagemann, S., Machenhauer, B., Jones, R., Christensen, O. B., Déqué, M., Jacob, D. & Vidale, P. L. (2004). Evaluation of water and energy budgets in regional climate models applied over Europe. *Clim. Dyn.* **23**, 547–567.

Hamed, K. H. (2008). Trend detection in hydrologic data: The Mann–Kendall trend test under the scaling Hypothesis. *J. Hydrol*. **349**, 350–363.

Hamlet, A. F. & Lettenmaier, D. P. (1999). Effects of Climate Change on Hydrology and Water resources: Objectives in the Columbia River Basin. *Water Resour. Bulletin* **35**(6), 1597-1623.

Hansen, J., Nazarenko, L., Ruedy, R., Sato, Mki., Willis, J., Del Genio, A., Koch, D., Lacis, A., Lo, K., Menon, S., Novakov, T., Perlwitz, J., Russell, G., Schmidt, G. A. & Tausnev, N. (2005). Earth's energy imbalance: Confirmation and implications. *Science* **308**, 1431-1435, DOI: 10.1126/science.1110252.

Hargreaves G. H. & Z. A. Samani (1985). Reference crop evapotranspiration from temperature. Appl. Eng. Agric. 1(2), 96–99.

Hargreaves, G. H. & Allen, R. G. (2003). History and evaluation of Hargreaves evapotranspiration equation. J. Irrig. Drain. Eng. ASCE 129(1), 53–63.

Hargreaves, G. L., Hargreaves, G. H. & Riley, J. P. (1985). Irrigation water requirements for Senegal River Basin. *J. Irrig. Drain. Eng.*, **111**(3), 265–275.

Harrold, T. I. & Jones, R. N. (2003). Downscaling GCM rainfall: a refinement of the perturbation method. In MODSIM2003. *International Congress on Modelling and Simulation*, Townsville, Australia, 14–17.

Hegerl, G. C., Stoot, P. A., Allen, M. R., Mitchell, J. F. B., Tett, S F. B. & Cubasch, U. (2000). Optimal detection and attribution of climate change: Sensitivity of results to climate model differences. *Clim. Dyn.* **16**, 737–754.

Hipel, K. W. & MCLeod, A. I. (1994). *Time series modeling of water resources and environmental systems*. Develop. Water Sci., Elsevier Science, Amsterdam, The Nederlands, 203-234.

Hosking, J. R. M. & Wallis, J. R. (1993). Some statistics useful in regional frequency analysis. *Water Resour. Res*. **29**(2), 271-281.

Hosking, J. R. M. & Wallis, J. R. (1997). *Regional frequency analysis: an approach based on L-moments*. Cambridge University Press., Cambridge, UK.

Hosking, J. R. M. (1990). *L*-moments analysis and estimation of distributions using linear combination of order statistics. *J. Royal Statist. Soc.* **52**, 105-124.

Hosking, J. R. M., Wallis, J. R. & Wood, F. (1985). Estimation of the generalized extreme-value distribution by the method of probability weighted moments. *Technometrics* **27**(3), 251-261.

Hosking, J. R. M., Wallis, J. R. (1987). Parameter and quantile estimation for the generalized Pareto distribution. *Technometrics* **29**(3), 339-349.

Houghton, J. T., Ding, Y., Griggs, D. J., Noguer, M., van der Linden, P. J., Dai, X., Maskell, K. & Johnson, C. A. (2001). *Clim. Change*: *The Scientific Basis. Contribution of Working Group I to the Third Assessment Report of the Intergovernmental Panel on Climate Change*. Cambridge, UK, and New York, NY: Cambridge University Press, 881.

Hreiche, A., Najem, W. & Bocquillon, C. (2007). Hydrological impact simulations of climate change on Lebanese coastal rivers. *Hydrol. Sci. J.,* **52**(6) 1119–1133.

Humphrey, M. D., Istok, J. D., Lee, J. Y, Hevesi, J. A. & Flint, A. L. (1997). A new method for automated dynamic calibration of tipping-bucket rain gauges. *J. Atmos. Oceanic Technol.*, **14**, 1513–1519.

Ines, A. V. M. & Hansen, J. W. (2006). Bias correction of daily GCM rainfall for crop simulation studies. *Agric. Meteorol.* **138**, 44–53.

IPCC (1994). Technical guidelines for assessing climate change impacts and adaptations. *IPCC Special Report to the First Session of the Conference of the Parties to the UN Framework Convention on Climate Change, Working Group II*, *Intergovernmental Panel on Climate Change*, T.R. Carter, M.L. Parry, S. Nishioka & H. Harasawa, Eds., University

College London and Center for Global Environmental Research, National Institute for Environmental Studies, Tsukuba, 59.

IPCC (2001a). *Clim. Change*: *The scientific basis*. Cambridge University Press, Cambridge.

IPCC (2007). Summary for Policymakers. In: *Clim. Change: The Physical Science Basis*. *Contribution of Working Group I to the Fourth Assessment Report of the Intergovernmental Panel on Climate* Change (ed. by Solomon, S., Qin, D., Manning, M., Chen, Z., Marquis, M., Averyt, K. B., Tignor, M. & Miller), H. L., 1–18. Cambridge University Press, UK.

Itenfisu, D., Elliott, R. L., Allen, R. G. & Walter, I. A. (2003). Comparison of reference evapotranspiration calculation as part of the ASCE standardization effort. J. Irrig. Drain. Eng. ASCE 129(6), 440–448.

Izenman, A. J. (1991). Recent developments in nonparametric density Estimation. *J Am. Stat. Assoc.* **86**(413), 205-224.

Jacob, D. J., Field, B. D., Li, Q., Blake, D. R., de Gouw, J., Warneke C., Hanse, A., Wisthaler, A., Singh, H. B. & Guenther, A. (2005). Global budget of methanol: Constraints from atmospheric observations. *J. Geophys. Res.***110***,* D08303, DOI: 10.1029/2004JD005172.

Jain, S. & Lall, U. (2000). Magnitude and timing of annual maximum floods: Trends and large-scale climatic associations for the Blacksmith Fork River, Utah. *Water Resour. Res*. **36**, 3641–3651.

Jenkinson, A. F. (1955). The frequency distribution of the annual maximum (or minimum) values of meteorological events. *Quart. J. Royal Meteorol. Soci.* **81**, 158–72.

Jeong, C. S., Jun-haeng, H., Deg, H. B. & Konstantine, P. G. (2005). Utility of high-resolution climate model simulations for water resources prediction over the Korean Peninsula: a sensitivity study. *Hydrol. Sci. J.* **50**(1), 139–153.

Kaspar, F. (2004). Development and uncertainty analysis of a global hydrologic model. *PhD Dissertation.* University of Kassel, Kassel, Germany, ISBN3-89958-071-0, German.

Katz, R. W. (1992). Role of statistics in the validation of general circulation models. *Clim. Res.* **2**, 35-45.

Keefer, D. L. & Verdinic, W. A. (1993). Better Estimation of PERT Activity Time Parameters. *Manage. Sci.* **39**, 1086–1091.

Kendall, M. G. (1975). *Rank Correlation Methods*. Griffin, London.

Kharin, V. V. & Zwiers, F. W. (2005). Estimating extremes in transient climate change simulations. *J. Clim.* **18**, 1156–1173.

King'uyu, S. M., Ogallo, L. A. & Anyamba, E. K. (1999). Recent Trends of Minimum and Maximum Surface Temperatures over Eastern Africa. *J. Clim.* **13**, 2876-2886.

Kistemann, T., Classen, T., Koch, C., Dagendorf, F., Fischeder, R., Gebel, J., Vacata, V. & Exner, M. (2002). Microbial load of drinking water reservoirs tributaries during extreme rainfall and runoff. *Appl. Environ. Microbiol.* **68**, 2188–2197.

Kitanidis, P. K., & Lane, R. W. (1985). Maximum likelihood parameter estimation of hydrologic spatial processes by the Gauss-Newton method. *J. Hydrol.* **79**(1-2), 53-71.

Kizza, M., Rodhe, A., Xu, C.-Y., Ntale, H. K., & Halldin, S. (2009). Temporal rainfall variability in the Lake Victoria Basin in East Africa during the twentieth century. *Theor Appl. Climatol*. **98**,119–135.

Klauer, B. & Brown, J. D. (2004). Conceptualizing imperfect knowledge in public decision making: Ignorance, uncertainty, error and 'risk situations'. *Eng. Manage.* **27**(1), 124-128.

Knutti, R., Joos, F., Muller, S. A, Plattner, G. K & Stocker, T. F. (2005). Probabilistic climate change projections for CO2 stabilization profiles. *Geophy. Res. Lett.* **32**(20), L20707, DOI: 10.1029/2005GL023294.

Knutti, R., Stocker, T. F., Joos, F. & Plattner, G. K. (2002). Constraints on radiative forcing and future climate change from observations and climate model ensembles. *Nature* **416**, 719–723.

Koutsouris, A. J., Destouni, G., Jarsjo, J. & Lyon, S. W. (2010). Hydro-climatic trends and water resource management implications based on multi-scale data for the Lake Victoria region, Kenya. *Environ. Res. Lett.* **5**, 034005 (7pp), DOI: 10.1088/1748-9326/5/3/034005.

Krishnamurti, T. N., Kishtawal, C. M., Zhang, Z., Larow, T., Bachiochi, D., Williford, E., Gadgil, S. & Surendran, S. (2000). Multimodel ensemble forecasts for weather and seasonal climate. *J. Clim.* **13**, 4196–4216, DOI: 10.1175/1520-0442(2000)013!4196:MEFFWAO2. 0.CO;2.

Kundzewicz, Z. W. (2004). Change detection in hydrological records a review of the methodology. *Hydrol. Sci. J.* **49**(1) 7–19.

Kundzewicz, Z. W., Mata, L. J., Arnell, N. W., Döll, P., Jimenez, B., Miller, K., Oki, T., Sen, Z. & Shiklomanov, I. (2008). The implications of projected climate change for freshwater resources and their management. *Hydrol. Sci. J.* **53**(1), 3-10.

Kundzewicz, Z. W., Mata, L. J., Arnell, N., Döll, P., Kabat, P., Jiménez, B., Miller, K., Oki, T., Şen, Z. & Shiklomanov, I. (2007). Freshwater resources and their management. *Clim. Change: Impacts, Adaptation and Vulnerability.Contribution of Working Group II to the Fourth Assessment Report of the Intergovernmental Panel on Climate Change*

(ed. by M. L. Parry, O. F. Canziani, J. P. Palutikof, P. J. van der Linden & C. E. Hanson), 173–210. Cambridge University Press, UK.

Kunkel, K. E., Andsager, K. & Easterling, D. R. (1999). Long-term trends in extreme precipitation events over the conterminous United States and Canada. *J. Clim.* **12**, 2515–2527.

Lall, U. (1995). Nonparametric function estimation: Recent hydrologic applications. *Reviews Geophysics* **33**, 1093–1102.

Lall, U., Rajagopalan, B. & Tarboton, D. G. (1996). A nonparametric wet/dry spell model for resampling daily Precipitation. *Water Resour. Res*. **32**(9), 2803–2823.

Lambert, S. J. & Boer, G. J. (2001). CMIP1 evaluation and intercomparison of coupled climate models. *Clim. Dynam*. **17**, 83–106, DOI: 10.1007/PL00013736.

Lehner, B., Döll, P., Alcamo, J., Henrichs, H. & Kaspar, F. (2005). Estimating the impact of global change on flood and drought risks in Europe: a continental, integrated assessment. *Clim. Change* **75**, 273–299.

Lenderink, G., Buishand, A. & van Deursen, W. (2007). Estimates of future discharges of the river Rhine using two scenario methodologies: direct versus delta approach, *Hydrol. Earth Syst. Sci*. **11**, 1145–1159.

Linsley, R. K., Kholer, M. A. & Paulhus, J. L. H. (1949). *Applied Hydrology*. McGraw Hill, New York.

López-Moreno, J. I., Beguería, S. & García-Ruiz, J. M. (2007). Trends in high flows in the central Spanish Pyrenees: response to climatic factors or to land-use change. *Hydrol. Sci. J*. **51**(6), 1039–1050.

Lu, G. Y. & Wong, D. W. (2008). An adaptive inverse-distance weighting spatial interpolation technique. *Computers Geosci.* **34**, 1044–1055.

Machiwal, D. & Jha, M. K. (2008). Comparative evaluation of statistical tests for time series analysis: application to hydrological time series. *Hydrol. Sci. J*. **53**(2) 353–365.

Madsen, H. (2000). Automatic calibration of a conceptual rainfall-runoff model using multiple objectives. *J. Hydrol*. **235**, 276–288.

Madsen, H., Rasmussen, P. F. & Rosbjerg, D. (1997). Comparison of annual maximum series and partial duration series methods for modeling extreme hydrologic events. 1. At-site modelling, *Water Resour. Re*s. **33**(4), 747-757.

Madsen, H., Wilson G., & Ammentorp H. C. (2002). Comparison of different automated strategies for calibration of rainfall-runoff models. *J. Hydrol*. **261**, 48-59.

Mann, H. B. (1945). Nonparametric tests against trend. *Econometrica* **13**, 245–259.

MathWorks Inc, MATLAB (2008). *Application programme interface reference version 7.0*. The MathWorks Inc., Natick, MA, USA

McDonnell, J. J. (2009). Classics in physical geography revisited. Hewlett, J. D. & Hibbert, A. R. (1967). Factors affecting the response of small watersheds to precipitation in humid areas. *Progress Phy. Geogr.* **33**(2), 288–293.

Meehl, G. A., Stocker, T. F., Collins, W. D., Friedlingstein, P., Gaye, A. T., Gregory, J. M., Kitoh, A., Knutti, R., Murphy, J. M., Noda, A., Raper, S. C. B., Watterson, I. G., Weaver, A. J. & Zhao, Z.-C. (2007). Global Climate Projections. *In Clim. Change 2007. The Physical Science Basis. Contribution of Working Group I to the Fourth Assessment Report of the Intergovernmental Panel on Climate Change* [Solomon, S., Qin, D., Manning, M., Chen, Z., Marquis, M., Averyt, K. B., Tignor, M. & Miller, H. L. (eds.)]. Cambridge University Press, Cambridge, United Kingdom and New York, NY, USA.

Middelkoop, H., Daamen, K., Gellens, D., Grabs, W., Kwadijk, J. C. J., Lang, H., Parmet, B. W. A. H., Schädler, B., Schulla, J. & Wilke, K. (2001). Impact of climate change on hydrological regimes and water resources management in the Rhine basin. *Clim. Change* **49**, 105–128.

Miller, M. P. (2005). Alleles In Space (AIS): Computer Software for the Joint Analysis of Interindividual Spatial and Genetic Information. *J. Heredity* **96**(6), 722–724.

Milly, P. C. D., Dunne, K. A. & Vecchia, A. V. (2005). Global pattern of trends in streamflow and water availability in a changing climate. *Nature* **438**, 347–350.

Mirza, M. M. Q., Warrick, R. A. & Ericksen, N. J. (2003). The implications of climate change on floods of the Ganges, Brahmaputra and Meghna rivers in Bangladesh. *Clim. Change* **57**, 287–318.

Mohamed, Y. A., van den Hurk, B. J. J. M., Savenije, H. H. G. & Bastiaanssen, W. G. M. (2005). Hydroclimatology of the Nile: results from a regional climate model. *Hydrol. Earth Syst. Sci.* **9**, 263–278.

Mpelasoka, F. S. & Chiew, F. H. S. (2009). Influence of rainfall scenario sonstruction methods on runoff projections. *J. Hydromet.* **10**, 1168–1183, DOI: 10.1175/2009JHM1045.1.

MWE (2011). *The declining trends of water resources in Uganda: A Case study of River Ruizi, Lake Wamala, Lake Victoria Catchments and representative Groundwater Monitoring stations.* Water Resources Monitoring & Assessment Division, Department of Monitoring and Assessment, Directorate of Water Resources Management Ministry of Water and Environment, Entebbe, Uganda.

Naess, A., Asce, M. & Clausen, P. H. (2000). The Peaks Over Threshold method and bootstrapping for estimating long return period design

values. *8th ASCE Specialty Conf. on Probabilistic Mechanics and Structural Stability*, July 23-26, 2000, University of Notre Dame.

Nakicenovic, N., Alcamo, J., Davis, G., de Vries, B., Fenhann, J., Gaffin, S., Gregory, K., Grübler, A., Jung, T. Y., Kram, T., La Rovere, E. L., Michaelis, L., Mori, S., Morita, T., Pepper, W., Pitcher, H., Price, L., Riahi, K., Roehrl, A., Rogner, H.-H., Sankovski, A., Schlesinger, M., Shukla, P., Smith, S., Swart, R., van Rooijen, S., Victor, N. & Dadi, Z. (2000). IPCC *Special Report on Emissions Scenarios*. Cambridge University Press, Cambridge, UK and New York, NY, USA.

Nash, J. E. & Sutcliffe, J. V. (1970). River flow forecasting through conceptual models part I - A discussion of principles. *J. Hydrol.* **3**, 282–290.

Nathan, R. J. & McMahan, T. A. (1990). Evaluation of automated techniques for baseflow and recession analysis. *Water Resour. Res*. **26**(7), 1465-1473.

Niringiye, A., Wambugu, S., Karugia, J. & Wanga, E. (2010). An Investigation of the Poverty- Environmental Degradation Nexus: A Case Study of Katonga Basin in Uganda. *Res. J. Environ. Earth Sci.* **2**(2), 82-88.

Nóbrega, M. T., Collischonn, W., Tucci, C. E. M. & Paz, A. R. (2011). Uncertainty in climate change impacts on water resources in the Rio Grande Basin, Brazil. *Hydrol. Earth Syst. Sci*. **15**, 585-595, DOI: 10.5194/hess-15-585-2011, 2011.

Nohara, D., Kitoh, A., Hosaka, M. & Oki, T. (2006). Impact of climate change on river runoff. *J. Hydromet.* **7**, 1076–1089.

Norbiato, D., Borga, M., Sangati, M. & Zanon, F. (2007). Regional frequency analysis of extreme precipitation in the eastern Italian Alps and the August 29, 2003 flash flood. *J. Hydrol.* **345**, 149– 166.

Notter, B., MacMillan, L., Viviroli, D., Weingartner, R. & Liniger, H.-P. (2007). Impacts of environmental change on water resources in the Mt. Kenya region. *J. Hydrol.* **343,** 266–278.

Ntegeka, V. & Willems, P. (2008). Trends and multidecadal oscillations in rainfall extremes, based on a more than 100-year time series of 10 min rainfall intensities at Uccle, Belgium. *Water Resour. Res*. **44**(W07402), DOI: 10.1029/2007WR006471.

Ntegeka, V., (2011). *Assessment of the observed and future climate variability and change in the hydroclimatic and hydrological extremes*. *PhD dissertation,* Arenberg Doctoral school of Science, Engineering and Technology, Katholieke Universiteit Leuven, Belgium.

Nyenzi, B. S. (1990). An analysis of the interannual variability of rainfall over East Africa. *Proc. 2nd Technical Conf. on Weather Forecasting*, Sept. 1990, E. & S. Africa, Nairobi, Kenya, 36–41.

Ogallo, L. (1979). Rainfall variability in Africa. *Mon. Wea. Rev*. **107**, 1133–1139.

Ogallo, L. (1989). The spatial and temporal patterns of the East African seasonal rainfall derived from principal component analysis. *Int. J. Clim* **9**, 145–167.

Olsson, J., Berggren, K., Olofsson, M. & Viklander, M. (2009). Applying climate model precipitation scenarios for urban hydrological assessment: A case study in Kalmar City, Sweden. *Atmos. Res*. **92**, 364–375, DOI: 10.1016/j.atmosres.2009.01.015.

Owor, M., Taylor, R. G., Tindimugaya, C. & Mwesigwa, D. (2009). Rainfall intensity and groundwater recharge: empirical evidence from the Upper Nile Basin. *Environ. Res. Lett*. **4**(035009), 6, DOI: 10.1088/1748-9326/4/3/035009.

Parida, B. P., Kachroo, R. K. & Shrestha, D. B. (1998). Regional flood frequency analysis of Mahi-Sabarmati basin (Sub-zone 3a) using index flood procedure with L-Moments. *Water Resour. Manage.* **12**, 1-12.

Parry, M. (2002). Scenarios for climate Impact and Adaptation Assessment. *Global Environ. Change* **12**, 149-153.

Parry, M., Arnell, N., McMichael, T., Nicholls, R., Martens, P., Kovats, S., Livermore, M., Rosenzweig, C., Iglesias, A. & Fischer, G. (2001). Millions at risk: defining critical climate change threats and targets. *Global Environ. Change* **11**, 181-183.

Paturel, J. E., Barrau, C., Mahé1, G., Dezetter, A. & Servat, E. (2007). Modelling the impact of climatic variability on water resources in West and Central Africa from a non-calibrated hydrological model. *Hydrol. Sci. J.* **52**(1) 38–48.

Peel, M. C. & McMahon, T. A. (2006). A quality-controlled global runoff data set. *Nature* **444**(E14), DOI: 10.1038/nature05480.

Peel, M. C., Wang, Q. J., Vogel, R. M. & McMahon, T. A. (2001). The utility of L-moment ratio diagrams for selecting a regional probability distibution. *Hydrol. Sci. J*. **46**, 147-155.

Piani, C., Haerter, J. O. & Coppola, E. (2010). Statistical bias correction for daily precipitation in regional climate models over Europe. *Theor. Appl. Climatol*. **99**, 187–192, DOI: 10.1007/s00704-009-0134-9.

Pickands, J. (1975). Statistical inference using extreme order statistics. *Ann. Statist*. **3**, 119-131.

Prudhomme, C., Reynard, N. & Crooks, S. (2002). Downscaling of global climate models for flood frequency analysis: Where are we now? *Hydrol. Process*. **16**, 1137–1150.

Pujol, N., Neppel, L. & Sabatier, R. (2007). Regional tests for trend detection in maximum precipitation series in the French Mediterranean region. *Hydrol. Sci. J.* **52**(5) 956–973.

Rajagopalan, B. & Lall, U. (1999). A k-nearest-neighbor simulator for daily precipitation and other variables. *Water Resour. Res*. **35**(10), 3089–3101.

Rajagopalan, B., Lall, U., Tarboton, D. G. & Bowles, D. S. (1997). Multivariate nonparametric resapling scheme for generation of daily weather variables. *Stochastic Hydrol. Hydraul*. **11**(1), 523–547.

Randall, D. A., Wood, R. A., Bony, S., Colman, R., Fichefet, T., Fyfe, J., Kattsov, V., Pitman, A., Shukla, J., Srinivasan, J., Stouffer, R. J., Sumi, A. & Taylor, K. E., (2007). Cilmate Models and Their Evaluation. In: *Clim. Change*: *The Physical Science Basis. Contribution of Working Group I to the Fourth Assessment Report of the Intergovernmental Panel on Climate Change* [Solomon, S., D. Qin, M. Manning, Z. Chen, M. Marquis, K.B. Averyt, M. Tignor & H.L. Miller (eds.)]. Cambridge University Press, Cambridge, UK and NY, USA.

Refsgaard, J. C. & Knudsen, J. (1996). Operational validation and intercomparison of different types of hydrological models. *Water Resour. Res*. **32**(7), 2189–2202.

Refsgaard, J. C. van der Sluijs, J. P., Højberg, A. L. & Vanrolleghem, P. A. (2007). Uncertainty in the environmental modelling process: A framework and guidance. *Environ. Modelling Software* **22**(11), 1543-1556.

Robertson, A. W., Lall, U., Zebiak, S. E. & Goddard, L. (2004). Improved combination of multiple atmospheric GCM ensembles for seasonal prediction. *Mon. Weather Rev.* **132**, 2732–2744, DOI: 10.1175/MWR2818.1.

Robson, A. J. & Reed, D. W. (1999). *Flood Estimation Handbook* **3**: *Statistical Procedures for Flood Frequency Estimation*. Institute of Hydrology, Wallingford, UK.

Sahoo, G. B., Ray, C. (2006). Flow forecasting for a Hawaii stream using rating curves and neural networks. *J. Hydrol.* **317**(1–2), 63–80.

Salas, J. D., Delleur, J. W., Yevjevich, V. & Lane, W. L. (1980). Applied Modelling of Hydrologic Time Series. *Water Resour. Pubs.*, Littleton, Co., USA.

Schmidli, J. & Frei, C. (2005). Trends of heavy precipitation and wet and dry spells in Switzerland during the 20th century. *Int. J. Climatol.* **25**, 753–771, DOI: 10.1002/joc.1179.

Schulzweida, U. & Kornblueh, L. (2011). *Climate Data Operators **1.5***. MPI for Meteorology, Germany.

Sen, P. K. (1968). Estimates of the regression coefficient based on Kendall's tau. *J. American Stat. Assoc.* **63**, 1379–1389.

Serrat-Capdevila, A., Valdés, J. B., Pérez, J. G., Baird, K., Mata, L. J. & Maddock III, T. (2007). Modeling climate change impacts – and uncertainty – on the hydrology of a riparian system: The San Pedro Basin, Arizona/Sonora. *J. Hydrol.* **347**, 48-66. DOI: 10.1016/j.jhydrol.2007.08.028.

Setegn, S. G., Rayner, D., Melesse, A. M., Bijan, D. & Srinivasan, R. (2011). Impact of climate change on the hydroclimatology of Lake Tana Basin, Ethiopia Water Resour. Res. **47**(W04511), 13: DOI: 10.1029/2010WR009248.

Sevruk, B. (1982). *Methods of correction for systematic error in point precipitation measurement for operational use*. Operational Hydrology Rep. **21**, WMO Rep. No. 589.

Sewagudde, S. M. (2009). Lake Victoria's Water Budget and the Potential Effects of Climate Change in the 21st Century. *African J. Tropical Hydrobiol. Fisheries* **12**, 22-30.

Shahin, M., Van Oorschot, H. J. L. & De Lange, S. J. (1993). *Statistical Analysis in Water Resources Engineering*. A. A. Balkema, Rotterdam, The Netherlands.

Shaw, E. M. (1983). *Hydrology in Practice*. Van Nostrand Rheinhold (UK) Co. Ltd., Wokingham.

Sheather, S. J., Jones, M. C. (1991). A reliable data-based bandwidth selection, method for kernel density estimation. *J. Royal Statist. Soc*. **53**, 683-690.

Sheng, Y. & Chun, Y. W. (2004). Possible regional probability distribution type of Canadian annual stream flow by L-moments. *Water Resour. Manage* **18**, 425-438.

Shepard, D. (1968). A Two-Dimensional Interpolation Function for Irregularly Spaced Data. *Proc. 23rd Nat. Conf. ACM*, 517-523.

Shoemaker, L., Lahlou, M., Bryer, M., Kumar, D. & Kratt, K. (1997). *Compendium of tools for watershed assessment and TMDL development*. U.S. Environmental Protection Agency, EPA841-B-97-006.

Sivapalan, M., Blosch, G., Zhang, L. & Vertessy, R. (2003). Downward approach to hydrological prediction. *Hydrol. Process.* **17**, 2101–2111.

Smith, R. L., (1987). Estimating tails of probability distributions. *Ann. Statist.* **15**, 1174-1207.

Sneyers, R. (1990). *On the Statistical Analysis of Series of Observations*. World Meteorological Organization, Technical Note **143**, WMO, 415.

Stager, J. C., Ruzmaikin, A., Conway, D., Verburg, P. & Mason, P. J. (2007). Sunspots, El Niño, and the levels of Lake Victoria, East Africa. *J. Geophysical Res*. **112**(D15106), 13, DOI: 10.1029/2006JD008362.

Stager, J. C., Ryves, D., Cumming, B. F., Meeker, L. D. & Beer J. (2005). Solar activity and the levels of Lake Victoria, East Africa, during the last millennium. *J. Paleolimnol.* **33**, 243–251.

Stedinger, J. R., Vogel, R. M. & Foufoula-Georgiou, E. (1993). *Frequency analysis of extreme events, chapter 18*. *In*: *Handbook of Hydrology*, edited by D. R. Maidment, McGraw-Hill, Inc.

Stehr, A., Debels, P., Romero, F. & Alcayaga, H. (2008). Hydrological modelling with SWAT under limited conditions of data availability: evaluation of results from a Chilean case study. *J. Hydrol. Sci*. **53**, 588–601.

Svensson, C. & Jones, D. A. (2010). Review of methods for deriving areal reduction factors. *J. Flood Risk Manage.* **3**, 232–245.

Svensson, C., Kundzewicz, Z. W. & Maurer, T. (2005). Trend detection in river flow series: 2. Flood and low-flow index series. *Hydrol. Sci. J*. **50**(5), 811–824.

Takemura, T., Nozawa, T., Emori, S., Nakajima, T. Y. & Nakajima, T. (2005). Simulation of climate response to aerosol direct and indirect effects with aerosol transport-radiation model. *J. Geophys. Res*. **110**(D02202), DOI: 10.1029/2004JD005029.

Takemura, T., Tsushima, Y., Yokohata, T., Nozawa, T., Nagashima, T. & Nakajima, T. (2006). Time evolutions of various radiative forcings for the past 150 years estimated by a general circulation model. *J. Geophys. Res*. **33***,* L19705, DOI: 10.1029/2006GL026666.

Taye, M. T., Ntegeka, V., Ogiramoi, N. P. & Willems, P. (2011). Assessment of climate change impact on hydrological extremes in two source regions of the Nile River Basin. *Hydrol. Earth Syst. Sci.* **15**(1), 209-222.

Tebaldi, C. & Knutti, R. (2007). The use of the multi-model ensemble in probabilistic climate projections. *Phil. Trans. Roy. Soc. A*. **365**, 2053–2075.

Theil, H. (1950). A rank-invariant method of Linear and polynomial regression analysis, I, II, III. *Nederl. Akad. Wetensch. Proc.* **53**, 386–392, 512–525, 1397–1412.

Trenberth, K. E, Dai, A., Rasmussen, R. M. & Parsons, D. B. (2003). The changing character of precipitation. *Bull. Am. Meteorol. Soc*. **84**, 1205–1217, DOI: 10.1175/BAMS-84-9-1205.

Trenberth, K. E., Jones, P. D., Ambenje, P., Bojariu, R., Easterling, D., Klein Tank, A., Parker, D. Rahimzadeh, F., Renwick, J. A., Rusticucci, M., Soden, B. & Zhai, P. (2007). Observations: Surface and Atmospheric Climate Change. In Clim.Change 2007. The Physical

Science Basis. Contribution of Working Group I to the Fourth Assessment Report of the Intergovernmental Panel on Climate Change [Solomon, S., Qin, D., Manning, M., Chen, Z., Marquis, M., Averyt, K.B., Tignor, M. & Miller, H.L. (eds.)]. Cambridge University Press, Cambridge, UK.

Vergara, W., Deeb, A. M., Valencia, A. M., Bradley, R. S., Francou, B., Zarzar, A., Grünwaldt, A. & Haeussling, S. M. (2007). Economic impacts of rapid glacier retreat in the Andes. *EOS.* **88**(25), 261–264.

Vidal, J.-P. & Wade, S. D. (2008). Multimodel projections of catchment-scale precipitation regime. *J. Hydrol.* **353**, 143–158.

Villarini, G. & Smith, J. A. (2010). Flood peak distributions for the eastern United States. *Water Resour. Res.* **46**(W06504), DOI: 10.1029/2009WR008395.

von Mises, R., (1954). La distribution la plus grande de n valeurs. In: *Selected papers of Richard von Mises* (P. Frank, Ed.). 271–294. *Am. Math. Soc. Providence* RI. Reprint (first published in *Rev. Math. Union. Interbalcanique* **1**, 141–160, 1936).

Walker, W. E., Marchau, V. A. W. J. & Swanson, D. (2010). Addressing deep uncertainty using adaptive policies: Introduction to section 2. *Technol. Forecasting Social Change*, **77** (6), 917-923.

Wang, H. & Lau, K. M. (2006). Hydrologic cycles in the tropics in twentieth century coupled climate simulations. *Int. J. Climatol.* **26**, 655-678.

Wang, Y, Leung, L. R., McGregor, J. L., Lee, D. K., Wang, W. C, Ding, Y. & Kimura, F. (2004). Regional climate modeling: Progress, Challenges and Prospects. *J. Metorol. Soc. Japan* **12**, 825-847.

Ware, C., Knight, W. & Wells, D. (1991). Memory intensive algorithms for multibeam bathymetric data. *Computers Geosci.* **17**(7), 985-993.

Willems, P. & Vrac, M. (2011). Statistical precipitation downscaling for small-scale hydrological impact investigations of climate change. *J. Hydrol.* **402**, 193–205.

Willems, P. (2000). Probabilistic immission modelling of receiving surface waters. *PhD thesis,* Catholic University of Leuven, Belgium.

Willems, P. (2000b). Compound intensity/duration/frequency-relationships of extreme precipitation for two seasons and two storm types', *J. Hydrol*. **33**, 189 – 205.

Willems, P. (2009). A time series tool to support the multi-criteria performance evaluation of rainfall-runoff models. *Environ. Modelling Software* **24**(3), 311-321.

Willems, P., Arnbjerg-Nielsen, K., Olsson, J., Nguyen, V. T. V. (2011). Climate change impact assessment on urban rainfall extremes and urban

drainage: methods and shortcomings. *Atmospheric Research*, DOI: 10.1016/j.atmosres.2011.04.003.

Willems, P., Guillou, A. & Beirlant, J. (2007). Bias correction in hydrologic GPD based extreme value analysis by means of a slowly varying function. *J. Hydrol.* **338**, 221–236.

Willems, P., Sonbol, M., Gamal, S., Mkhandi, A., Opere, A., Tedesse, L., Tedesse L., Abdel Motaleb, M., Farid, S., Zaki, A. & Al-Weshah, R. (2005). Regional flood frequency analysis in the Nile basin. *Int. Conf. UNESCO Flanders FIT FRIEND/Nile Project-"Towards a better cooperation", CD-ROM Proc.* **18**. Sharm El-Sheikh, Egypt, 12-14 November, 2005,

WMO (1986). *Manual for Estimation of Probable Maximum Precipitation*. Operational Hydrology Report no.1, WMO No. **332**, Geneva.

WMO (1994). *Guide to Hydrological Practices*. WMO No. **168**, Geneva.

WMO (2000) Detecting trends and other changes in hydrological data. *WMO/TD No*. **1013**, WHO, Geneva, 168.

Yanjun, S., Taikan, O., Nobuyuki, U., Shinjiro, K. & Naota, H. (2008). Projection of future world water resources under SRES scenarios: water withdrawal. *Hydrol. Sci. J.*, **53**(1), 11–33.

Yazdani, M. R., Khoshhal, D. J., Mahdavi, M. & Sharma, A. (2011). Trend detection of the rainfall and air temperature data in the Zayandehrud basin. *J. Applied Sci.* **11**(12), 1225–2134.

Yin, X. & Nicholson, S. E. (1998). The water balance of Lake Victoria. *Hydrol. Sci*. **43**(5) 789-811.

Yue, S. & Wang, C. Y. (2002). Applicability of prewhitening to eliminate the influence of serial correlation on the Mann-Kendall test. *Water Resour. Res*. **38**(6), 1068, DOI: 10.1029/2001WR000861.

Yue, S. & Wang, C. Y. (2004). The Mann-Kendall test modified by effective sample size to detect trend in serially correlated hydrological series. *Water Resour. Manage.* **18**, 201–218.

Yue, S., Pilon, P. & Cavadias, G. (2002a). Power of the Mann-Kendall and Spearman's rho tests for detecting monotonic trends in hydrological series. *J. Hydrol.* **259**, 254– 271.

Yue, S., Pilon, P., Phinney, B. & Cavadias, G. (2002b). The influence of autocorrelation on the ability to detect trend in hydrological series. *Hydrol. Process.* **16**, 1807–1829.

Yue-Cong, W. & Barry, A. (2010). *Climate change and its impacts on water supply and demand in Sydney*. Summary report: NSW office for water, Sydney, NSW, 12.

AUTHOR'S RESUME

Paul Nyeko Ogiramoi graduated with an upper second class BSc. degree in Civil Engineering in 2001 from Makerere University Kampala, Uganda. He, then, joined the Directorate of Water Development, under the Ministry of Water and Environment (MWE/DWD), Uganda, in 2002 as a graduate Engineer and worked in the Planning and Development Division of the Rural Water and Sanitation Department. While in the MWE/DWD, he was involved in many water recourses engineering planning and development projects. In 2003, Ogiramoi enrolled for a two-year MSc. under the Interuniversity Programme in Water Resources Engineering (IPWARE), managed at Katholieke Universiteit Leuven (KULeuven) and Vrije Universiteit Brussel, Belgium. He successfully completed the first year with a Complementary degree in Water Resources Engineering (WRE). After the end of the second year, he graduated with a MSc. in WRE with a grade of great distinction. In 2005-2007, Ogiramoi worked in the MWE/DWD as a Water Resources Engineer in charge of Technical Support Unit that lumped together the districts of the West Nile region, Uganda. In 2008, The Uganda Government accredited him with a legal certificate that qualified him as a lawful practicing professional engineer in the country. In the same year, 2008, with the funding from VLIR (Flemish Interuniversity Council), Belgium, Eng. Ogiramoi enrolled for a PhD programme in civil engineering at KULeuven, Belgium, under the supervision of Prof. Willems Patrick of KULeuven, Belgium and Prof. Ngirane-Katashaya Gaddi of Makerere University, Kampala, Uganda.

PUBLICATIONS

Articles in internationally reviewed scientific journals

Nyeko-Ogiramoi, **P**., Ngirane-Katashaya, G., Willems, P. & Ntegeka, V. (2010). Evaluation and inter-comparison of Global Climate Models' performance over Katonga and Ruizi catchments in Lake Victoria basin. *Phy. Chem. Earth* **35**, 618–633.

Taye, M. T., Ntegeka, V., **Nyeko-Ogiramoi**, **P.** & Willems, P. (2011). Assessment of climate change impact on hydrological extremes in two source regions of the Nile River Basin. *Hydrol. Earth Syst. Sci.* **7**, 5441–5465.

Nyeko-Ogiramoi, **P.**, Willems, P. & Ngirane-Katashaya, G. (2011). Trend and variability in the observed hydrometeorological extremes in the Lake Victoria basin. *J. Hydrol.* (under review).

Nyeko-Ogiramoi, **P.**, Willems, P., Mutua, F. M. & Moges, S. A. (2011). An elusive search for regional flood frequency estimates in the River Nile basin based on hierarchical clustering. *Hydro. Sc. J*. (in revision).

Book chapter, internationally recognized scientific publisher

Nyeko-Ogiramoi, **P**., Willems, P. Ngirane-Katashaya, G. & Ntegeka, V. (2011). Nonparametric statistical downscaling of precipitation from Global Climate Models. In: *Climate Models* (ed. L. Druyan), InTech ISBN 979-953-307-338-4.

Article in other type of scientific journals

Willems, P., **Nyeko-Ogiramoi, P**., Mutua, F. M., Gamal, A., Kabub, J., Hassan, F. A., Sonbol, M., Lotfy, A., Kimaro, T. A., Mkhand, S., Opere, A., Yosif, A. I., Kizza, M., Tadesse, L., Abdel, M. M., Farid, S., Zaki, A. & Al-Weshah, R. (2010). Regional Flood Frequency Analysis for the River Nile Basin. *Bull. Séanc. Acad. R. Sci. Outre-Mer*, **55**, 555-570.

Papers presented at international conferences and symposia published in full in proceedings

Nyeko-Ogiramoi, **P.**, Willems, P. & Ngirane-Katashaya, G. (2011). Perturbation downscaling for the assessment of the impact of climate change on extreme precipitation and temperature events over the upper River Nile basin. *Pro. Int. Conf. Future Environ. Energy* (ICFEE), **E10011**, 25-27 March, 2011, Sanya, China.

Nyeko-Ogiramoi, P., Willems, P. & Ngirane-Katashaya, G. (2011). Assessment of the impact of climate change on extreme precipitation and temperature events over the upper River Nile basin. *Proc. Advances in Eng. & Technol. Int. conf.* **109**(1410AET2011), January 30–February 1, 2011, Entebbe, Uganda.

Nyeko-Ogiramoi, P., Willems, P. & Ntegeka, V. (2008). Climate change scenarios for the River Nile basin. *Proc. Nile Basin Develop. Forum*, 654-666, 17-19 November, 2008, Khartoum - Sudan.

Abstracts, presented at international conferences published and in full in proceedings

Nyeko-Ogiramoi, P., Ngirane-Katashaya, G. & Willems, P. (2009). Using quantile analysis to evaluate GCM's performance over Katonga and Ruizi Catchments in Lake Victoria Basin. *10th*

WaterNet/WARFSA/GWP-SA Symp., 28-30 October 2009, Makerere University, Entebbe, Uganda.

Nyeko-Ogiramoi, P., Ntegeka, V. & Willems, P. (2009). GCM based perturbation analysis over Katonga and Ruizi Catchments in Lake Victoria basin. *Int. Symp. Developing Countries facing Global Warming: a Post-Kyoto Assessment*, Brussels, 12 - 13 June 2009.

Articles in preparation, internationally reviewed scientific journals

Impact of climate change on the hydrological extremes in the Lake Victoria catchments.

GCM-based climate change scenarios for the assessment of the impacts of climate change on the hydrology and water resources at catchment scale in the River Nile basin.

APPENDIX A

Supplementary Tables

Tables A.1-A.6 contain information on the properties of the long-term mean annual rainfall, temperature and streamflow data for selected stations in the Lake Victoria basin, River Ruizi and Katonga catchments. Longitude (Lon) and Latitude (Lat) are in decimal degrees; Alt represents the altitude. The Max and Min are the respective maximum and minimum of the long-term mean of the annual variable for the record length (number of years) considered.

Table A.1 Selected rainfall stations in the Lake Victoria basin.

Catch-ment	Station name (No. in Figure. 3.4)	Station ID	Lon	Lat	Alt (m)	Mean (mm)	CV	Skew-ness	Max (mm)	Min (mm)	Begin year	No. years
Issanga	Maswa (1)	9333005	33.77	-3.17	1341	838	0.21	0.49	1344	524	1928	79
Kagera	Rugari (2)	10149	30.40	-2.73	1650	1201	0.36	2.43	3004	577	1943	64
Katonga	Kamenyami (3)	9031026	31.67	-0.30	1320	1033	0.24	0.33	1679	592	1952	48
Mara	Nyabassi (4)	9134008	34.57	-1.35	1829	1435	0.28	0.70	2627	748	1926	79
Nyando	Londiani (5)	9035127	35.62	-0.05	2690	1216	0.20	-0.18	1751	664	1960	45
Nzoia	Turbo Forest (6)	8935076	35.02	0.67	2034	1326	0.24	0.19	2141	611	1960	45
Ruizi	Mbarara M (7)	9030003	30.68	-0.60	1420	915	0.18	0.48	1520	519	1918	87
Yala	Loliondo (8)	9235000	35.62	-2.05	2134	894	0.32	0.30	1529	433	1934	62
Insidelake	Nansio (9)	9233008	33.08	-2.12	1181	1223	0.21	0.42	1923	735	1950	57
Rusumo	Kayanga (10)	9131028	31.17	-1.53	1362	1080	0.18	0.72	1793	560	1960	47

Table A.2 Selected temperature stations in the Lake Victoria basin.

Catch-ment	Station name (No. in Figure 3.5)	WMO ID	Annual mean (°C)	CV	Skew-ness	Maximum (°C)	Minimum (°C)	Begin year	No. years
Kagera	Biharamulo {1}	9231011	16.73	0.05	0.09	18.15	15.12	1970	31
Katonga	Bukasa (2)	9032010	17.38	0.06	-1.09	18.84	14.62	1970	23
Nzoia	Kadenge {3}	8934140	17.02	0.10	-0.94	20.47	11.18	1971	30
Insidelake	Kayanga {4}	9232027	15.88	0.07	0.42	18.15	13.56	1970	31
Nyando	Kisii Water Supply {5}	60462	17.76	0.05	1.36	20.81	16.11	1970	37
Ruizi	Mbarara Met {6}	9030003	16.18	0.05	0.71	18.15	15.00	1970	31
Mara	Narok {7}	60750	14.28	0.16	-3.94	16.21	2.61	1970	35
Yala	Ukerewe-Island {8}	9132002	18.13	0.07	1.27	20.79	16.31	1970	32
Issanga	Ukiriguru ({9}	9233044	17.20	0.07	0.30	20.25	14.78	1970	35

Table A.3 Selected streamflow gauging stations in the Lake Victoria basin.

Station name (No. in Figure 4.4)	Station ID	Lon	Lat	Mean ($m^3 s^{-1}$)	CV	Skew-ness	Max ($m^3 s^{-1}$)	Min ($m^3 s^{-1}$)	Begin year	No. years
Simiyu [1]	112022	33.45	-2.59	202.92	0.28	-0.42	289.30	95.43	1969	28
Nyakizumba [2]	81248	30.08	-1.32	22.26	0.43	0.34	43.88	5.12	1956	45
Katonga [3]	81259	31.95	-0.09	10.42	1.05	2.55	51.03	1.42	1965	42
Nyando [4]	104172	35.04	-0.10	177.37	0.42	0.83	359.86	50.54	1961	39
Nzoia Rwamba [5]	1EF02	34.08	0.13	376.41	0.48	1.33	936.26	157.81	1950	51
Ruizi [6]	81224	30.65	-0.62	25.55	0.57	0.65	58.19	9.06	1970	31
Sio [7)]	1AH01	34.14	0.39	56.08	0.18	-0.52	71.12	31.76	1958	43

Table A.4 Selected temperature stations in the River Katonga and Ruizi catchments.

Katonga				Ruizi			
Station ID	Lon	Lat	Alt (m)	Station ID	Lon	Lat	Alt (m)
8931008	31.83	0.55	1350	9030006	30.65	-0.63	1410
8932099	32.12	0.30	1245	9030013	30.43	-0.37	1650
9031030	31.63	-0.08	1260	9030019	30.35	-0.72	1500
9032001	32.02	-0.02	1170	9030021	30.32	-0.57	1560

Table A.5 Selected rainfall stations in the River Katonga catchment.

Station name	WMO ID	Annual mean (mm)	CV	Skew-ness	Maximum (mm)	Minimum (mm)	Begin year	No. years
Kassanda	8931008	1021	0.28	0.43	1764	526	1943	64
Madu	8931017	1060	0.19	0.45	1502	713	1943	64
Kanoni	8931022	1168	0.16	0.52	1586	860	1957	50
Ngando Hydromet	8931029	1164	0.16	0.02	1509	710	1972	35
Bakijulula	8932061	1240	0.18	0.80	1986	854	1944	63
Senda	8932062	1265	0.20	0.85	2068	870	1944	63
Bulera	8932072	1237	0.20	0.29	1865	622	1951	56
Kibibi	8932077	1281	0.20	0.86	1935	893	1954	53
Mwera	8932099	1284	0.20	1.18	2108	884	1961	46
Mubende DFI	8932129	1212	0.16	0.68	1685	909	1974	33
Katigondo WFM	9031003	1222	0.22	0.59	2032	765	1943	64
Masaka Forest	9031004	1170	0.21	0.87	1988	813	1944	63
Kalungu	9031007	1129	0.21	0.37	1646	693	1943	64
Butenga	9031018	1090	0.23	0.33	1771	715	1943	64
St. Henrys College Kito	9031023	1157	0.17	0.36	1639	759	1948	59
Kamenyami	9031026	1033	0.23	-0.03	1508	587	1952	55
Bigasa	9031030	1097	0.18	0.55	1546	794	1958	49
Jubiya Forest	9031034	1315	0.17	0.26	1766	965	1964	43
Nkozi Exp Farm	9032001	1136	0.18	-0.20	1490	656	1943	64
Bukakata Pier	9032003	1285	0.16	0.29	1740	953	1943	64

Table A.6 Selected rainfall stations in the River Ruizi catchment.

Station name	WMO ID	Annual mean (mm)	CV	Skew-ness	Maximum (mm)	Minimum (mm)	Begin year	No. years
Mbarara Met	9030003	945	0.19	0.72	1520	637	1918	89
Mbarara High School	9030006	932	0.21	0.42	1505	372	1943	64
Rwoho Forest	9030012	1016	0.24	0.22	1608	539	1948	59
Nsika	9030013	1075	0.18	1.03	1802	737	1950	57
Ndeizha	9030019	1103	0.18	0.04	1555	721	1950	57
Rubare Farm	9030021	1081	0.19	0.47	1625	672	1951	56
Rubare Farm	9030021	1081	0.19	0.47	1625	672	1951	56
Mbarara Stock Farm	9030025	955	0.19	0.96	1581	603	1957	50
Bugamba Forest	9030027	1048	0.19	0.82	1695	725	1958	49
Kikunda Rwoho	9030042	997	0.24	-0.15	1582	388	1975	32
Mary Hill High School	9030043	963	0.16	1.07	1528	653	1969	38
Rwanyamahembe	9030046	1036	0.17	0.76	1619	727	1951	56
Rubindi	9030047	1046	0.18	0.57	1612	711	1950	57
Muko Range	9030051	944	0.24	-0.26	1568	281	1971	36

Tables A.7 and A.8 provide information on the AR4 IPCC GCMs whose data were used in this study; the models' resolutions, given in Lon and Lat, are in decimal degrees. The models (Table A.7) marked with * demonstrated high inconsistency with observed rainfall over the Lake Victoria basin.

Table A.7 Information on the GCMs whose data were used in this study.

Modeling institution, country	Center acronym	Model acronym	Model resolution		Availability of scenario:			
			Lon	Lat	20C3M	A2	A1B	B1
Bjerknes Centre for Climate Research, Norway Norway	BCCR	BCM2.0	2.813	2.791	✔	✔	✔	✔
Canadian Centre for Climate Modelling & Analysis, Canada	CCCma	CGCM3.1(T47)	3.750	3.711	✔	✔	✔	✔
		CGCM3.1(T63)	3.750	3.711	✔	✘	✔	✔
Centre National de Recherches Meteorologiques, France	CNRM	CM3	2.813	2.791	✔	✔	✔	✔
Australia's Commonwealth Scientific and Industrial Research Organisation, Australia	CSIRO	Mk3.0	1.875	1.865	✔	✔	✔	✔
		Mk3.5	1.875	1.865	✔	✔	✔	✔
Max-Planck-Institute for Meteorology, Germany	MPI-M	ECHAM4-OM	3.750	3.711	✔	✔	✘	✔
		ECHAM5-OM	1.875	1.865	✔	✔	✔	✔
Research Institute of KMA, Germany/Korea	MIUB	ECHO-G	3.750	3.711	✔	✔	✔	✔
Institute of Atmospheric Physics, China	LASG	FGOALS-g1.0*	2.500	2.022	✔	✘	✔	✔
Geophysical Fluid Dynamics Laboratory, USA	GFDL	CM2.0	2.500	2.022	✔	✔	✔	✔
		M2.1	2.500	2.022	✔	✔	✔	✔
Goddard Institute for Space Studies, USA	GISS	AOM	3.750	3.711	✔	✘	✔	✔
		E-H	5.000	4.000	✔	✘	✔	✘
		E-R	5.000	4.000	✔	✔	✘	✘
Institute for Numerical Mathematics, Russia	INM	CM3.0	5.000	4.000	✔	✔	✔	✔
Institut Pierre Simon Laplace, France	IPSL	CM4	3.750	2.535	✔	✔	✔	✔
National Institute for Environmental Studies, Japan	MRI	CGCM2.3.2a*	2.813	2.791	✔	✔	✔	✔
Meteorological Research Institute, Japan	NIES	MIROC3.2(hires)	2.813	2.791	✔	✘	✔	✔
		MIROC3.2(medres)	2.813	2.791	✔	✔	✔	✔
National Center for Atmostpheric Research, USA	NCAR	CCSM3.0*	1.406	1.401	✔	✔	✔	✔
		PCM1*	2.813	2.791	✔	✔	✔	✔
Hadley Centre for Climate Prediction and Research Met Office, United Kingdom	UKMO	HadCM3	3.750	2.750	✔	✘	✘	✘
		HadGEM1	1.875	1.250	✔	✘	✘	✘

Table A.8 Definitions of the IPCC SRES scenarios used in this study.

Scenario	Data set	Description	Simulation period	Data available for
20C3M	20th Century simulation	Model input forcings or initial conditions (e.g., solar irradiance, ozone, sulfates, greenhouse gases) are temporally and spatially varied	1870-2000	1961-2000
SRES B1	550 ppm CO_2 maximum (SRES B1)	Atmospheric CO_2 concentrations reached 550 ppm in the year 2100 in a world characterized by low population growth, high GDP growth, low energy use, high land-use changes, low resource availability and medium introduction of new and efficient technologies.	2001-2100	2046-2065 2081-2100
SRES A1B	720 ppm CO_2 maximum (SRES A1B)	Atmospheric CO_2 concentrations reach 720 ppm in the year 2100 in a world characterized by low population growth, very high GDP growth, very high energy use, low land-use changes, medium resource availability and rapid introduction of new and efficient technologies.	2001-2100	2046-2065 2081-2100
SRES A2	850 ppm CO_2 maximum (SRES A2)	Atmospheric CO_2 concentrations reach 850 ppm in the year2100 in a world characterized by high population growth, medium GDP growth, high energy use, medium/high land-use changes, low resource availability and slow introduction of new and efficient technologies.	2001-2100	2046-2065 2081-2100

APPENDIX B

Some classical statistical models

Mann-Kendall test

The MK (Mann-Kendall) test is based on the test statistic S defined as follow:

$$S = \sum_{i=1}^{n-1} \sum_{j=i+1}^{n} \operatorname{sgn}(x_j - x_i) \tag{B.1}$$

where x_j are the sequential data values at respective time j, n is the length of the data set, and

$$\operatorname{sgn}(\theta) = \begin{cases} 1 & \text{if} \quad \theta > 0 \\ 0 & \text{if} \quad \theta = 0 \\ -1 & \text{if} \quad \theta < 0 \end{cases} \tag{B.2}$$

A very high positive value of S is an indicator of an increasing trend and a very low negative value indicates a decreasing trend. Mann (1945) and Kendall (1975) have documented that when $n \geq 8$, the statistic S is approximately normally distributed with the mean and the variance as follows:

$$E(S) = 0 \tag{B.3}$$

$$V(S) = \frac{n(n-1)(2n+5) - \sum_{i=1}^{g} t_i(t_i-1)(2t_i+5)}{18} \tag{B.4}$$

where t_i is the number of ties (data points) in the i^{th} group and g is the number of ties (a set of sample data having the same value). The standardized statistic Z is computed by

$$Z_{\text{MK}} = \begin{cases} \dfrac{S-1}{\sqrt{\operatorname{Var}(S)}} & S > 0 \\ 0 & \text{S} = 0 \\ \dfrac{S+1}{\sqrt{\operatorname{Var}(S)}} & S < 0 \end{cases} \tag{B.5}$$

Modifier of the MK variance

To remove the effect of the lag-1 autoregressive (AR(1)) from the MK test result, the variance $V(S)$ is modified by an effective sample size (ESS) and is thus able to limit the effect of AR(1). The modified variance $V^*(S)$ is given by

$$V^*(S) = V(S).\frac{n}{n^*} \tag{B.6}$$

where n is the actual sample size (ASS) of the sample data, n^* is the ESS given by equation (B.7), and n/n^* is termed the correction factor. The ESS is given by (Bayley and Hammersley, 1946)

$$n^* = \frac{n}{1 + 2.\sum_{k=1}^{n-1}\left(1 - \frac{k}{n}j\right).\rho_k} \tag{B.7}$$

where ρ_k is the lag-k serial correlation coefficient, which can be represented by the sample lag-k serial correlation coefficient, given by (Salas et al., 1980)

$$r_k = \frac{\frac{1}{n-k}\sum_{t=1}^{n-k}\left(x_t - \overline{x}_t\right)\left(x_{t+k} - \overline{x}_t\right)}{\frac{1}{n}\sum_{t=1}^{n}\left(x_t - \overline{x}_t\right)^2} \tag{B.8a}$$

$$\overline{x}_t = \frac{1}{n}\sum_{t=1}^{n} x_t \tag{B.8b}$$

Matalas and Langbein (1962) provided a formula for computing n^* for the lag-1 autoregressive process:

$$n^* = \frac{n}{1 + \frac{2.\rho_1^{n+1} - n.\rho_1^2 + (n-1).\rho_1}{n(\rho_1 - 1)^2}} \tag{B.9}$$

It is referenced in Yue and Wang (2004) that formulae B.7 and B.9 appeared in the work of Lettenmaier (1976). The P-value (probability value, p) of the MK statistic, S, of the sample data can be estimated using the normal CDF:

$$p = \Phi(|Z|)\ (Z = Z_{MK}, Z_{SR}) \tag{B.10}$$

$$\left(\Phi(|Z|) = \frac{1}{\sqrt{2\pi}} \int_0^{|Z|} e^{-t^2/2} \mathrm{d}t \right) \tag{B.11}$$

If the *P*-value is large enough, for example, than the set confidence limit, the trend is quite unlikely to be caused by random sampling. At the significant level of 0.05, if $p \geq 0.95$, the existing trend is considered statistically significant. The positive or the negative value of *Z*-value indicates an increasing or a decreasing trend, respectively.

Magnitude of the slope of a monotonic trend

The magnitude of the slope of the trend is estimated using the approach proposed by Theil (1950) and Sen (1968), which is given by

$$b = \text{Median}\left(\frac{x_j - x_i}{j - i} \right), \ \forall j > i \tag{B.12}$$

where *b* is the estimate of the slope of the trend and x_i is the i^{th} observation. Note that *b*, the slope of the trend in the time series, is a robust measure of the magnitude of a monotonically increasing trend and essentially computes the median of all the pair wise slopes in the particular time series.

Autocorrelation test

The lag-1 autocorrelation coefficient for the sample data is calculated as:

$$r_1 = \frac{\sum_{i=1}^{n-1} (x_i - \overline{x})(x_{i+1} - \overline{x})}{\sum_{i=1}^{n} (x_i - \overline{x})^2} \tag{B.13}$$

which is related to equation (B.8a). If the time series data come from a random process, the expected value and variance of r_1 are:

$$E(r_1) = -\frac{1}{n} \tag{B.14}$$

$$Var(r_1) = -\frac{\left(n^3 - 3n^2 + 4\right)}{\left[n^2(n^2 - 1)\right]} \tag{B.15}$$

The *Z*-statistic is therefore (the critical test statistic values for various significance levels can be obtained from normal probability distribution of equation B.11) given by:

$$Z = \frac{\left|r_1 - E(r_1)\right|}{Var(r_1)^{0.5}} \tag{B.16}$$

Given a significant level α, it is possible to obtain the upper and lower values of r_1 (also see Yue et al., 2002).

The Nash-Sutcliffe model performance criterion

The Nash-Sutcliffe coefficient of efficiency, *RE*, is defined by the following equation (Nash and Sutcliffe, 1970):

$$RE = 1 - \frac{\sum_{i=1}^{n}\left(Q_{o,i} - Q_{s,i}\right)^2}{\sum_{i=1}^{n}\left(Q_{o,i} - \overline{Q_{o,i}}\right)^2} \tag{B.17}$$

where

RE = Nash-Sutcliffe coefficient of efficiency [-]
$Q_{o,i}$ = observed streamflow at the i^{th} time interval [$m^3\ s^{-1}$]
$\overline{Q_{o,i}}$ = mean of the observed streamflow [$m^3\ s^{-1}$]
$Q_{s,i}$ = simulated streamflow at the i^{th} time interval [$m^3\ s^{-1}$]
n = the number of time steps of the observations [-]

***ET*$_o$ estimation**

FAO Penman-Monteith equation

The FAO Penman-Monteith equation (Allen et al., 1998) is given by:

$$ET_o = \frac{0.408\Delta(R_n - G) + \gamma\frac{900}{T+273}u_2(e_s - e_a)}{\Delta + \gamma(1 + 0.34u_2)} \tag{B.18}$$

where ET_o reference evapotranspiration [mm day^{-1}],
Δ slope of the saturated vapour pressure [kPa $°C^{-1}$]
R_n net Radiation [MJ $m^{-2}.day^{-1}$]
γ psychrometric constant [kPa $°C^{-1}$]

e_s-e_a vapour pressure deficit [kPa]
T mean temperature [°C]
u_2 windspeed at x m above soil surface [m s^{-1}]
G soil heat flux density [MJ m^{-2} day^{-1}],

The soil heat flux is considered very small compared to R_n, particularly when the surface is covered by vegetation and calculation time steps are 24 hours or longer. The estimation of G is thus ignored in most computational environment. The details on how the different variables are estimated with data or with some missing data are provided in the FAO Irrigation and Drainage Paper n° 56 for daily and 10-daily time periods. Several day-dependent variables can be estimated from maximum and minimum temperature.